Lancaster University
Division of Biomedical and Life Sciences

Investigation of a Tau aggregation inhibitor peptide and peptide-conjugated liposomes as a potential treatment for Alzheimer's Disease

Thesis submitted in total fulfilment of the requirements of the degree of Doctor of Philosophy

Niklas Philipp Reich
BSc, MSc

Date of submission: 1st May 2023

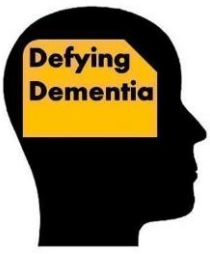

Abstract

Although amyloid beta (Aβ)-targeting antibodies have recently been approved to reduce cognitive decline in Alzheimer's disease (AD), the most common form of dementia, the utility of these drugs is questionable due to dangerous side effects. As a therapeutic alternative to Aβ, inhibiting the pathological aggregation of Tau has gained traction. Our group has recently developed a Tau aggregation inhibitor peptide, RI-AG03, to complement our Aβ aggregation inhibitor peptide RI-OR2.

My aim in this thesis was to investigate the protective effects of RI-AG03 in Tauopathy cell models and 1N4R Tau (P301S)-transgenic PS19 mice. This included the use of doxycycline-inducible and full-length (2N4R) Tau (P301L)-expressing SH-SY5Y cells, termed Clone 4, and Tau RD (V337M/P301L)-EYFP-expressing HEK293 cells, termed Clone 9, to test the peptide. Moreover, the cellular uptake mechanisms and subcellular distributions of polyarginine (polyR)- or transactivator of transcription (TAT)- cell penetrating peptide-linked variants of RI-AG03, unconjugated liposomes and RI-AG03-conjugated liposomes were studied.

RI-AG03-polyR treatment increased total Tau levels in Tauopathy cell and animal models. In Clone 9 cells, RI-AG03-polyR weakly co-localised with monomeric and oligomeric, but not larger, Tau RD-EYFP inclusions. Curiously, both RI-AG03-polyR and a scrambled control peptide reduced the proportions of soluble Tau in Clone 9 cells, while image analysis showed that Cy5-RI-AG03-polyR treatment increased the number of aggregates, suggesting a pro-aggregatory effect. Despite this, RI-AG03-polyR or RI-AG03-TAT improved cell viability and reduced membrane rupture in Clone 9 cells (this effect was even more pronounced when the peptides were conjugated to liposomes), whilst a scrambled control peptide had no such effects. Cellular trafficking studies revealed that only the uptake of RI-AG03-polyR/TAT-conjugated liposomes, whose internalisation was 3-fold higher than that of unconjugated liposomes, was significant in SH-SY5Y cells. Uptake occurred mainly via direct membrane penetration and macropinocytosis, in agreement with fair or moderate co-localisation

with lysosomes and macropinosomes. Strikingly, conjugating RI-AG03-polyR to liposomes avoided peptide entrapment in cell organelles.

Due to using too young animals in a preliminary *in vivo* study, the potential effects of RI-AG03-polyR on cerebral Tau pathology and glial inflammation in PS19 mice could not be characterised. However, immunoblotting showed that RI-AG03-polyR administration doubled baseline postsynaptic density protein 95 (PSD-95) levels in the brains of both wild-type and PS19 mice, whilst both RI-AG03-polyR and its scrambled version increased cerebral pro-apoptotic caspase 3 activity *in vivo*. Finally, RI-AG03-polyR-treated control animals showed two-fold increased p62 levels, but no changes in the autophagy markers Beclin 1 and LC3.

Overall, my findings suggest that RI-AG03 and RI-AG03-conjugated liposomes protect from Tau propagation and toxicity in non-neuronal cells. However, given that the data suggests negative effects of the dosing regimen used in the *in vivo* pilot studies, substantial further studies are necessary to determine whether the peptides might represent an effective AD therapy in pre-clinical models.

Declaration

I hereby declare that the intellectual content in this thesis is my own and that these experimental results have not been submitted, in part or in whole, for any other degree. If not referenced or acknowledged otherwise, the work presented is my own.

Niklas Reich

1st May 2023

Lancaster University

Acknowledgements

I want to thank my recently deceased supervisor, Prof. David Allsop, for his trust and the freedom he gave me in pursuing my research independently. I believe that he was a true pioneer in the field of AD and, for a great article, see Alzforum (2021). Moreover, I want to thank my second supervisor, Dr. Neil Dawson, for his expertise and support with the animal work. I also have to emphasise the support provided by Dr. Edward Parkin, who helped me designing transfection plasmids and with whom I also enjoyed many intellectual discussions and collaborations on projects and grant applications. Finally, I want to express my gratitude to Prof. Christian Holscher. The experience I gained by joining his weekly paper discussions during my time as MSc Biomedicine student and by working as Visiting Researcher in his laboratory were crucial in securing this PhD position.

I would also like to thank Dr. Anthony Aggidis, who developed the Tau aggregation inhibitor peptide RI-AG03 and Callum Ross, a former MRes student, who also introduced me to making liposomes. I also learned multiple methods from Dr. Mark Taylor, who is a good friend. I further want to thank Dr. Leonie Unterholzner and Dr. Jessica Almine. The methods that I learned from them during my MSc dissertation project were the basis for the cell culture experiments and cell line selection in the current work. I also appreciate the aid of Dr. Elisabeth Shaw, who taught me confocal microscopy and flow cytometry, Dr. Nigel Fullwood, who introduced me to transmission electron microscopy, Dr. Nikki Copeland for his assistance with flow cytometry, Dr. Alexandre Benedetto, an expert in microscope image analysis, and Dr. Jayde Whittingham-Dowd who advised me on western blotting. I am further grateful to Dr. Shreyasi Chatterjee from the University of Southampton and Dr. Marc Diamond from the UT Southwestern, who shared Clone 9 cells with me.

Special thanks also goes to Dr. Penny Foulds and ‘Defying Dementia’ whose passionate volunteers and donors funded my research at Lancaster University. Most importantly, I want to thank my parents, who have supported me all along the way.

Table of contents

List of Tables

List of Figures

List of abbreviated terms

AD	Alzheimer's disease
ADAM	A disintegrin and metalloproteinase
AICD	Amyloid precursor protein intracellular domain
AMPAR	Alpha-amino-3-hydroxy-5-methyl-4-isoxazolepropionic acid receptor
ANOVA	Analysis of variance
APF	Annular protofibril
APP	Amyloid precursor protein
ARIA	Amyloid-related imaging abnormalities
ATP	Adenosine triphosphate
Aß	Amyloid beta
BACE1	Beta amyloid precursor protein cleaving enzyme 1
BBB	Blood brain barrier
BDNF	Brain derived neurotrophic factor
BSA	Bovine serum albumin
CAMSAP	Calmodulin-regulated spectrin-associated protein
CBD	Corticobasal degeneration
Ca^{2+}	Calcium

CavME	Caveolae-mediated endocytosis
cdk	Cyclin-dependent kinase
CFP	Cyan fluorescent protein
CPP	Cell penetrating peptide
CLASP	CLIP-associating protein
CLIC/GEEC	Clathrin-Independent carriers / glycosylphosphatidylinositol-enriched endosomal compartments-type endocytosis
CLIP	Cytoplasmic linker protein
CMA	Chaperone-mediated autophagy
CME	Clathrin-mediated endocytosis
CNS	Central nervous system
CREB	cAMP response element-binding protein
CSF	Cerebrospinal fluid
Cy5	Cyanine-5
DMEM	Dulbecco's Modified Eagle Medium
DMSO	Dimethyl sulfoxide
DSPE-PEG(2000)-Mal	1,2-distearoyl-sn-glycero-3-phosphoethanolamine-N-[maleimide(polyethylene glycol)-2000]
Dox	Doxycycline

EB	End binding
EDTA	Ethylenediaminetetraacetic acid
EIPA	5-(N-Ethyl-N-isopropyl)amiloride
ER	Endoplasmic reticulum
ERK	Extracellular signal-regulated kinase
EYFP	Enhanced yellow fluorescent protein
FAD	Familial Alzheimer‘s disease
FBS	Fetal bovine serum
FITC	Fluorescein isothiocyanate
FRET	Fluorescence resonance energy transfer
FTDP-17	Frontotemporal dementia with parkinsonism linked to chromosome 17
GFAP	Glial fibrillary acidic protein
GSK-3ß	Glycogen synthase kinase 3ß
GTO	Granular Tau oligomer
HEK293	Human embryonic kidney 293
Hsc70	Heat shock cognate protein 70
IBA1	Ionized calcium binding adaptor molecule 1
IGC	Inter-gel control
IL	Interleukin
i.p.	Intraperitoneally

iPSC	Induced pluripotent stem cell
JNK	c-jun N-terminal kinase-interacting protein 1
LAMP-2A	Lysosome-associated membrane protein-2A
LDH	Lactate dehydrogenase
LPS	Lipopolysaccharide
LTP	Long-term potentiation
MAP	Microtubule-associated protein
MAPT	Microtubule-associated protein tau
MCI	Mild cognitive impairment
N	N-terminal region (of Tau)
NEB	New England Biolabs
NF-κB	Nuclear factor-kappa B
NFTs	Neurofibrillary tangles
NO	Nitric oxide
NMDAR	N-methyl-D-aspartate receptor
PBS	Phosphate-buffered saline
PEG	Polyethylene glycol
PET	Position emission tomography
PFA	Paraformaldehyde
PHF	Paired helical filament
PiD	Pick's disease

PINP	Peptide inhibitor nanoparticle
PKA	Protein kinase A
polyR	Polyarginine
PP	Protein phosphatase
PRD	Proline-rich domain (in Tau)
PSD-95	Postsynaptic density protein 95
PSEN	Presenilin
PSP	Progressive supranuclear palsy
R	Repeat (in Tau)
RD	Repeat domain (R1 - R4 in Tau)
RIPA	Radioimmunoprecipitation assay
ROS	Reactive oxygen species
SDS	Sodium dodecyl sulfate
SDS-PAGE	Sodium dodecyl sulfate polyacrylamide gel electrophoresis
SF	Straight filament
SM	Sphingomyelin
TAT	Transactivator of transcription
TBE	Tris Borate EDTA
TBS	Tris-buffered saline
TE	Tris-HCl-EDTA

TEM	Transmission electron microscopy
ThS	Thioflavin S
ThT	Thioflavin T
TNF-α	Tumour necrosis factor α
T2DM	Type 2 diabetes mellitus
WT	Wild-type
YFP	Yellow fluorescent protein
6-FAM	6-carboxyfluorescein

1. Introduction

1.1. Alzheimer's disease

1.1.1. Background

It is thought that there are 50 million cases of dementia worldwide and this number is excepted to triple by 2050. Alzheimer's disease (AD) accounts for two-thirds of dementia cases, making it the most frequent neurodegenerative disease. Typically, AD manifests sporadically in individuals over the age of 65, ultimately affecting 50 % of the world population above the age of 85. In 2 - 5 % of cases, the presence of a familial AD (FAD)-associated genetic mutation results in early-onset AD, with symptoms manifesting between ages of 30 - 50 (Zerovnik, 2010; Qiu et al., 2009; Zhang et al., 2021b). Besides aging and genetic predispositions, one-third of AD cases develop as a consequence of modifiable risk factors. AD-associated risk factors accelerating disease onset and shortening lifespan post diagnosis include cardiovascular diseases, diabetes, smoking, air pollution, alcoholism, low educational status, decreased mental, physical and social activity, depression, chronic stress, disturbed sleep, a diet deprived of vitamins and minerals and head injuries (Qiu et al., 2009; Zhang et al., 2021b).

Patients initially develop a preliminary condition, known as mild cognitive impairment (MCI), in which minor mental impairments become apparent. As time passes, a subset of MCI patients transition to AD. In the latter cases, the symptoms progressively worsen, with patients experiencing major deficits in cognitive function, memory and the ability to learn new information. Besides cognitive symptoms, emotional and behavioural alterations also manifest. In more advanced stages of AD, the inability to speak (aphasia) and physical impediments can be observed. Death usually occurs 3 - 9 years after disease onset (Zerovnik, 2010; Helzner et al., 2008).

The first pathologic changes in the AD-afflicted brain, including the aggregation of amyloid beta (Aß) and Tau into senile plaques and neurofibrillary tangles (NFTs), respectively, are believed to occur as early as 25 - 30 years prior to appearance of symptoms (Gandy and DeKosky, 2013; Wischik et al.,

2014). As such, recent efforts towards a therapy have focussed on developing diagnostic methods for early disease detection. Typically, clinical diagnosis of AD relies on the assessment of the clinical history, age and cognitive function of a patient, but is only rarely combined with an investigation of the senile plaque burden, NFT load, blood flow and white matter loss via computed tomography, magnetic resonance imaging or position emission tomography (PET). The current diagnostic accuracy for AD is low, and discrimination from other forms of dementia can only be verified through post mortem examination of the brain (NIH, 2017; Dubois et al., 2021).

In addition to AD, other Tau-exclusive diseases of the brain, termed Tauopathies, exist, including frontotemporal dementia with parkinsonism linked to chromosome 17 (FTDP-17), Pick's disease (PiD), progressive supranuclear palsy (PSP) and corticobasal degeneration (CBD). These conditions differ from AD by the absence of Aß plaques as well as differences in the affected brain areas and symptoms (Avila et al., 2004).

1.1.2. The amyloid cascade hypothesis

The amyloid cascade hypothesis has been the dominant causation theory underlying AD for over two decades and is based on the assumption that the accumulation of Aß and deposition of the peptides in senile plaques are the major pathological events in AD (Hardy and Allsop, 1991; Hardy and Higgins, 1992). Aß fragments between 40 and 43 amino acids are created from the amyloid precursor protein (APP) through sequential proteolytic cleavage by ß-secretase (beta amyloid precursor protein cleaving enzyme 1; BACE1) and the γ-secretase complex, consisting of nicastrin, presenilin enhancer 2, anterior pharynx-defective 1 and presenilin (PSEN)1/2 (Figure 1.1). However, under physiological conditions, the majority of APP is processed through a non-amyloidogenic pathway by α-secretase, mainly involving a distintegrin and metalloproteinases (ADAMs) 9, 10 and 17 (Figure 1.1) (Zhang and Song, 2013).

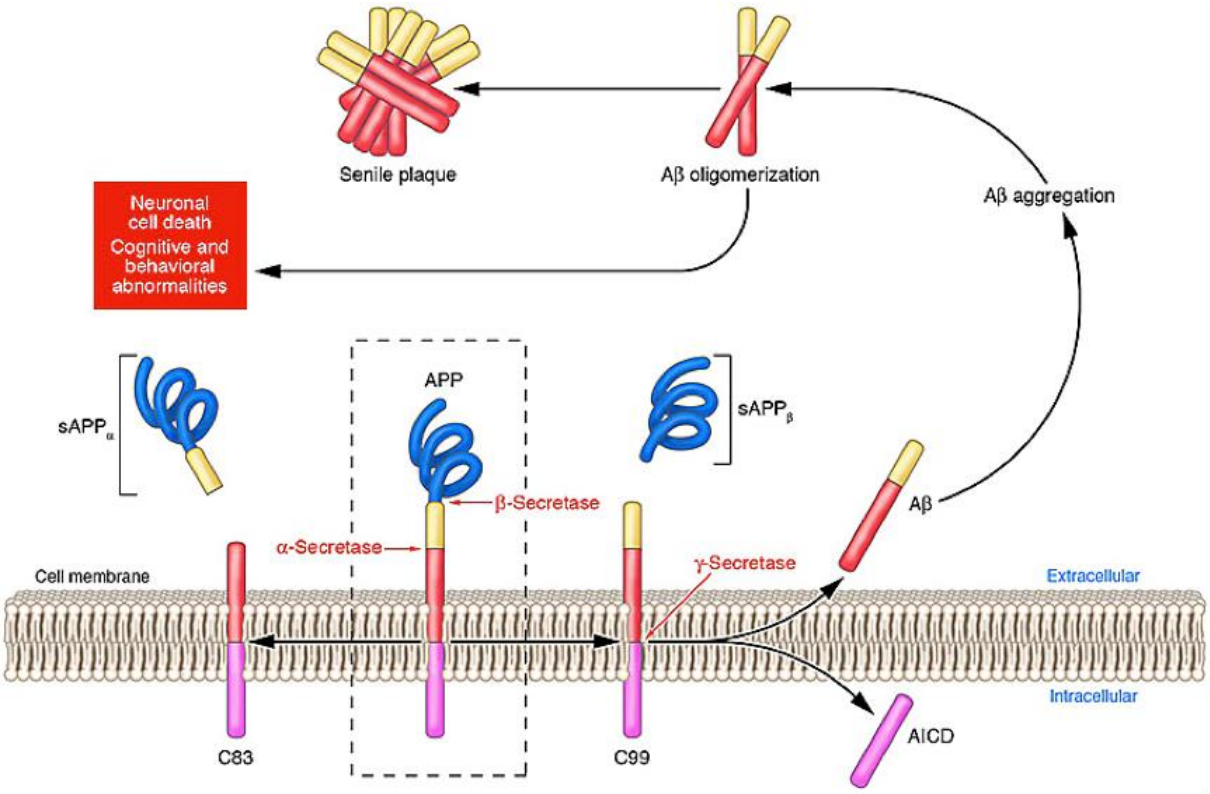

Figure 1.1: Amyloidogenic and non-amyloidogenic proteolysis of APP. The majority of APP undergoes proteolytic processing via the non-amyloidogenic pathway. In this pathway, APP is cleaved by members of the ADAM family, collectively known as α-secretases, creating a fragment known as soluble APPα (sAPPα). The remaining, membrane-bound C-terminal fragment (C83) is processed by γ-secretase, leading to formation of p3 (not shown) and the APP intracellular domain (AICD). Alternatively, in the amyloidogenic pathway, APP may be cleaved by ß-secretase (BACE1) first, leading to the formation of sAPPß. Digestion of the C-terminal APP fragment (C99) by γ-secretase ultimately creates the aggregation-prone $Aß_{1-40}$ and $Aß_{1-42}$ peptides along with AICD. In AD, Aß abnormally accumulates and oligomerises, forming senile plaques that are thought to be implicated in neuronal dysfunction and death. Figure taken from Gandy (2005).

According to the amyloid cascade hypothesis, FAD mutations, impaired degradation and clearance of Aß and accumulation of neurotoxic $Aß_{42}$ initiate a vicious cascade involving senile plaque formation, synaptic dysfunction, neuroinflammation, Tau fibrillisation, neuronal death and, ultimately, dementia (Figure 1.2) (Kametani and Hasegawa, 2018). Notably, all FAD mutations presently identified affect the *APP* or *PSEN1/2* genes encoding for catalytic subunits of γ-secretase, leading to elevated Aß production or an increase in the $Aβ_{42}/Aβ_{40}$ ratio, an increased Aß plaque load and early onset AD (Alzforum, 2019; Hampel et al., 2021). Similarly, due to the trisomy of chromosome 21 and,

thus, the presence of three copies of the *APP* gene, people with Down syndrome show a 1.5-fold increase in Aß generation and premature cognitive decline at around 40 years old (Kolata, 1985).

Despite recent therapeutic success, the validity of the amyloid hypothesis is strongly debated. Over the last 2 decades, numerous Aß-targeting therapeutics have been developed to reduce Aß load, impede amyloidogenic APP processing, impair amyloid aggregation and deposition or immunise against Aß (Wischik et al., 2014). These Aß-modifying approaches have failed to improve cognition in phase 2 and 3 clinical trials in AD patients (Wischik et al., 2014). Nevertheless, for the first time in history, a disease-modifying drug, the anti-Aß antibody aducanumab developed by Biogen, was approved by the FDA for the treatment of MCI and mild dementia/AD in June 2021 (Mozersky et al., 2022). Aducanumab is highly criticised, however, because the antibody was not approved based on its ability to slow cognitive decline, but because of clearing Aß plaques. Due to lack of benefits on brain function and severe side effects, including brain swelling and bleeding (amyloid-related imaging abnormalities; ARIA), Medicare funding for aducanumab was restricted to clinical trials and the FDA requested the acquisition of additional clinical data until 2030. Unlike aducanumab, lecanemab, an antibody targeting soluble Aß protofibrils, has been demonstrated to both lower Aß burden and cognitive decline in a double-blind phase 3 clinical trial involving patients with MCI or early AD (van Dyck et al., 2023). These results led to the FDA approval of lecanemab for early AD (M.M.a.B.W.C., 2023). However, lecanemab has shown severe adverse effects, such as infusion-related reactions (26.4 %), ARIA-H (cerebral micro- and macrohemorrhages or superficial siderosis; 17.3 %) and ARIA-E (cerebral edema; 12.6 %) (van Dyck et al., 2023). The antibody's long-term utility for moderate and advanced AD, risk/benefit ratio, i.e. reduction in cognitive decline vs. ARIA, patient burden and treatment costs ($26,500 per patient annually) have been questioned (M.M.a.B.W.C., 2023). Comparable positive results in a phase 3 AD trial have also recently been reported for another Aß antibody, donanemab (Sims et al., 2023), although the drug may only slow memory loss for an estimated time of 7 months (Hamilton, 2023). Notably, senile plaque load poorly correlates with cognitive impairment and, despite its requirement for an AD diagnosis, is not specific for AD

patients; non-demented, elderly individuals commonly develop plaques as well (Bancher et al., 1996; Terry et al., 1991; Aizenstein et al., 2008). Furthermore, it has been argued that the available clinical data does not support that lowering Aß levels benefits cognition in AD (Mozersky et al., 2022), indicating that more research is necessary.

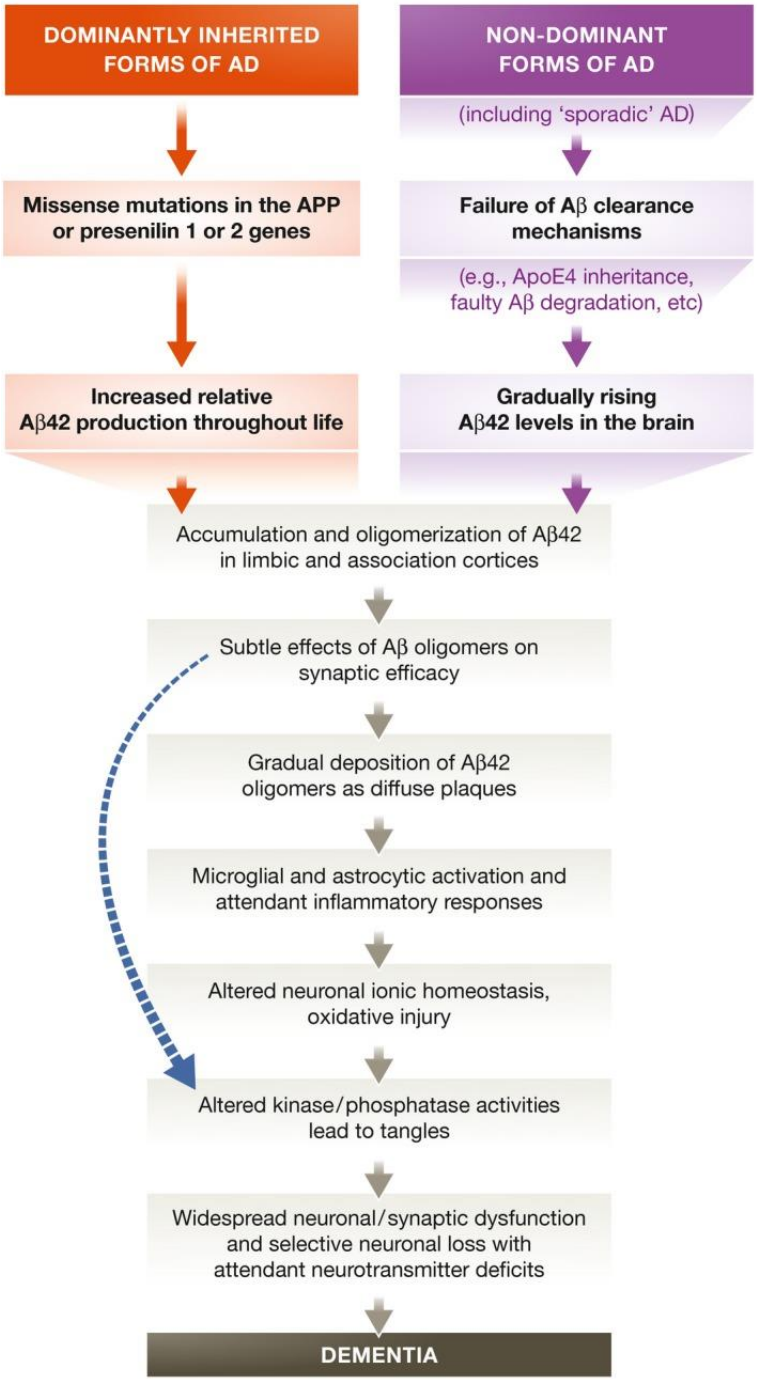

Figure 1.2: Updated version of the amyloid cascade hypothesis in AD. Based on the research of several groups, including ours in Hardy and Allsop (1991), the initial hypothesis was presented in Hardy and Higgins (1992), then amended twice in Hardy and Selkoe (2002) and Selkoe and Hardy

(2016). Depicted are the major steps involved in the Aß-driven development of dementia, as suggested by the amyloid hypothesis. Aß species, in particular soluble oligomers, are strongly implicated in the initiation of Tau pathology (as marked by the blue arrow). Despite the failure of many Aß-alleviating drugs and a growing existential debate, Aß is still deemed to be an essential disease-initiating, albeit not disease-driving, factor in AD (reviewed in Selkoe and Hardy (2016)). Taken from Selkoe and Hardy (2016).

1.1.3. The Tau hypothesis

A Tau-focused hypothesis of neurodegeneration has been postulated in AD (Arnsten et al., 2021). Initially, an inflammatory trigger, for example Aß or pathogen-associated molecular patterns such as lipopolysaccharide (LPS), stimulates cytokine secretion by microglia. These pro-inflammatory cytokines, in turn, induce neuronal MAP kinases, leading to the hyperphosphorylation of Tau, subsequent inability of the protein to bind to microtubules, Tau aggregation into soluble oligomers and insoluble NFTs, the sequestration of microtubule-bound Tau and other MAPs by seeding-competent, oligomeric Tau species and, finally, microtubule depolymerisation (Kametani and Hasegawa, 2018; Alonso et al., 1997; Barron et al., 2017; Maccioni et al., 2010). Furthermore, pathological Tau is released in a free or vesicle-incorporated form into the extracellular space, then internalised by proximate neurons, where seeding-competent Tau species evoke the aggregation of endogenous Tau (Figure 1.3) (De La-Rocque et al., 2021). As such, Tau propagates across nearby neurons. While Tau-burdened neurons ultimately die, there is no evidence that intracellular Tau is released by apoptotic neurons (De La-Rocque et al., 2021), suggesting that Tau propagation involves alive neurons. Following the death and disintegration of Tau-containing neurons, ghost tangles may remain, however (Figure 1.3) (Moloney et al., 2021).

It is debated whether the Aβ or Tau pathology emerges first. Tauists have argued that sporadic AD might be initiated by Ca^{2+} dysregulation and concomitant Tau hyperphosphorylation in vulnerable glutamatergic projection neurons in the association cortex (Arnsten et al., 2021). Phospho-Tau (Ser^{214}) was hypothesised to generate ‘traffic jams’ on dendritic microtubules, potentially interfering with the trafficking of APP-containing endosomes. As a consequence of APP and BACE1

accumulation, Aß production may also be heightened via the phospho-Tau-associated destruction of axonal microtubules (Sadleir et al., 2016; Arnsten et al., 2021).

Emerging evidence suggests that the Tau pathology, and not Aß, ultimately drives cognitive decline and neurodegeneration in AD. In support of this view, the accumulation of phosphorylated Tau and its' aggregation into paired helical filaments (PHFs) correlates more strongly with neurodegeneration, synapse loss and memory deficits than the Aß load (Harrington et al., 1994; Arriagada et al., 1992; Giannakopoulos et al., 2003; Gomez-Isla et al., 1997). It must be noted, however, that the strongest correlate of cognitive decline, even more critical than NFT burden, is synapse loss (Subramanian et al., 2020). In favour of a pathological role of Tau, the presence of Tau appears to be a prerequisite for Aß-driven toxicity. For example, deletion of murine or human transgenic Tau in hippocampal neurons or brain slices prevents the cell death induced by externally applied Aß fibrils, and prevents the Aß-induced reduction in long-term potentiation (Rapoport et al., 2002; Shipton et al., 2011). Likewise, reducing endogenous Tau in hAPP-transgenic mice (with FAD mutations) significantly ameliorated cognitive deficits and excitotoxin-induced seizures, without impacting Aß pathology (Roberson et al., 2007). It is now believed that Aß is an important disease-initiating factor, yet other mechanisms, including the abnormal processing of Tau, may ultimately drive neurodegeneration and cognitive decline in AD (Kopeikina et al., 2012).

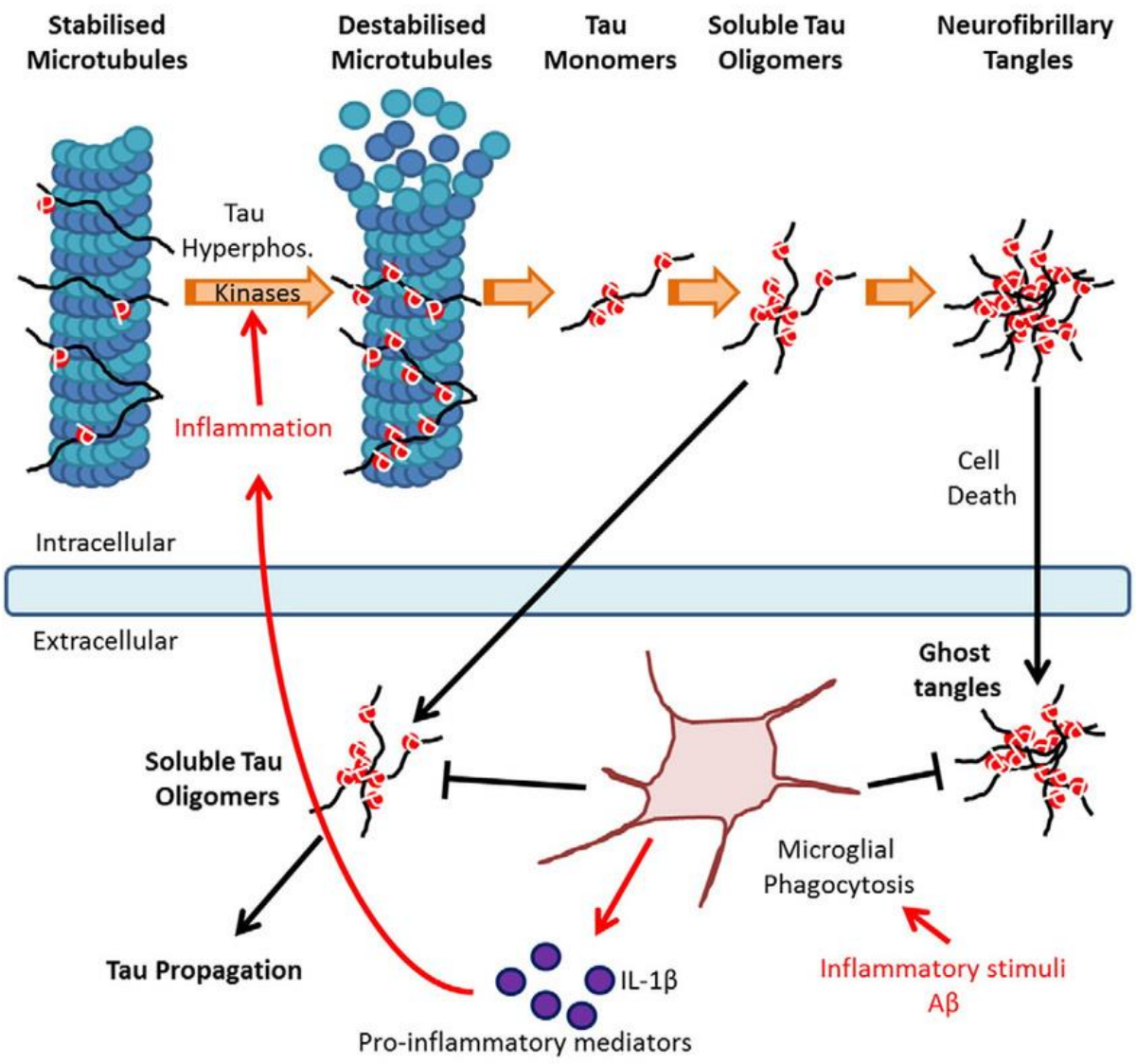

Figure 1.3: Advancement of the Tau pathology in AD. The presence of inflammatory stimuli, e.g. pathogen-associated molecular patterns such as LPS or Aß, leads to the activation of microglia and pro-inflammatory cytokine production. By binding to their respective receptors on neurons, these pro-inflammatory cytokines induce the activation of cellular kinases. Subsequent Tau hyperphosphorylation promotes dissociation of Tau from microtubules and stimulates the protein's self-aggregation into soluble oligomers and mature NFTs. Since both physiological and pathologic Tau are released and endocytosed by neighbouring neurons, aggregated Tau species may propagate between neurons by instigating aggregation of native, microtubule-bound Tau. Following the death of Tau-burdened neurons, ghost tangles, which are remnants of originally intracellular NFTs, may remain in the extracellular space. Notably, activated microglia are also involved in the clearance of extracellular Tau, but chronic inflammation, as characteristic for AD, exacerbates Tau pathology. Taken from Barron et al. (2017).

1.1.4. Interaction of the Amyloid Beta and Tau pathologies in Alzheimer's disease

The link between Aß and Tau pathologies in AD is highly debated. As stipulated by the amyloid cascade hypothesis (Figure 1.2), Aß may exacerbate Tau-mediated neurodegeneration (Selkoe and Hardy, 2016). Since Aß peptides are known to trigger inflammatory responses (Cai et al., 2014) that, in turn, stimulate Tau kinase activity and Tau hyperphosphorylation (Barron et al., 2017), inflammation is a major link between the Aß and Tau pathologies. In addition, *in vitro* and *in vivo* studies have demonstrated that recombinant Aß oligomers as well as oligomers formed in an APP-transgenic mouse model were capable of cross-seeding the aggregation of native Tau (Lasagna-Reeves et al., 2010; Castillo-Carranza et al., 2015).

However, more recent reviews emphasise that Aβ is a required, but not sufficient, factor in the Tau pathology of AD (Roda et al., 2022). Specifically, it was shown that multiple Aß-based animal models, some of them even co-expressing native human Tau in their brains (5xFAD mice), exclusively developed Aß plaques (He et al., 2018). To trigger Tau aggregation into insoluble inclusions, however, cerebral microinjections of PHFs purified from the brain of AD patients (as Tau seeds) were necessary. Once a Tau seed was administered into the brain, the cerebral plaque load in the Aß animal models correlated with the subsequent formation of NFTs and neuropil threads (He et al., 2018). This suggests that Aß accelerates an already present Tau pathology, yet is not the initiator of Tau aggregation. In support of this hypothesis, an *in vitro* study demonstrated that other 'stress factors' besides Aß peptides, such as hydrogen peroxide-mediated oxidative stress, an excess of glutamate, adenosine triphosphate (ATP) overload (resulting in excessive Ca^{2+} influx) or serum deprivation, all increased kinase-associated Tau hyperphosphorylation and spine degeneration in primary hippocampal neurons (Zempel et al., 2010). Instead of Aß species, it has been suggested that non-degraded junk proteins in the cytoplasm (mitochondrial proteins and lipofuscin), accumulating due to defects in cellular degradation and clearance mechanisms, might elicit the sequestration of Tau into PHFs and straight filaments (SFs) (Wischik et al., 2014). Interestingly, a 'dual pathway hypothesis' has been postulated (Small and Duff, 2008), suggesting that there are

similar upstream factors that initiate both amyloid pathologies, such as the AD-accelerating apolipoprotein E4 genotype, activation of the stress kinase GSK-3β or retromer sorting pathway deficiencies. Once induced, Aβ and Tau then jointly drive synapse dysfunction and neuronal death during AD (Roda et al., 2022; Rapoport et al., 2002; Shipton et al., 2011; Roberson et al., 2007).

A potential co-inducer of the Aβ and Tau pathologies in AD is neuronal insulin resistance. Type 2 diabetes mellitus (T2DM) is a well-known risk factor of AD (Holscher, 2019). Furthermore, independent of peripheral insulin resistance in T2DM, AD patients showed desensitised insulin-signalling in the brain (Talbot et al., 2012; Moloney et al., 2010; Steen et al., 2005), caused by aging-associated chronic neuroinflammation or accumulation of Aβ peptides (Holscher, 2019). Importantly, insulin resistance in neurons leads to loss of Akt-signaling and, thus, excessive activity of the Tau-phosphorylating kinase GSK-3β (Hong and Lee, 1997; Schubert et al., 2004). On the other hand, insulin regulates Aβ production, for example by inducing the expression of the Aβ-degrading insulin-degrading enzyme (McClean and Holscher, 2014; Park et al., 2021; Paladugu et al., 2021) or promoting the activity of the non-amyloidogenic α-secretase ADAM10 (Figure 1.1) (Ohtake et al., 2014). Additionally, GSK-3β activation, as suppressed by insulin-signalling (Holscher, 2019), elicits the NF-κB-mediated expression of BACE1, thus aggravating Aβ generation in neurons (Ly et al., 2013; Perry et al., 2003; Jantrapirom et al., 2020; Park et al., 2021; Yu et al., 2020). Indeed, inducing insulin resistance in cultured neurons, amongst other adverse effects, stimulated GSK-3β-induced Tau hyperphosphorylation and aggregation, while enhancing BACE1 activity, Aβ generation and plaque formation (Jantrapirom et al., 2020; Gupta et al., 2011). Thus, neuroinflammation-associated insulin resistance in neurons possibly initiates the Aß and Tau pathologies, followed by cooperation of both amyloids to drive neurodegeneration in AD (Small and Duff, 2008; Roda et al., 2022; Ittner et al., 2010).

1.2. Tau protein in Alzheimer's disease

1.2.1. Tau protein

Tau is a member of the family of microtubule-associated proteins (MAPs) and expressed in neurons, where it predominantly localises to the axonal compartment (De Anda-Hernández et al., 2012; Buee et al., 2000). The presence of a diffusion barrier in the axonal initial segment has been shown to limit retrograde Tau trafficking into the soma and dendrites (Li et al., 2011). Besides the brain, trace amounts of Tau have also been demonstrated in peripheral tissue, for example in fibroblasts and pancreatic acinar cells (Ingelson et al., 1996; Vanier et al., 1998).

The gene encoding Tau, *MAPT*, consists of 16 exons, yet transcription of exons 4A, 6 and 8 has not been described in the central nervous system (CNS) (Figure 1.4A) (Buee et al., 2000). Although components of the *MAPT* promotor, exon -1 and exon 14, are integrated in the mRNA transcript, but they are not translated (De Anda-Hernández et al., 2012; Andreadis et al., 1992). During early embryonic development, expression of the shortest isoform of Tau, devoid of exon 2, 3 and 10, is thought to play an important role in the development of the CNS (Figure 1.4B) (Buee et al., 2000; Kosik et al., 1989). In the adult brain, however, splicing results in the production of 6 different Tau isoforms, present in varying ratios throughout the brain (Figure 1.4B) (Andreadis et al., 1992). These Tau splicing products consist of either 3 or 4 evolutionary conserved repeats (R) of 31 - 32 amino acids in length. Each R domain is composed of an 18 amino acid-long repeat motif that is preceded by a 13 - 14 amino acid-long spacer sequence. Jointly, R1 - R4 are involved in the microtubule-binding of Tau. Additionally, zero, one or two N-terminal regions (N) of either 29 or 58 amino acids in length, respectively, may be inserted (Goedert et al., 1989; Butner and Kirschner, 1991). Based on these splicing-mediated differences, Tau isoforms have been categorised as 3R and 4R species with 0 - 2 N-terminal inclusions. The longest isoform, featuring all four R domains and both N-terminal regions, 2N4R, has a length of 441 amino acids and a molecular weight of 45 kDa, whereas the shortest isoform, 0N3R, is 352 amino acids long, with a molecular weight of 37 kDa (Figure 1.4B).

Structurally, all isoforms share an N-terminal projection domain, comprising of an initial array of acidic amino acids that transition into a proline-rich domain (PRD), as well as the microtubule-binding repeat domain (RD), containing R1 - R4 (Figure 1.4C) (De Anda-Hernández et al., 2012; Goedert and Spillantini, 2017). Importantly, the ^{275}VQIINK^{280} and ^{306}VQIVYK^{311} sequences within the spacer sequence of R2 or R3, respectively, are thought to play a major pathological role (Aillaud and Funke, 2022).

Notably, mutations in the *MAPT* gene do not lead to AD, but result in the development of Tau-exclusive forms of dementia (Tauopathies), such as FTDP-17. Over 30 disease-promoting mutations of Tau have been discovered, either negatively affecting microtubule binding affinity, altering Tau isoform splicing, increasing substrate availability for kinases or elevating the aggregation tendency of the native polypeptide (Alzforum, 2019; Goedert and Jakes, 2005).

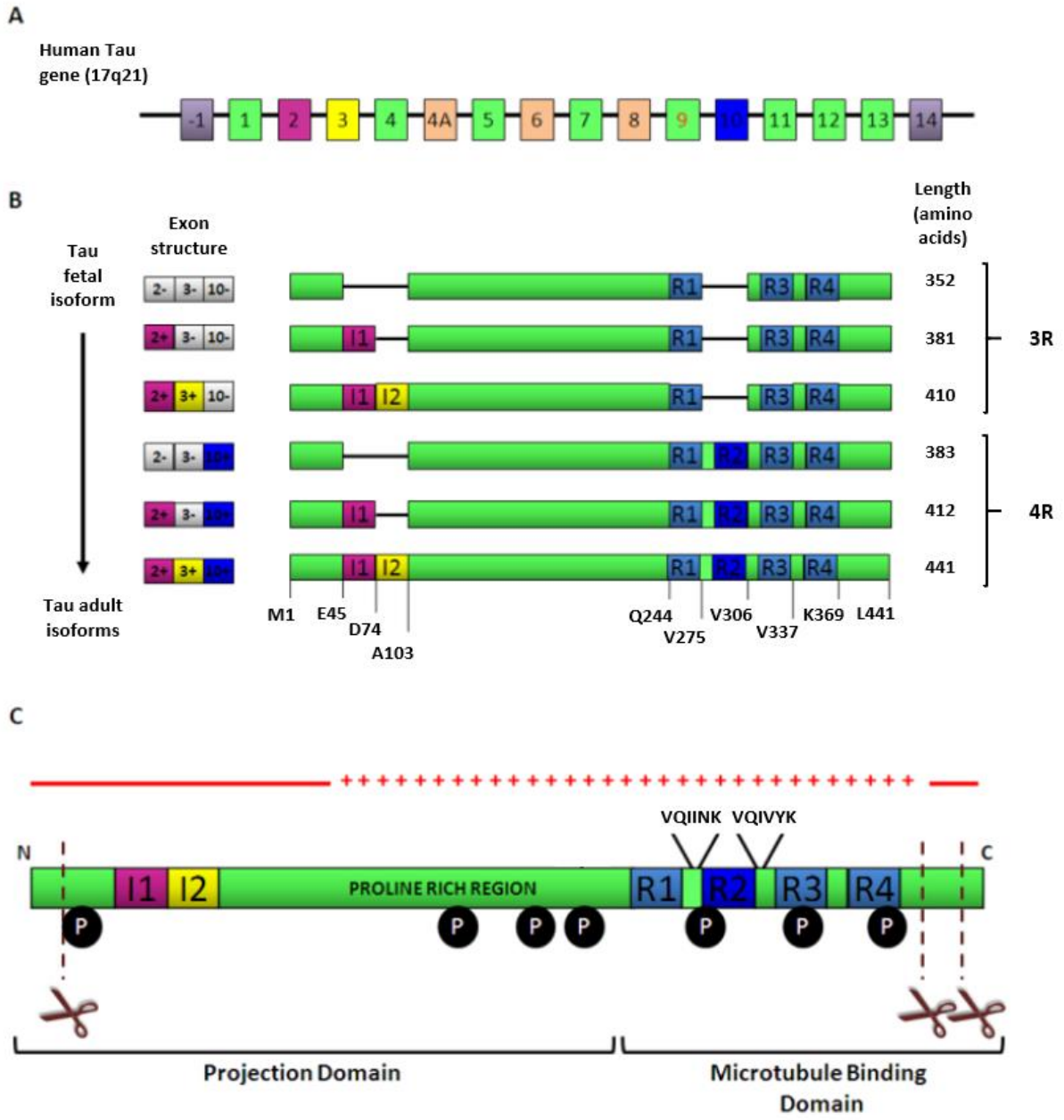

Figure 1.4: Splicing products of Tau and sequence characteristics. (A) Exons of human *MAPT*. Exon 4A, 6 and 8 are not expressed in the brain, whereas exon -1 and 14 are only transcribed, but not translated. (B) Tau isoforms. Depending on the incorporation or exclusion of exon 2, 3 and 10, Tau isoforms can be subdivided into 3R and 4R species with 0 - 2 N-terminal regions. Thus, alternative splicing may create 0N3R, 1N3R, 2N3R, 0N4R, 1N4R and 2N4R isoforms of Tau (top to bottom), ranging from 352 - 441 amino acids in length. While expression of the shortest, 0N3R isoform dominates during the fetal stage, thought to be involved in cerebral development, longer constructs are produced as the human brain ages. In the adult brain, all isoforms are expressed in brain region-specific ratios. (C) Structural subdomains of Tau. R1 - R4 denote the 18 amino acid-long microtubule-binding repeats of Tau that are preceded by 13 - 14 amino acid-long spacer sequences (green space between Rs). The four imperfect repeats, comprising R1 (Glu^{244} - Lys^{274}), R2 (Val^{275} - Ser^{305}), R3 (Val^{306} - Glu^{336}) and R4 (Val^{337} - Asn^{368}), are essential for the physiological function of Tau, but are also involved in Tau pathology (Mandelkow et al., 2007). C-terminal truncation of Tau at Asp^{421} and Glu^{391}

in AD and other tauopathies is believed to be a pathology-associated step (Guillozet-Bongaarts et al., 2005). Adapted from De Anda-Hernández et al. (2012).

1.2.2. Microtubules and the physiological function of Tau

Microtubules are tubular elements of the cytoskeleton in neurons that consist of α- and ß-tubulin subunits (reviewed in Baas et al. (2016)). In addition to providing structural support to axons and dendrites, microtubules are implicated in neurite outgrowth and used as 'highways' for cell organelle positioning and the trafficking of cargo, e.g. neurotransmitter-metabolising enzymes, via the motor proteins kinesin (anterograde – away from the neuronal body and towards the synaptic terminals) and dynein (retrograde – reversed direction). Given their role in axonal architecture and intraneuronal transport, microtubules are critically involved in the physiological brain function, connectivity and development (De Anda-Hernández et al., 2012; Hirokawa et al., 2010; Mokhtar et al., 2013).

To generate or dissolve microtubules, which can vary between less than one to hundreds of micrometers in length, tubulins are dynamically added to, or cleared from, the plus end, while the other (minus) end remains static (Baas et al., 2016). Microtubules may be found in the entire neuronal body, including the soma, dendrites and axons (Figure 1.5A). As a key difference between cell processes, it was shown that axonal microtubules are uniformly packed, with their plus ends facing away from the soma, whereas dendritic microtubules are bidirectionally oriented (1:1 ratio minus-end- vs. plus-end-distal) (Baas et al., 1988; Baas et al., 1989). Moreover, microtubules exhibit a stable domain close to the minus end and a more flexible labile domain towards the plus end (Baas et al., 2016). It was demonstrated that approximately 58 % of the axonal microtubule mass in primary (rat) neurons is stable, whereas the other 42 % are labile and more strongly tyrosinated. In contrast to their axonal counterparts, dendritic microtubules show a comparably lower percentage of stable, and thus greater labile, microtubule mass (Baas and Black, 1990; Baas et al., 2016). Notably, younger neurons have a higher degree of labile domains in the axon, and stable axonal

microtubule mass may differ between different types of neurons (e.g. sympathetic vs. hippocampal) (Baas et al., 2016).

Besides a range of post-translational modifications that regulate microtubule stability (Figure 1.5B), various proteins, including MAPs and Tau, modulate microtubule assembly. Over 40 years ago, it was discovered that Tau can induce the chain assembly of purified α- and ß-tubulin subunits into mature microtubules (Weingarten et al., 1975). These studies also showed that Tau promotes the elongation and prevents the shortening of microtubules, thus acting as a microtubule stabiliser (Panda et al., 1995). However, more recent findings revealed that Tau selectively stabilises the labile portion of microtubules (Figure 1.5B), whilst depletion of Tau, in fact, increases stable microtubule mass in cultured neurons (Qiang et al., 2018). On the other hand, MAP6 (previously known as stable tubule only polypeptide, STOP) was shown to be a genuine stabiliser that protects microtubules from cold-induced disassembly (Slaughter and Black, 2003; Margolis et al., 1990; Qiang et al., 2018), and whose interaction with labile domains is restricted by Tau (Qiang et al., 2018).

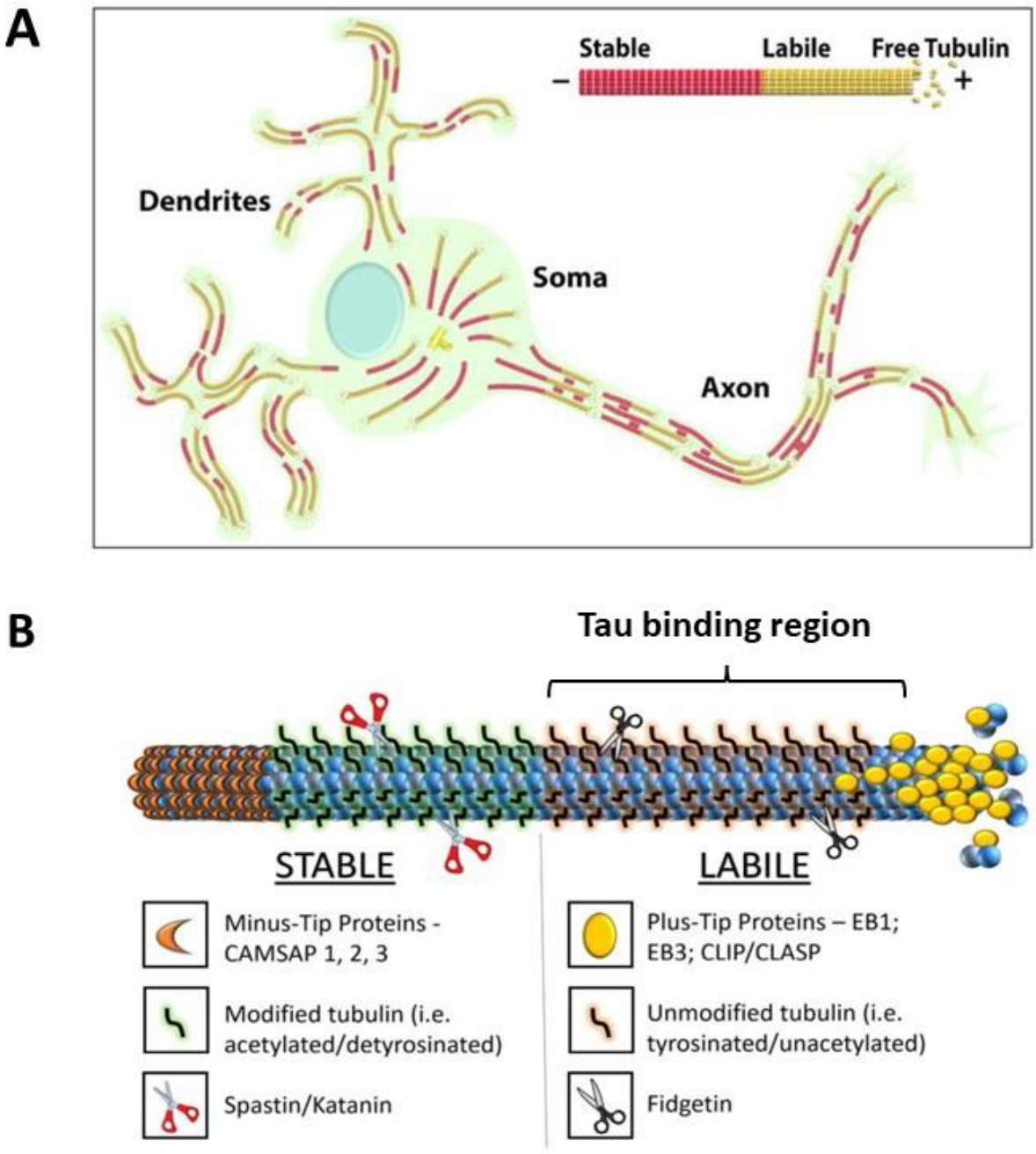

Figure 1.5: Localisation of microtubules and their modifications in vertebrate neurons. (A) Neuronal microtubule architecture. Microtubules are tubular polymers dynamically assembled from α- and ß-tubulins added to the plus end. Microtubules initially nucleate at the centrosome in the soma, but are transported by motor proteins into growing axons and dendrites during neuronal development, where they continue to polymerise. A mature neuron features uniform, plus-end-distal-oriented microtubules in the axon and non-uniform (bidirectionally) oriented microtubules in dendrites. Moreover, individual microtubules consist of a stable and a labile region. A key contrast is that dendritic microtubules show a lower amount of stable, but more labile, microtubule mass. (B) Post-translational tubulin modifications and protein interactions. The stable domain of microtubules is generally modified via detyrosination (but not always entirely) and acetylation, whereas the labile domain is tyrosinated and unacetylated. Other modifications affecting stability include

phosphorylation, polyglycation, polyamination and polyglutamylation (not shown). Minus-tip proteins calmodulin-regulated spectrin-associated protein (CAMSAP) 1-3 prevent depolymerisation at the minus end, while their plus-tip counterparts end binding (EB)1, EB3, cytoplasmic linker protein (CLIP) and CLIP-associating protein (CLASP) associate with the plus end. Region-specific severing proteins also exist, such as spastin, katanin (both stable domain) and fidgetin (labile). If microtubules are cut in the stable region, they may break into two individual tubules that are capable of growing. By contrast, if severed in the labile portion, the microtubule is shortened. Importantly, Tau selectively interacts with labile microtubule domains. Modified from Baas et al (2016).

Emerging evidence also suggests physiological roles for Tau in modulating kinesin/dynein motility (Dixit et al., 2008), DNA protection upon oxidative and heat stress (Sultan et al., 2011), cerebral insulin-signalling (Marciniak et al., 2017), the regulation of the RNA metabolism and stress-associated protein translation, as mediated by (hyper)phosphorylated and oligomerised Tau that is (mis)sorted into stress granules in dendrites (Cruz et al., 2019; Koren et al., 2020), and postsynaptic plasticity (Ittner and Ittner, 2018).

In light of the main physiological function of Tau, the interaction with microtubules has been extensively characterised. Curiously, the binding affinity of Tau towards tubulin was reported to be surprisingly weak (Butner and Kirschner, 1991) and only lasts ~40 ms in living neurons (Janning et al., 2014). It was proposed that Tau may jump between microtubules in a 'kiss-and-hop' manner (Janning et al., 2014), which likely contributes to the flexibility of labile domains (Janning et al., 2014; Kadavath et al., 2015). Binding to microtubules is predominantly established by certain residues within the RD of Tau, although the PRD also partially contributes (Butner and Kirschner, 1991; Kadavath et al., 2015; Goode et al., 1997). As depicted in Figure 1.6A, a recent study revealed that a handful of lysine residues in the Tau protein interact with Lys^{336} and Lys^{338} of α-tubulin. These important residues of Tau comprise Lys^{225} and Lys^{240} (PRD flanking R1), Lys^{257} (R1), Lys^{311} (linker sequence between R2 & R3) and lys^{383} (located shortly after R4). This was confirmed using the competitive ligand vinblastine, a tubulin-binding molecule which interacts with α-tubulin near Lys^{336} and Lys^{338} (Figure 1.6B) (Kadavath et al., 2015). In addition to the key binding sites, mutational experiments have revealed further residues that appear to be involved in microtubule binding, for

example Lys^{215}, Lys^{216} and Arg^{221} in the PRD (Goode et al., 1997). Notably, the 18 amino acid-long long spacer sequences between R1-R4 as well as the N-terminal tail of Tau (projection domain) remain unbound (Kadavath et al., 2015). It has been proposed that the unbound projection domain assures adequate spacing between microtubules, thus regulating the axonal shape (Chen et al., 1992).

Affinity-wise, there are major differences between 3R and 4R Tau isoforms. In direct comparison, absence of the R1-R2 linker domain as well as R2 (in particular the ^{275}VQIINK^{280} motif) in 3R Tau isoforms leads to a 3-fold decreased binding strength compared to 4R Tau, even though none of the key amino acids, as depicted in Figure 1.6A, are missing (Kadavath et al., 2015; Lu and Kosik, 2001; Goode and Feinstein, 1994). It was argued that 3R and 4R Tau undergo an "induced fit" upon binding to microtubules, adopting a conformation that facilitates the interaction with microtubules. Structural differences between 3R and 4R isoforms presumably affect the exposure of key binding residues of Tau towards α-tubulin, explaining the varying binding affinity (Kadavath et al., 2015).

The association of Tau with tubulin is dynamically regulated by the phosphorylation state of the former protein. Constant modification by cellular kinases and phosphatases regulates the binding (unphosphorylated) or detachment (phosphorylated) of Tau to α-tubulin, thus modulating microtubule (de)polymerisation and cargo delivery (Kolarova et al., 2012).

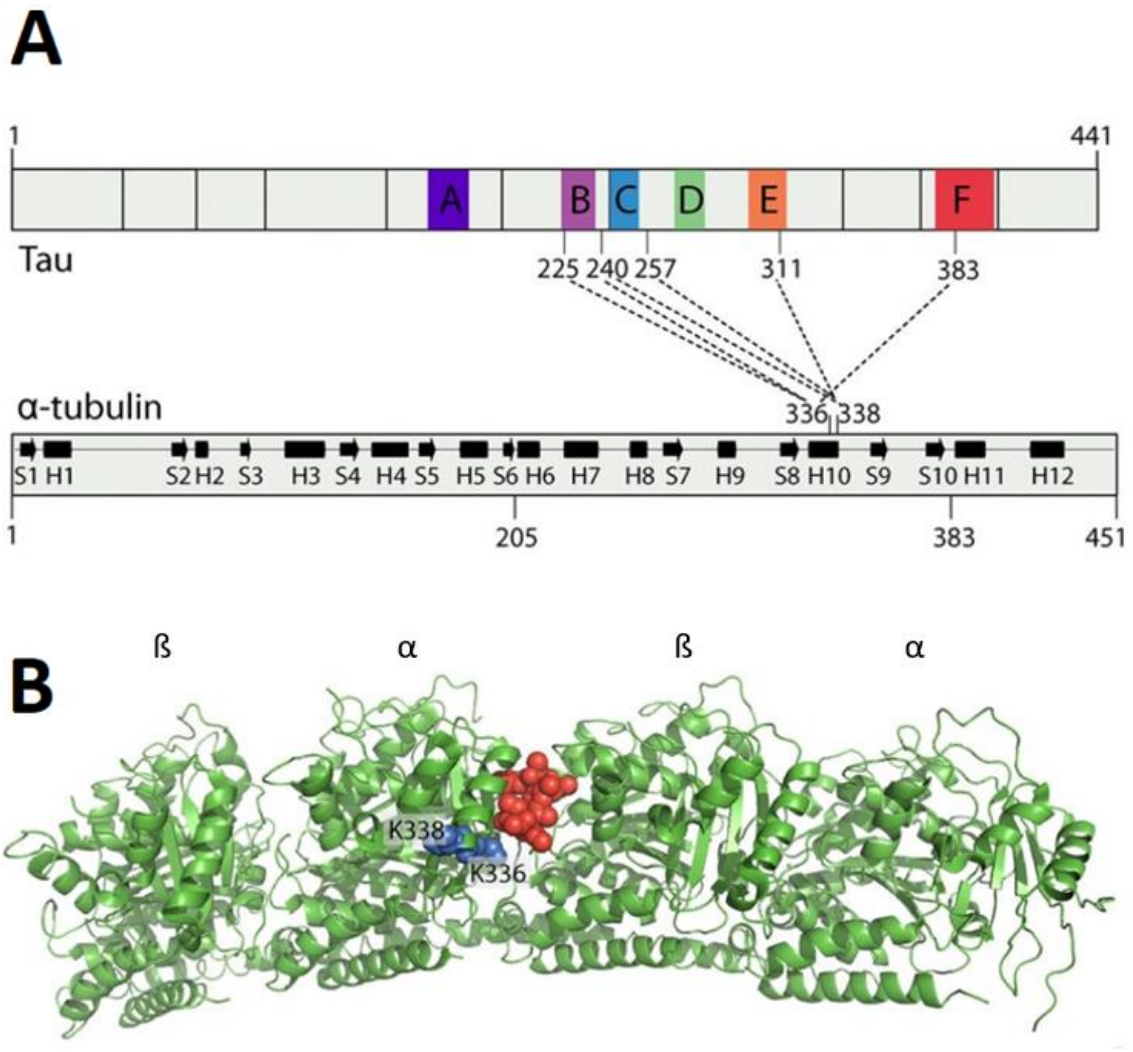

Figure 1.6: Binding interactions between Tau and microtubules. (A) A set of five key amino acids surrounding and within the RD (R1-4) region of Tau, comprising Lys^{225}, Lys^{240}, Lys^{257}, Lys^{311} and Lys^{383}, mediate the binding of Tau to Lys^{336} and Lys^{338} of α-tubulin. This establishes a loose, yet dynamic, interaction of Tau with microtubules. (B) Vinblastine (red), a microtubule-associating agent that binds between α- and ß- tubulin dimers (green), prevents microtubule-binding of tau by sterically impeding the interaction of Tau with Lys^{336} and Lys^{338} (blue) of α-tubulin. Adapted from Kadavath et al. (2015).

1.2.3. Post-translational modifications of Tau

A range of post-translational modifications of Tau, including phosphorylation, acetylation, methylation, ubiquitinylation, SUMOylation, O-GlcNAcylation and N-glycosylation, have been identified (Alquezar et al., 2020). Collectively, these modifications mainly affect phase separation,

aggregation, microtubule assembly and degradation of Tau (Ye et al., 2022). The physiological and pathological role of these is discussed below.

Generally, dynamic phosphorylation and dephosphorylation of Tau regulates the protein's interaction with microtubules (Kolarova et al., 2012). Selective, minor and presumably temporally regulated phosphorylation at Ser^{262}, Ser^{324} and Ser^{356} in the Tau RD was shown to lower the binding affinity of Tau for microtubules, thus modulating neuronal polarity and the outgrowth of neurites (Biernat et al., 2002; Biernat and Mandelkow, 1999). Furthermore, Tau is implicated in axogenesis through a phosphorylation gradient in neurons, with Tau more strongly dephosphorylated in the axonal growth cone compared to somatodendritic regions (Mandell and Banker, 1996). It was also suggested that Tau phosphorylation at Ser^{199}, Ser^{202}, Thr^{205} and Ser396 affects postsynaptic plasticity and N-methyl-D-aspartate receptor (NMDAR) activity by altering the interaction of Tau with other synaptic proteins, such as postsynaptic density protein 95 (PSD-95) or Fyn (Ittner and Ittner, 2018). Due to playing a key role in the progression of Tau pathology, Tau hyperphosphorylation will be covered in more detail in a separate section.

Regarding acetylation, it was demonstrated that cysteine residues in the RD of Tau mediate self-acetylation of the protein (Cohen et al., 2013). This process, e.g. including acetylation at Lys^{280}, has mostly been associated with loss-of-function and exacerbation of the Tau pathology (Min et al., 2010; Cohen et al., 2011; Irwin et al., 2012). On the other hand, acetate removal via histone deacetylase 6 at Lys^{321} enhances Tau aggregation by revealing a disease-associated phosphorylation site at Ser^{324} (Carlomagno et al., 2017), although deacetylation of Tau at Lys^{174} by sirtuin 1 reduces Tau accumulation (Min et al., 2018). While the physiological role of acetylation is not well characterised, this post-translational modification might competitively regulate that of others, such as ubiquitination, SUMOylation, methylation and glycation (Alquezar et al., 2020).

Ubiquitination mediates the degradation of Tau. Carboxyl terminus of Hsc70-interacting protein-driven ubiquitination of Tau at Lys^{48} and Lys^{63}, in cooperation with the chaperone heat shock protein

70, was shown to induce the proteasomal and autophagy-induced elimination of native and hyperphosphorylated Tau (Petrucelli et al., 2004; Shimura et al., 2004; Zhang et al., 2008; Tan et al., 2008). By contrast, Otub1 may deubiquitinate Lys^{48} and prevents clearance of Tau, if overexpressed (Wang et al., 2017a). Notably, insoluble Tau aggregates are hyperubiquitinylated and the pathologic significance of this event it is yet unknown (Alquezar et al., 2020).

Preferentially non-microtubule-bound Tau can be SUMOylated by small ubiquitin-like modifiers (SUMOs) at Lys340 in the RD, which was demonstrated to decrease Tau degradation (Luo et al., 2014; Dorval and Fraser, 2006). This post-translational modification is still incompletely understood, but was hypothesised to compete with ubiquitination to navigate Tau clearance (Alquezar et al., 2020).

Methylation at multiple sites has been shown for mouse Tau in wild-type and hAPP mice *in vivo* (at Arg^{126}, Arg^{155} and Arg^{349}) (Morris et al., 2015) and Tau derived from the brain of both healthy individuals and AD patients (Thomas et al., 2012; Huseby et al., 2019). If not excessive, methylation does not seem to affect microtubule-binding (tubulin polymerisation), but was shown to reduce aggregation of recombinant 2N4R Tau induced with thiazine red (Funk et al., 2014). Since aging and disease progression were both suggested to promote Tau methylation (Alquezar et al., 2020), this modification might be a compensatory and protective mechanism. Clearly, further studies are necessary to investigate the impact of Tau methylation.

N-glycosylation appears to be specific for pathologic Tau derived from the brains of AD patients (Wang et al., 1996a; Sato et al., 2001; Liu et al., 2002), whereas O-GlcNAcylated Tau was shown to be less common in AD relative to controls (Liu et al., 2004a; Robertson et al., 2004). The former modification is incompletely understood. N-glycosylation occurs within the ER and Golgi, where Tau is usually not present, indicating that it likely does not have a physiological role (Kizuka et al., 2017). However, it has been speculated that N-glycosylation could promote Tau phosphorylation or lower its' effect on microtubule polymerisation. On the other hand, O-GlcNAcylation of intracellular

proteins is reciprocally regulated by the cytoplasmic enzymes O-GlcNAc transferase and O-GlcNAcase (Yang and Qian, 2017). Tau O-GlcNAcylation, for example identified at Thr^{123}, Ser^{208}, Ser^{400} and between $Ser^{409-413}$, (Yuzwa et al., 2011; Yuzwa et al., 2012), was shown to counteract Tau phosphorylation at neighbouring sites, suggesting that this post-translational modification exerts a protective function (Liu et al., 2004a; Lefebvre et al., 2003; Smet-Nocca et al., 2011). Indeed, O-GlcNAcylation seems to improve the solubility of Tau and prevent Tau aggregation, also *in vivo*. (Yuzwa et al., 2012; Yuzwa et al., 2014). Notably, there is also a non-enzymatic variant known as glycation, which describes the spontaneous modification of Tau by sugar or metabolites thereof (Alquezar et al., 2020). This represents a predominantly pathologic process that has been linked to increased Tau aggregation and PHFs (Ko et al., 1999; Ledesma et al., 1996).

Additionally, Tau may be protonated, oxidated or nitrated, and further research is necessary to determine the impact of these post-translational modifications on Tau (Alquezar et al., 2020).

1.2.4. Hyperphosphorylation of Tau

At the time when fibrillated Tau was first characterised, it was noticed that dephosphorylation of brain tissue derived from AD patients improved recognition of NFTs by monoclonal antibodies raised against non-phosphorylated Tau (Wood et al., 1986). Therefore, it was concluded that aggregated Tau is abnormally phosphorylated in AD (Grundke-Iqbal et al., 1986; Kopke et al., 1993; Wood et al., 1986). Subsequent studies confirmed that levels of phospho-Tau are elevated in brain homogenates and tissue of AD patients (Khatoon et al., 1992; Khatoon et al., 1994). Indeed, phospho-Tau pools were 3 - 4-fold higher in AD compared to control brains, with as much as 40 % of total Tau being hyperphosphorylated in AD patients (Kopke et al., 1993). In this context, it is likely that disproportionate Tau phosphorylation by kinases and reduced dephosphorylation by phosphatases drive Tau pathology (Kolarova et al., 2012). Full-length 2N4R Tau contains 85 theoretical

phosphorylation sites, of which up to 45 are deemed to be pathologically relevant (Figure 1.7) (Mandelkow et al., 2007; Wang and Liu, 2008; Hanger et al., 2009).

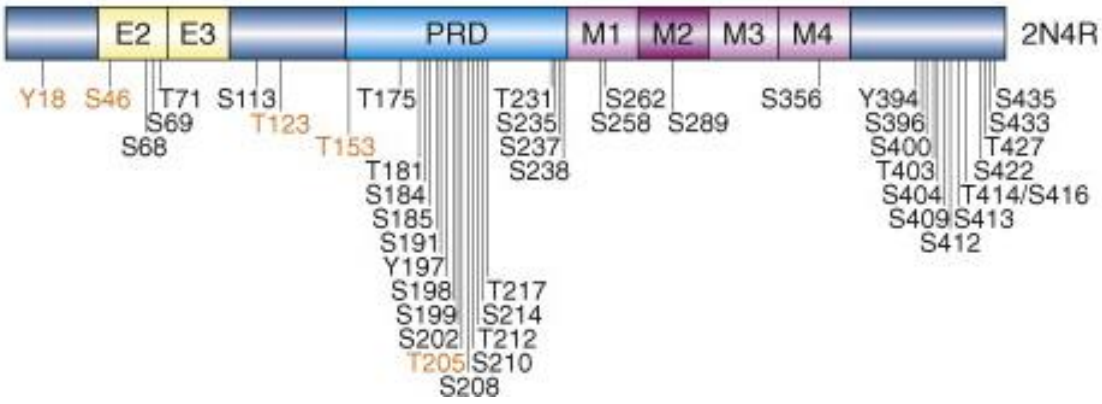

Figure 1.7: Pathology-implicated phosphorylation sites in 2N4R Tau. The majority of phosphorylated sites are in the proline-rich domain (PRD) and C-terminal region of Tau, but not in the microtubule-associating RD of Tau (M1 - M4). Orange text denotes sites detected through antibodies, whereas the remaining sites were determined via mass spectrometry or Edman degradation. Taken from Hanger et al. (2009).

Two main classes of Tau kinases have been identified, comprising the proline-directed protein kinases, glycogen synthase kinase 3ß (GSK-3ß), cell division cycle 2 kinase, cyclin-dependent kinase 2 (cdk2), cdk5 and extracellular signal-regulated kinase 1/2 ($ERK_{1/2}$), as well as the non-proline-directed protein kinases, encompassing protein kinase A (PKA), PKC, MAP-microtubule affinity regulating kinase, P70S6K, calcium- and calmodulin-dependent protein kinase II (CaMKII), brain-specific kinase (BRSK), and casein kinase I plus casein kinase II (Kopeikina et al., 2012; Wang and Liu, 2008; Timm et al., 2008). A list of individual Tau residues modified by GSK-3ß, cdk5 and other Tau kinases is given in (Hanger et al., 2009), but, importantly, the interplay of kinases is considered to be critical. For instance, whilst it was discovered that GSK-3β phosphorylated the most residues in Tau, only the combination of several kinases was able to recreate the phosphorylation pattern seen in AD (Wang et al., 2007a). The detrimental role of GSK-3ß in AD is well established and a GSK-3β-based hypothesis of neurodegeneration has been proposed (Hooper et al., 2008).

Kinase-mediated phosphorylation is counterbalanced by several serine/threonine protein phosphatases (PP), including PP-1, PP-2A, PP-2B and PP-5 (Kopeikina et al., 2012; Wang and Liu, 2008). Of the PPs, PP-2A, the most efficient enzyme, and PP-1 predominantly control Tau dephosphorylation (Wang et al., 1996b). Interestingly, a significant reduction in PP-2A, but not PP-1, activity was observed in white and grey matter of AD patients, indicating a reduced neuronal phosphatase ability to deal with the Tau hyperphosphorylation (Gong et al., 1993).

Once initiated, Tau phosphorylation appears to attract further kinases, encouraging hyperphosphorylation (Zhang et al., 2006b). For example, initial phosphorylation with PKA renders Tau a better substrate for GSK-3ß (Liu et al., 2004b). Hyperphosphorylated Tau is incapable of associating with microtubules and dephosphorylation is needed for Tau to regain its physiological properties (Alonso et al., 1994). In short, an increase in kinase and concomitant lessening in phosphatase activity likely invoke Tau hyperphosphorylation, resulting in the detachment of native Tau from microtubules and the breakdown of the microtubular and axonal cytoskeletal networks. Nevertheless, the role of hyperphosphorylation is incompletely understood, as phosphorylation at specific sites has been proposed to be protective against Tau pathology (Wang and Liu, 2008).

1.2.5. The process of Tau aggregation

The phenomenon of Tau hyperphosphorylation is thought to initiate the pathological aggregation of Tau (Kolarova et al., 2012). Hyperphosphorylation enhances the hydrophilicity of Tau and elicits its detachment from microtubules (Alquezar et al., 2020). Adding anionic phospho-groups to Tau in the PRD and RD, in particular at Ser^{214}, Thr^{231}, Ser^{235} and Ser^{262} (Figure 1.7), neutralises the intrinsic positive charge of the protein, thus lowering its affinity towards negatively charged microtubules (Carroll et al., 2021; Alquezar et al., 2020).

Wild-type (WT) Tau actually aggregates poorly, but self-association may be artificially enhanced, for example by adding polyanionic sulfoglycosaminoglycans (heparin) or arachidonic acid (Arrasate et

al., 1999; Wilson and Binder, 1997). However, Tau hyperphosphorylation induces structural re-arrangements in the protein. This new conformation, known as "Alz50", is structurally relaxed, more prone to aggregation and features the interaction of the N-terminal tail with the RD (R3 area) (Guillozet-Bongaarts et al., 2005; Kim et al., 2012). Once ALz50 Tau monomers have assembled into ß sheet-positive, yet still soluble, polymers, C-terminal truncation by cellular proteases produces a confirmation termed "Tau-66" (Figure 1.8A) (Guillozet-Bongaarts et al., 2005). In particular, the carboxy-terminal truncation of Tau at position Asp^{421} and then Glu^{391} (Figure 1.4C) was shown to augment amyloid nucleation and lower the critical Tau monomer concentrations necessary to generate insoluble Tau aggregates (Yin and Kuret, 2006). A recent study confirmed that the removal of the initial 150 N-terminal and last 50 C-terminal amino acids of full-length Tau, likely via steric barrier elimination, encourages the phosphorylation and aggregation of the protein (Gu et al., 2020).

Collectively, hyperphosphorylation-mediated accumulation of Tau in the cytosol, changes in folding and loss of repellent positive charge in the RD enable the self-association of Tau (Guillozet-Bongaarts et al., 2005; Berriman et al., 2003; Kolarova et al., 2012). Importantly, Tau aggregation is dependent on two ß sheet-containing motifs in the RD, including ^{306}VQIVYK^{311} (exon 11, also referred to as PHF6*) within R3 and ^{275}VQIINK^{280} (exon 10, known as PHF6) in the inter-repeat of R2 (Figure 1.4C) (von Bergen et al., 2001; von Bergen et al., 2000; Mamsa and Meloni, 2021). Because the RNA region encoding the ^{275}VQIINK^{280}-containing R2 area (exon 10) is subject to alternative splicing, ^{275}VQIINK^{280} is not present in 3R Tau isoforms (Figure 1.4B) (De Anda-Hernández et al., 2012). Studies have suggested that the ^{275}VQIINK^{280} and ^{306}VQIVYK^{311} motifs work in concert to promote the oligomerisation of 4R Tau isoforms, whilst oligomerisation of 3R Tau is exclusively mediated by ^{306}VQIVYK^{311} (von Bergen et al., 2001; von Bergen et al., 2000).

Ultimately, truncated and soluble Tau polymers mislocalise from the axonal to somatodendritic compartments in neurons, where they sequentially interact to form insoluble Tau filaments and NFTs (Kopeikina et al., 2012). Visually, Tau filaments isolated from the brains of AD patients may adopt a twisted conformation in the form of PHFs or appear as SFs (Figure 1.8B). Moreover, hybrid

species that transition from one Tau filament architecture to the other have been detected (Crowther, 1991b). Immunohistochemical labelling of post-mortem brain tissue of AD patients with antibodies revealed that insoluble Tau inclusions accrue within the neuronal body, in axons (denoted as neuropil threads) and as part of dystrophic neurites in close proximity to extracellular Aβ plaques (Figure 1.8C) (Iqbal et al., 1989).

Notably, over 50 mutations in the *MAPT* gene have been identified to date (Strang et al., 2019). Usually point mutations, some of these may encourage the development of selected Tauopathies, but not AD, by rendering Tau a more favourable kinase substrate, altering the native protein structure, decreasing microtubule affinity and/or facilitating aggregation (Alonso Adel et al., 2004; Strang et al., 2019).

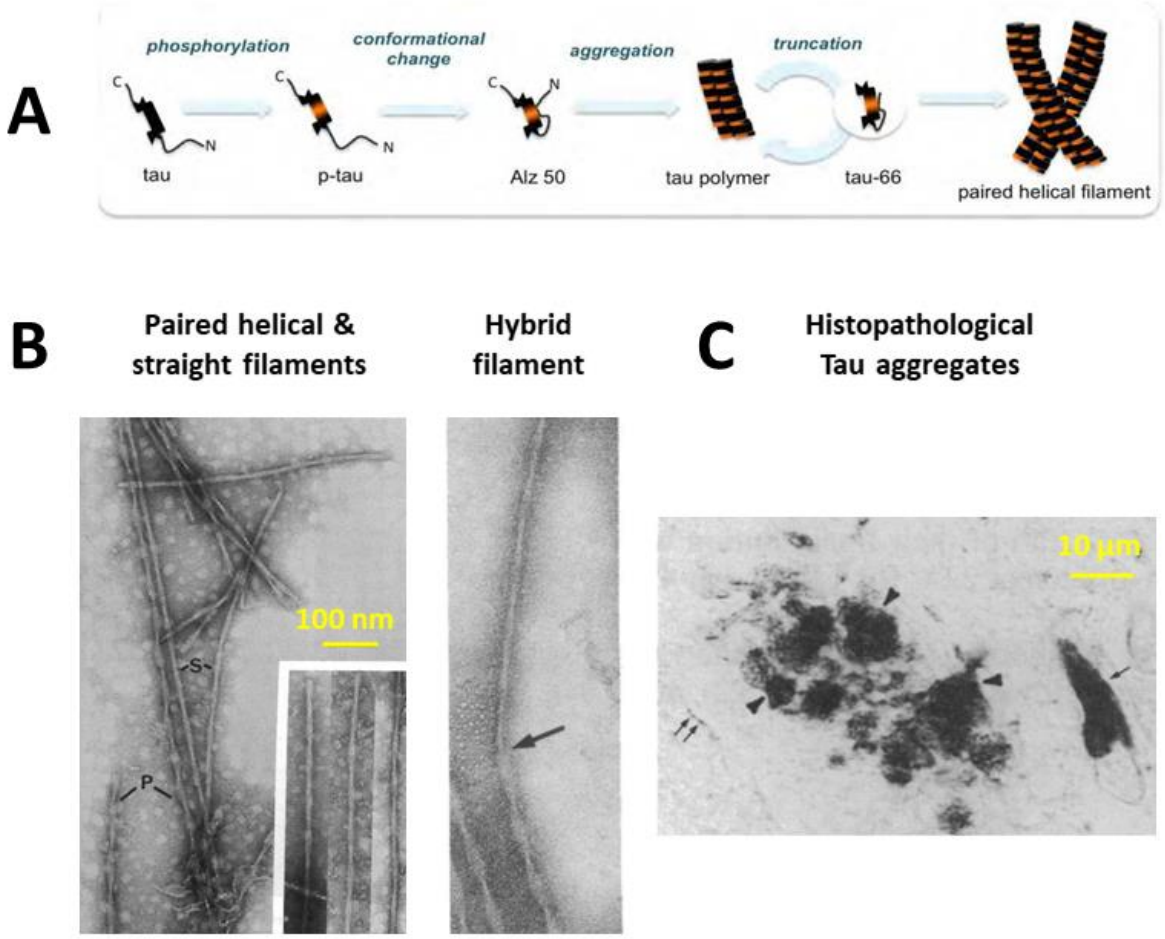

Figure 1.8: The process of Tau aggregation into insoluble Tau filaments and NFTs. (A) Initiated by hyperphosphorylation, Tau undergoes a series of modifications and conformational alterations that encourage self-aggregation into soluble polymers, insoluble Tau filaments and NFTs. (B) Electron microscope images of twisted PHFs (P) and SFs (S). Hybrid Tau filaments show characteristics of both twisted and straight filaments. The arrow marks the transitioning point between both architectures. (C) Histopathological manifestations of insoluble Tau fibrils in post-mortem brain tissue derived from and AD brain. Depicted are Tau inclusions within the neuronal body (single arrow), fine neuropil threads in the neuronal axon (double arrow) and dystrophic neurites that associate with Aβ-composed senile plaques (arrowheads). Adapted from Kim et al. (2012), Iqbal et al. (1989) and Crowther (1991a).

1.2.6. Tau propagation

It is well established that misfolded Tau may act as a seed, stimulating Tau aggregation in a prion-like manner throughout the CNS (Goedert et al., 2017). Almost three decades ago, it was demonstrated that AD-derived hyperphosphorylated Tau sequesters soluble Tau as well as MAP1(A/B) and MAP2,

thus destroying microtubules (Alonso et al., 1996; Iqbal et al., 2008). In 2009, a pioneering study by (Frost et al., 2009) demonstrated that the addition of extracellular aggregated, but not monomeric, Tau into the medium of human embryonic kidney 293 (HEK293) cells resulted in their internalisation and subsequent interruption of Tau-tubulin interactions and promoted fibrillization of native 2N4R Tau overexpressed by the same cells. This seed-like function of pathologic Tau was subsequently confirmed *in vivo* (Clavaguera et al., 2009). The authors demonstrated that cerebral injection of brain extract derived from NFT-forming Tau (P301S)-transgenic mice or human Tauopathy patients into 2N4R Tau-expressing ALZ17 mice induced local Tau aggregation that spread into brain regions adjacent to the administration site (Clavaguera et al., 2009; Clavaguera et al., 2013).

Multiple i*n vitro* studies have demonstrated that overexpressed or oligomeric Tau and PHFs are released by cells, then internalised by proximate cells to invoke the oligomerisation of soluble and/or microtubule-associated Tau into insoluble inclusions (Kfoury et al., 2012; Simon et al., 2012; Santa-Maria et al., 2012; Sanders et al., 2014). However, it must be noted that all six endogenously expressed Tau isoforms are actively packaged into secretory vesicles (exosomes) and are constantly released into the extracellular space, even in the absence of Tau pathology (Karch et al., 2012). There is also no evidence that cell death induces the release of Tau species and transcellular Tau propagation (De La-Rocque et al., 2021). Endocytosed Tau may also accumulate in endosomes/lysosomes, forming proteolytically-resistant seeds (Michel et al., 2014). Cell culture studies suggests that, once triggered, Tau propagation may become permanent (Sanders et al., 2014). Conversely, the sequestration of extracellular Tau species with monoclonal antibodies has been shown to halt the transcellular spread of misfolded Tau (Kfoury et al., 2012), further rescuing cognitive deficits when cerebrally infused into a mouse model exhibiting Tau propagation (Yanamandra et al., 2013).

It is not entirely clear what initiates the Tau pathology. While Aβ contributes to the misfolding of Tau, predominantly by stimulating pro-inflammatory cytokine production and subsequent activation of Tau-hyperphosphorylating kinases in neurons, other factors might play a leading role (Roda et al.,

2022). Notably, initial purification studies identified that proteins other than Tau were sequestered into PHFs, such as mitochondrial effectors (i.e. the energy-producing ATP-synthase, also known as complex 5) or lipofuscin. The authors postulated that the age-associated dysfunction in cellular autophagy, proteasomal removal or other clearance mechanisms (summarised in Xin et al. (2018)) led to the cytosolic amassment of the aforementioned waste proteins that serve as substrates to trigger Tau aggregation (Wischik et al., 2014). In addition, the impairment of these clearance mechanisms may also facilitate the accumulation of seeding-competent Tau oligomers in neurons (Wischik et al., 2014).

Three mechanisms are thought to drive the transcellular spread of Tau (Fig. 1.9). First, it has been proposed that soluble Tau monomers and small oligomers are internalised by CMA (Simic et al., 2016). Second, it has been shown that extracellularly applied Tau fibrils, as produced through the heparin-induced aggregation of synthetic Tau RD, interact with heparan sulfate proteoglycans on the cellular membrane to evoke macropinocytosis-mediated uptake (Holmes et al., 2013). Third, hyperphosphorylated Tau is transmitted across synapses within exosomes between anatomically connected neurons (Wang et al., 2017b; Saman et al., 2012). Such exosomes, containing seeding-competent monomeric and oligomeric Tau species, have also been detected in the CSF of AD patients (Saman et al., 2012). Various studies suggest that Tau oligomers are internalised and propagate more effectively than Tau monomers, whilst larger Tau fibrils do not propagate effectively (Frost et al., 2009; Wu et al., 2013; Takeda et al., 2015). Oligomeric Tau composed of at least 3 degradation-resistant Tau RDs (R1-4) was shown to be the smallest seeding-competent Tau species (Mirbaha et al., 2015). PET-tracing of Tau in AD patients, combined with computational modelling, recently suggested that up to 70 % of the Tau spreading pattern throughout the CNS is predictable and explained by trafficking of Tau seeds across connected neurons (Vogel et al., 2021). As such, Tau therapeutics must be capable of intercepting the transcellular propagation of Tau.

Interestingly, microglia have a key role in Tau propagation. Generally, both microglia (Brelstaff et al., 2018) and astrocytes (Martini-Stoica et al., 2018) contribute to the clearance of extracellular Tau

species, while microglia also eliminate Tau inclusion-containing neurons. However, the microglia-induced phagocytosis of Tau-burdened neurons and hyperphosphorylated Tau aggregates result in the exosome-driven secretion of additional Tau seeds, with their uptake by nearby neurons further promoting Tau propagation *in vivo* (Asai et al., 2015). Interestingly, inflammatory stimulation of microglia with LPS aggravated Tau exocytosis, whereas the drug-mediated suppression of ionized calcium binding adaptor molecule 1 (IBA1)-immunoreactive microglia (or exosome formation) prevented Tau pathology in the brains of Tau (P301S)-transgenic PS19 mice (Asai et al., 2015). Specifically, the elevated release of phagocytosed Tau aggregates by microglia and subsequent Tau propagation in neurons throughout the CNS of PS19 mice were shown to be dependent on the induction of the pro-inflammatory transcription factor tumour necrosis factor α (TNF-α) in microglia (Wang et al., 2022). These findings support the suggestion that microglial activation and pro-inflammatory cytokine production drive pathology-associated Tau propagation.

In addition to neurons, oligodendrocytes endogenously express Tau (Ksiezak-Reding et al., 2003). An animal model with selective Tau knockdown in neurons showed that Tau propagated in oligodendrocytes across the white matter, in a manner independent of neuronal axons, instigating the death of these glial cells (Narasimhan et al., 2020; Zareba-Paslawska et al., 2020). This separate Tau pathology in oligodendrocytes not only interfered with the oligodendrocyte-mediated myelination of neuronal axons, which is critical for axonal integrity and function, but also fostered neurodegeneration *in vivo* (Higuchi et al., 2005).

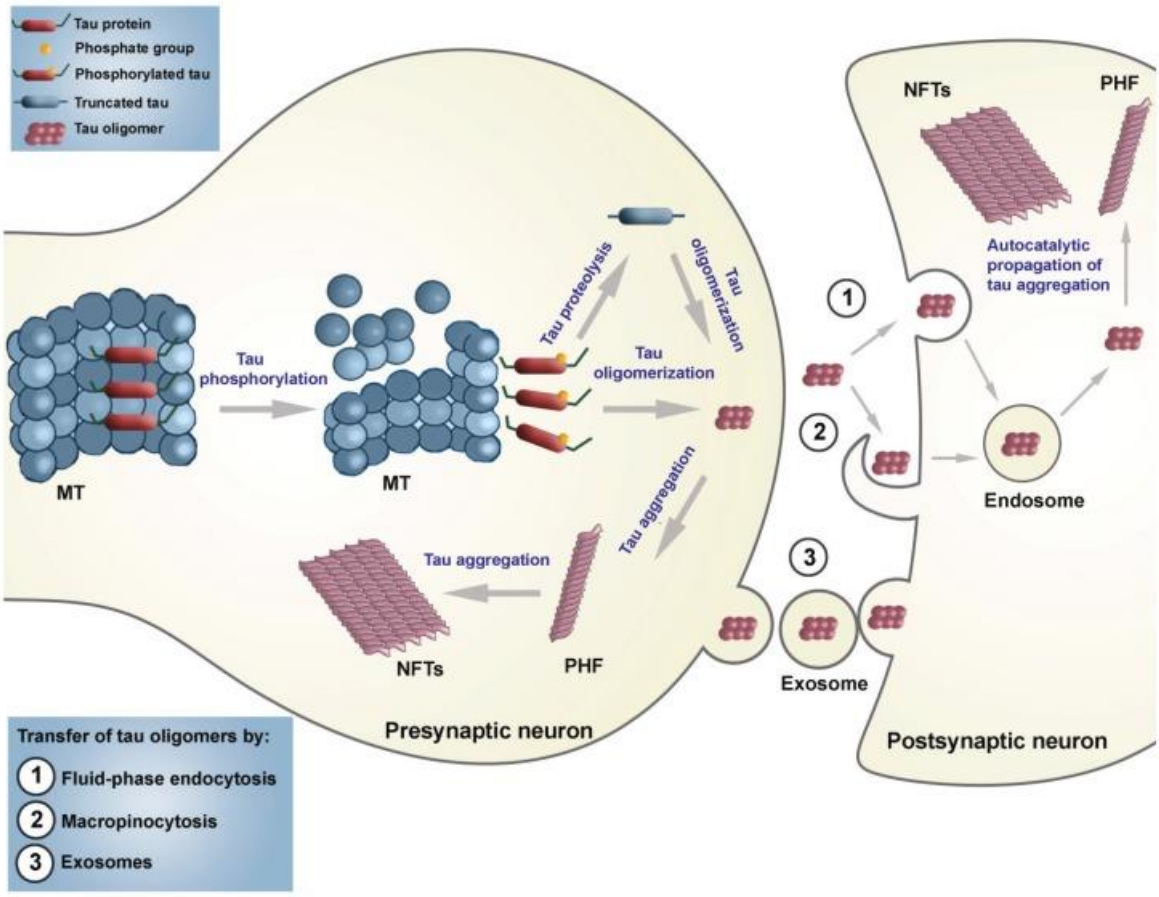

Figure 1.9: Transneuronal Tau propagation in AD and Tauopathies. Pathology-associated hyperphosphorylation evoke the detachment of Tau from microtubules and promote polypeptide misfolding. Tau truncation by cellular proteases leads to the formation of a degradation-resistant RD fragment. These fragments self-oligomerise to create a propagation-competent Tau seed that consists of at least three truncated Tau RDs. Tau seeds may sequester microtubule-bound native Tau into PHFs/SFs and NFTs or traffic between anatomically connected neurons by three means, including (1) fluid-phase endocytosis, (2) macropinocytosis and (3) exosome-mediated delivery across synapses. Taken from Simic et al. (2016).

The structural core of Tau filaments consists of either a 10 or 12 kDa-long pronase-resistant fragment of about 100 amino acids in length, derived from the RD (amino acids 244 - 368) of Tau (Figure 1.10A) (Wischik et al., 1996; Wischik et al., 1988). The 12 kDa fragment (Ile^{297}-Ala^{390} of Tau), when immobilised on a solid matrix, captured aqueous full-length Tau and induced its misfolding (Figure 1.10B) (Wischik et al., 1996). Digestion of the N-terminal fuzzy coat of captured Tau via the addition of proteases enabled the binding of further Tau monomers to the solid phase. This

established an auto-catalytic and self-propagating binding/digestion cycle that potentially drives the assembly of Tau into insoluble fibrils consisting of truncated RD fragments (Wischik et al., 1996; Wischik et al., 2018). Indeed, Wischik and colleagues showed that the co-expression of small amounts of the 12 kDa Tau fragment with 2N4R Tau induced the highly toxic propagation of Tau in fibroblasts (Harrington et al., 2015). Similarly, a transgenic mouse line overexpressing the 12 kDa fragment ($Tau_{296-390}$) showed severe Tau pathology in the hippocampus and entorhinal cortex as well as memory deficits from an early age of three months, supporting a key pathological role for this Tau fragment (Melis et al., 2015).

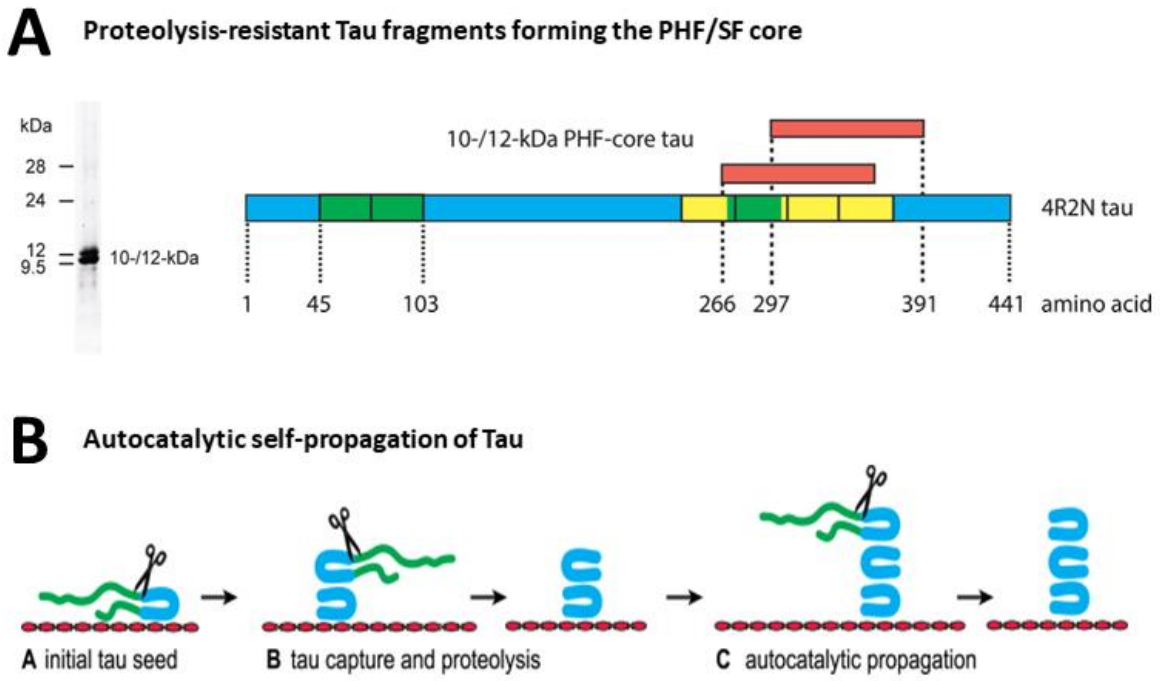

Figure 1.10: Characteristics of Tau seeds and pathologic self-propagation. (A) Degradation-resistant and seeding-competent Tau fragments that form the core of Tau filaments. Proteolysis of regions flanking the RD of Tau (yellow) by cellular proteases generates a fragment of 10 kDa or 12 kDa in size (red bars). Which Tau fragment is produced depends on alternative splicing and the inclusion or exclusion of R2 (green) in 4R Tau or 3R Tau isoforms, respectively. The truncated 10 - 12 kDa fragments of Tau misfold into a pathology-associated protofilament structure. Two protofilaments subsequently interact to form a Tau protofilament core that further sequestrates into PHF/SFs. (B) Truncation-induced Tau propagation. Tau aggregation and the self-induced (prion-like) assembly into fibrils can be stimulated by primase digestion *in vitro*. In this viscous cycle, full-length native Tau is bound with high affinity by truncated Tau RD fragments, which induces misfolding of the RD in native Tau. Proteolytic digestion of the captured native Tau then initiates an autocatalytic and self-propagating binding/digestion cycle. Adapted from Wischik et al. (2018).

Notably, the predominant spreading Tau isoform, either 3R or 4R Tau, differs between Tauopathies (Strang et al., 2019; Boyarko and Hook, 2021). AD and FTDP-17 show a balanced ratio of 3R and 4R Tau isoforms that aggregate, accrue and propagate across the brain. In contrast, PSP and CBD are 4R Tau-dominant, whereas PiD exhibits almost exclusive propagation of 3R Tau inclusions (Strang et al., 2019; Boyarko and Hook, 2021). Of over 50 known *MAPT* point mutations, one third directly affect alternative splicing and the inclusion of exon 10, thus skewing the ratio of 3R versus 4R Tau isoforms (Strang et al., 2019; Niblock and Gallo, 2012).

Particularly relevant in the context of the current dissertation, both the P301L and P301S mutations in R2/Exon 10 favour the generation of 4R Tau inclusions (Strang et al., 2019). However, unlike e.g. the N279K, L284L, N296/H/N or S305N/S mutations that promote the inclusion of exon 10, the P301L/P301S mutations are unique because they promote the formation of 4R Tau aggregates without altering the splicing of Exon 10 (Andreadis, 2012; Strang et al., 2019).

Tau isoform ratios also play a pathological role. For example, a study used mRNA-binding and Tau isoform-switching antisense oligonucleotides to upregulate the ratio of 4R/3R Tau in hTau mice (Schoch et al., 2016), which were previously bred to exclusively express human Tau isoforms (predominantly 3R Tau) (Andorfer et al., 2003). Upregulation of the 4R/3R Tau ratio in these mice, without changing total Tau levels, aggravated Tau phosphorylation and oligomerisation, the occurrence of seizures and nesting deficits (Schoch et al., 2016). Concomitantly, the trans-splicing-mediated increase in 4R Tau, in order to normalise excessive 3R Tau production and lowered 4R/3R isoform ratios, rescued the accumulation of hyperphosphorylated and insoluble Tau in the prefrontal cortex, rescued neuronal firing and improved novel object recognition memory in hTau mice (Espindola et al., 2018). Given the typical 1:1 ratio of 3R and 4R Tau isoforms in the brain (Andreadis, 2005; Gasparini et al., 2007), along with the fact that both alterations of this isoform ratio are neurotoxic (Schoch et al., 2016; Espindola et al., 2018), it has been suggested Tau isoform imbalance might drive the cerebral pathology in some Tauopathies (Andreadis, 2012). As indicated earlier, disharmonious 3R to 4R Tau isoform ratios do not seem to play a role in AD, however, as both 3R and 4R Tau-containing inclusions are formed in equal amounts (Strang et al., 2019; Boyarko and Hook, 2021).

In relation to Tau propagation in AD, Braak and Braak (1991) mapped histopathological spread and disease severity in a 6-stage system, with deposition of Tau fibrils commencing at stage II. In a series of events, Tau characteristically spreads from transentorhinal layer pre-alpha (phase I) to the CA1 region of the hippocampus (phase II) and limbic regions (phase III - IV), which includes the entirety of the hippocampus, the basolateral amygdala and nuclei of the thalamus, finally reaching the isocortex

(phase V - VI). Transition between stages is thought to require approximately ten years (Wischik et al., 2014; Braak and Braak, 1991; Markesbery, 1997). In agreement with the scaling system, it has repeatedly been demonstrated that cognitive decline correlates well with Braak staging (Bancher et al., 1996; Grober et al., 1999; Duyckaerts et al., 1997; Geddes et al., 1996). Specifically, AD patients have been shown to exhibit mild mental impairments at stage III (especially once the hippocampus, the centre of long-term memory formation, is affected), transitioning to severe cognitive deficits in phase V.

1.2.7. Mechanisms of Tau toxicity

It is arguable as to which Tau species drives neurodegeneration and, as proposed by Kopeikina et al. (2012), there are three major views in the literature. The first is that insoluble NFTs are the key species driving neurodegeneration and cognitive impairment. The second argues that hyperphosphorylated forms of Tau that abnormally accumulate in cell compartments other than axons, including both Tau monomers and oligomers, are the main toxic entity, whereas their sequestration into NFTs is a protective mechanism. The most likely, third view is that soluble Tau monomers and oligomers and insoluble PHFs/SFs and NFTs are all detrimental through different pathological mechanisms and at different stages of the disease. The current consensus is that excessive post-translational modifications, Tau missorting and conformational changes in the Tau protein structure are all key pathological events (Kopeikina et al., 2012).

Indeed, various studies suggest that propagation-inducing, soluble species of Tau, including truncated, hyperphosphorylated or oligomeric Tau, are more cyto- and synaptotoxic than native Tau monomers or larger fibrils (Alonso Adel et al., 2006; de Calignon et al., 2010; Guerrero-Munoz et al., 2015). Soluble Tau species might be more detrimental than other forms of Tau due to their ability to sequester native Tau, thus accelerating the destruction of microtubules (Simic et al., 2016). On the other hand, aggregation of hyperphosphorylated or oligomeric Tau into insoluble inclusions was

shown to be a protective mechanism that slowed Tau propagation and microtubule depolymerisation *in vitro* (Alonso Adel et al., 2006; Dubey et al., 2008), whilst suppressing neuronal death *in vivo* (de Calignon et al., 2009; de Calignon et al., 2010). However, in favour of the aforementioned third view, the accumulation of degradation-resistant, mature NFTs in the cytoplasm may eventually become toxic, for example via the physical interference of NFTs with basic cellular and transportation processes (Kopeikina et al., 2012). It has been suggested that accumulating Tau oligomers invoke memory deficits and neuronal atrophy in the early stages of AD, whilst NFTs might become toxic in more advanced disease stages (Berger et al., 2007).

Tau toxicity manifests due to both loss-of-function and gain-of-toxicity. As implied earlier, Tau hyperphosphorylation induces a loss of microtubule binding affinity (Kolarova et al., 2012). This is further aggravated by the fact that propagation-competent Tau oligomers are capable of sequestering microtubule-associating Tau into insoluble inclusions (Wischik et al., 2018). Loss of Tau results in destruction of microtubules in neuronal processes and impedes intracellular transport by the microtubule-utilising motor proteins kinesin and dynein (Kopeikina et al., 2012; Stamer et al., 2002). Notably, Tau was shown to maintain labile, but not stable, microtubule domains, questioning how the loss of Tau leads to microtubule loss in AD (Qiang et al., 2018). Potential reasons have been debated, including that Tau-lacking axonal microtubules might become more prone to severing by katanin and that pathologic Tau could trigger excessive polyglutamation of dendritic microtubules and concomitant spastin activation (Baas et al., 2016). Inverse to expectations, microtubules could, in fact, be overstabilised due to binding of MAPs etc to Tau-depleted labile domains. Moreover, it was suggested that other toxic effects of aggregated Tau species may indirectly damage microtubules, e.g. the Tau-induced activation of kinases that modify microtubule-stabilising proteins or sequestration of these by Tau seeds.

On the other hand, ample evidence suggests that Tau directly deregulates motor protein activity. Tau showed a ten-fold higher binding affinity to kinesin, as compared to dynein (Dixit et al., 2008). In agreement with this difference in binding strength, overexpression of 3R, 4R or full-length 2N4R Tau

selectively inhibited kinesin-associated anterograde transport towards distal axons in cultured cells (Dixit et al., 2008; Dubey et al., 2008; Stamer et al., 2002; Stoothoff et al., 2009; Thies and Mandelkow, 2007). Because the RD of Tau was sufficient to impede kinesin motor activity, it was proposed that binding of accumulating Tau to microtubules physically blocks kinesin-mediated transport (Dixit et al., 2008). Another hypothesis was that Tau acts as a cargo for kinesin, thus displacing other cargo (Dubey et al., 2008). Besides native Tau, hyperphosphorylated Tau was shown to trap c-Jun N-terminal kinase-interacting protein 1, a protein linking cargo to the kinesin motor protein complex, in the cytoplasm, as observed in primary neuronal cells, *in vivo* and in the brains of AD patients (Ittner et al., 2009). GSK-3β-phosphorylated Tau was shown to have a greater binding affinity to kinesin than native Tau, suggesting that abnormally phosphorylated Tau may compete with other kinesin-associated cargo in AD (Cuchillo-Ibanez et al., 2008). Further studies showed that increased exposure of the phosphatase-activating domain (amino acids 2 - 18 of Tau) in fibrillated and insoluble, but not soluble, Tau species blocked kinesin-driven fast axonal transport by activating PP-1 and GSK-3β (Kanaan et al., 2011; LaPointe et al., 2009). Thus, the pathologic accumulation of native, hyperphosphorylated and aggregated insoluble (PHF) Tau all interfere with the activity of kinesin.

Negative consequences of Tau-impaired anterograde transport by kinesin were morphological changes and decreased cellular proliferation (Ebneth et al., 1998). Moreover, kinesin-associated cell organelle transport was interrupted, resulting in clustering of mitochondria in the perinuclear area and ER shrinkage (Ebneth et al., 1998). Lack of mitochondria in axonal compartments subsequently triggered local ATP deficits, synapse and spine degeneration and axonal retraction (Thies and Mandelkow, 2007; Dubey et al., 2008). Besides cell organelles, the intracellular trafficking of Golgi-originating vesicles, neurofilaments, APP and ROS-detoxifying peroxisomes was interrupted, leading to increased oxidative stress (Stamer et al., 2002). Finally, Tau mis-sorting from axons into cytosolic and dendritic regions was observed (Thies and Mandelkow, 2007). It has been suggested that accumulating, pathology-associated Tau species are delivered in retrograde direction to

somatodendritic compartments, where they can aggregate into NFTs in order to protect microtubule-associated transport (Kolarova et al., 2012). Collectively, the latter pathological events culminate in caspase-mediated neuronal apoptosis (Figure 1.11) (Kopeikina et al., 2012; de Calignon et al., 2010; Spires-Jones et al., 2008).

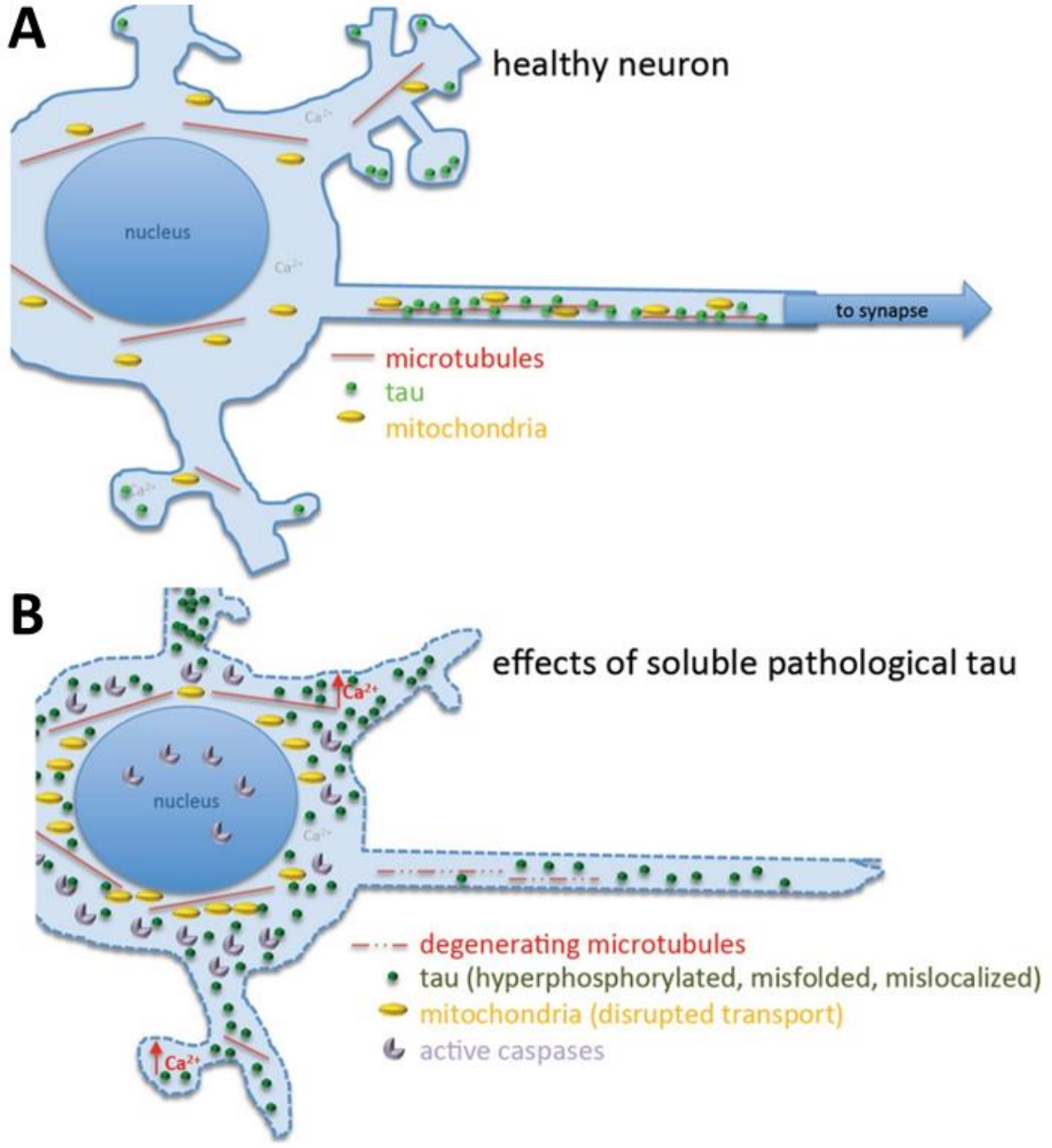

Figure 1.11: Detrimental consequences of Tau-induced microtubule transport defects in neurons. (A) In the healthy neuron, Tau stabilises the microtubule network and axonal integrity. Transport of cargo, such as Golgi-derived vesicles, across intact microtubules is mediated from the cellular body to synapses (anterograde) or in reverse direction (retrograde) via the motor proteins kinesin and

dynamin, respectively. Microtubule-associated transport further regulates the intracellular positioning of cell organelles, for example mitochondria. (B) Under pathologic conditions, hyperphosphorylation or sequestration by seeding-competent Tau species render Tau unable to associate with microtubules, promoting the disassembly of microtubules. Moreover, accumulating native, hyperphosphorylated or aggregated Tau inhibit kinesin-driven anterograde transport of cargo and cell organelles towards distal axons. This results in the axonal depletion of mitochondria, local ATP deficits, spine and axonal atrophy as well as synaptic dysfunction. Since the kinesin-mediated transport of peroxisomes is impaired, oxidative stress is enhanced. In an effort to rescue the occurring transport deficits, pathology-associated Tau species are missorted in retrograde direction from axonal to somatodendritic compartments, where Tau aggregates and insoluble Tau inclusions accumulate. Ultimately, elevated ROS levels and impaired mitochondrial energy production trigger caspase activation and cellular apoptosis. Taken from Kopeikina et al. (2012).

On the other hand, certain pathology-associated Tau species exert direct cytotoxic effects. Truncation of Tau by cellular proteases generates a multitude of fragments that exert various detrimental outcomes, including the stimulation of Tau phosphorylation or aggregation, synaptotoxic effects, mitochondrial dysfunction, oxidative stress, blockade of autophagy and lysosomal degradation, axonal injury and intracellular transport deficits (Boyarko and Hook, 2021).

Aggregated Tau also disrupts neuronal membranes (de Calignon et al., 2009), possibly via the oligomerisation of Tau into pore-forming annular protofibrils (APFs) (Lasagna-Reeves et al., 2014). In this context, NFT formation may limit the generation of APFs, suppressing membrane rupture, caspase activation and neuronal death (de Calignon et al., 2009; de Calignon et al., 2010).

Interestingly, a recent study found a positive correlation between NFT deposition and transposable element activation in the CNS of AD patients, which was confirmed in native or mutant Tau-overexpressing *Drosophila* models (Guo et al., 2018). Notably, retrotransposon activation may be harmful and is usually suppressed to prevent genomic rearrangements and insertional mutagenesis in cells (Levin and Moran, 2011). Brain aging impedes the regulation of transposable elements, however, leading to memory impairments, genome instability and neuronal atrophy (Li et al., 2013; Maxwell et al., 2011; Wood et al., 2016). Thus, the age-associated accumulation of pathologic Tau species may drive genomic instability and neuronal death during AD (Guo et al., 2018). In addition,

as compared to respective controls, Tau-based cell, mouse and fly models all showed elevated Ser^{139}-phosphorylated histone H2AX levels (Ser^{137}-phsophorylated H2Av in flies), which serve as a marker for DNA double strand breaks, whilst Tau-overexpressing *Drosophila* displayed an increase in single- and double-strand DNA breaks in comet tail assays (Khurana et al., 2012). This Tau-driven DNA damage and concomitant oxidative stress further resulted in heterochromatin loss in the CNS of Tauopathy mouse and fly models and AD patients (Frost et al., 2014). As a likely consequence of this Tau-induced chromatin damage, AD patients also exhibited an aberrant induction of usually heterochromatin-silenced genes in their brains (Frost et al., 2014). Furthermore, DNA lesions are increased in hippocampal neurons during AD (Adamec et al., 1999; Madabhushi et al., 2014), suggesting that the abnormal accumulation and deposition of Tau might contribute to AD through DNA damage.

The negative impact of Tau on cellular Ca^{2+} homeostasis is well documented. Overexpression of human Tau, which upregulated the transient receptor potential channel 1/store-operated Ca^{2+} entry pathway, induced Ca^{2+} influx, ER stress, the subsequent activation of the Tau kinases GSK-3β and CaMKI and inactivation of the Tau-dephosphorylating enzyme PP2A (Ye et al., 2020). In cultured neurons, Tau overexpression suppressed cAMP response element-binding protein (CREB) activity, a nuclear key transcription factor involved in memory formation and neuronal survival (Sharma and Singh, 2020), via the induction of the Ca^{2+}-sensing CREB-phosphatase calcineurin (Yin et al., 2016). There is also evidence that extracellular Tau, when dephosphorylated *in situ* by tissue-non-specific alkaline phosphatase, interacts with muscarinic M1/M3 receptors to trigger neurotoxic Ca^{2+} increases in SH-SY5Y cells (Diaz-Hernandez et al., 2010). Aggregated Tau was further shown to integrate into neuronal membranes, causing the opening of voltage-gated Ca^{2+} channels and nicotinamide adenine dinucleotide phosphate oxidase activation, thus enhancing oxidative stress (Esteras et al., 2021).

Pathologic Tau is also implicated in Ca^{2+}-mediated excitotoxicity resulting from excessive ionotropic receptor activation (especially NMDARs), leading to excessive cytosolic Ca^{2+} levels, mitochondrial

dysfunction and neuronal atrophy (Wang and Reddy, 2017; Esteras and Abramov, 2020). It should also be noted that Tau is required for Aβ-driven neuronal death (Ittner et al., 2010) and that Aβ monomers and oligomers stimulate synaptic NMDARs to induce NMDAR-dependent excitotoxicity (Texido et al., 2011; Ferreira et al., 2012). In this context, Tau recruits the NMDAR-phosphorylating protein Fyn and PSD-95 to the postsynaptic space, promoting aberrant glutamate- or Aβ-induced Ca^{2+}-influx through alpha-amino-3-hydroxy-5-methyl-4-isoxazolepropionic acid receptors (AMPARs) and NMDARs (Ittner et al., 2010). In addition, Tau phosphorylated at Tyr^{18} by Fyn and A152T-mutant Tau are sufficient to cause NR2-NMDAR-driven excitotoxicity (Miyamoto et al., 2017; Decker et al., 2016). As such, these studies suggest that Tau species that are missorted into dendritic synapses (Kopeikina et al., 2012; Thies and Mandelkow, 2007) might trigger excitotoxicity in concert with Aβ, glutamate, Fyn and PSD-95 (Ittner and Ittner, 2018).

In relation to a further potential toxic mechanism, Tau disturbs the tightly balanced fusion/fission dynamics in mitochondria (Cheng and Bai, 2018). Hyperphosphorylated Tau interacts with the mitochondrial fission protein dynamin-like protein 1 (Manczak and Reddy, 2012), whilst Asp^{421}-truncated Tau downregulates the levels of the fusion-mediator optic atrophy protein 1 (OPA1) (Perez et al., 2018), promoting mitochondrial fragmentation. In turn, the overexpression of full-length Tau in both HEK293 cells and primary hippocampal neurons elicited the expression of the fusion-triggering modulators OPA1, mitofusin 1 and 2, leading to decreased ATP generation, complex 1 activity and a loss of cell viability (Li et al., 2016). It has been proposed that Tau accumulation initially enhances mitochondrial fusion to protect from AD-associated hyperfission, whereas hyperphosphorylated or truncated Tau exacerbates fission at more advanced disease stages (Cheng and Bai, 2018).

Evidence also exists for a reciprocal relationship between Tau pathology and neuroinflammation. Even at low concentrations (0.5 μM), misfolded synthetic Tau has been shown to stimulate microglial immunoreactivity, inducing the transcription factors activator protein 1 and nuclear factor-kappa B (NF-κB) and promoting production of the inflammatory cytokines interleukin (IL)-1ß,

IL-6, and TNF-α, along with nitric oxide (NO) in microglial and astrocyte co-cultures (Kovac et al., 2011). Similarly, pro-inflammatory stimuli, such as LPS, mouse hepatitis virus, Aß or Tau oligomers, can evoke pro-inflammatory cytokine generation by glial cells that induce Tau kinase activation and hyperphosphorylation in neurons (reviewed in Barron et al. (2017)).

Moreover, the chronic activation of pro-inflammatory cytokine receptors on neurons induces a range of serine kinases, including c-jun N-terminal kinase-interacting protein 1 (JNK), IκB kinase β and protein kinase R, that phosphorylate and inactivate IRS-1, a component of the insulin-signalling pathway (Holscher, 2019; Akhtar and Sah, 2020). Thus, neuroinflammation is thought to trigger neuronal insulin resistance in AD and other neurodegenerative diseases. In turn, insulin resistance-associated loss of Akt-signalling results in GSK-3β hyperactivity and concomitant Tau hyperphosphorylation (Akhtar and Sah, 2020; Holscher, 2019; Reich and Holscher, 2020).

1.2.8. Pathology-associated structural changes in Tau and Tau peptide-interactions

Interestingly, Tau is a natively unstructured protein, exhibiting total α-helix and β sheet contents of <5% and <15 %, respectively (Schweers et al., 1994). Fluorescence resonance energy transfer (FRET) and electron paramagnetic resonance analysis of full-length 2N4R Tau suggests that the polypeptide adopts a 'paperclip'-like, yet weak and still highly flexible, tertiary conformation (Jeganathan et al., 2006). This conformation involves the folding of the C-terminus onto the RD, followed by the folding of the N-terminal tail over the C-terminal region (Figure 1.12A).

The aggregation pattern and structure of pathologic Tau have been characterised in AD. Generally, misfolding is induced via hyperphosphorylation, which adds negative charge. This neutralises intra-molecular charge differences in the Tau protein and results in a relaxed conformation that is more prone to self-association (Kolarova et al., 2012).

Tau aggregation is facilitated by the presence of the ^{275}VQIINK^{280} sequence (R2) and also requires the ^{306}VQIVYK^{311} (R3) motif (Falcon et al., 2015). Tau oligomerisation further involves disulfide bridge

formation between two cysteine residues in adjacent Tau monomers (Cys^{291} in R2 and Cys^{322} in R3) (Saito et al., 2021), but may also occur in a cysteine-independent fashion via electrostatic attraction between the cationic N-terminal region and anionic PRD/RD areas (Wang et al., 2021). Soluble and insoluble Tau species are structurally highly heterogenic, with only some Tau aggregates being propagation-competent or cytotoxic (Wang et al., 2021).

In AD, two misfolded Tau monomers initially generate a still soluble protofilament core, followed by their sequestration into either PHFs or SFs (Figure 1.8B) (Fitzpatrick et al., 2017). Tau filaments are composed of a detergent- and proteolysis-resistant core consisting of two identical, crosslinked protofilaments (Figure 1.12B&C). This protofilament core is also referred to as a 'Tau seed' that can stimulate the aggregation of native Tau (section 1.2.6). An individual protofilament comprises amino acids 306 - 378 of Tau, consisting of R3, R4 and 10 additional amino acids of the C-terminus. This protofilament core is flanked by an unstructured (and ultimately degraded) fuzzy coat, formed from the C- and N-termini of Tau (Figure 1.12B). Two protofilaments may associate in a symmetric or asymmetric manner with each other (Figure 1.12C), the nature of which determines their subsequent assembly into PHFs or SFs, respectively. Structurally, a single $Tau_{306-378}$ protofilament contains eight β sheet-positive regions (β1-8), with ~80 % of amino acid residues exhibiting a β-strand conformation. Driving the characteristic C-shaped architecture of protofilaments, hydrophobic groups of the ^{306}VQIVYK^{311} motif in β1 of $Tau_{306-378}$ interact with residues 374 - 378 in β8. This structure is further stabilised through polar zipper formation between β2 and β8 (Figure 1.12D) (Fitzpatrick et al., 2017).

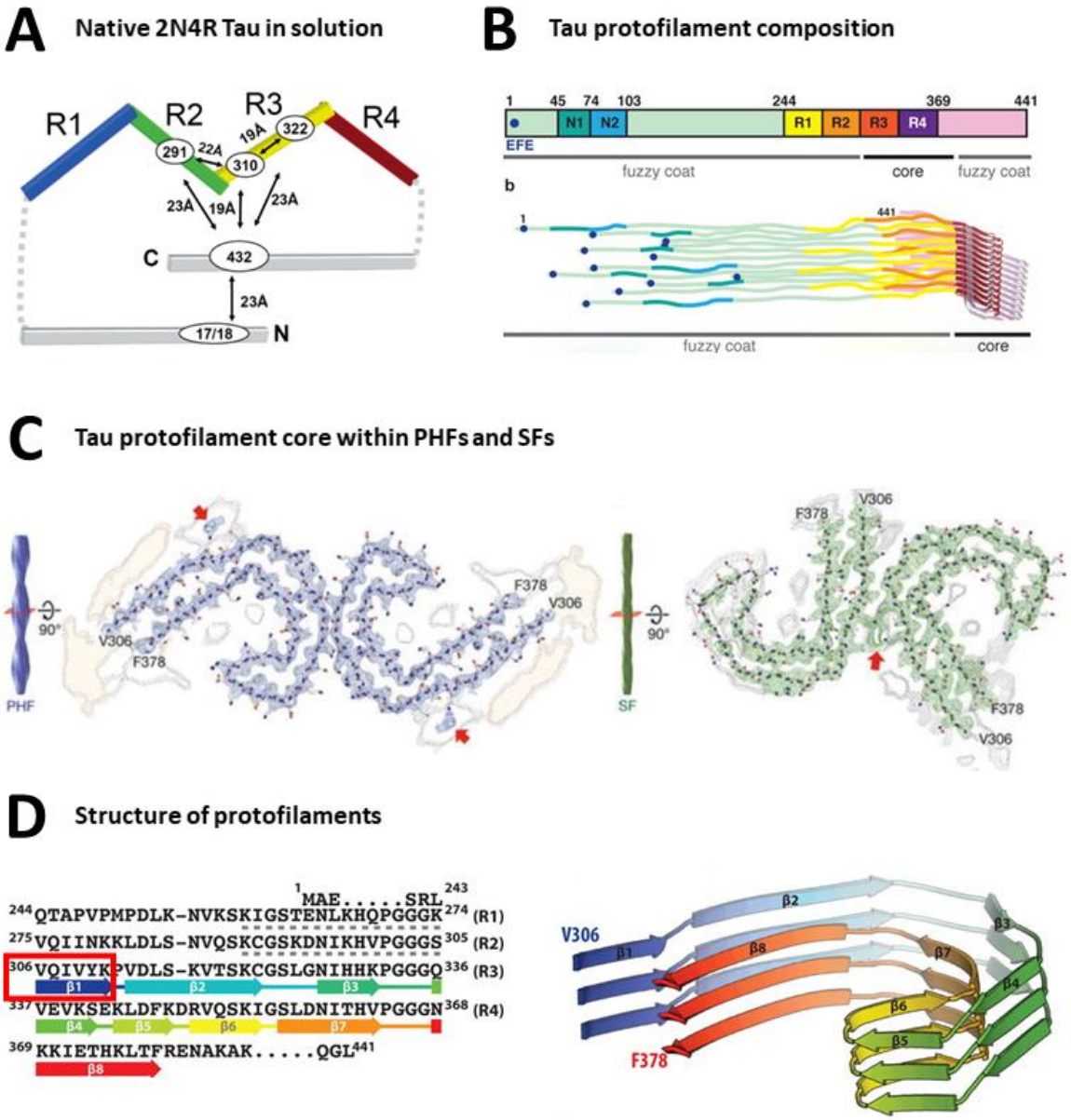

Figure 1.12: Native and pathology-associated protofilament structures of Tau in AD. (A) The conformation of native 2N4R Tau. Tau is a 'natively unfolded' and structurally dynamic protein. Nonetheless, structural studies suggest that Tau adopts a 'paperclip'-like architecture in solution. The distances between closely associating amino acids are shown in Å. (B) The composition of AD-associated Tau protofilaments. During pathology-associated misfolding, R3, R4 and part of the C-terminus ($Tau_{306-378}$) form a proteolytically-resistant core that is integrated into Tau filaments and NFTs. The remining N- and C-terminal residues of Tau appear as unstructured, fuzzy and ultimately misfolded Tau protofilaments ($Tau_{306-378}$). (C) Symmetrically associating Tau protofilament cores stack into PHFs (left), whereas their asymmetrically interacting counterparts pack into SFs (right). (D) Folding of individual Tau protofilaments. Approximately ~80 % of the amino acid residues in misfolded $Tau_{306-378}$ show β sheet conformation, featuring eight separate β-strand regions (β1-8). The characteristic folding of Tau protofilaments is achieved by the inclusion of β sheet-breaking prolines (Pro^{312}, Pro^{332} and Pro^{364}), protein chain-turning glycines (Gly^{323} and Gly^{355}) and curve-

inducing Glu^{342} and Asp^{348} residues. The Tau aggregation-inducing ^{306}VQIVYK^{311} sequence in β1 (highlighted with red box) associates with amino acids 374 – 378 through the direct packing of hydrophobic side chains, as complemented by polar zipper formation between β2 and β8. Alternating (thus neutral) charge of amino acids 338 (beginning of β4) to 349 (end of β5) enables tight inter-molecular packing of the β4 - β7 regions. Modified from Jeganathan et al. (2006) and Fitzpatrick et al. (2017).

Symmetrically assembled protofilament cores (Figure 1.12C, left) are created by hydrogen bridge formation between ^{332}PGGGQ^{336} residues (more specifically the ^{333}GGG^{335} glycine tripeptide) of two protofilaments. These symmetric protofilament cores are then layered on top of each other to generate PHFs (Figure 1.13A). Hydrogen-bonding between ^{332}PGGGQ^{336} motifs not only creates symmetric protofilament cores, but also stabilises the interface between protofilament cores in the assembling PHF. In contrast, SFs are made up of asymmetric protofilament cores (Figure 1.12C, right) stacked in an irregular manner. In the case of SFs, protofilament core formation involves interactions between ^{321}KCGS^{324} in the first and ^{313}VELSK^{317} in the second Tau protofilament, cross-linked by an anionic tri-glutamate group (^{7}EEE^{9}) in the amino-terminal region of Tau (Figure 1.13B) (Fitzpatrick et al., 2017). Notably, Tau filament foldings are unique for each Tauopathy. For instance, in contrast to the above arrangement seen in AD, CBD-derived Tau filaments incorporate the R1 and R2 areas of Tau into the protofilament core (Arakhamia et al., 2020).

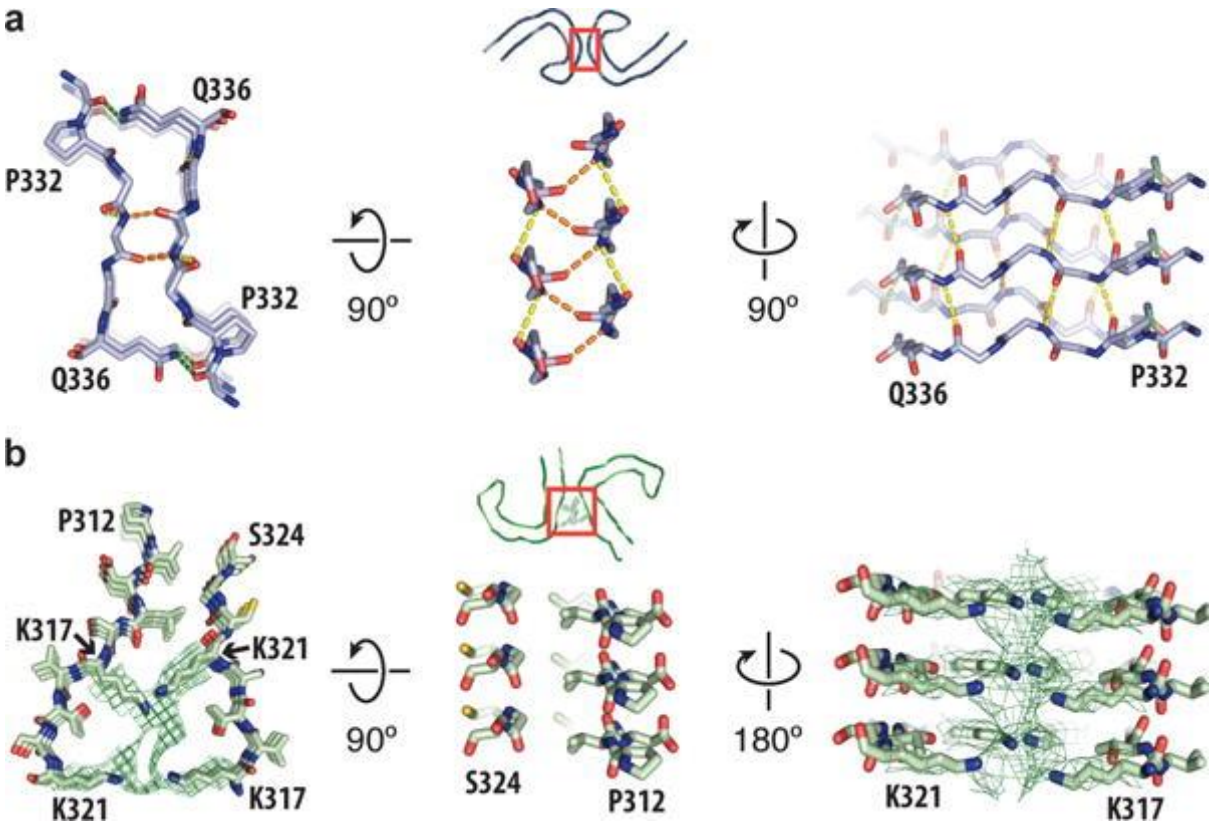

Figure 1.13: Inter-molecule stacking of Tau protofilament cores into insoluble PHFs and SFs in AD. (a) Packing of PHFs. The protofilament core consists of two mirroring Tau protofilaments ($Tau_{306-378}$ each) which associate via hydrogen-bonding (orange) between their ^{333}GGG^{335} residues (indicated by red box). Protofilament cores further pack on top of each other in a staggered fashion, as stabilised by inter-core hydrogen bonds between ^{332}PGGGQ^{336} regions (yellow). (b) Composition of SFs. Asymmetrically interacting Tau protofilaments, forming the core of SFs, involve interactions of the ^{321}KCGS^{324} in the first and ^{313}VELSK^{317} sequence in the second protofilament. In contrast to the hydrogen bond-stabilised core in PHFs, the protofilament core of SFs does not involve hydrogen-bonding or hydrophobic group interactions. Instead, an additional density (green mesh), postulated to represent a negatively charged glutamate group (^{7}EEE^{9}) in the N-terminal region of Tau, appears to insert between protofilaments to form salt bridges with cationic Lys^{317}, Lys^{321} and Thr^{319}. Asymmetric protofilament cores ultimately stack in a straight manner to generate SFs. Taken from Fitzpatrick et al. (2017).

Importantly, heparin-aggregated Tau, commonly used as a model system *in vitro*, adopts a different architecture to that observed in AD and other Tauopathies (Zhang et al., 2019). In the case of 2N4R Tau, cryo-electron microscopy showed that the use of heparin generated four different Tau filament architectures, denoted as snake (~45 %), twister (~30 %), hose (~20 %) and jagged (~5 %) conformations. In contrast, when exposed to heparin, 2N3R Tau folded into a single and fifth

filament conformation (Figure 1.14A) (Zhang et al., 2019). Moreover, while protofilaments derived from PHFs or SFs in AD consist of eight β sheet regions and Tau residues 306 - 378, protofilaments of heparin-aggregated 2N4R recombinant Tau, such as the Tau snake filament (6QJH), include only six β sheet motifs and comprise amino acids 272 - 330 of Tau (compare Figure 1.14B and C) (Fitzpatrick et al., 2017; Zhang et al., 2019). These conformational differences between Tau aggregates have to be considered for the design of effective structure-based Tau aggregation inhibitors (Wang et al., 2021).

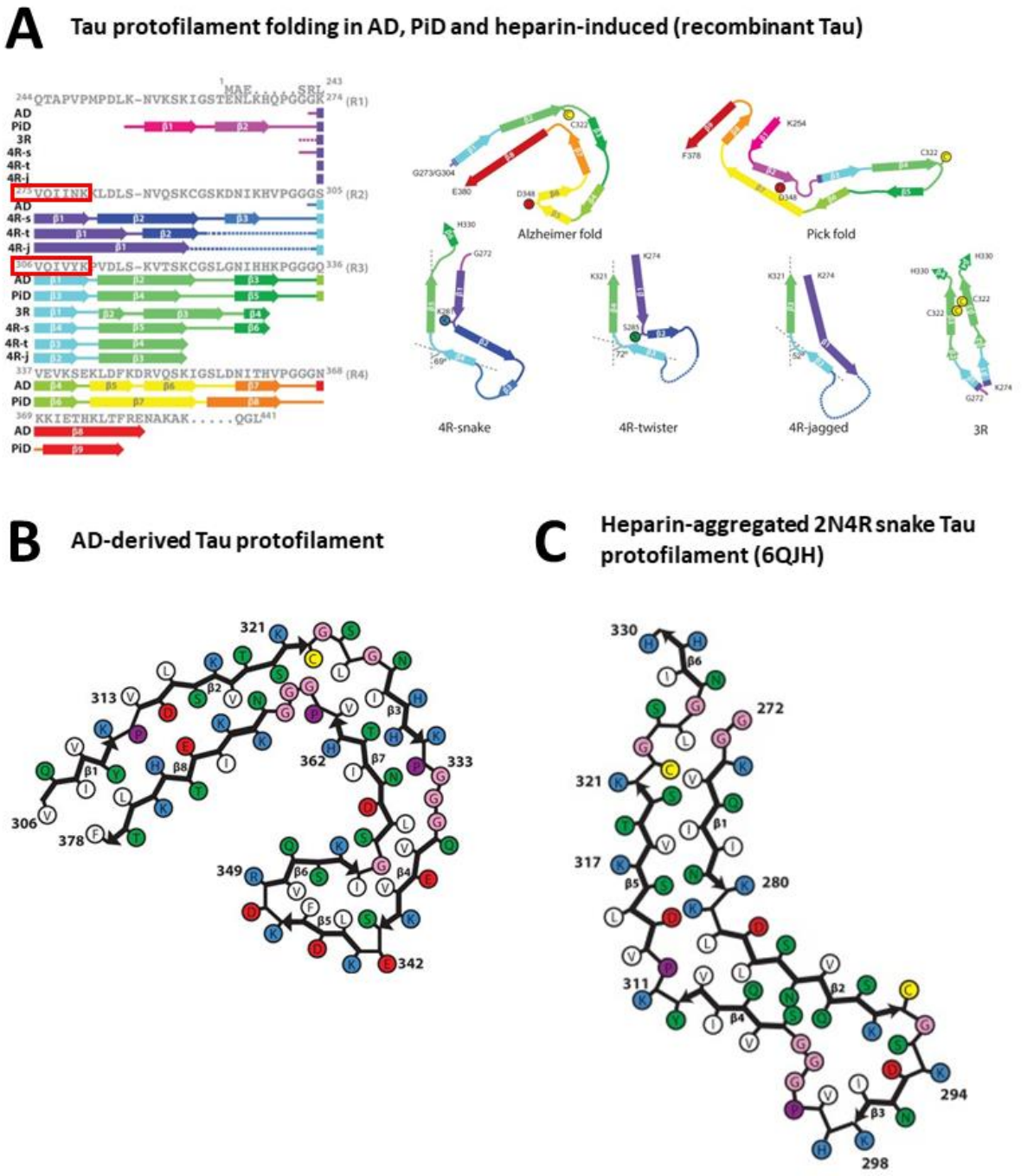

Figure 1.14: Comparison of Tau protofilament structures of heparin-aggregated, recombinant Tau and protofilaments derived from AD and PiD. (A) Alternate folding of Tau into various pathology-associated protofilament architectures. The ^{275}VQIINK^{280} (PHF6*) and ^{306}VQIVYK^{311} (PHF6) sequences, required for Tau aggregation, are highlighted with red boxes. 3R and 4R Tau structures (bottom row) represent conformations achieved with heparin. Amongst heparin-assembled 4R Tau protofilaments, the snake conformation is the most common (~45 %) (B) Structure of Tau protofilaments isolated from AD patients ($Tau_{306 - 378}$) as compared to (C) the heparin-aggregated snake Tau protofilament ($Tau_{272 - 330}$). Note that the ^{275}VQIINK^{280} motif is only contained in protofilaments produced with heparin treatment of recombinant 4R Tau, but not present in protofilaments isolated from AD brain tissue. Modified from Zhang et al. (2019).

While the literature supports the fact that ^{275}VQIINK^{280} (PHF6*) and ^{306}VQIVYK^{311} (PHF6) cooperate to mediate Tau oligomerisation, this might not apply for every Tau aggregate. Studies have shown that the deletion of ^{275}VQIINK^{280} lowered, whereas removal of ^{306}VQIVYK^{311} completely prevented, β sheet- and PHF-formation by 4R Tau monomers in the presence of heparin (von Bergen et al., 2001; Li and Lee, 2006). In the case of 4R Tau, it has been predicted that ^{275}VQIINK^{280} and ^{306}VQIVYK^{311} interact with each other to drive the oligomerisation of the protein (Ganguly et al., 2015). Indeed, using 2N4R Tau snake filaments (6QJH), our own modelling experiments confirmed that recombinant VQIVYK peptides are capable of associating with both PHF6* and PHF6 motifs (Aggidis A. et al., 2021). As 3R Tau isoforms lack ^{275}VQIINK^{280} (due to the splicing-associated removal of R2; Figure 1.4B), their aggregation is entirely dependent on ^{306}VQIVYK^{311} (von Bergen et al., 2001; Li and Lee, 2006). (Seidler et al., 2018) recently highlighted that ^{275}VQIINK^{280} was a more potent mediator of 4R Tau aggregation than ^{306}VQIVYK^{311}, but it should be emphasised that this was in the context of using heparin. ^{275}VQIINK^{280} (β1) and ^{306}VQIVYK^{311} (β4) are both part of $Tau_{272-330}$ protofilaments in 6QJH 2N4R Tau snake filaments (Figure 1.14A; red boxes). However, $Tau_{306-378}$ protofilaments that assemble into PHFs and SFs in AD only contain ^{306}VQIVYK^{311} (β1), whilst ^{275}VQIINK^{280} is part of the (degraded) N-terminal fuzzy coat (Fitzpatrick et al., 2017; Zhang et al., 2019). This suggests that ^{275}VQIINK^{280} is relevant for the heparin-induced 4R Tau aggregation *in vitro*, yet its importance for physiological Tau aggregation in AD is questionable.

1.2.9. Tau-based AD therapeutics

Historically, AD has shown a high drug failure rate of 99.6 % (Qiu et al., 2009; Patterson, 2018). From a clinical perspective, there has been a strong focus on amyloid pathology, especially Aβ, in AD (Roda et al., 2022; Huang et al., 2020). Besides recently emerged and FDA-approved Aβ-targeting therapies, including the antibodies aducanumab and lecanemab (Mozersky et al., 2022; M.M.a.B.W.C., 2023), there are drugs improving the memory- and behaviour-associated symptoms

of AD, including cholinesterase inhibitors, AMPAR modulators and NMDAR antagonists (Breijyeh and Karaman, 2020). Additionally, alternative approaches based on Tau pathology have gained traction in recent years. However, compared to Aß, substantially fewer research efforts have focused on the development of compounds that prevent Tau pathology. Nonetheless, some Tau-targeted therapies have reached the stage of clinical trials (Huang et al., 2020; Roda et al., 2022).

A popular approach in terms of Tau therapeutics is the development of structure-based drugs. Such Tau therapeutics fall into one of two functional categories (Wang et al., 2021). They may aim to stabilise the native ‘paperclip'-conformation of soluble Tau in order to prevent misfolding and favour microtubule association. An example would be inhibitors of the Tau-hyperphosphorylating kinase GSK-3β, such as lithium, which reduce the dissociation of Tau from tubulin (Wang et al., 2021). Alternatively, other indirect agents may be employed, for instance the BBB-penetrant and Tau-mimicking microtubule-stabiliser epothilone D (Ballatore et al., 2012). On the other hand, aggregation inhibitors, such as our RI-AG03 peptide, intercept pathologic Tau oligomerisation by preventing interactions between Tau monomers (Wang et al., 2021; Aggidis A. et al., 2021).

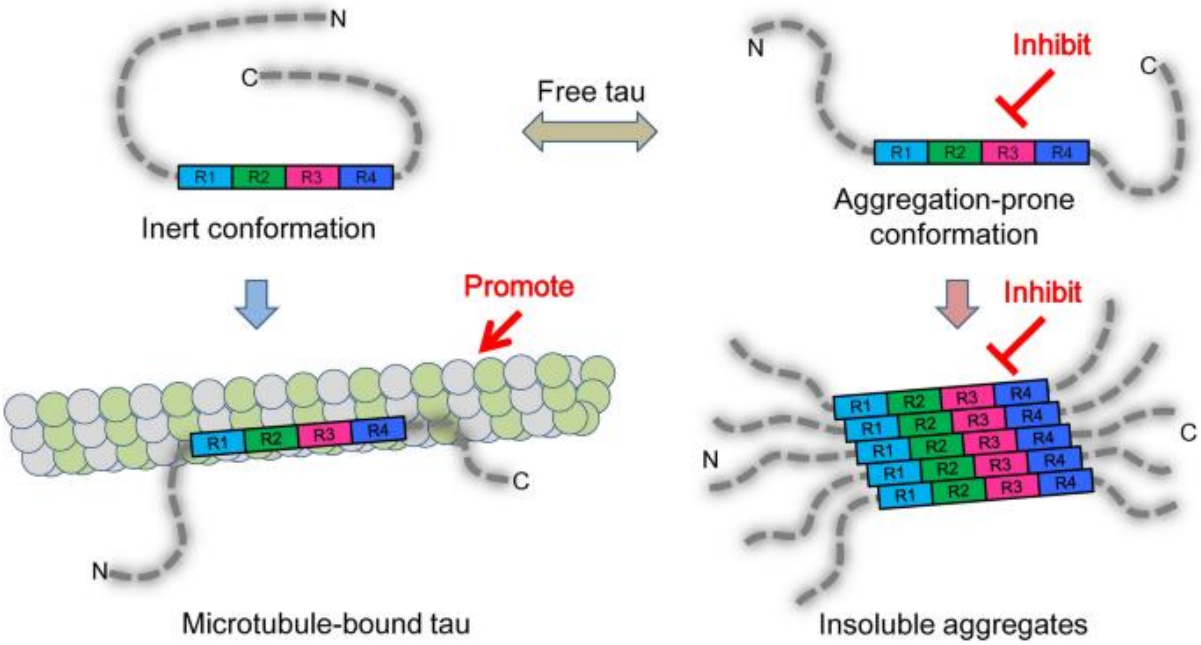

Figure 1.15: Improvement of the Tau pathology by structure-based Tau therapeutics in AD and Tauopathies. Anti-Tau drugs may help to retain the native structure of Tau and/or microtubule stability (left) or block the pathology-associated assembly of misfolded Tau into soluble and insoluble Tau inclusions (right). Taken from Wang et al. (2021).

A few peptide-based Tau aggregation inhibitors have been tested in phase I or II clinical trials (Wang et al., 2021; Aillaud and Funke, 2022). However, there also exist various non-peptide Tau aggregation inhibitors, notably the phenothiazine methylene blue, discovered by Wischik et al. (1996). The compound was able to inhibit the aggregation of recombinant Tau *in vitro* and even disassemble preformed PHFs, without negatively affecting the physiological binding of Tau to microtubules (Wischik et al., 1996; Taniguchi et al., 2005). The drug also demonstrated favourable effects in a range of Tauopathy animal models (O'Leary et al., 2010; Congdon et al., 2012; Melis et al., 2015) and in a 50 week (extended) phase II clinical trial for patients with mild to moderate AD (Wischik et al., 2015). In AD patients, drug administration maintained cognitive function and improved cerebral blood flow (Wischik et al., 2015). Mechanistically, it was initially thought that methylene blue prevented Tau aggregation by oxidising the key residues Cys^{291} and Cys^{322}, similar to aminothienopyridazines (Akoury et al., 2013; Crowe et al., 2013). However, more recent studies

imply that methylene blue-induced inhibition of Tau oligomerisation is cysteine-independent (Al-Hilaly et al., 2018). Unfortunately, the compound was unsuccessful in three phase III studies in all-cause dementia, AD and frontotemporal dementia patients (Alzforum; Roda et al., 2022). However, an improved version of methylene blue, LMTX (or TRx0237), is currently the subject of a phase III clinical trial for AD (NCT03446001).

Another group of Tau aggregation inhibitors are polyphenols. While these compounds were shown to interact with misfolded Tau monomers and potently block aggregation at low doses (µM range), polyphenols exhibit multiple undesirable properties (Rauch et al., 2017). Disadvantages include the inability to dissipate Tau fibrils, self-oligomerisation and interference with the commonly used thioflavin T (ThT) (Tau aggregation) assay, hence encouraging false positive results (Pickhardt et al., 2015; Lo et al., 2019).

In addition to Tau aggregation inhibitors, vaccines and various antibodies targeting extra- or intracellular Tau have been developed and tested in patients (Sandusky-Beltran and Sigurdsson, 2020). Most Tau antibodies are intended to halt the extracellular spread of propagation-competent Tau seeds, whilst promoting the microglial phagocytosis of antibody-tagged Tau inclusions. Some of these antibodies are further internalised by neurons or glia through receptor-driven endocytosis and thought to disassemble Tau aggregates accumulating in endosomes and lysosomes (Sandusky-Beltran and Sigurdsson, 2020). Moreover, the recently developed 'Trim Away' system, which combines tripartite motif protein 21- and Tau-targeting antibodies to mediate the proteasomal clearance of pathologic Tau species in neurons potentially exhibits some promise (McEwan et al., 2017; Clift et al., 2018).

Other means to address the Tau pathology include microtubule stabilisers, such as paclitaxel (Ballatore et al., 2012), and Tau kinase or acetylation inhibitors, for example the GSK-3β-blocking lithium or p300-inhibting Salsalate (Sayas, 2020). However, due to toxic side effects and poor clinical efficacy, both of these therapeutic approaches have been discontinued (Congdon and Sigurdsson,

2018). Moreover, small molecules that modulate chaperone-associated Tau degradation and folding have emerged (Gorantla and Chinnathambi, 2018). More recent developments include antisense RNAs (morpholinos) that impede Tau translation, for instance IONIS MAPTRx by Ionis Pharma, Inc. that is currently being tested in phase I/II clinical trials (NCT03186989) (Roda et al., 2022).

1.3. Mechanisms of endocytosis

Cellular endocytosis is a process by which parts of the plasma membrane are internalised in the form of lipid vesicles, allowing the cell to take up fluids, plasma membrane-bound proteins and macromolecules (Doherty and McMahon, 2009). Together with exocytosis, the delivery of vesicle-enclosed molecules to the extracellular space, both mechanisms regulate the interaction of cells with their environment. For example, endo- and exocytosis control the cell surface density of receptors (Doherty and McMahon, 2009).

Notably, cellular uptake of cargo by endocytosis, or phagocytosis in specialised cells (macrophages, microglia and astrocytes), are ATP-dependent. Furthermore, there are multiple energy/ATP-requiring subclasses of endocytosis, including clathrin-mediated endocytosis (CME), clathrin-independent endocytosis, such as caveolae-mediated endocytosis (CavME) or flotillin-dependent endocytosis, and macropinocytosis (Doherty and McMahon, 2009; Foroozandeh and Aziz, 2018; Vercauteren et al., 2010). The most relevant endocytosis pathways for nanocarriers are illustrated in Figure 1.16.

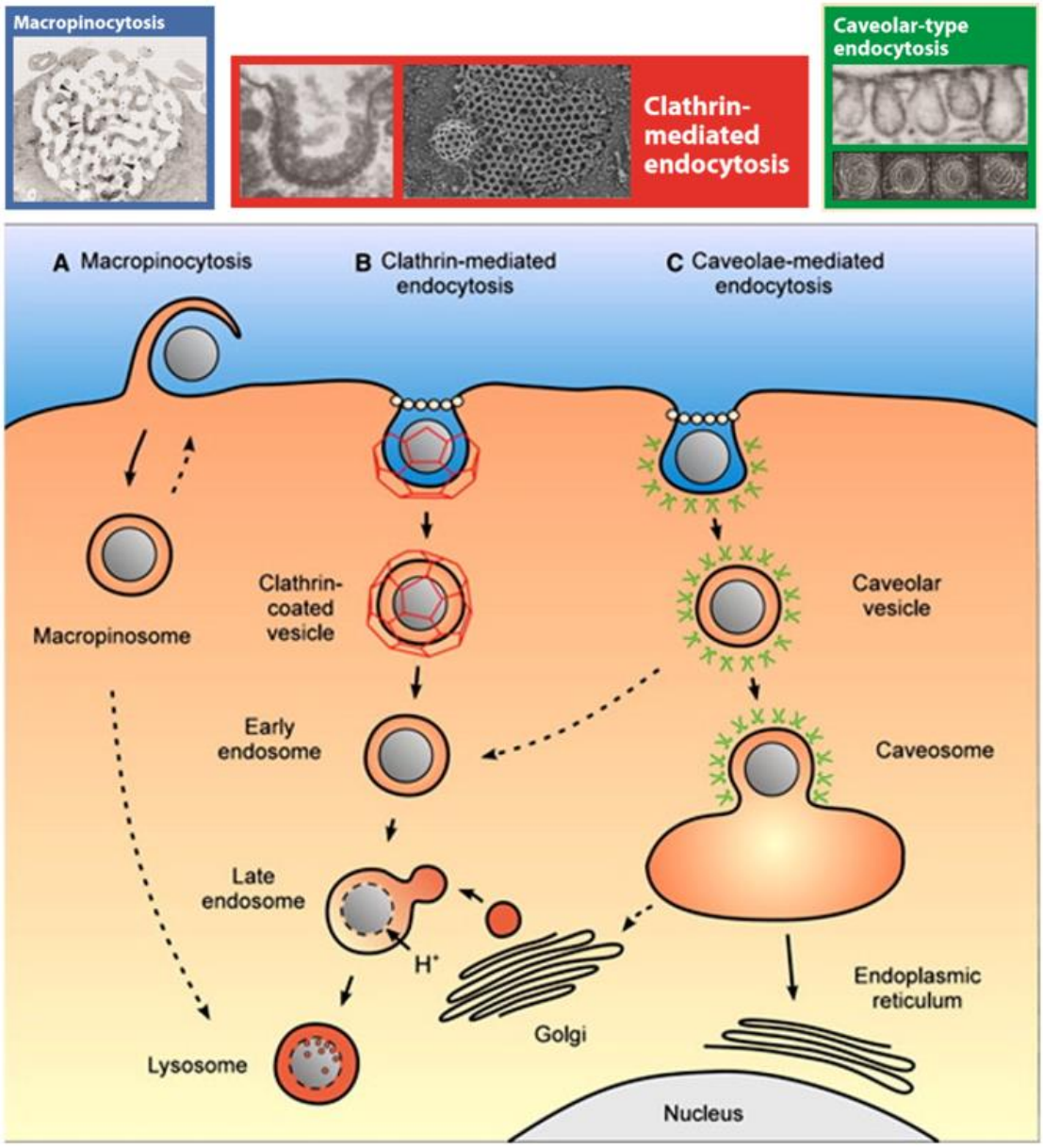

Figure 1.16: Illustration of the three major endocytosis pathways of therapeutic nanoparticles. (A) *Macropinocytosis*. In this actin-driven process, extensive ruffling of the cellular plasma membrane entraps proximate cargo through the inward-folding of ruffles and fusion with the plasma membrane. The macropinosomes generated may subsequently merge with lysosomes. (B) *Clathrin-mediated endocytosis*. Usually receptor-triggered, adaptor proteins, such as adaptor protein 2, recruit clathrin, leading to formation of a characteristic clathrin lattice around the budding vesicle. Following scission by dynamin and invagination of the vesicle, clathrin is removed by various uncoating proteins, including auxillin and heat shock cognate 70, resulting in the maturation of early endosomes. In most cases, early endosomes traffic to late endosomes/lysosomes, but redirection to the plasma membrane may ensue. (C) *Caveolae-mediated endocytosis*. Occurring at lipid rafts, caveolae-specific cargo may trigger the internalisation of plasma membrane-embedded caveolae, which resemble a "bunch of grapes". In co-operation, caveolins, structural proteins that form a distinct, spike-like coat around caveolae, and cavins promote membrane curvature of caveolae, followed by dynamin-mediated cleavage. Liberated caveolae typically diffuse to the caveosome, a

sorting and fusion station for caveolae. In contrast to what is depicted, a recent study has revealed that caveosomes correspond to late endosomes coated by caveolin-1 (Hayer et al., 2010). Following sorting in caveosomes, depending on the cargo, caveolae may be sent to the ER, Golgi or lysosomes. Modified from Doherty and McMahon (2009) and Saraswathy and Gong (2013).

Macropinocytosis is predominantly associated with macrophages and dendritic cells and its role is to aid the non-selective internalisation of nutrients, soluble macromolecules and antigens (Figure 1.16A). Typically, cellular exposure to growth factors, such as epidermal growth factor or macrophage colony-stimulating factor 1 (Haigler et al., 1979; Racoosin and Swanson, 1989), evokes the restructuring of the actin cytoskeleton, resulting in plasma membrane ruffling (Lim and Gleeson, 2011). Subsequently forming membrane protrusions may fold onto themselves, capturing extracellular cargo, and merge at their base with the cellular bilipid membrane to create unevenly shaped macropinosomes of up to 5 mm in diameter (Doherty and McMahon, 2009; Lim and Gleeson, 2011). Following intracellular maturation, these vesicles are delivered to lysosomes (Racoosin and Swanson, 1993), although their final destination appears to be cell-type dependent (Doherty and McMahon, 2009; Lim and Gleeson, 2011).

The best understood endocytic pathway is CME (Figure 1.16B) which is responsible for internalisation of various G-protein-coupled receptors (Cao et al., 1998; Popova et al., 2013). Upon ligand recognition, plasma membrane invaginations form, as assisted by adaptor protein 2 (AP2), ß-arrestins and clathrin. The latter forms a characteristic clathrin lattice around the budding lipid vesicle to support membrane curvature. Subsequent cleavage by dynamin and elimination of the clathrin coat leads to formation of early endosomes. The latter may be targeted to late endosomes and lysosomes for degradation or recirculate to the plasma membrane (Mettlen et al., 2018; Popova et al., 2013). Examples of clathrin-internalised cargo include transferrin receptors (Liu et al., 2010), low-density lipoprotein receptors (Garuti et al., 2005), μ-opioid neuropeptide receptors (Henry et al., 2012) and even death receptors (Reis et al., 2017). Dynamin-regulated CMA is also strongly involved

in vesicle recycling and transport of macromolecules, such as neurotransmitters, at synaptic terminals in neurons (Mettlen et al., 2018; Smillie and Cousin, 2005).

Another frequently reported endocytic mechanism is CavME (Figure 1.16C) (Doherty and McMahon, 2009). Caveolae ("little caves") are tubular structures of 60 - 80 nm diameter within the plasma membrane. Characteristically, caveolae are enriched in cholesterol and sphingomyelin (SM) and feature a spiky coat, consisting of oligomerised caveolin-1 and caveolin-2 proteins (Doherty and McMahon, 2009; Monier et al., 1995; Rothberg et al., 1992). Typically found as multicaveolar assemblies in the cellular bilipid membrane, it is believed that caveolae represent a subdomain of gycolipid rafts (Nabi and Le, 2003). When stimulated by cargo, cavins assist the membrane curvature of embedded caveolae, similar to clathrin. This is followed by the intracellular cleavage of the lipid vesicles by dynamin, allowing the trafficking of caveolae to the caveosome (Nabi and Le, 2003; Oh et al., 1998; Busija et al., 2017). The latter was initially thought to be a fusion or sorting platform for incoming caveolae (Nabi and Le, 2003), differing from early endosomes due to the surface presentation of caveolin-1, absence of endosomal markers and acidification (Pelkmans et al., 2001). However, in contrast to what is depicted in Figure 1.16C, a recent study revealed that caveosomes are, in fact, caveolin-1-displaying late endosomes that are targeted for lysosomal degradation (Hayer et al., 2010). From the caveosome, delivery to the ER and the Golgi apparatus has been described, yet the final destination appears to be cargo-dependent (Le and Nabi, 2003). Examples of caveolae-internalised cargo include cholera toxin (Shogomori and Futerman, 2001; Montesano et al., 1982), autocrine motility factor (Benlimame et al., 1998), sphingolipids and sphingolipid-interacting compounds (Puri et al., 2001), growth hormone (Lobie et al., 1999), endothelin receptor type A (Okamoto et al., 2000) or IL-2 receptors (Lamaze et al., 2001) and some bacteria (Duncan et al., 2002; Shin et al., 2000; Sukumaran et al., 2002).

Reviewed in Doherty and McMahon (2009), other less well characterised endocytic pathways include flotillin-dependent endocytosis, phagocytosis, clathrin-Independent carriers / glycosylphosphatidylinositol-enriched endosomal compartments-type endocytosis (CLIC/GEEC),

entosis and circular dorsal ruffles. Importantly, the relative distribution of clathrin-mediated versus clathrin-independent endocytosis varies between cells, suggesting that is of high importance to study the internalisation of drugs in the target cell population of interest (Doherty and McMahon, 2009).

1.4. Development of amyloid aggregation inhibitor peptides and peptide-conjugated liposomes for the treatment of Alzheimer's disease

Because AD is a multi-factorial disease, with multiple pathologic factors exacerbating each other, it has been suggested multi-target treatments might be necessary to prevent cognitive decline in every AD patient (Iqbal and Grundke-Iqbal, 2010; Huang et al., 2020; Reich and Holscher, 2020). In particular, it has recently been highlighted that combination therapies, addressing the pathologic interplay between Aβ and Tau, might be more promising for the successful treatment of AD (Roda et al., 2022). With this in mind, the overarching aim of our research is to combine our previously developed Aβ aggregation inhibitor peptide, RI-OR2 (Taylor et al., 2010; Parthsarathy et al., 2013; Gregori et al., 2017), with the subject of the current study, the Tau aggregation inhibitor peptide RI-AG03 (Aggidis A. et al., 2021; Aggidis, 2019), to generate a combination therapy for the treatment of AD.

1.4.1. Amyloid beta aggregation inhibitor peptide development

Our group initially developed Aβ aggregation inhibitor peptides to halt the formation of plaques in the brain. Out of two candidates, the more effective peptide called 'OR2' was chosen (Figure 1.17A) (Taylor et al., 2010; Austen et al., 2008). Modelled to bind to the aggregation-driving ^{16}KLVFF^{20} sequence in Aβ peptides (Figure 1.17B) (Austen et al., 2008), OR2 was further retro-inverted to generate RI-OR2, which rendered the peptide highly resistant to proteolysis (Figure 1.17C) (Taylor et al., 2010). We demonstrated that OR2 and RI-OR2 prevented the oligomerisation and fibrilisation of

recombinant $A\beta_{1-40}$ or $A\beta_{1-42}$, whilst pre-treatment of $A\beta_{1-42}$ peptides with RI-OR2 rescued SH-SY5Y cells from death (Taylor et al., 2010).

To make the peptide more effective *in vivo*, a few modifications were made. To mediate cellular uptake, the TAT cell penetrating peptide (CPP) sequence was added to RI-OR2 (Figure 1.17D) (Parthsarathy et al., 2013). Fluorescein-based biodistribution studies verified that intraperitoneally (i.p.) injected RI-OR2 modified with TAT also crossed the BBB in APP/PSEN1 mice (Figure 1.17E) (Parthsarathy et al., 2013). Furthermore, daily peripheral injections of RI-OR2 for 21 days lowered Aβ oligomer and plaque load, microgliosis and oxidative stress in the cerebral cortex, while enhancing neurogenesis in the hippocampal dentate gyrus, in the APPswe/PS1ΔE9 mouse model of AD (Parthsarathy et al., 2013).

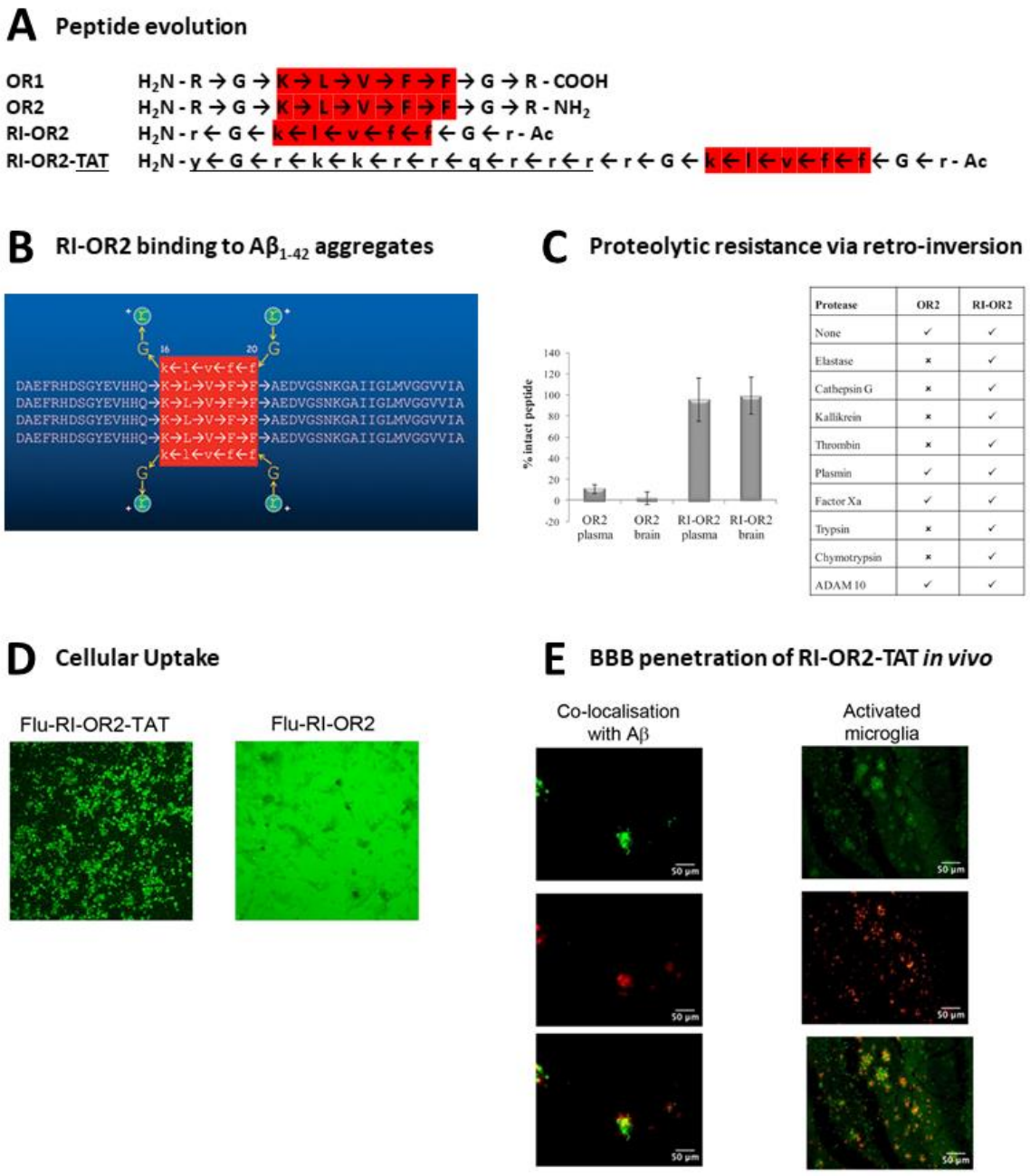

Figure 1.17: Development and characteristics of the Aβ aggregation inhibitor RI-OR2-TAT. (A) Sequences of various peptide candidates. Peptide residues binding to the pro-aggregatory ^{16}KLVFF^{20} motif in Aβ are highlighted in red. Small letters represent D-amino acids and CPPs are underlined. (B) Binding of RI-OR2 to the aggregation-driving ^{16}KLVFF^{20} motif in (oligomeric) $Aβ_{1-42}$. (C) 1 mM peptide incubated with 50 mg/mL human brain or 5 mg/mL human plasma extract (left; diagram illustrates the mean ± SEM % of reversed-phase HPLC absorbance of 3 independent replicates at 220 nm) or 0.1 mg/mL proteases (right; √ = stable and x = degraded) at 37 °C for 24 h shows that RI-OR2 is proteolytically resistant, whilst OR2 is not. (D) Representative confocal images showing that 10 µM fluorescein (Flu)-RI-OR2-TAT is internalised by SH-SY5Y cells after a 10 min treatment period, whereas Flu-RI-OR2 (without TAT CPP) is not. (E) 100 nmol/kg Flu-RI-OR2-TAT was i.p. injected into 17 month-old APP/PSEN1 mice, rodents were sacrificed 1 h later and brain sections subjected to immunohistochemistry using anti-Aβ and anti-IBA1 antibodies. BBB crossing *in vivo* is apparent

because Flu-RI-OR2-TAT (green) co-localised with Aβ plaques (red; left panels) and activated microglia stimulated by Aβ pathology (red; right panels). Figures and data were adapted from Taylor et al. (2010) and Parthsarathy et al. (2013). For details regarding the Aβ aggregation-inhibiting effects of RI-OR2(-TAT), please see the aforementioned publications.

1.4.2. Tau aggregation inhibitor peptide development

To complement RI-OR2-TAT, our gorup recently tested various Tau aggregation inhibitor peptide candidates (Aggidis A. et al., 2021; Aggidis, 2019). The first generation inhibitor AG01 was designed to interact with ^{275}VQIINK^{280} present in R2 in 4R Tau isoforms, whilst subsequent peptides were constructed to bind the pathologically more critical ^{306}VQIVYK^{311} sequence in R3 in all six Tau isoforms (Figure 1.18A) (von Bergen et al., 2001; von Bergen et al., 2000; Mamsa and Meloni, 2021; Falcon et al., 2015). Screening of our peptides in ThT assays showed that AG03-polyR was the best inhibitor of heparin-induced $Tau_{\Delta 1-250}$ aggregation, also exhibiting a low propensity to self-oligomerise (Figure 1.18B) (Aggidis A. et al., 2021). Strikingly, adding proteolytic resistance though retro-inversion, but not N-methylation, potently improved the anti-aggregatory effects of AG03-polyR, resulting in approximately ~94 % reduced $Tau_{\Delta 1-250}$ aggregation (IC_{50} of RI-AG03-polyR = 7.83 µM) (Figure 1.18C) (Aggidis A. et al., 2021). Using heparin-$Tau_{\Delta 1-250}$ preparations, TEM visually confirmed that RI-AG03-polyR prevented the formation of insoluble Tau fibrils and, instead, generated β sheet-negative, spherical Tau structures (red arrows in Figure 1.18D) (Aggidis A. et al., 2021). Suggestive of its therapeutic potential, feeding RI-AG03-polyR to transgenic *Drosophila* models with eye-localised or systemic overexpression of full-length (2N4R) human Tau ameliorated ocular degeneration and enhanced survival (Aggidis A. et al., 2021).

Notably, considering that Tau is an intracellular protein that propagates in a prion-like fashion across interconnected neurons in AD and Tauopathies (Vogel et al., 2021), the incorporation of a CPP, such as the polyR sequence in RI-AG03, is mandatory to enhance BBB penetration and neuronal uptake (Juliano et al., 2008; Palm-Apergi et al., 2012; Shi et al., 2014). Furthermore, in agreement with the anti-aggregatory effects of arginine-rich peptides (Mamsa and Meloni, 2021), our initial experiments

confirmed that additional arginine residues in AG02 peptide variants, specifically in AG02R9, improved their Tau aggregation-blocking effects (Figure 1.18A&B). Thus, a polyR sequence was incorporated into (RI-)AG03.

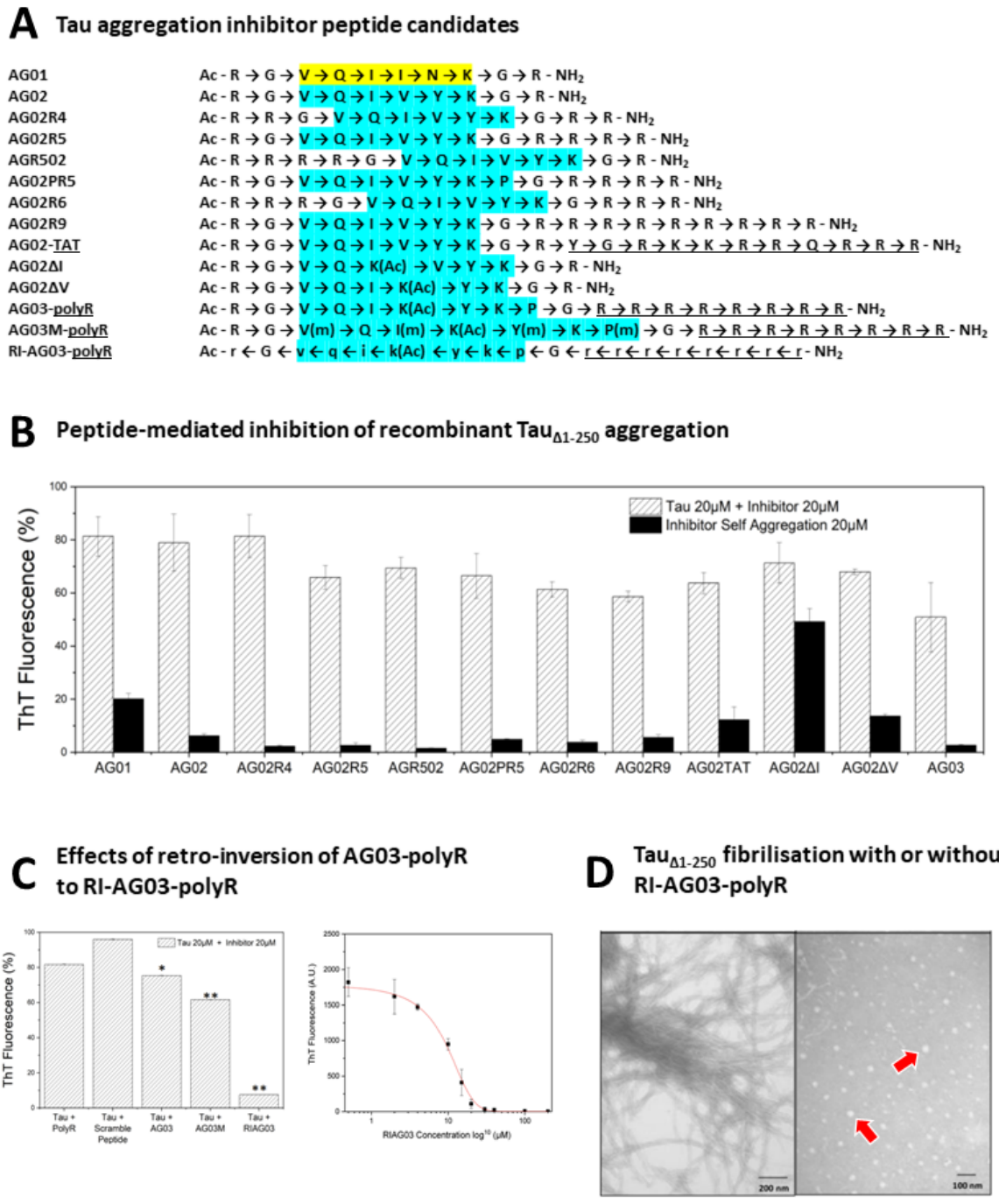

Figure 1.18: Selection of the Tau aggregation inhibitor peptide RI-AG03-polyR. (A) Sequences of previously tested Tau aggregation inhibitor peptide candidates. Peptide regions that are predicted to bind to the aggregation-inducing ^{275}VQIINK^{280} and ^{306}VQIVYK^{311} sequences in Tau are highlighted in yellow (AG01) and blue (AG02 and AG03 variants), respectively. CPPs are underlined and letters in small cases represent D-amino acids. (B) 20 µM recombinant Tau$_{\Delta 1-250}$ was incubated in aggregation

buffer (Tris buffer 30 mM, DTT 1 mM, heparin 5 µM, pH 7.4) in the presence of equimolar concentrations of the peptides in (A) at 37 °C for 24 h, then ThT-associated fluorescence (β sheet content) was measured. Data was plotted as mean ± % of ThT fluorescence (n = 3). (C) $Tau_{\Delta 1\text{--}250}$ aggregation-inhibiting effects of the most effective peptide, AG03-polyR, its degradation-resistant N-methylated (AG03M-polyR) and retro-inverted forms (RI-AG03-polyR) and a control scrambled AG03-polyR peptide (Ac - R→ G→ Q→ P→ K→ I→ K(Ac) → Y→ V→ G→ R→ R→ R→ R→ R→ R→ R - NH_2) in ThT assays. Data was analysed with one-way ANOVA and Tukey's post hoc test; significance was * = < 0.05 and ** = < 0.01 compared to peptide-free ThT signal (left graph). The right diagram shows a dose-response curve of RI-AG03-polyR in ThT assays (IC_{50} to inhibit $Tau_{\Delta 1\text{--}250}$ aggregation = 7.83 µM). (D) 20 µM $Tau_{\Delta 1\text{--}250}$ in aggregation mix (see earlier) was incubated without or with equimolar RI-AG03-polyR concentrations at 37 °C for 24 h, counterstained on grids with 2 % phosphotungstic acid and visualised using TEM. Without inhibitor, $Tau_{\Delta 1\text{-}250}$ formed insoluble fibrils, whilst adding RI-AG03-polyR generated spherical Tau structures (mean diameter = 35.82 nm; see red arrows). Taken from Aggidis et al (2021).

By employing computational modelling, our group also modelled the interaction of non-retro-inverted AG03 with pathological Tau (Aggidis A. et al., 2021). Experimental docking (Figure 1.19A) demonstrated that AG03 associated with the ^{306}VQIVYK^{311} motif in $Tau_{306-378}$ (β1) and, to some extent, with the opposite β8-strand (^{368}NKKIETHKLTF^{378}; Figure 1.12D). Furthermore, modelling predicted that AG03 binds more potently to ^{306}VQIVYK^{311} than recombinant VQIVYK. We also computed the association of AG03 with heparin-aggregated Tau. As expected, computational modelling predicted that AG03 binds in an anti-parallel fashion to ^{306}VQIVYK^{311}, but also in a parallel manner to ^{275}VQIINK^{280}, in 2N4R Tau snake filaments (6QJH) (Figure 1.19B) (Aggidis A. et al., 2021). The interaction of our VQIVYK-based AG03 peptide with ^{275}VQIINK^{280} is similar to the pathologic association of ^{306}VQIVYK^{311} with ^{275}VQIINK^{280} that drives the aggregation of 4R Tau in the presence of heparin (Ganguly et al., 2015).

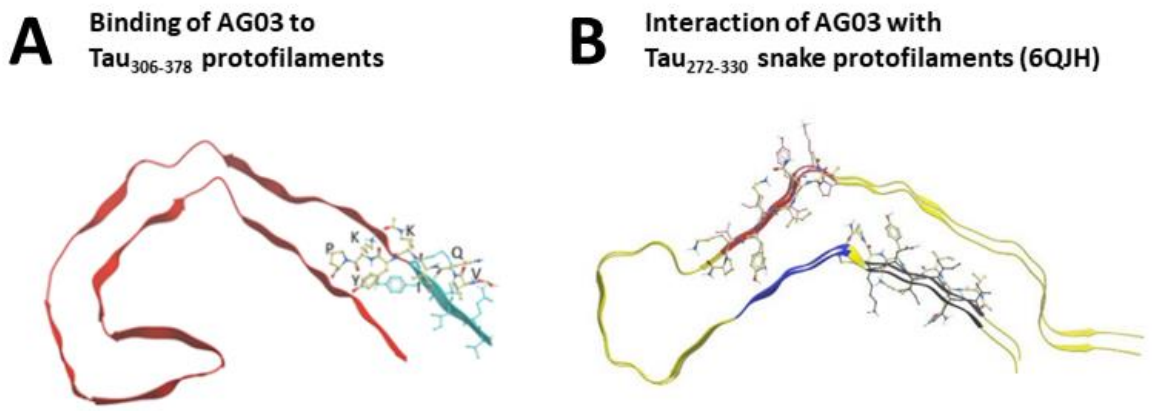

Figure 1.19: Computational modelling of the binding interactions between the non-retro-inverted Tau aggregation inhibitor peptide AG03 and AD-isolated and heparin-induced recombinant Tau protofilaments. (A) The key aggregatory ^{306}VQIVYK^{311} sequence in Tau is illustrated in cyan. (B) depicts ^{306}VQIVYK^{311} in red and ^{275}VQIINK^{280} in blue. Despite originally being designed against ^{306}VQIVYK^{311}, structural docking suggests that AG03 can also bind in parallel to ^{275}VQIINK^{280}. Adapted from Aggidis et al (2021).

While modelling suggests that AG03 has the potential to interact with the already formed protofilament core, it is not clear if peptide-binding prevents the misfolding of (hyperphosphorylated) Tau into its pathologic protofilament structure. Nonetheless, the interaction of the peptide with ^{306}VQIVYK^{311} presumably sterically interrupts the inter-molecule stacking of Tau protofilament cores into Tau polymers and, subsequently, PHFs or SFs.

In summary, the previous *in vitro* results of our group and computational structural investigations suggest that RI-AG03 can prevent heparin-induced or Tauopathy-specific aggregation of 3R and 4R Tau into β sheet-exhibiting insoluble filaments and NFTs.

1.4.3. Nanocarriers in the treatment of Alzheimer's disease

Nanocarriers are molecules in the range of 1 - 100 nm that are, for example, extensively used in the field of cancer (Khan et al., 2017; Jabr-Milane et al., 2008). By altering their composition and due to their high surface to volume ratio, nanocarriers can be fine-tuned for the delivery of single or

multiple therapeutic drugs. Additionally, agents can be conjugated to the surface of nanocarriers or incorporated into them, and the former of which can be employed to target the structures to specific cell or tissue types (Rachmawati et al., 2020; Khan et al., 2017). Additionally, these drug vehicles not only provide proteolytic protection of the incorporated cargo, but can be modified to facilitate either accelerated or delayed drug release (Khan et al., 2017). A prominent example of such multi-functional nanocarriers are liposomes; lipid-composed vesicles that are gradually becoming more popular as drug delivery shuttles in AD (Ross et al., 2018). Other examples include nanocarriers consisting of polymers, micelles, dendrimers, carbons, metal or silicon (Jabr-Milane et al., 2008).

One of the greatest challenges in relation to CNS-targeting drugs is to overcome the BBB; a cellular layer composed of tightly linked endothelial cells, further reinforced by astrocytes and pericytes, that restricts the entry of most blood-borne compounds into the CNS (Bhowmik et al., 2015; Foroozandeh and Aziz, 2018). Notably, besides the composition and administered dose, the size of liposomes is an important variable that determines their tissue-specific uptake and blood circulation times post injection (Abra and Hunt, 1981; Harashima and Kiwada, 1996). Advantageous for the treatment of AD, it has been suggested that smaller liposome diameters at or below 100 nm show better CNS uptake (Ross et al., 2018; Kahana et al., 2021). However, small liposome sizes (~50 nm) suffer from restricted encapsulation capacity and poorer half-life in the circulatory system (Ross et al., 2018). Dependent on their characteristics, liposomes translocate from the blood stream into the BBB using adsorptive-mediated, receptor-mediated or carrier-mediated transcytosis (Juhairiyah and de Lange, 2021), and various microdialysis studies have been performed to optimize liposomes for selective drug delivery into the brain (Gaillard et al., 2014; Hu et al., 2019; Hu et al., 2017; Lindqvist et al., 2013; Lindqvist et al., 2016).

As depicted in Figure 1.20, various strategies have been employed to enhance BBB translocation. Surface conjugation of ligands that are specifically internalised by or interact with receptors expressed on BBB endothelial cells, such as transferrin and lactoferrin receptors or glutathione (Qian et al., 2002; Fillebeen et al., 1999; Gaillard et al., 2014), have been shown to improve the CNS uptake

of injected nanocarriers (Ross et al., 2018). Another strategy involves the attachment of CPPs to liposomes. CPPs refer to short motifs, usually below 30 amino acids, that have the ability to infiltrate cells (Juliano et al., 2008). Typically positively charged, electrostatic attraction facilitates the association of CPPs with negatively charged lipids in the cellular plasma membrane, followed by energy-independent direct membrane penetration or, as dependent on the (experimental) conditions, cellular uptake via endocytosis (Juliano et al., 2008; Palm-Apergi et al., 2012; Shi et al., 2014).

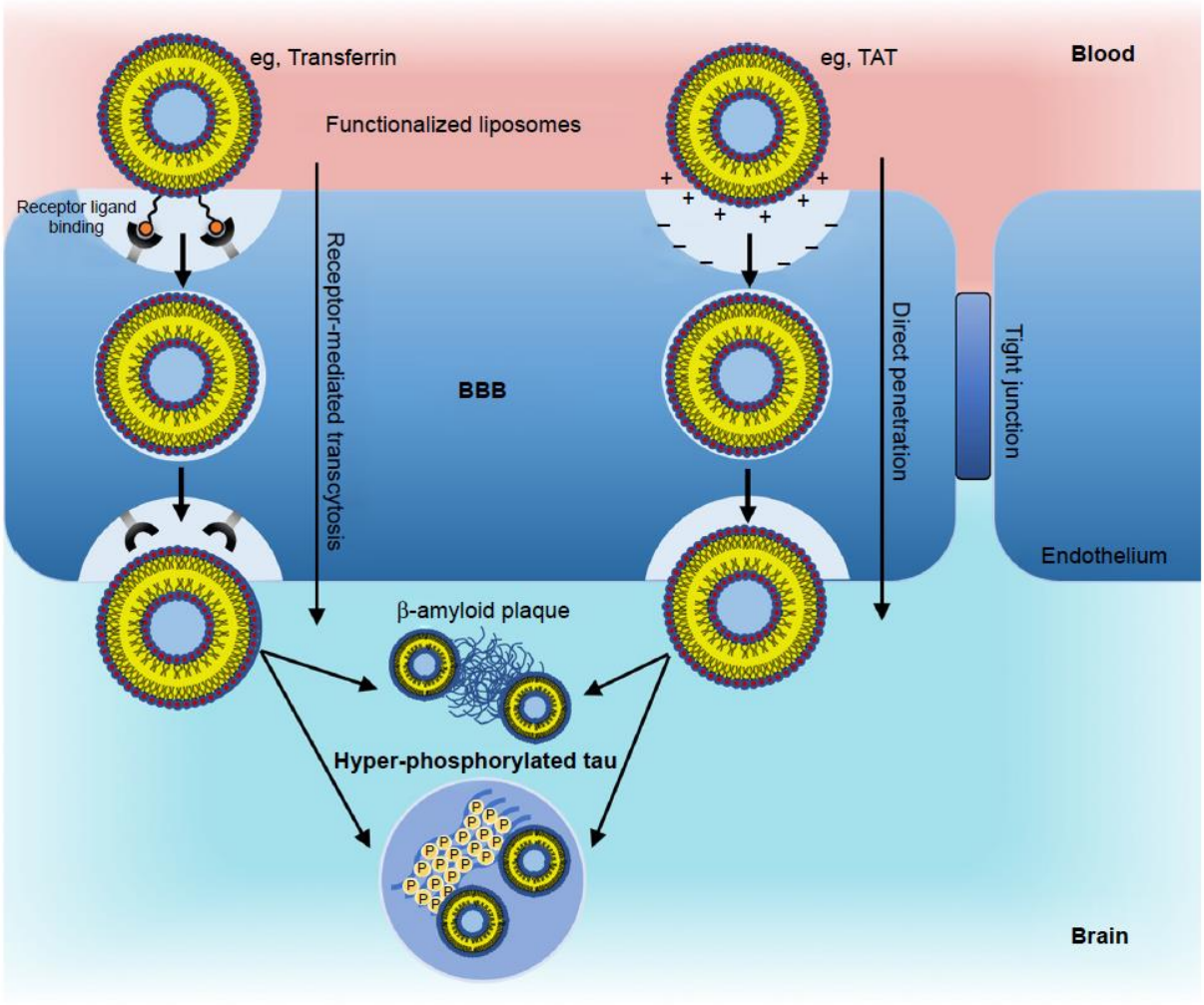

Figure 1.20: Potential modifications of liposomes to enhance BBB penetration. The liposome-mediated penetration of the BBB may be improved by targeting receptors that are densely expressed on endothelial cells that form the BBB, for example transferrin receptors (left) (Qian et al., 2002). Similarly, the conjugation of ligands that are constitutively transported through the BBB, such as glutathione (Gaillard et al., 2014), may promote translocation. Alternatively, surface attachment of cationic CPP, such as TAT, to liposomes facilitates the apposition and permeation of the negatively charged cell membrane of the BBB endothelium (right). The combinatorial linkage of translocation-enhancing CPPs and one or multiple therapeutic agents, for example drugs that address the Aß and Tau pathology, pose a promising strategy for the treatment of AD. Taken from Ross et al. (2018).

In relation to our own Aβ anti-aggregation peptide, our group previously incorporated a CPP, TAT, into RI-OR02 (Figure 1.17A) (Taylor et al., 2010). Moreover, we showed that both peripherally injected free and liposome-conjugated RI-OR02-TAT peptide entered the CNS *in vivo*, exerting neuroprotective effects in AD mouse models (Parthsarathy et al., 2013; Gregori et al., 2017). Besides

TAT, other promising CPPs include the BBB-translocating polyR (usually 8 or 9 arginine units) (Futaki et al., 2001; Mitchell et al., 2000; Gotanda et al., 2014; Pham et al., 2005) and motifs that selectively facilitate cerebral uptake, such as CPPs derived from trypanosomes (Goto et al., 2011) or zika viruses (Jun et al., 2017). As an alternative to injections and BBB passage, intranasal application of liposomes, allowing the cerebral transport of drug-loaded or -conjugated liposomes through the olfactory bulb and trigeminal nerves, has successfully been attempted. These early efforts need refinement, however (Zheng et al., 2015).

To improve the functionality of liposomes, the lipid composition may be adjusted. For example, the incorporation of cholesterol favours increased vesicle stability (Briuglia et al., 2015). Another common modification is the inclusion of polysaccharides, such as polyethylene glycol (PEG), to bestow useful "stealth" properties on liposomes. PEGylation, due to the adsorption of water molecules to PEG chains, generates a water coat, which protects the lipid vesicles from phagocytic clearance in the blood stream. This extension in the circulation time of PEGylated liposomes elevates their chance of BBB transcytosis (Ross et al., 2018; Veronese and Mero, 2008). Also, for more than 20 years, PEG has been a popular linker lipid for the conjugation of therapeutic compounds or CPPs to liposomes (Zalipsky, 1995).

1.4.4. Development of peptide inhibitor nanoparticles (PINPs) for the treatment of Alzheimer's disease

In order to potentially avoid injections and administer our Aβ aggregation inhibitor peptide via a nasal spray, RI-OR2 was conjugated to liposomes as nanocarriers (Gregori et al., 2017). Strikingly, these peptide-liposomes conjugates that our group named peptide inhibitor nanoparticles (PINPs) were 400-fold more potent in inhibiting the aggregation of recombinant $A\beta_{1-42}$ than free RI-OR2 peptide. Furthermore, PINPs crossed an *in vitro* BBB model, traversed the BBB of WT mice and improved object recognition memory in the Tg2576 mouse model of AD (Gregori et al., 2017).

Similarly, the inclusion of an additional cysteine residue and use of click chemistry allowed the covalent linkage of our Tau aggregation inhibitor peptide RI-AG03-polyR to liposomes (Figure 1.21A&B) (Mason and Thordarson, 2016). Our group subsequently showed that RI-AG03-conjuagted liposomes were 40-fold more effective in blocking heparin-induced $Tau_{\Delta 1\text{-}250}$ aggregation compared to the non-linked peptide *in vitro* (Aggidis A. et al., 2021).

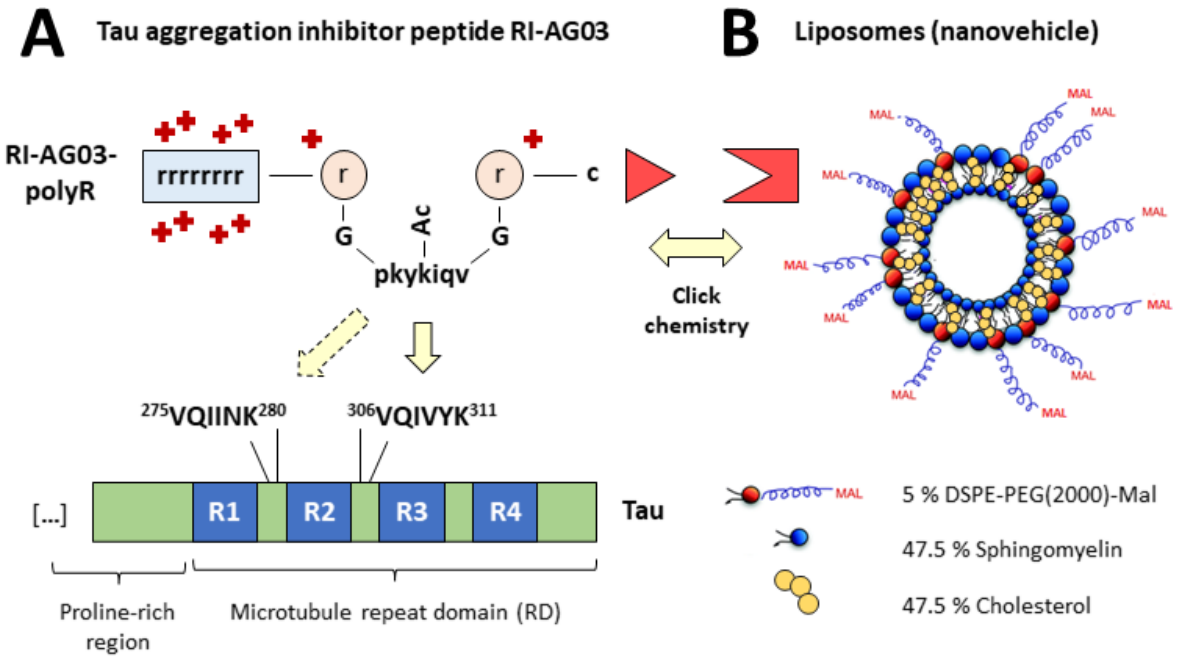

Figure 1.21: Properties of RI-AG03-polyR and liposomes. (A) Illustration of RI-AG03 and association with Tau. The peptide predominantly consists of D-amino acids (small cases) and was retro-inverted to prevent proteolytic breakdown. Computational modelling confirmed that RI-AG03 binds with its Tau-interacting sequence ('p-k-y-k(Ac)-i-q-v') to the aggregation-implicated ^{306}VQIVYK^{311} motif in R3 (spacer region) of Tau (Aggidis A. et al., 2021; von Bergen et al., 2001). Interestingly, an association of the peptide with the pathological ^{275}VQIINK^{280} sequence in R2 of 4R Tau isoforms was predicted (Aggidis A. et al., 2021). Positive charge imparted by arginine residues flanking the Tau-interacting sequence in RI-AG03 prevent self-oligomerisation (Aggidis A. et al., 2021; Mamsa and Meloni, 2021), whilst the addition of a cationic polyR sequence facilitates BBB translocation and cellular uptake (Futaki et al., 2001; Mitchell et al., 2000; Gotanda et al., 2014; Pham et al., 2005; Juliano et al., 2008). Synthesis of RI-AG03 with an additional cysteine enables covalent peptide conjugation to DSPE-PEG(2000)-Mal in liposomes via click chemistry (Mason and Thordarson, 2016). (B) Liposome composition. Liposomes serve as nanocarriers for the peptide and consist of the depicted relative molar lipid ratios. Partially modified from Chandrasekaran et al. (2014).

1.5. Project aims

To build on our previous results, the overarching experimental aims of my dissertation were as follows:

(i) Test the Tau aggregation inhibitor peptide RI-AG03, either in its free or liposome-conjugated form, in suitable cell and animal models of Tauopathy.

(ii) Determine how RI-AG03-conjugated liposomes enter neurons and their subcellular localisation relative to pathologic Tau in the cytoplasm. As such, I investigated the internalisation mechanisms and intraorganellar trafficking of unconjugated and peptide-conjugated liposomes *in vitro*. Furthermore, I aimed to characterise any differences between the polyR and TAT CPPs in relation to peptide uptake and distribution.

Ultimately, the intention of our group is to develop a multi-functional therapy for AD, combining both RI-OR2-TAT- and RI-AG03-polyR-conjugated liposomes, and to facilitate the subsequent transition into clinical trials.

2. Material and Methods

2.1. Materials

2.1.1. Solutions

Table 2.1: Standard buffer compositions. All buffer components were from Merck (Feltham, UK).

Buffer (1x)	Composition
Phosphate-buffered saline (PBS)	137 mM NaCl 2.7 mM KCl 20 mM Na_2HPO_4 1.8 mM KH_2PO_4 pH = 7.4
Tris-HCl	50 mM Tris base pH = 7.6
Tris-HCl-EDTA (TE)	10 mM Tris base 1 mM EDTA pH = 8
Tris-buffered saline (TBS)	50 mM Tris base 150 mM NaCl pH = 7.6
Tris Borate EDTA (TBE)	90 mM Tris base 90 mM boric acid 2 mM EDTA

2.1.2. Plasmids

pCMV-Tet3G, pIRESneo3 and pTRE3G-mCherry vectors as well as Linear Hygromycin Marker were purchased from Takara Bio Europe (Saint-Germain-en-Laye, France). pTRE3G-mCherry_ Tau_{441} P301L, which was pTRE3G-mCherry containing full length (2N4R) Tau with the P301L mutation and mCherry under the control of the doxycycline-regulated P_{TRE3GV} promoter (Takara Bio Europe), as well as

pIRESneo3_Tet-On 3G, consisting of pIRESneo3 containing the CMV promotor-regulated and constitutively expressed Tet-On 3G gene (derived from pCMV-Tet3G) in its multiple cloning site, were synthesised by Epoch Life Science, Inc (Missouri City, USA). The sequences of the constructed vectors and the gene of Tau are given in the Appendix (section 9.1).

2.1.3. Reagents

Table 2.2: Primary and secondary antibodies used for western blotting

Antibody target	Species	Epitope	Dilution	Catalogue no.	Supplier
Tau	Rabbit	*E. coli*-expressed human $Tau_{243-441}$	1:1000 (1:50)	A0024	Dako/Agilent, Cheadle, UK
Phospho-Tau	Mouse	Purified human PHF phospho-Tau (Ser^{202} & Thr^{205}; AT8)	1:500	MN1020	Invitrogen/ Thermo Fisher Scientific, Loughborough, UK
Synaptophysin	Rabbit	Ala_{230} of human recombinant synaptophysin	1:1000	5461	Cell Signaling Technology, Danvers, USA
Postsynaptic density protein-95 (PSD-95)	Rabbit	Gln_{53} of human recombinant PSD-95	1:1000	3450	Cell Signaling Technology
Caspase-3	Rabbit	p20 subunit of human recombinant caspase-3	1:1000	14220	Cell Signaling Technology
Beclin 1	Rabbit	Thr_{72} of human recombinant Beclin-1	1:1000	3495	Cell Signaling Technology
LC3A/B	Rabbit	Leu_{44} of human recombinant LC3B protein (conserved in LC3A)	1:1000	12741	Cell Signaling Technology

Antibody target	Species	Epitope	Dilution	Catalogue no.	Supplier
SQSTM1/p62	Rabbit	Residues surrounding the C-terminus of human recombinant SQSTM1/p62	1:1000	39749	Cell Signaling Technology
IBA1	Rabbit	Ala_{139} of human recombinant IBA1	1:1000	17198	Cell Signaling Technology
Glial fibrillary acidic protein (GFAP)	Rabbit	Asp_{395} of human recombinant GFAP	1:1000	12389	Cell Signaling Technology
Anti-rabbit IgG, HRP-linked Antibody	Goat	Primary rabbit antibodies	1:2000	7074	Cell Signaling Technology
Anti-mouse IgG, HRP-linked Antibody	Horse	Primary mouse antibodies	1:1000	7076	Cell Signaling Technology
F(ab')2 Anti-Rabbit IgG H&L (10nm Gold)	Goat	Primary rabbit antibodies	1:20	ab39601	Abcam, Cambridge, UK

Table 2.3: Cell organelle stains. All were from Invitrogen/Thermo Fisher Scientific.

Reagent	Stained cell organelle	Excitation/emission [λ]	Manual
LysoTracker™ Deep Red	Lysosomes	647/668 nm	(Thermo_Fisher_Scientific_Inc, 2013)
pHrodo™ Red Dextran	Macropinosomes	565/585 nm	(Thermo_Fisher_Scientific_Inc, 2012)
CellLight™ Plasma Membrane-RFP	Cell Membrane	555/584 nm	(Thermo_Fisher_Scientific_Inc, 2014)
CellLight™ Early Endosomes-RFP	Early endosomes	555/584 nm	(Thermo_Fisher_Scientific_Inc, 2014)
CellLight™ ER-RFP	ER	555/584 nm	(Thermo_Fisher_Scientific_Inc, 2014)
CellLight™ Golgi-RFP	Golgi	555/584 nm	(Thermo_Fisher_Scientific_Inc, 2014)
Cholera Toxin Subunit B (Alexa Fluor 594 Conjugate)	Lipid rafts	590/617 nm	/
HCS LipidTOX™ Red Neutral Lipid Stain	Caveosomes	637/655 nm	(Molecular Probes, 2006)

2.2. Methods

2.2.1. Bacterial transformation

To bulk up plasmid DNA (section 2.1.2), XL1-Blue Competent Cells (Agilent Technologies, Cheadle, UK) were thawed on ice. 20 µl of the competent cells were mixed with 0.3 µl of 1.42 M β-mercaptoethanol, incubated for 10 min on ice and gently shaken every 2 min. 100 ng of the transfection vector was added, the mixture incubated for another 15 min on ice, placed in a 42 °C heat block for 45 sec and chilled on ice for 2 min.

2.2.2. Bacterial culture

Transformed bacteria were plated on LB agar plates consisting of LB broth with agar (Miller; composed of 15 g/L agar, 10 g/L NaCl, 10 g/L tryptone and 5 g/L yeast extract) containing 100 µg/mL ampicillin (both Merck) and incubated overnight at 37 °C. Colonies were picked, transferred into 3 mL LB broth (Miller; composition as above without agar) (Merck) containing 100 µg/mL ampicillin in 15 mL Falcon tubes and cultivated overnight at a 45 ° angle at 37 °C under constant shaking. 0.5 mL of the bacterial culture was aseptically added into an autoclaved and foil-covered 250 mL shaking flask containing 50 mL LB broth (Miller) with 100 µg/mL ampicillin and grown at 250 rpm and 37 °C on an orbital shaker for another night.

2.2.3. Plasmid purification

Bacteria were then harvested by centrifugation at 6500 g for 20 min using a JA-20 rotor in a Avanti J-26S centrifuge (Beckman Coulter, High Wycombe, UK). The resulting pellet, containing the plasmid, was purified with the QIAGEN Plasmid Midi Kit (Qiagen, Manchester, UK) according to the manufacturer's instructions (QIAGEN, 2016).

2.2.4. Agarose gel electrophoresis

DNA samples as well as GeneRuler 100 bp DNA Ladder (100 - 1000 bp; Thermo Fisher Scientific, Loughborough, UK) were resolved on a 1 % (w/v) agarose gel in 0.5x TBE containing a final concentration of 1x GelRed® Nucleic Acid Stain (Millipore) for 1 h and visualised using the ChemiDoc™ Imaging System (Bio-Rad, Kidlington, UK).

2.2.5. Plasmid linearisation and ethanol precipitation

Prior to mammalian cell transfection, pIRESneo3_Tet-On3G and pTRE3G-mCherry_ Tau_{441} P301L vectors (30 µg) were linearised at 37 °C overnight by incubating with 5 µl New England Biolabs (NEB) Buffer™ (10 x), 1 µl PvuI (10 U/µl) (both NEB, Hitchin, UK), and 0.5 µl acetylated bovine serum albumin (BSA; 10 µg/mL; Promega, Southampton, UK) diluted to a total of 50 µl with distilled water. The following morning, 5 µL of 3 M sodium acetate (pH 5.2; Merck) and 100 µL cold absolute ethanol (VWR, Soulbury, UK) were added to the digests, which were then incubated at -20 °C for 1 h. The digests were then centrifuged at max speed (~17,000 g) for 5 min, washed with 80 % (v/v) cold absolute ethanol at max speed for 20 min and the DNA pellet resuspended in sterile distilled water in a laminar flow hood.

2.2.6. Mammalian cell culture

Human neuroblastoma SH-SY5Y cells were purchased from ATCC® (CRL-2266; Manassas, USA). The Tau RD (V337M/P301L)-enhanced yellow fluorescent protein (EYFP)-expressing HEK293 cell line, referred to throughout this thesis as Clone 9 HEK293 cells, was kindly supplied by Marc Diamond (UT Southwestern Medical Center, Dallas, USA) (Sanders et al., 2014).

SH-SY5Y cells were maintained in Dulbecco's Modified Eagle Medium (DMEM)-F12 (Gibco/Thermo Fisher Scientific, Warrington, UK) containing 10 % (v/v) heat-inactivated fetal bovine serum (FBS) and

1 % (v/v) antibiotic-antimycotic solution (both Merck) at 37 °C and with 5 % (v/v) CO_2. In the case of Clone 9 (HEK293) cells, the culture method was identical to that of SH-SY5Y cells except that DMEM was used in place of DMEM-F12. Clone 4 SH-SY5Y cells co-inducible for the expression of 2N4R Tau (P301L) and mCherry (selection process described below) were cultured as for normal SH-SY5Y, except for the use of Tet System Approved FBS (Takara Bio Europe) instead of normal FBS. Specifically to investigate the impact of Dox treatments on endogenous Tau expression and cell viability (section 3.1 and 9.2), SH-SY5Y cells were also cultured in DMEM-F12 containing Tet System Approved FBS. In order to induce the expression of 2N4R Tau (P301L) in Clone 4 SH-SY5Y cells, a final concentration of 500 ng/mL doxycycline hyclate (Dox) (Merck) was added to the culture medium. The Dox-containing medium was renewed every 48 h.

In order to passage cells, the medium was removed, the flask washed with PBS and cells were detached using 1x Trypsin-EDTA solution (Merck). The cells were then incubated at 37 °C and 5 % (v/v) CO_2 for ~5 min. Trypsin was inactivated with the addition of an equal amount (v/v) of growth medium. The cells were transferred into 50 mL Falcon tubes and centrifuged at 500 g for 5 min. The supernatant was removed, the cell pellet re-suspended in the respective growth medium (composition as explained above) and cells were seeded at ~10 - 20 % confluency into fresh T75-flasks for maintenance. Alternatively, cells were seeded at the indicated concentrations to conduct the experiments.

To freeze cells for long-term storage, the cell pellet was resuspended in 2 mL freezing medium (growth medium containing 10 % (v/v) dimethyl sulfoxide (DMSO; Scientific Laboratory Supplies, Nottingham, UK)), pipetted into 2 mL cryogenic vials, placed into a Corning® CoolCell™ FTS30 Cell freezing container (both Corning, Loughborough, UK) and frozen at -80 °C overnight. The next day, cryogenic vials were transferred into liquid nitrogen storage containers.

For cell resurrection, cryogenic vials were removed and promptly defrosted in a water bath at 37 °C. Once defrosted, the cells were transferred into 20 mL pre-warmed growth medium in 50 mL Falcon

tubes, centrifuged at 500 g for 5 min, the supernatant decanted and the cell pellet resuspended in fresh growth medium pre-warmed to 37 °C. All cell work was conducted in a sterile laminar flow hood.

2.2.7. Stable transfection

SH-SY5Y cells were cultured to confluency in T75-flasks, transfected with 30 µg linearised pIRESneo3_Tet-On3G via electroporation (square wave, 120 V, 25 msec, 2 mm path width; Gene Pulser Xcell™, Bio-Rad) and selected with 500 µg/mL G418 (Takara Bio Europe). Selection medium containing G418 was renewed every 2-3 days. Once the cells had reached confluency, they were sub-cultured into fresh T75-flasks in fresh 500 µg/mL G418-containing growth medium and grown to confluency a second time.

The resulting stably transfected cells, SH-SY5Y_Tet-On3G, were then co-transfected as described above with linearised 30 µg pTRE3G-mCherry_Tau_{441} P301L and 1.5 µg Linear Hygromycin Marker. In this case, normal FBS in the growth medium was replaced with tetracycline-free Tet System Approved FBS (Takara Bio Europe) and 150 µg/mL Hygromycin B (Gibco/Thermo Fisher Scientific) was added as selection antibiotic. From this point onwards, polyclonal SH-SY5Y_Tet-On3G_Tau_{441} P301L cells were maintained in tetracycline-free growth medium.

2.2.8. Reverse transcription-polymerase chain reaction (RT-PCR) for confirmation of Tet-On 3G expression in transfected SH-SY5Y cells

Successful expression of Tet-On 3G was confirmed in SH-SY5Y_Tet-On3G cells by RT-PCR. RNA was purified using the E.Z.N.A.® Total RNA Kit I (Omega Bio-Tek, Norcross, Georgia) according to the manufacturer's instructions (Omega_Bio-Tek, 2022). Prior to elution, DNA was removed through

incubation of the purification column membrane with DNase I solution (Thermo Fisher Scientific) for 20 min on ice. RNA was then eluted in RNAse-free water.

RT-PCR on the purified RNA was performed using a forward primer, 5'-ATGTCTAGACTGGACAAGAGCAA-3' and a reverse primer, 5'-TTACCCGGGGAGCATGTC-3' (both Eurofins Genomics, Ebersberg, Germany). Using 4 μg of purified RNA from pIRESneo3 (empty vector)- or pIRESneo3_Tet-On3G-transfected SH-SY5Y cells, RNA eluent (RNAse-free water; negative control) and 45 μM of each forward and reverse primers (final concentrations 0.9 μM each; 746 bp amplicon), RT-PCR was carried out using the Titanium® One-Step RT-PCR Kit (Takara Bio Europe) according to the manufacturer's instructions (Takara_Bio_Europe, 2011) and using the conditions detailed in Table 2.3. As an additional positive control, 1 μg mouse liver total RNA and 45 μM of each control mouse β-actin forward and reverse primers (final concentrations 0.9 μM each; 540 bp amplicon) supplied with the E.Z.N.A.® Total RNA Kit I (Omega Bio-Tek) were used as instructed. All amplified samples were subsequently run on agarose gels.

Amplification of RNA derived from pIRESneo3_Tet-On3G-transfected SH-SY5Y cells with Tet-On 3G primers produced the expected 746 bp amplicon, thus confirming expression of Tet-On 3G (Appendix, lane 3, Figure 9.1).

Table 2.4: Parameters for RT-PCR amplification of Tet-On 3G

Stage	Number of cycles	Temperature	Duration
1	1	50 °C	1 h
2	1	94 °C	15 min
3	40	94 °C	30 sec
		60 °C	30 sec
		72 °C	60 sec
4	1	72 °C	5 min
5	Hold	4 °C	/

2.2.9. Flow cytometry confirmation of mCherry expression

Dox-induced SH-SY5Y cells transfected as described in section 2.2.7 along with uninduced controls were grown to confluency, trypsinized, washed with 1x PBS, resuspended in 1x PBS and analysed with a CytoFLEX flow cytometer (mCherry $\lambda_{Ex/Em}$ = 587/610 nm) and CytExpert software (both Beckman Coulter, High Wycombe, UK). Cell debris was removed through consistent gating across samples. Fold-changes in the median cellular fluorescence intensity between mCherry-expressing and non-expressing cells and the % of fluorescing cells (Dox-induced mCherry expression) were determined to verify the suitability of polyclonal SH-SY5Y_Tet-On3G_Tau_{441} P301L cells for monoclonal cell line selection. Flow cytometry confirmed that 6.36 % and 7.01 % of analysed SH-SY5Y_Tet-On3G_Tau_{441} P301L cells exhibited mCherry expression following Dox-induction for 24 h and 96 h, respectively (Appendix, Figure 9.2C&D).

2.2.10. Selection of monoclonal cell lines by limiting dilutions

Polyclonal SH-SY5Y_Tet-On3G_Tau_{441} P301L cells were diluted to 1 cell per well in 96-well plates in growth medium containing tetracycline/Dox-free Tet System Approved FBS (Takara Bio Europe) and 150 µg/mL Hygromycin B (Gibco/Thermo Fisher Scientific). Wells were visually screened for colony appearance 14 days after seeding and the medium was exchanged as soon as single, outgrowing cells were discovered (every 7 - 14 days). Expression of mCherry was induced by supplementing the Tet System Approved FBS (Takara Bio)-containing growth medium with 500 ng/µL Dox (Merck) for 24 h and wells containing univocally red fluorescing cells were identified using confocal microscopy (ZEISS LSM880; Zeiss, Cambridge, UK). Five mCherry-positive clones, including Clone 4 SH-SY5Y cells used in the experiments, were detected, passaged and analysed for Tau expression in the presence of 500 ng/µL Dox via western blotting (section 2.2.16).

2.2.11. Peptide synthesis

RI-AG03-polyR ("c-r-r-r-r-r-r-r-r-G-p-k-y-k(Ac)-i-q-v-G-r-NH_2"), scrambled RI-AG03-polyR ("c-r-r-r-r-r-r-r-r-G-v-y-k-i-k(Ac)-p-q-G-r-NH_2"), RI-AG03-TAT ("c-r-r-r-q-r-r-k-k-r-G-y-G-p-k-y-k(Ac)-i-q-v-G-r-NH_2"), 6-carboxyfluorescein (6-FAM)-RI-AG03-polyR and 6-FAM-RI-AG03-TAT were synthesised by Severn Biotech Ltd (Kidderminster, UK). Cyanine-5 (Cy5)-RI-AG03-polyR was from Cambridge Peptides Ltd (Cambridge, UK). To allow liposome linkage, all peptides contained an additional cysteine (Mason and Thordarson, 2016). The peptides contained D-amino acids (as denoted by lower cases) except for glycine, because this amino acid does not possess a D-enantiomer.

2.2.12. Preparation of liposomes and click chemistry attachment of RI-AG03

Liposomes were made by dissolving relative molar proportions of the following lipids in chloroform (all Avanti Polar Lipids, Inc, Alabaster, USA): 47.5 % SM (egg-derived), 47.5 % cholesterol (plant-

derived) and 5 % 1,2-distearoyl-sn-glycero-3-phosphoethanolamine-N-[maleimide(polyethylene glycol)-2000] (DSPE-PEG(2000)-Mal). For the visualisation of liposomes via immunocytochemistry, 2 % of the cholesterol was replaced with TopFluor® (BODIPY) cholesterol (Avanti Polar Lipids, Inc.). The lipid mixture was dried under liquid nitrogen and the film resuspended in PBS using a water bath sonicator set to 37 °C for 15 min, or until fully dissolved. The mixture was then subjected to five freeze-thaw cycles in liquid nitrogen and extruded 11 times using a Mini-Extruder (Avanti Polar Lipids Inc.) with 0.1 µm Nuclepore™ Polycarbonate Track-Etched Membranes (Whatman, Maidstone, UK) and Hamilton 1000 µL Syringes (Avanti Polar Lipids Inc.), as described by Avanti Polar Lipids (Lipids).

Because DSPE-PEG(2000)-Mal is randomly incorporated into liposomes, with the maleimide group facing either inwards or outwards, approximately half of DSPE-PEG(2000)-Mal used is bioactive. For example, Oswald et al (2016) showed that ~63 % of DSPE-PEG(2000)-Mal in their liposomes was conjugation-competent. In the case of our liposomes, which contain 5 % DSPE-PEG(200)-Mal, this suggests that ~2.5 % of lipids can be used for peptide conjugation. To attach the cysteine residue of RI-AG03 to available DSPE-PEG(2000)-Mal chains via click chemistry (Mason and Thordarson, 2016), extruded liposomes were incubated in the presence of excess molar proportions of peptide equivalent to the molar concentration of DSPE-PEG(2000)-Mal (i.e. 2.5 %) x 1.2 for 2 h at 37 °C. The mixture was vortexed once after 1 h and rocked on a plate shaker at room temperature overnight. Unbound peptide was removed by ultracentrifugation for 1 h at 172,000 g (4 °C) and the liposome pellet was then resuspended in 1x PBS by using a water bath sonicator at 37 °C and three 15 min sonication cycles with vortexing in between cycles. To remove any potential liposome clumps for flow cytometry, the liposomes were centrifuged at max speed (~17,000 g) in a benchtop centrifuge for 4 min, using 0.22 µm Corning® Costar® Spin-X® centrifuge tube cellulose acetate filters (Corning).

2.2.13. Measurement of liposome concentrations

To determine the concentration of extruded liposomes, a modified version of the LabAssay™ Phospholipid kit (FUJIFILM Wako Shibayagi Corporation, Richmond, USA) was applied. Extruded liposomes in 1x PBS were mixed at a ratio of 1:1 (v/v) with a solvent mixture consisting of 65% (v/v) methanol (VWR), 33 % (v/v) chloroform (VWR) and 2 % v/v sodium dodecyl sulfate (SDS) (Merck; using 20 % (w/v) SDS dissolved in PBS as stock solution). Samples were incubated in a heat block at 72 °C for 15 min, then sonicated at 72 °C for 5 min in a water bath sonicator. 2 µL of the samples, the standard solution supplied with the LabAssay™ Phospholipid kit, a blank control solution (solvent mixture and distilled water) and BSA diluted in blank control solution (ranging from 0.2 to 1.5 mg/mL, w/v) each were pipetted in triplicates into 96-well plates. The chromogenic substrate was then added to each well and the plates were shaken for 20 - 30 sec prior to incubation at 37 °C for 5 min. The plate was then measured at 600 nm and 700 nm with an Infinite M200 Pro plate reader (Tecan UK ltd., Reading, UK). Blanks and reference wavelength measurements (700 nm) were subtracted from the sample measurements, a standard curve (in mg/mL) was calculated using the corrected BSA absorbance values and sample concentrations were estimated. Finally, the sample concentrations (mg/mL) were converted to molar concentrations.

As the assay results reflected the phospholipid content in liposomes (representing the 47.5 % SM and 5 % DSPE-PEG(2000)-Mal contents of the liposomes), equation 1 (see below) was used to determine the molar liposome concentration. In this context, the molar concentration of SM in liposomes was equal to cholesterol (both 47.5 %). For simplicity, even though only the DSPE moiety represents a phospholipid, DSPE-PEG(2000)-Mal (5 %) was considered as a full phospholipid.

Equation 1: $[c\ (cholesterol) * 2] + \frac{c\ (cholesterol) * 0.05}{0.475} = c\ (liposomes)$

2.2.14. Cell lysis and separation of soluble and insoluble Tau

Cells were trypsinized, washed twice with PBS, resuspended in native lysis buffer (Abcam, Cambridge, UK) containing 1x Halt™ Protease and Phosphatase Inhibitor Cocktail (Thermo Fisher Scientific), left on ice for 30 min and subjected to a freeze-and-thaw cycle. The cell lysate was clarified by sequential centrifugations at 500 g and 1000 g for 5 min each and the supernatant was retained as total lysate, which contains both soluble and insoluble Tau. In order to separate soluble and insoluble Tau, the total cell lysate was ultracentrifuged at 100,000 g for 1 h at 4 °C and the supernatant collected as the soluble Tau-containing fraction (Sanders et al., 2014).

2.2.15. Protein assay

The DC™ Protein Assay Kit II (Bio-Rad) was used according to the manufacturer's instructions (Bio-Rad, 2022) in order to quantify the protein concentrations of the lysate samples, using BSA (Merck) diluted to 0.2 - 1.5 mg/mL in distilled water (w/v) as a standard curve. Lysates were then aliquoted and kept at -20 °C until use in western blots (section 2.2.16).

2.2.16. Sodium dodecyl sulfate polyacrylamide gel electrophoresis (SDS-PAGE) and western blotting

Samples diluted to 20 µg total protein with distilled water were mixed at a 1:3 ratio with 4x Laemmli Sample Buffer (Bio-Rad) and boiled for 10 min at 100 °C. 8 µL Precision Plus Protein™ All Blue Prestained Protein Standard (10 - 250 kDa; Bio-Rad) and protein samples were loaded into wells of Any kD™ Mini-PROTEAN® TGX Stain-Free™ Protein Gels (Bio-Rad) which were then run in Tris/Glycine/SDS buffer (diluted with distilled water from a 10x stock; Bio-Rad) at 130 V for 1 h at room temperature. Total protein bands in the gel were activated with the 'stain-free gel' setting, for 1 min, in the ChemiDoc™ Imaging System (Bio-Rad).

For immunoblotting, proteins were transferred to 0.2 µm nitrocellulose membranes (Bio-Rad) via the semi-dry 'mixed MW' program of a Trans-Blot Turbo Transfer Systems (Bio-Rad). Using the ChemiDoc™ Imaging System, the total protein levels on the membranes were visualised for later total protein normalisation. Membranes were then blocked in TBST (TBS containing 0.1 % (v/v) Tween20; Merck) containing 5 % (w/v) skimmed milk powder or, when primary phospho-antibodies were employed, 5 % (w/v) BSA (Merck), for 1 h at room temperature. Then, the blocking solution was decanted, fresh blocking solution containing the diluted primary antibodies, as shown in Table 2.1, was added and the membranes were incubated with constant agitation at 4 °C overnight. The following morning, blots were washed three times with TBST for 5 min at room temperature, then probed with secondary antibodies diluted in blocking solution (Table 2.1) for 1 h at room temperature. Membranes were then washed three times with TBST for 5 min, exposed to ECL™ Select Western Blotting Detection Reagent (Cytiva, Cardiff, UK; an equal amount of luminol solution A and peroxide solution B) and developed for 5 min. The membrane was then immediately visualised with the ChemiDoc™ Imaging System using ImageLab™ software (Bio-Rad).

In addition to total protein normalisation, to compare samples from different blots, an inter-gel control (IGC) was run on every gel and all samples on the same gel/blot normalised to it. This IGC was the lysate of untreated, untransfected SH-SY5Y cells or untreated Clone 4 SH-SY5Y cells (chapter 3), Clone 9 HEK293 cells (chapter 4) or the brain homogenate of a PBS-injected PS19 mouse (chapter 6).

2.2.17. Flow cytometry to quantify liposome uptake

SH-SY5Y cells were seeded at a density of 350,000 cells per well in 12-well plates and allowed to settle in an incubator overnight (37 °C with 5 % (v/v) CO_2). Cells were treated with a final concentration of 75 µM BODIPY-liposomes, RI-AG03-polyR-BODIPY-liposomes or RI-AG03-PolyR-BODIPY-liposomes for 4 h. To investigate the primary endocytosis pathways, vehicle solution (DMSO,

Scientific Laboratory Supplies) or a final concentration of 10 µM chlorpromazine hydrochloride (clathrin-mediated endocytosis (CME) inhibitor), 7.5 µM cytochalasin D (macropinocytosis and partial CME and caveolae-mediated endocytosis (CavME) inhibitor), 5 µg/mL filipin III from streptomyces filipinensis (CavME inhibitor) or 50 µM 5-(N-Ethyl-N-isopropyl)amiloride (EIPA; macropinocytosis inhibitor) (all from Merck) dissolved in DMSO were added 30 min prior to the liposomes and the cells then co-incubated with the liposomes for 4 h at 37 °C. All incubations were performed in triplicates. Cells were then trypsinized, pelleted and resuspended in 1 mL 1x PBS. An equal volume of 4 % (w/v) paraformaldehyde (PFA; Merck) in 1x PBS was added for a final concentration of 2 % PFA and the cells were fixed for 30 min at 4 °C in the dark. The median cellular fluorescence (fluorescein isothiocyanate (FITC) filter set; $\lambda_{Ex/Em}$ = 490/525 nm) following the uptake of BODIPY-liposomes, as compared to untreated cells, was quantified using flow cytometry (CytoFLEX; Beckman Coulter, High Wycombe, UK) and CytExpert software (Beckman Coulter) with a minimum cell count of 10,000 cells. Consistent gating across samples was applied to remove cell debris.

2.2.18. Immunocytochemistry and image analysis

150,000 SH-SY5Y cells were seeded onto poly-L-lysine coated coverslips and allowed to adhere overnight. The next day, to monitor intracellular trafficking of fluorophore-labelled RI-AG03 peptides with either a polyR or TAT CPP (6-FAM-RI-AG03-polyR and 6-FAM-RI-AG03-TAT peptides), fluorescent liposomes (unconjugated BODIPY-liposomes), fluorescent liposomes conjugated to RI-AG03 (RI-AG03-polyR-BODIPY-liposomes or RI-AG03-TAT-BODIPY-liposomes), liposomes linked to fluorophore-labelled RI-AG03 peptides (6-FAM-RI-AG03-polyR-liposomes or 6-FAM-RI-AG03-TAT-liposomes) and dual fluorescing peptide-liposomes (Cy5-RI-AG03-polyR-BODIPY-liposomes), SH-SY5Y cells were treated with the latter constructs for 16 h at 37 °C and 5 % (v/v) CO_2. To assess co-localisation of the peptides, liposomes and peptide-liposomes with various cell organelles, the cell

organelle stains listed in Table 2.2 (section 2.1.3) were used according to the referenced manufacturer's instructions. To co-stain for lipid rafts, cells were washed twice in ice-cold 1x PBS, immersed in 1x PBS containing the aforementioned fluorescent peptides or liposome constructs as well as 20 µg/mL Cholera Toxin Subunit B (Alexa Fluor 594 Conjugate) (Invitrogen/Thermo Fisher Scientific) and left on ice for 30 min. The cells were then washed in 1x PBS, fixed in 4 % (w/v) PFA (Merck) in 1x PBS (4 °C, 30 min) and mounted with ProLong™ Diamond Antifade Mountant containing DAPI (Invitrogen/Thermo Fisher Scientific). The coverslips were subsequently sealed with nail varnish and stored at 4 °C in the dark. To show that HCS LipidTOX™ Red Neutral Lipid Stain (Invitrogen/Thermo Fisher Scientific) is unsuitable due to staining both caveosomes and internalised liposomes (see Appendix, chapter 9.5), coverslips with PFA-fixed and treated SH-SY5Y cells were kept in 24-well plates and immersed into 500 µL 1x LipidTOX™ Deep Red Neutral Lipid Stain diluted in PBS. Plates were sealed and incubated for 30 min at room temperature, without any further washing.

To investigate the intracellular co-localisation of the peptide and peptide-liposomes with Tau RD (P301L/V337M)-EYFP, Clone 9 cells were seeded onto coverslips in 24-well plates and incubated with Cy5-RIAG03-polyR or Cy5-RIAG03-polyR-liposomes for 2 h or 16 h. Cells were fixed, mounted and stored as described above.

Using a 63x oil immersion objective (Plan-APOCHROMAT, 63x/1.40 Oil DIC M27) on a ZEISS LSM880 confocal microscope and ZEN software (both Zeiss, Cambridge, UK), at least three images across separate coverslips were taken for each treatment. To produce representative images comparing SH-SY5Y cell fluorescence following unconjugated BODIPY-liposome, RI-AG03-polyR-BODIPY-liposome or RI-AG03-TAT-BODIPY-liposome treatment, consistent microscope settings for the pinhole size (1 AU), laser strength and gain were applied for the green channel (FITC). Excitation/emission spectra were λ = 365/440 nm (DAPI), λ = 490/525 nm (FITC; for BODIPY, 6-FAM and Tau RD (P301L/V337M)-EYFP) and λ = 651/670 nm (Cy5). The excitation/emission values of each of the cell organelle stains are given in Table 2.2.

To analyse co-localisation between cell organelles (red channel) and drugs (green channel), which was either 6-FAM-RI-AG03-polyR/TAT peptide, BODIPY-liposomes, BODIPY-liposomes conjugated to RI-AG03-polyR/TAT or liposomes conjugated to 6-FAM-RI-AG03-polyR/TAT peptide, the Colocalization Threshold plugin of ImageJ was used. The Costes Method was applied to set intensity thresholds. Pearson's correlation coefficient Rcoloc (a value from -1 to 0 and 1) was subsequently calculated as a measure of co-localisation and interpreted according to Chan YH (none, poor, fair, moderate, very strong and perfect) (Akoglu, 2018). For Tau RD (P301L/V337M)-EYFP aggregate counts and size in Clone 9 cells, Otsu thresholding was applied to the whole images (green channels) to separate aggregates, then analysed using ImageJ. To determine the average number of aggregates per cell, nuclei (DAPI in the respective blue channels) were additionally counted with ImageJ.

2.2.19. Viability and toxicity assays

Cell viability was assessed using Cell Counting Kit 8 (WST-8 / CCK8) (Abcam; (Abcam, 2020)) or the Cell Proliferation Kit I (MTT) (Roche; (Merck, 2022). Cell death was quantified using the CyQUANT™ lactate dehydrogenase (LDH) Cytotoxicity Assay (Invitrogen/Thermo Fisher Scientific; (Thermo_Fisher_Scientific_Inc, 2019)). For all assays, the manufacturers' instructions were followed and colorimetric substrate conversion in the plates was evaluated with an Infinite M200 Pro plate reader (Tecan UK ltd.).

2.2.20. Transmission electron microscopy (TEM)

Soluble and insoluble Tau in Clone 9 HEK293 cell lysate was separated, as described in section 2.2.14. The resulting Tau pellet was resuspended in 30 µL Tris-HCl (50 mM, pH 7.4), after which 15 µL of the resuspension was pipetted onto a 400-mesh Formvar/carbon film-coated copper grid (Merck) and left for 5 min, then washed twice with 10 µL 1x TBS (the droplet was dipped off). A humidified

chamber was assembled by placing a wet Kimwipe, overlayed by a piece of parafilm, into a Petri Dish. 100 µL blocking buffer (2 % (w/v) skimmed milk powder in 1x TBST) was pipetted onto the parafilm and the grid floated on the droplet (sample side down) for 1 h at room temperature. The grid was then transferred onto a droplet containing primary rabbit anti-Tau antibody (1:50; Dako/Agilent) diluted in blocking solution, the humidified chamber was sealed and the sample incubated overnight at 4 °C. The grid was washed twice by placing on a 1x TBST droplet (100 µL) for 5 min, sequentially rinsed with 10 µL of each 1x TBST and distilled water (by adding and dipping the liquids off) and then incubated on a 100 µL droplet consisting of secondary Goat F(ab')2 Anti-Rabbit IgG H&L (10nm Gold) (1:20; Abcam) diluted in blocking solution for 1 h at room temperature. The grid was then washed with 10 µL 1x TBST and distilled water each. 10 µL of 2 % (w/v) phosphotungstic acid (Merck) diluted in distilled water was added to the grid and incubated at room temperature for 2 min, the excess was then dipped off and the grid flushed with 10 µL distilled water. The grid was subsequently subjected to TEM, with images taken at 200,000x magnification, using a Jeol JEM-1010 electron microscope (Jeol UK ltd, Welwyn Garden City, UK).

2.2.21. Animals

Wild-type mice (C57BL/6NJ; strain #005304), abbreviated to WT mice throughout, and 1N4R Tau (P301S)-transgenic PS19 mice (B6N.Cg-Tg(Prnp-MAPT*P301S)PS19Vle/J; strain #024841) (Yoshiyama et al., 2007), abbreviated to PS19 mice throughout, were purchased from The Jackson Laboratory (Bar Harbor, USA). Animals were group housed (4 - 6 per cage) under standard conditions (individually ventilated cages, 21 °C, 45 - 65 % humidity, 12 h:12 h dark/light cycle, lights on at 07:00) with food and water access ad libitum. Animal experiments were carried out in compliance with the UK Animals (Scientific Procedures) Act 1986 and approved by the Lancaster University Animal Welfare and Ethics Review Board (AWERB).

2.2.22. Genotyping

Ear notches were collected and incubated in 500 mL digestion buffer (50 mM Tris-HCl, 100 mM EDTA pH 8.0, 100 mM NaCl and 1 % SDS; all Merck) and 50 µL of 1 mg/mL Proteinase K (Merck) overnight at 37 °C. Hair and debris was removed through centrifugation at 13,000 rpm for 5 min. 300 µL isopropanol (VWR) was added to fresh centrifuge tubes, the digests were added, vortexed and the DNA precipitated by leaving the tubes for 15 min at room temperature. DNA was pelleted by centrifugation at 13,000 rpm for 10 min, washed with 300 µL 70 % (v/v) ethanol (VWR) and any traces of ethanol were removed by pipette. DNA was then dissolved by incubation in TE buffer (10 mM Tris-HCl and 1 mM EDTA) for 1 h at 56 °C.

For PCR analysis the following primers were employed: Control forward (5'-CAAATGTTGCTTGTCTGGTG-3'), control reverse (5'-GTCAGTCGAGTGCACAGTTT-3'), MAPT transgenic forward (5'-GGCATCTCAGCAATGTCTCC-3') and MAPT transgenic reverse (5'-GGTATTAGCCTATGGGGGACAC-3'); with corresponding amplicon sizes of 200 bp (WT mice) and ~450 bp (PS19 mice) (The_Jackson_Laboratory, 2022). All primers were synthesised by Eurofins Genomics (Ebersberg, Germany).

For each sample, 9 µL of a master mix consisting of 5 µL Hotshot Diamond (Clent Life Science, Stourbridge, UK) and 1 µL of a 9 µM stock of each of the four primers above dissolved in UltraPure™ DNase/RNase-Free Distilled Water (Invitrogen/Thermo Fisher Scientific; final primer concentrations in master mix 1 µM) was prepared. The 9 µL master mix was then combined with 1 µL DNA sample (diluted 1:70 in distilled water) or blank (digestion buffer) and DNA was amplified using the conditions described in Table 2.4.

Table 2.5: PCR parameters for genotyping

Stage	Number of cycles	Temperature	Duration
1	1	94 °C	2 min
2	14	94 °C	20 sec
		64 °C	20 sec (-0.5 °C per cycle)
		68 °C	10 sec
3	35	94 °C	15 sec
		57 °C	20 sec
		72 °C	10 sec
4	1	72 °C	2 min
5	Hold	4 °C	/

2.2.23. Animal treatments and tissue collection

WT and PS19 mice were split into groups of n = 3 - 6, as outlined in Table 2.5. Notably, PS19 mice were reported to develop glial inflammation and synaptic degeneration at an age of 3 - 6 months, followed by Tau pathology, cognitive impairments and neuronal loss at and beyond 6 months of age (Yoshiyama et al., 2007; Takeuchi et al., 2011; Lasagna-Reeves et al., 2016; Maruyama et al., 2013). Thus, 6 month-old animals were chosen to investigate the effects of peptide treatment in the presence of Tau pathology. Starting at an age of 6 months, animals were injected i.p. with 2.2 mL/kg 1x PBS, 100 nmol/kg RI-AG03-polyR in 1x PBS or 100 nmol/kg scrambled RI-AG03-polyR in 1x PBS every other day for a total of 44 days. The latter peptide dose was informed by our previous *in vivo* studies using unconjugated or liposome-conjugated of the Aβ aggregation inhibitor peptide RI-OR2-TAT (Parthsarathy et al., 2013; Gregori et al., 2017). On the final day, at an age of around ~7.5

months, mice were culled, the brains removed, the individual hemispheres separated and immediately snap-frozen in liquid nitrogen and stored at -80 °C until use.

Table 2.6: Mouse features and groups in the *in vivo* pilot experiments.

Group	Treatment	Mouse ID number	Sex	Total group numbers (n)
WT	1x PBS	M3 M4 M14 M16 M19 M123	F F F F M M	6
	RI-AG03-polyR	M109 M113 M115 M116	F F M F	4
PS19	1x PBS	M5 M6 M7 M8 M110 M120	F M M M M F	6
	RI-AG03-polyR	M111 M114 M117 M124	F M F M	4
	Scrambled RI-AG03-polyR	M112 M122 M125	F M M	3

2.2.24. Mouse brain homogenisation

Snap-frozen mouse brain hemispheres were immersed in radioimmunoprecipitation assay (RIPA) buffer (Merck) in PowerBead Tubes containing ceramic 1.4 mm beads (Qiagen) and homogenised using a FastPrep^{R}-24 (MP Biomedicals, Illkirch Graffenstaden, France) with 3x20 sec pulses at 6.0 m/sec with 30 sec rest intervals between pulses. Brain homogenates were then centrifuged (10,000 g for 10 min at 4 °C) and the supernatants (total lysate) collected. Half of the total lysate fractions were ultracentrifuged at 100,000 g for 1 h at 4 °C to remove insoluble Tau from the soluble fractions, as outlined in section 2.2.14. The protein concentrations of each sample were quantified as detailed in section 2.2.15. Both the total and soluble fractions were aliquoted and stored at -20 °C until use in western blotting.

2.2.25. Statistical and power analysis

Significant differences between groups were determined using one-way, two-way or three-way analysis of variance (ANOVA) followed by Tukey's post-hoc test. Normal distribution was assessed using the Shapiro-Wilk test. In the case that the data was not normally distributed, the nonparametric Kruskal-Wallis test was applied instead of ANOVA. Significance was set at $p < 0.05$ and the corresponding p, F and df values were calculated using JASP (University of Amsterdam, Amsterdam, The Netherlands) and SPSS (IBM, London, UK). Data in all graphs were plotted as group means ± SEM.

In this thesis, if not referred to otherwise, technical replicates (n = 3 - 6), which were separate wells or flasks of cells treated at the same time, were used and analysed. By contrast, three biological (independent experimental) replicates, each with n = 3 technical replicates, were used to determine the uptake of unconjugated and peptide-conjugated BODIPY-liposomes in the absence or presence of endocytosis inhibitors in SH-SY5Y cells (section 5.3.1 and 5.3.2). In this case, the average of the technical replicates (n = 3) from biological replicate 1, 2 and 3 each was analysed using ANOVA.

G*Power was used to calculate effect size (Cohen's f) and power of the *in vivo* pilot experiments, with an assumed α error probability of 0.05 (Faul et al., 2007).

3. Generation and characterisation of a tauopathy cell model for *in vitro* testing of RI-AG03

3.1. Introduction

Previously, we designed and screened multiple Tau aggregation inhibitor peptide candidates for their ability to inhibit the aggregation of recombinant $Tau_{\Delta 1\text{-}250}$.The peptides were modelled to interact with the pro-aggregatory ^{306}VQIVYK^{311} sequence present in all 6 isoforms of Tau (Aggidis A. et al., 2021; De Anda-Hernández et al., 2012). The results showed that the most potent Tau aggregation inhibitor was RI-AG03 ("G-p-k-y-k(Ac)-i-q-v-G-r-NH_2") (Aggidis A. et al., 2021).

Having confirmed the anti-aggregatory effects on recombinant Tau (Aggidis A. et al., 2021), the next objective was to create a suitable cell model of Tauopathy to test RI-AG03. For this purpose, multi-functional SH-SY5Y cells were chosen. SH-SY5Y are a human-derived cell line subcloned from metastatic, bone marrow-originating SK-N-SH neuroblastoma cells (Ross et al., 1983) and have previously been employed to investigate Tau sorting and pathology (reviewed in Bell and Zempel (2022a) and Bell and Zempel (2022b)). The many advantages of SH-SY5Y cells include easy handling and genetic modification (Bell and Zempel, 2022a). Resembling mature neurons, SH-SY5Y cells endogenously express small amounts of all six Tau isoforms (Uberti et al., 1997; Agholme et al., 2010). Specifically, undifferentiated SH-SY5Y cells predominantly express the fetal 0N3R Tau isoform (Dupont-Wallois et al., 1995; Smith et al., 1995; Tanaka et al., 1995; Uberti et al., 1997), with lower expression levels of the remaining 3R and 4R Tau isoforms, including full-length (64 kDa) 2N4R Tau (Agholme et al., 2010; Dupont-Wallois et al., 1995). Prolonged cultivation (maturation) times and cell differentiation change the Tau isoform ratio in SH-SY5Y cells to be more similar to that observed in neurons, with equal proportions of 3R and 4R Tau isoforms (Bell and Zempel, 2022a). If differentiated with compounds such as retinoic acid or brain derived neurotrophic factor (BDNF), SH-SY5Y cells exhibit increases in Tau expression, neurite outgrowth, microtubule formation and show neuron-like sorting of endogenous Tau in axon-like structures (Bell and Zempel, 2022a; Agholme et al., 2010). Comparable to observations in primary neurons, SH-SY5Y cells also missort overexpressed,

truncated Tau into somatic regions (Bell and Zempel, 2022a; Bell et al., 2021), and have a Tau phosphorylation index which parallels that seen in the human brain and during AD (Bell and Zempel, 2022a; Tanaka et al., 1995; Smith et al., 1995; Majd et al., 2018). Furthermore, SH-SY5Y cells express a range of Tau kinases and phosphatases, with phosphatase inhibitors, such as okadaic acid, resulting in AD-like Tau hyperphosphorylation, aggregation, microtubule damage and cell death (Boban et al., 2019; Dupont-Wallois et al., 1995; Tanaka et al., 1998). Finally, protocols to differentiate SH-SY5Y cells towards a cholinergic, noradrenergic or dopaminergic phenotype have been established (Bell and Zempel, 2022a). As such, the AD-associated Tau pathology of neurons in different brain regions and utilising different neurotransmitters can be mimicked using SH-SY5Y cells (Bell and Zempel, 2022a; Bell and Zempel, 2022b).

There are some caveats to using SH-SY5Y cells (Bell and Zempel, 2022a; Bell and Zempel, 2022b). Undifferentiated SH-SY5Y cells show excess 0N3R Tau, more relative amounts of 3R compared to 4R Tau and weaker expression of 2N Tau isoforms in comparison to neurons (Agholme et al., 2010). Moreover, Tau mostly localises to nuclear and cytoplasmic compartments in undifferentiated SH-SY5Y cells, contrasting with the predominant axonal localisation seen in neurons (Uberti et al., 1997). To create a Tau isoform pattern similar to the human brain and improve neuritic (axonal) Tau distribution, differentiation of SH-SY5Y cells is necessary (Bell and Zempel, 2022a; Agholme et al., 2010; Uberti et al., 1997). Other disadvantages include chromosomal abnormalities, such as trisomy of chromosome 7 and copy gains of the *MAPT* gene on chromosome 17 (Yusuf et al., 2013), and incompletely characterised differentiation profiles (Bell and Zempel, 2022a). Finally, as is the case for all cell culture platforms, SH-SY5Y cell cultures lack the extracellular environments and interactions with other cell types that are present *in vivo* (Bell and Zempel, 2022a; Bell and Zempel, 2022b).

To create a translationally relevant SH-SY5Y-based Tau cell model, four criteria were considered:

(i) Tau is predominantly expressed by neurons and spliced into various isoforms (Wang and Mandelkow, 2016). Thus, all 6 isoforms of Tau had to be endogenously expressed in the chosen cell

line. This allows us to assess whether RI-AG03 interferes with the physiological function of endogenous Tau, for instance by disrupting microtubule formation and intracellular transport, in a toxic manner (Wang and Mandelkow, 2016).

(ii) Tauopathies are not characterised solely by a disease-specific propagation pattern of Tau across the CNS, but also by different Tau isoform ratios. For instance, AD and FTDP-17 demonstrate pathological aggregation and spreading of both 3R and 4R Tau isoforms, whilst PiD and CBD predominantly exhibit 3R Tau aggregates (Boyarko and Hook, 2021). Thus, all Tau isoforms should be present in the chosen cell line in order to model a broader range of neurodegenerative diseases.

(iii) The cell model should be Dox-inducible to facilitate cellular maintenance and to have a non-pathologic control state.

(iv) Native Tau is highly soluble and shows a poor aggregation propensity in the absence of hyperphosphorylation or truncation (Lim et al., 2014), yet it was desirable to express the full *MAPT* gene (2N4R Tau) to enable splicing into all isoforms of Tau. Therefore, the coding DNA for full-length 2N4R Tau with the P301L mutation was employed. Several studies indicate that this mutation induces conformational changes that facilitate β sheet and PHF formation (Barghorn et al., 2000; von Bergen et al., 2001).

Based on the above criteria, it was opted to generate a monoclonal and Dox-inducible SH-SY5Y neuroblastoma cell line expressing full-length 2N4R Tau (P301L) to test RI-AG03.

3.2. Experimental goals

- Select a monoclonal, Dox-inducible and 2N4R Tau (P301L)-overexpressing SH-SY5Y cell line
- Check total Tau expression, soluble Tau levels (as an inverted estimate of insoluble Tau formation) and the cell viability of the selected Tauopathy cell line in the presence and absence of Dox
- Investigate the effects of RI-AG03-polyR, in comparison to a scrambled control peptide, on total and soluble Tau and cell viability in both control SH-SY5Y and Tauopathy-modelling SH-SY5Y cells

3.3. Creation and characterisation of a Tau-expressing SH-SY5Y cell model (Clone 4)

To create a neuronal cell model of Tauopathy, SH-SY5Y cells were stably transfected first with a regulator plasmid consisting of the coding DNA for the tetracycline transactivator protein, Tet-On 3G, under the control of a constitutive promoter (plasmid 1). Plasmid-containing cells were then selected using G418. The resulting cell line (SH-SY5Y_TetOn3G) was then co-transfected with a hygromycin resistance marker and a response plasmid consisting of the coding DNA for 2N4R Tau (P301L) and mcherry under the control of a Dox-inducible promoter regulated by transactivator binding (plasmid 2; see Appendix section 9.1 for plasmid maps), followed by antibiotic selection to generate SH-SY5Y_Tet-On3G_Tau_{441} P301L cells. Finally, limiting dilutions were applied to establish 5 monoclonal Tau-expressing SH-SY5Y clones ('Methods' sections 2.2.7 - 2.2.10).

According to Takara (Saint-Germain-en-Laye, France), Dox concentrations of 10 ng/mL are sufficient to induce maximal protein expression with the Tet-On 3G system (Zhou et al., 2006; Takara). To guarantee maximal induction, an excess of 500 ng/mL Dox was used during the clone selection process and for all subsequent experiments.

To confirm inducibility of Tau expression in the selected clones, untransfected SH-SY5Y cells (control) and Clone 1 - 4 SH-SY5Y cells were exposed to Dox for 4 days. The lysate of these cells was then

analysed via western blotting using total $Tau_{243-441}$ antibodies and Tau band intensity of every sample was normalised to that of the same inter-gel control (IGC; untreated, untransfected SH-SY5Y cell lysate) that was loaded on every gel. Statistical analysis showed that Tau expression significantly differed between clones ($F(4, 20) = 5.48$, $p = 0.004$; two-way ANOVA) and that Dox treatment significantly increased Tau levels predominantly in the selected clones ($F(1, 20) = 11.72$, $p = 0.003$) (Figure 3.1A). There was no significant interaction of both variables, however. Relative to control SH-SY5Y cells, only Clone 4 cells, but none of the other cell clones, had a significantly higher Tau expression ($p < 0.01$). Clone 4 cells also expressed more Tau compared to Clone 2 cells ($p < 0.05$). Clone 1 - 4 all showed elevated Tau expression when exposed to Dox, with Clone 4 exhibiting the highest (14.38 ± 2.07-fold) increase in Tau levels in an induced state (Figure 3.1A). Dox-induction (+) resulted in the appearance of a 68 kDa band representing 2N4R Tau in Clone 1 – 4 cells (Figure 3.1B). Lower MW bands, presumably Tau degradation products, were also visible in Dox-induced Clone 1, Clone 3 and Clone 4 cells between 25 - 60 kDa. As seen in Figure 3.1C, Clone 1 - 4 cells all exhibited a multangular morphology and short neurites, similar to untransfected SH-SY5Y cells. Clone 5 cells, however, showed a deformed, 'squashed' morphology. These Clone 5 cells also grew slowly and were, hence, excluded. Due to showing the best Tau expression and good growth, Clone 4 cells were further characterised.

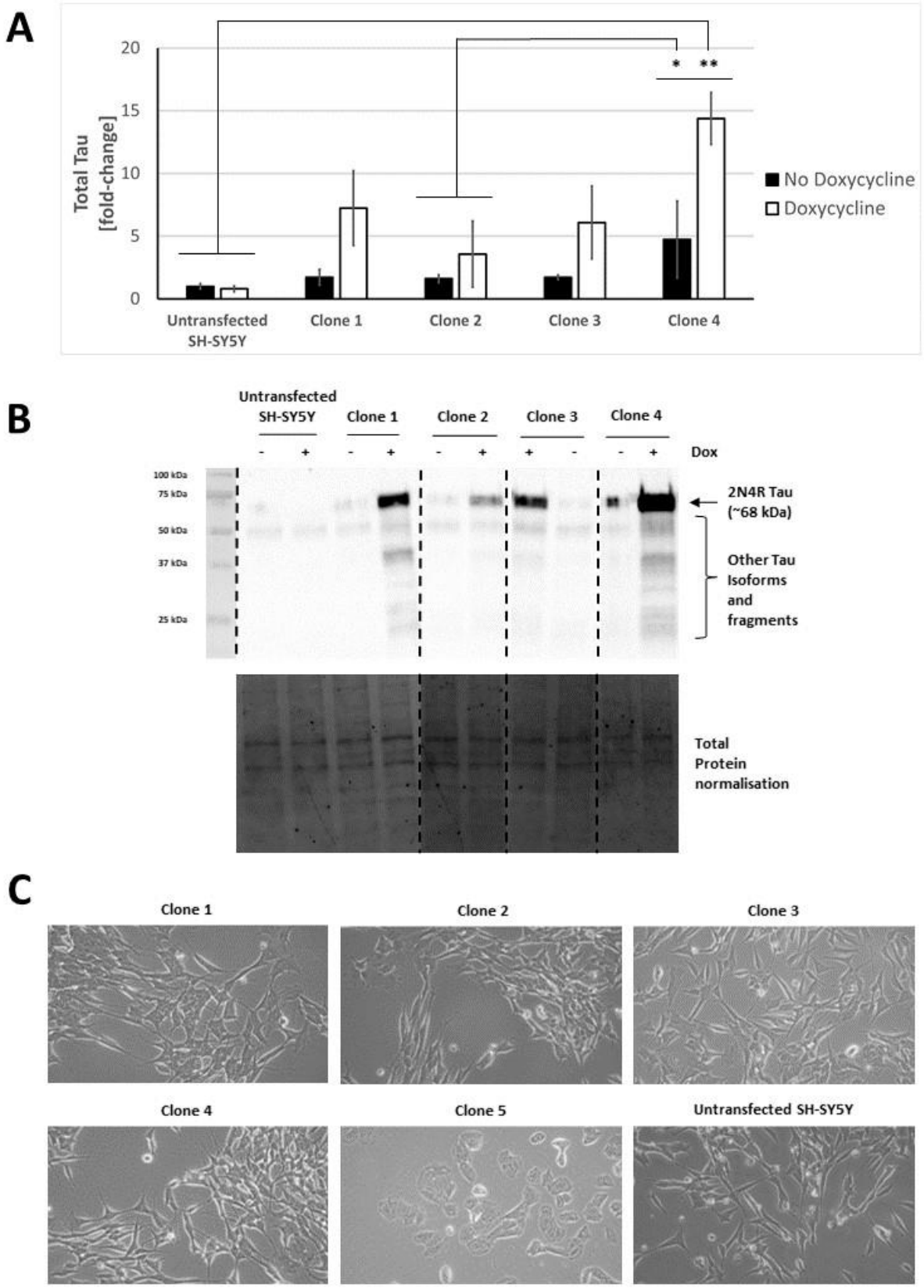

Figure 3.1: Dox-induction of Tau expression in Clone 1 - 5 SH-SY5Y cells. (A) Total $Tau_{243-441}$ levels of untransfected control SH-SY5Y cells and Clone 1 - 4 cells in the absence and presence of Dox (500 ng/mL) after a 4 day treatment. (B) Representative immunoblots showing total Tau with (+) or

without (-) Dox treatment (upper panel) and total protein normalisation (lower panel). Dotted lines show different blots or omitted areas. (C) Morphologies of untransfected SH-SY5Y cells and Clone 1 - 5 cells. Clone 5 showed a deformed morphology and was, thus, not assessed for Tau expression. To compare results across blots, Tau bands were additionally normalised to those of the same IGC run on every gel (non-Dox-treated SH-SY5Y cells). Shown is the mean ± SEM fold-change as compared to untreated and untransfected SH-SY5Y cells (n = 3 technical replicates; separate cell wells/flasks treated at the same time). Data were analysed by two-way ANOVA and Tukey's post-hoc test. Levels of significance are * = $p < 0.05$ and ** = $p < 0.01$.

3.3.1. Doxycycline-inducible Tau expression in untransfected SH-SY5Y and Clone 4 cells

Initially, to exclude the possibility that Dox had unexpected effects on the expression of endogenous Tau in control SH-SY5Y cells, the influence of Dox treatment on untransfected SH-SY5Y cells was assessed in more detail. SH-SY5Y cells were cultured for a period of 7 days in the absence or presence of Dox, lysates were prepared and subjected to immunoblotting using polyclonal antibodies detecting total Tau (residues 243-441). For comparison across blots, as in the previous section, the same lysate of untransfected SH-SY5Y cells was used as IGC on every gel to normalise Tau levels in all samples.

Statistical analysis revealed a significant interaction between the application of Dox and days in culture ($F(3, 16) = 4.51$, $p = 0.018$; two-way ANOVA). As expected, the results demonstrated that Dox treatment of SH-SY5Y cells for 1 - 7 days had no effect on total endogenous Tau levels relative to cells cultivated for the same time in the absence of Dox (Figure 3.2A). Interestingly, endogenous Tau levels were significantly lower on day 2 compared to day 7 ($p = 0.005$) in Dox-untreated cells. In the presence of Dox, Tau levels were significantly higher on day 7 compared to day 1 ($p < 0.001$), day 2 ($p < 0.001$) and day 4 ($p < 0.001$) (Figure 3.2A). This variability in Tau levels might reflect that SH-SY5Y cells change Tau isoform and, likely, total Tau expression with increasing maturity and cultivation times, as previously reported (Bell and Zempel, 2022a; Agholme et al., 2010).

As seen in Figure 3.2C, untransfected SH-SY5Y cells endogenously expressed four Tau bands at ~64 kDa (2N4R Tau), ~52 kDa (2N3R Tau), ~40 kDa (most likely 1N3R Tau) and ~25 kDa (0N3R Tau) in

the total fraction (T). Another band at ~30 kDa (0N4R Tau) was also visible in some soluble fractions (S). The weak expression of 0N4R Tau and absence of 1N4R Tau in these SH-SY5Y cells (passage 8) is likely related to the fact that 4R Tau isoforms are weakly expressed in young cells (Bell and Zempel, 2022a; Agholme et al., 2010).

To measure the influence of Dox on soluble Tau, the same SH-SY5Y cell lysates were ultracentrifuged to remove insoluble Tau (Sanders et al., 2014). The resulting total and soluble fractions were subsequently subjected to immunoblotting with polyclonal total $Tau_{243-441}$-recognising antibodies and the results (Figure 3.2B) expressed in terms of the soluble Tau as a percentage of the total detected Tau (soluble plus insoluble). Most of the total Tau in untransfected SH-SY5Y cells was soluble (on average 90.45 ± 5.01 % without Dox and 83.87 ± 5.57 % with Dox across the 7 days). Due to high variability, the data were analysed using the Shapiro-Wilk test, which revealed that the data is not normally distributed ($p < 0.001$). Subsequent application of the nonparametric Kruskal-Wallis test indicated there were no significant differences in the proportions of soluble Tau between day 1 - 7 (Figure 3.2B). Importantly, the application of Dox also did not significantly alter the proportions of soluble Tau in SH-SY5Y cells, as compared to non-treated SH-SY5Y cells.

When compared under Dox-free culture conditions across 7 days, the Tau levels of Clone 4 cells were similar to that seen in untransfected SH-SY5Y cells (Figure 3.2D). A significant interaction between cell type and days in culture on Tau expression was found ($F(3, 16) = 12.04$, $p > 0.001$; two-way ANOVA). Post-hoc analysis confirmed that Tau expression was not significantly different in Clone 4 cells, as compared to untransfected SH-SY5Y cells on day 1, 4 or 7. However, Tau expression levels were significantly higher in Clone 4 cells than in untransfected SH-SY5Y cells on day 2 ($p = 0.003$). Analysis of the temporal variations in Tau expression for each cell line revealed that untransfected SY5Y cells showed lower Tau levels on culture day 2 relative to all other days (versus day 1, $p = 0.031$; day 4, $p = 0.025$; day 7, $p < 0.001$). By contrast, in Clone 4 cells, Tau expression levels were significantly reduced on day 2 compared to day 4 ($p = 0.031$). Overall, these results suggest that Clone 4 SH-SY5Y cells do not exhibit increased Tau expression in the absence of Dox in

comparison to untransfected SH-SY5Y cells. However, there appear to be fluctuations in Tau expression across days in culture that may be different between Clone 4 and untransfected SH-SY5Y cells. This could in part be related to the earlier noted variability in endogenous Tau expression in SH-SY5Y cells, which is associated with the cell maturity and cultivation time (Bell and Zempel, 2022a; Agholme et al., 2010).

In summary, these findings suggest that Dox does not influence the expression of endogenous Tau or the proportions of soluble Tau in untransfected SH-SY5Y cells. Moreover, due to being derived from SH-SY5Y cells, non-Dox-treated Clone 4 cells express similar levels of endogenous Tau to that seen in control SH-SY5Y cells.

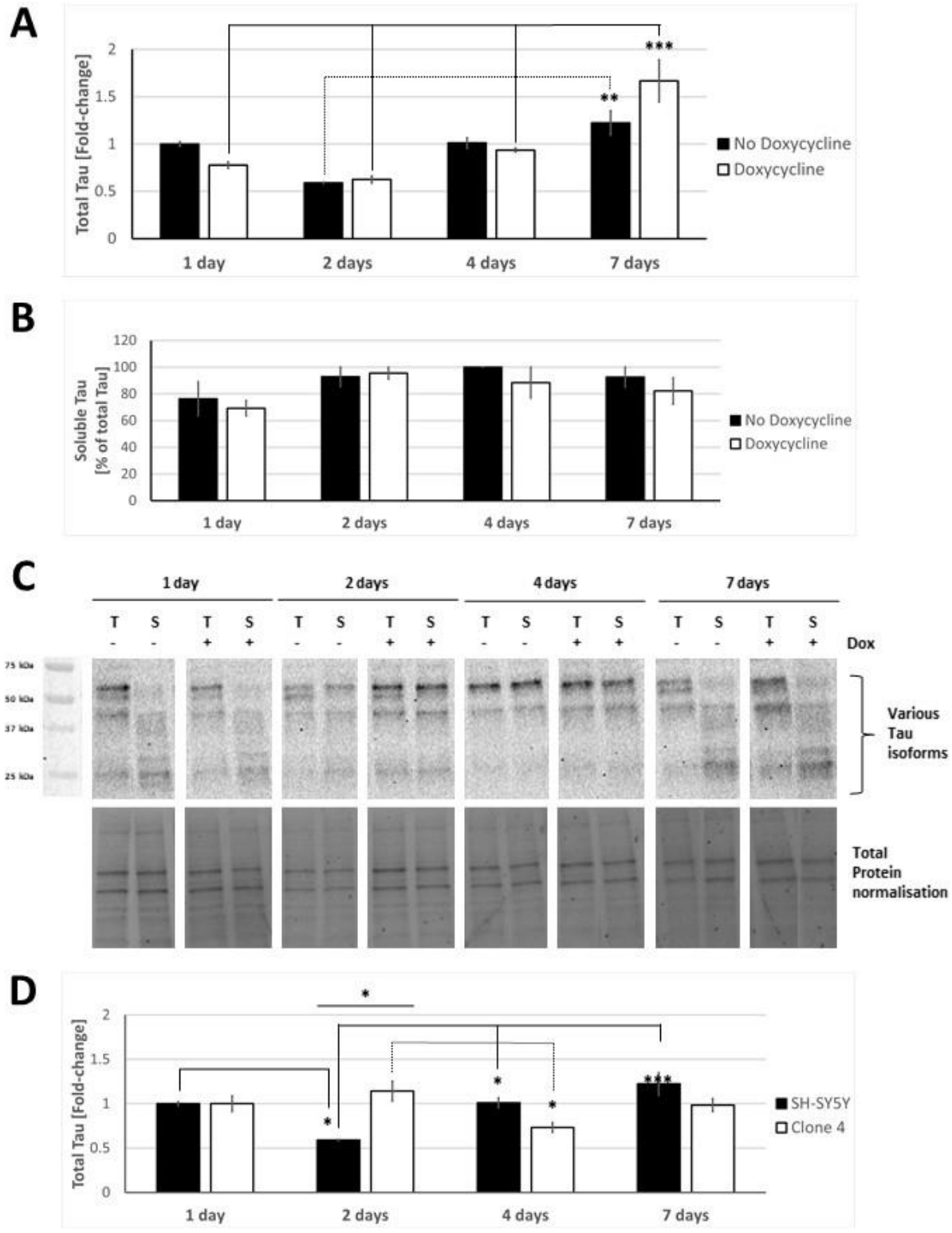

Figure 3.2: Impact of Dox treatments on Tau expression and soluble Tau in untransfected SH-SY5Y cells. (A) Intracellular total Tau and (B) Soluble Tau levels of untransfected SH-SY5Y cells in the presence or absence of Dox (500 ng/mL) over a 1 - 7 day culture period. Tau was probed with polyclonal $Tau_{243-441}$ antibodies. (C) Representative immunoblots. The upper panel shows Tau in the total (T) and soluble (S) fractions of SH-SY5Y cells, either with (+) or without (-) Dox treatment, for cultivation periods of 1 - 7 days. The lower panel depicts the respective total protein blots used for

normalisation. (D) Comparison of the endogenous total Tau levels in SH-SY5Y and Clone 4 cells in tetracycline (Dox)-free medium across 1 - 7 days. Tau bands of all samples were normalised to the same IGC (untreated, untransfected SH-SY5Y cell lysate) loaded on each gel. Results are the mean ± SEM fold-change as compared to untreated SH-SY5Y cells at day 1 (n = 3 technical replicates; separate cell wells/flasks treated at the same time). Data were analysed by two-way ANOVA followed by Tukey's post-hoc test. Levels of significance are * = $p < 0.05$, ** = $p < 0.01$ and *** = $p < 0.001$.

In the next series of experiments, the impact of Dox-induced 2N4R Tau (P301L) overexpression on total and soluble Tau levels in Clone 4 SH-SY5Y cells was assessed. For cross-blot comparison and normalisation of Tau band intensities of all samples, the same IGC (untreated Clone 4 cell lysate) was loaded on every gel. For total Tau levels, there also was a significant interaction between Dox treatment and days in culture ($F(3, 16) = 44.59$, $p > 0.001$). In the presence of Dox and in comparison to uninduced cells on the same day, total Tau levels were significantly increased 5.69-fold at day 1 ($p < 0.001$), 9.92-fold at day 2 ($p = 0.001$), 15.79-fold at day 4 ($p < 0.001$) and 15.98-fold at day 7 ($p < 0.001$) (Figure 3.3A). When cultivated in tetracycline-free medium, endogenous Tau levels in Clone 4 cells did not change across the 7 days. On the other hand, in Dox-treated Clone 4 cells, total Tau levels were increased on day 2 compared to day 1 ($p < 0.001$) and day 4 relative to day 2 ($p < 0.001$). However, total Tau levels in Clone 4 cells were unaltered between day 4 and 7 (Figure 3.3A). Thus, Dox-induced 2N4R Tau (P301L) expression gradually increased total Tau levels from day 1, then plateaued at day 4 in Clone 4 cells.

In terms of soluble Tau (Figure 3.3B), this form of the protein showed notable variability. Indeed, the Shapiro-Wilk test confirmed that the dataset is not normally distributed ($p < 0.001$). Thus, the Kruskal-Wallis test was applied. This nonparametric test revealed that the intracellular proportions of soluble Tau were not affected by the cultivation time (1 - 7 days) and Dox treatment. Similar to untransfected SH-SY5Y cells (Figure 3.2B), the averaged proportions of soluble Tau in Clone 4 cells were high across the 7 days (89.31 ± 2.86 % of total Tau in Dox-untreated and 88.69 ± 8.26 % in Dox-treated cells; Figure 3.3B).

As expected, Dox treatment visibly induced the expression of the transfected 2N4R Tau isoform (~68 kDa) in Clone 4 cells (Figure 3.3C). Moreover, smaller molecular weight bands between 25 - 50 kDa became more pronounced in the presence of Dox. These are likely degradation products of the overexpressed 2N4R Tau (Figure 3.3C).

Collectively, these results suggest that Clone 4 SH-SY5Y cells are a suitable, inducible and 2N4R Tau-overexpressing cell model. However, as indicated by unaltered proportions of soluble Tau, there is no evidence for Tau aggregation in this Tauopathy cell model for up to 7 days of Dox-induction.

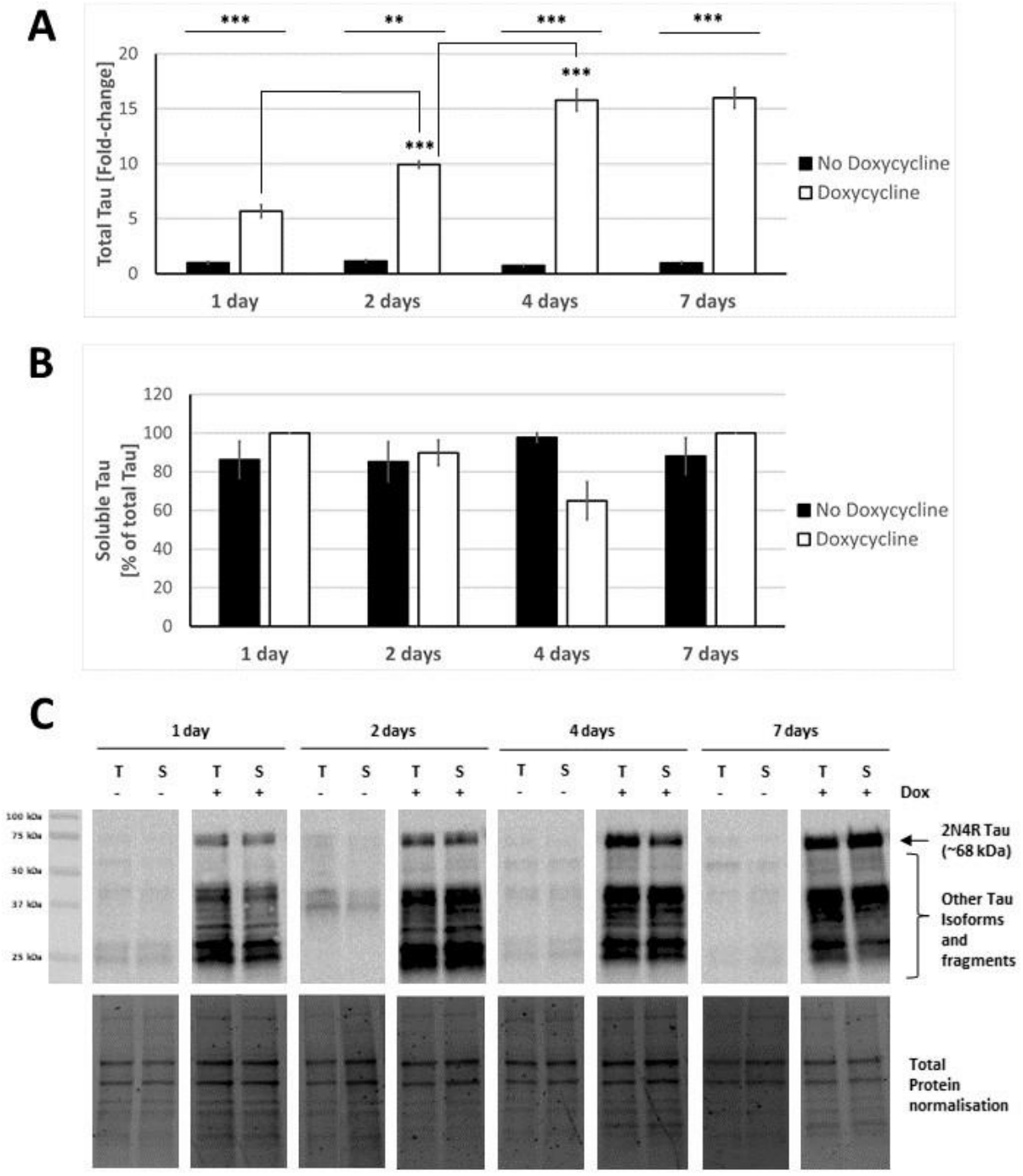

Figure 3.3: Tau characterisation following Dox treatment of Clone 4 SH-SY5Y cells. Clone 4 is a cell line stably transfected with the Tet-On 3G system for Dox-inducible 2N4R Tau (P301L) expression. (A) Total Tau and (B) intracellular soluble Tau levels in Clone 4 cells following Dox treatment (500 ng/mL) for 1 - 7 days. Tau was detected using polyclonal $Tau_{243-441}$ antibodies. (C) Immunoblots showing Tau expression and fragments in the total (T) and soluble (S) fractions (upper panel) and the respective total protein normalisation blots (lower panel) following Dox treatment for 1 - 7 days. All samples were normalised to the same untreated, unprocessed Clone 4 cell lysate loaded on every gel (IGC). Values are the mean ± SEM fold-change in comparison to Clone 4 in tetracycline-free medium at day 1 (n = 3 technical replicates; separate cell wells/flasks treated at the same time).

Data were analysed by two-way ANOVA followed by Tukey's post-hoc test. Levels of significance are ** = $p < 0.01$ and *** = $p < 0.001$.

3.3.2. Toxicity following Tau induction in Clone 4 SH-SY5Y cells

Having established that Dox treatment enhanced the expression of 2N4R Tau in Clone 4 cells, the cytotoxic effects of Dox-induced Tau expression were assessed. Following Dox-induction for 2 days (48 h) or 4 days (96 h), cell viability was assessed using the WST-8 assay. The results showed that Tau induction did not affect cell viability over this time frame (Figure 3.4A). Furthermore, cell death, using the LDH assay, was assessed. These results also demonstrated no change in cell death at day 2 or 4 (Figure 3.4B). Collectively, these data indicate that Tau induction was not toxic in Clone 4 cells.

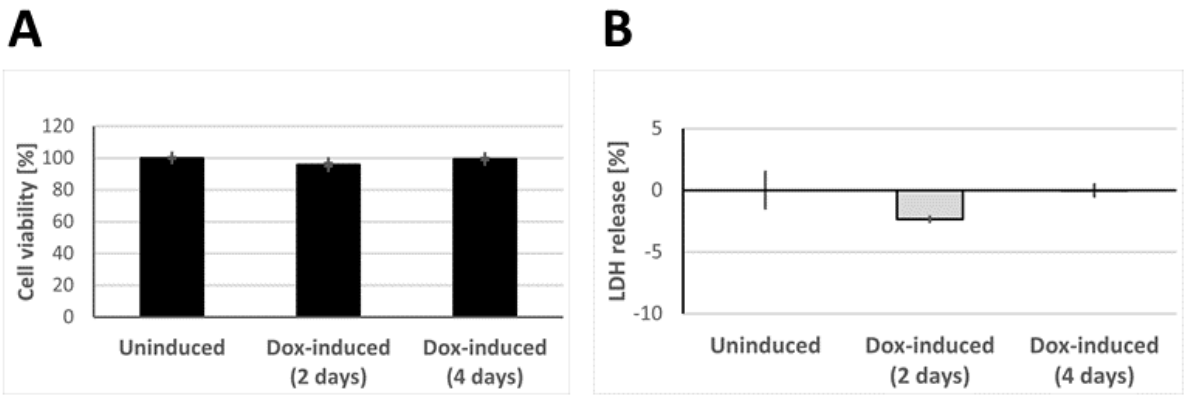

Figure 3.4: Cell viability and toxicity of in response to Dox-mediated Tau overexpression in Clone 4 cells. Clone 4 cells were cultured in the presence of Dox for 2 days (48 h) and 4 days (96 h). (A) Cell viability, as assessed via the colorimetric conversion of WST-8. (B) Cell death, measured through membrane rupture and consequent LDH release. Values are the mean ± S.E.M. % of cell viability or LDH release, respectively, as compared to uninduced control cells in tetracycline-free medium (n = 6 technical replicates; separate cell wells/flasks treated at the same time). One-way ANOVAs and Tukey's post hoc test showed that Tau overexpression was not toxic over time.

3.4. Testing of RI-AG03-polyR in Clone 4 SH-SY5Y cells

3.4.1. Effects of RI-AG03-polyR on intracellular total and soluble Tau

To investigate the Tau-interacting effects of RI-AG03 in a cell environment, the peptide was modified. In order to facilitate cellular uptake, it was synthesized with the internalisation-promoting

sequence of the CPP polyarginine (polyR; 8 arginine residues) (Shi et al., 2014). Because pathological Tau aggregates intracellularly and predominantly propagates between interconnected neurons (Simic et al., 2016; Vogel et al., 2021), adding a CPP is essential for efficient access of the peptide to cytosolic Tau.

With Clone 4 cells established, the effects of RI-AG03-polyR on intracellular Tau levels were assessed. As determined earlier, Dox treatment elicits the expression of 2N4R Tau (P301L) in Clone 4 cells, which significantly and gradually increased total Tau levels in Clone 4 cells over 1 - 4 days (Figure 3.3A). For these experiments, a 2 day (48 h) treatment period was chosen because longer time periods would have required to change the Dox- (and peptide-) containing medium. To ensure the specificity of the effects of the Tau binding sequence in RI-AG03-polyR, a scrambled RI-AG03-polyR peptide, featuring a shuffled Tau-interacting sequence and an intact polyR CPP ('Methods' section 2.2.11), was used as the control. Additionally, Tau levels in each sample were normalised to that of the same IGC (untreated Clone 4 cell lysate) run on every gel.

Statistical evaluation found a significant interaction between peptide type (RI-AG03-polyR vs. scrambled peptide), peptide concentration (10 - 5000 nM) and Dox treatment (Dox vs. no Dox) ($F(3, 32) = 10.40$, $p < 0.001$; three-way ANOVA). This suggests that different concentrations of RI-AG03-polyR or the scrambled peptide exert distinct effects on total Tau levels, and that this may depend on whether Clone 4 cells are cultivated in Dox-free or Dox-containing medium.

Therefore, to assess this relationship, each peptide concentration (10 nM, 100 nM, 1000 nM and 5000 nM) was analysed individually using two-way ANOVAs, with peptide type and Dox treatment as the independent variables. At all peptide concentrations, peptide type and Dox treatment significantly interacted (10 nM: ($F(2, 12) = 18.57$, $p < 0.001$; 100 nM: $F(2, 12) = 4.99$, $p = 0.026$; 1000 nM: $F(2, 12) = 4.55$, $p = 0.034$ and 5000 nM: $F(2, 12) = 45.85$, $p < 0.001$).

As confirmed earlier (Figure 3.3A), Dox-treated Clone 4 cells showed significantly higher total Tau levels compared to cells cultivated in Dox-free medium (not shown; 0 nM, Figure 3.5A). At a peptide

concentration of 10 nM and in the absence of Dox, post hoc analysis revealed that the scrambled peptide and RI-AG03-polyR had no effect on total Tau levels in Clone 4 cells relative to Dox- and peptide-untreated cells. However, in the presence of Dox, treatment with 10 nM scrambled peptide ($p < 0.001$) or RI-AG03-polyR ($p = 0.001$) significantly increased total Tau pools compared to Dox-induced and peptide-untreated cells. There was no difference in the effect of both peptides under Dox-exposed and Dox-free culture conditions (Figure 3.5A).

Using 100 nM, there was no effect of both peptides on total endogenous Tau levels in Dox-free medium. By contrast, when Dox was co-applied, the scrambled peptide, but not RI-AG03-polyR, elevated total Tau levels in the presence of Dox, as compared to Dox-exposed and peptide-untreated Clone 4 cells ($p = 0.021$). However, the impact of the scrambled peptide on total Tau levels was not significantly different from that of RI-AG03-polyR.

Similar to lower peptide concentrations, the exposure of Dox-untreated Clone 4 cells to 1000 nM scrambled peptide or RI-AG03-polyR did not significantly influence total endogenous Tau levels relative to non-Dox- and non-peptide-treated cells. In comparison to Dox-induced Clone 4 cells, co-treatment with Dox and 1000 nM RI-AG03-polyR, but not the scrambled peptide, significantly enhanced total Tau levels ($p = 0.007$). However, the effect of RI-AG03-polyR was not significantly greater than that of its scrambled version.

In the absence of Dox, scrambled peptide and RI-AG03-polyR concentrations of 5000 nM also did not alter total endogenous Tau levels. In turn, when added to Dox-containing culture medium, the scrambled peptide ($p < 0.001$) and RI-AG03-polyR ($p < 0.001$) heightened total Tau levels in Clone 4 cells relative to Dox-exposed, but peptide-untreated, cells. At 5000 nM, the total Tau-increasing effects of RI-AG03-polyR were significantly greater than those of the scrambled peptide in the presence of Dox ($p < 0.001$) (Figure 3.5A).

In summary, the peptides did not affect endogenous Tau levels in Clone 4 cells under Dox-free culture conditions following a 48 h treatment period. Inducing the expression of 2N4R Tau (P301L)

with Dox over the same time period raised total Tau levels in Clone 4 cells 6.17-fold. Moreover, the co-exposure to Dox and 10 nM, 100 nM or 5000 nM scrambled peptide further significantly increased total Tau levels 14.78-fold, 10.55-fold or 18.88-fold, respectively. Similarly, in the presence of Dox, RI-AG03-polyR concentrations of 10 nM, 1000 nM and 5000 nM significantly heightened total Tau levels 11.85-fold, 15.79-fold and 31.64-fold, respectively, as compared to Dox-induced and peptide-untreated Clone 4 cells. In comparison, RI-AG03-polyR evoked a bigger increase in total Tau levels than its scrambled version at the highest concentration used (5000 nM).

Examination of the immunoblots indicates that both peptides cause the accumulation of the overexpressed 2N4R Tau (P301L) in Clone 4 cells, in particular of smaller molecular weight degradation products between 20 - 40 kDa (e.g. '5000 nM RI-AG03-polyR + Dox' compared to 'control + Dox'; Figure 3.5B). Reasons for peptide-induced Tau accumulation in cells, such as potential proteasome inhibition or interactions with intracellular Tau, are further debated in section 3.5.3.

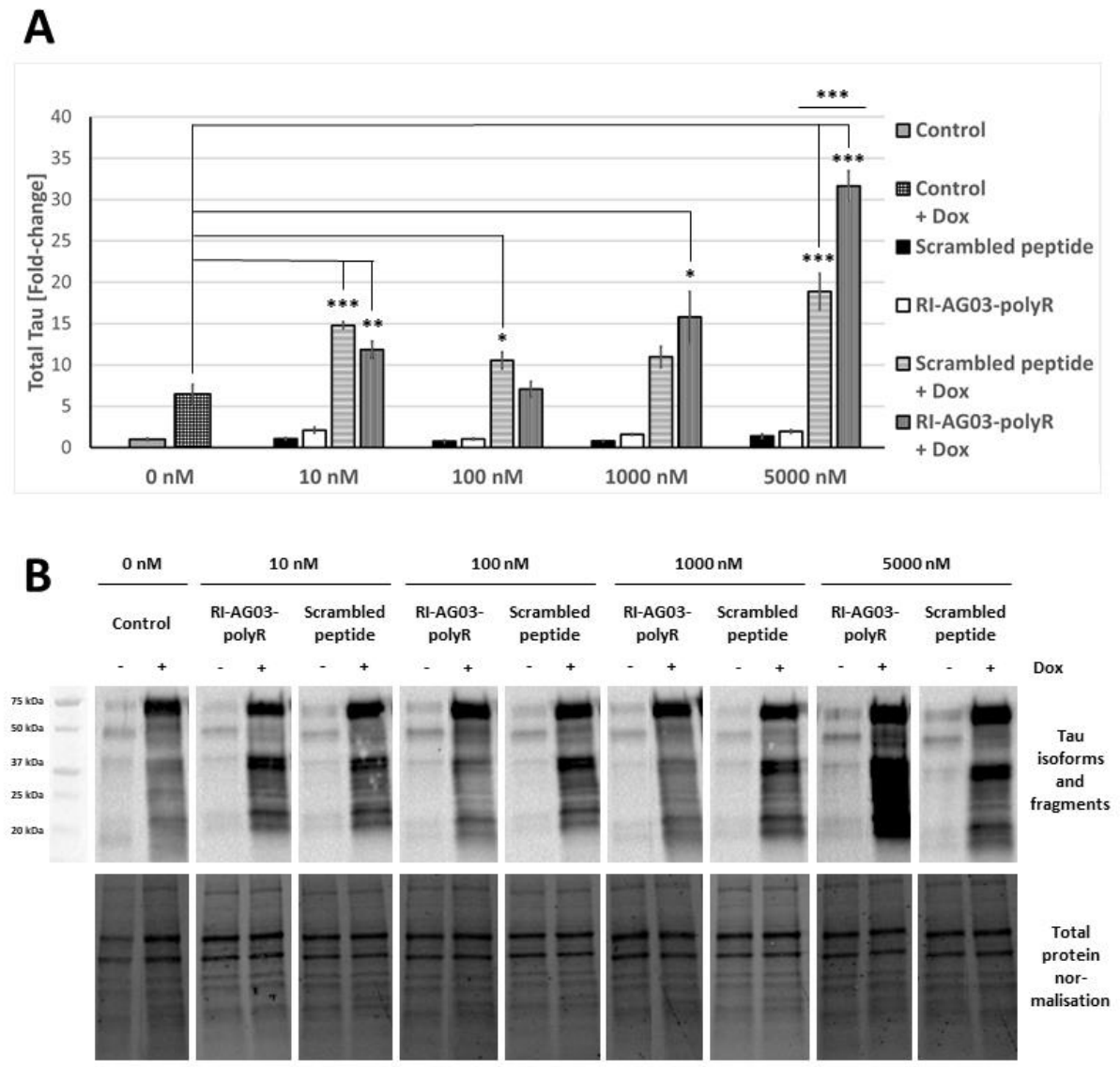

Figure 3.5: Effects of RI-AG03-polyR and scrambled RI-AG03-polyR peptide treatments on total Tau levels in Clone 4 cells. (A) Total Tau levels without and with Dox (500 ng/mL)-induced 2N4R Tau (P301L) overexpression in Clone 4 cells treated with 10 - 5000 nM of the scrambled control or RI-AG03-polyR peptide for 48 h. (B) Representative immunoblots, illustrating total Tau (upper panel) and total protein normalisation (lower panel) blots. These show that Dox-induction increases 2N4R Tau expression, whilst treatment with scrambled RI-AG03-polyR and RI-AG03-polyR peptide cause intracellular Tau accumulation. Tau band intensities of each sample were normalised to those in the same untreated Clone 4 cell lysate (IGC) on all gels. Data are shown as the mean ± S.E.M. fold-change in total Tau compared to peptide-untreated cells in tetracycline-free medium (n = 3 technical replicates; separate cell wells/flasks treated at the same time). The data were analysed using three-way ANOVA and two-way ANOVAs for individual peptide concentrations (10, 100, 1000 or 5000 nM) followed by Tukey's post hoc test. The shown significant differences reflect the results of the two-way-ANOVAs/Tukey's tests with * = $p < 0.05$, ** = $p < 0.01$ and *** = $p < 0.001$. Notably, Dox-treated Clone 4 cells showed significantly increased total Tau levels compared to Dox-untreated cells in the absence of the peptides (0 nM; not shown), as confirmed earlier.

3.4.2. Effects of RI-AG03-polyR on cell viability

Earlier experiments showed that Dox-induced expression of 2N4R Tau (P301L) is not toxic to Clone 4 cells (Figure 3.4). However, since RI-AG03-polyR and scrambled RI-AG03-polyR affected total Tau levels (Figure 3.5) and to investigate if the peptide has potential detrimental effects, the cell viability of Clone 4 cells, both under Dox-induced and Dox-free culture conditions, was evaluated following 48 h and 96 h treatments using the colorimetric WST-8 conversion assay.

Consistent with earlier results, post hoc tests showed that Dox had no effect on the cell viability of Clone 4 cells, irrespective of the length of induction (Figure 3.6). Likewise, neither RI-AG03-polyR, nor scrambled RI-AG03-polyR, affected the viability of uninduced or Dox-induced Clone 4 cells at peptide concentrations between 10 nM - 5000 nM following a 48 h (Figure 3.6A) or 96 h (Figure 3.6B) exposure period. In every case, there was no significantly different effect between the scrambled peptide and RI-AG03-polyR.

Identical results were also observed when untransfected SH-SY5Y cells were cultivated with the peptides in the presence or absence of Dox for 48 h (Appendix, Figure 9.3A). However, over a 96 h time period, three-way ANOVA using Dox treatment (Dox-treated or Dox-free), peptide type (RI-AG03-polyR vs. scrambled peptide) and peptide concentration (10 - 5000 nM) as independent variables revealed a significant interaction between peptide type and concentration ($F(4, 96) = 3.67$, $p = 0.008$; Appendix, Figure 9.3B). In fact, Tukey's test showed that the exposure of either Dox-treated or Dox-untreated SH-SY5Y cells to 5000 nM RI-AG03-polyR significantly enhanced cell viability relative to peptide-untreated cells in Dox-containing or Dox-free culture medium ($p < 0.001$). Moreover, independent of whether Dox was present, 5000 nM RI-AG03-polyR enhanced cell viability significantly more than the same concentration of the scrambled peptide ($p = 0.002$) after 96 h (Figure 9.3B).

Therefore, despite triggering the cytosolic amassment of overexpressed Tau in Clone 4 cells, RI-AG03-polyR or scrambled RI-AG03-polyR are not toxic at concentrations up to 5000 nM *in vitro*.

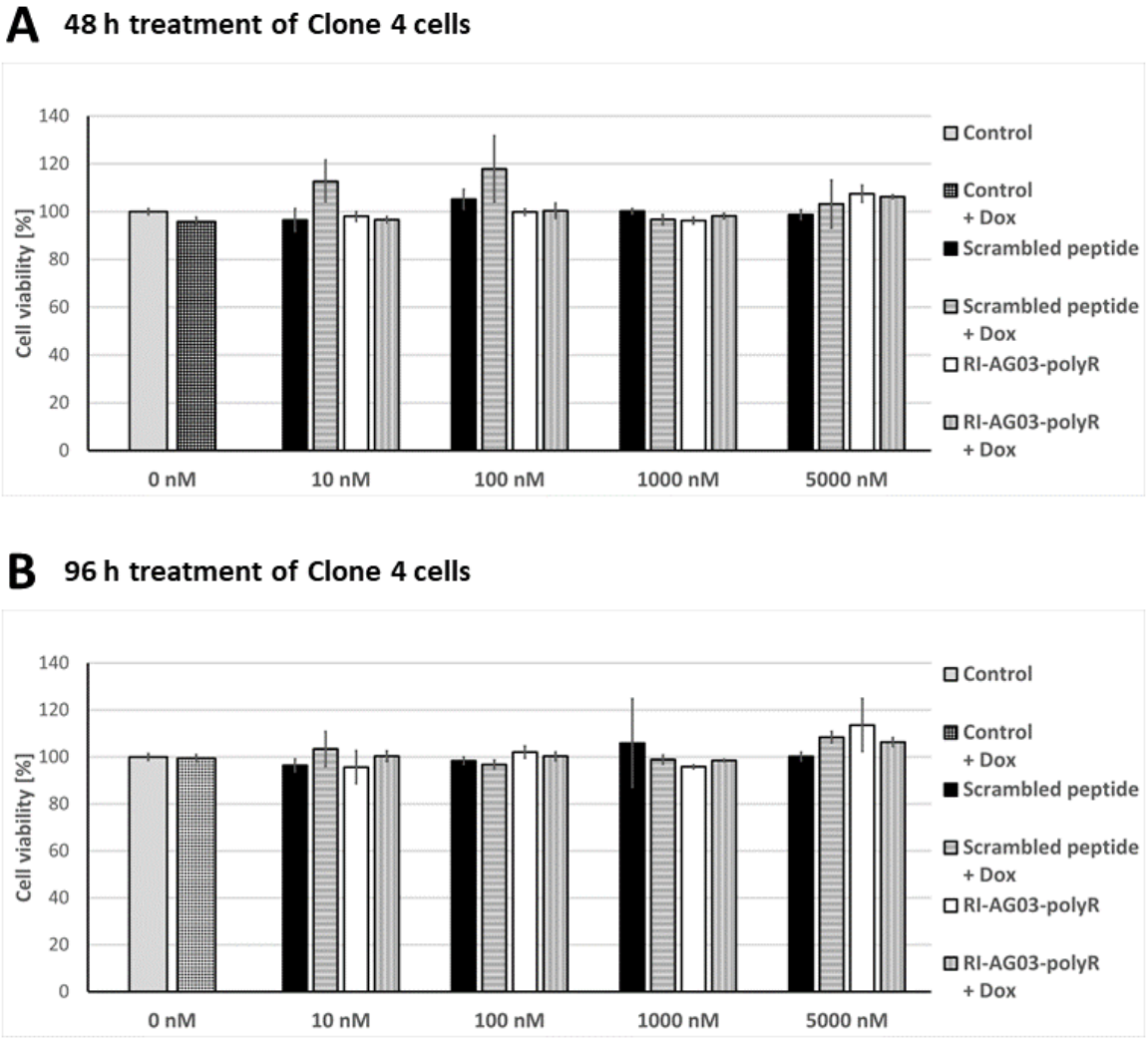

Figure 3.6: Cell viability of Clone 4 cells treated with Dox, RI-AG03-polyR or scrambled RI-AG03-polyR. (A) Exposure of Clone 4 cells to various scrambled RI-AG03-polyR and RI-AG03-polyR peptide concentrations for 48 h. (B) Treatment as described for (A), but for 96 h. Cell viability was measured in the absence or presence of Dox (500 ng/mL)-induced 2N4R Tau overexpression via colorimetric WST-8 conversion. Shown are the mean ± SEM % of cell viability, in comparison to Dox/peptide-untreated Clone 4 cells in Dox-free medium (n = 6 technical replicates; separate cell wells/flasks treated at the same time). No significant differences were found using three-way ANOVA and Tukey's post hoc test, suggesting that Dox-induced Tau expression and the peptides are non-toxic to cells.

3.5. Discussion

3.5.1. The relationship between 2N4R Tau (P301L) over-expression, aggregation and cytotoxicity

Over the last two decades, various Tau-based cell culture models have been developed to study the pathology-associated mutational effects, post-translational modifications, missorting, aggregation, intercellular propagation and the toxicity of Tau (Khlistunova et al., 2006; Bandyopadhyay et al., 2007; Vogelsberg-Ragaglia et al., 2000; Guo and Lee, 2011; Nonaka et al., 2010; Lu and Kosik, 2001; Chun and Johnson, 2007; Kfoury et al., 2012; Chun et al., 2007; Tak et al., 2013; Harrington et al., 2015). Other utilities of such Tauopathy cell models include the investigation of microtubule-related implications, the identification of biomarkers or the screening of potential drug candidates. Non-neuronal cell lines, for example HEK293 cells (Bandyopadhyay et al., 2007; Chun and Johnson, 2007; Chun et al., 2007; Kfoury et al., 2012; Tak et al., 2013), chinese hamster ovary epithelial cells (Vogelsberg-Ragaglia et al., 2000), fibroblasts (Lu and Kosik, 2001; Harrington et al., 2015), SH-SY5Y (Nonaka et al., 2010) and N2a neuroblastoma cell models (Khlistunova et al., 2006) have been employed. Previously, researchers have used cells transiently or stably transfected with aggregation-prone truncated Tau, such as the R1-4-containing K18 (Khlistunova et al., 2006) or R1/3/4-containing K19 fragment (Chun et al., 2007). Alternatively, Tau isoforms, such as the 441 amino acid-long (full-length) 2N4R Tau, also known as Tau-40, were introduced (Bandyopadhyay et al., 2007; Vogelsberg-Ragaglia et al., 2000; Guo and Lee, 2011; Lu and Kosik, 2001; Chun and Johnson, 2007; Chun et al., 2007; Tak et al., 2013; Harrington et al., 2015). These Tau isoforms or fragments were regulated by either a constitutive (Vogelsberg-Ragaglia et al., 2000; Lu and Kosik, 2001; Tak et al., 2013) or tetracycline/Dox-inducible promotor (Khlistunova et al., 2006; Bandyopadhyay et al., 2007). Finally, Tau constructs containing disease-associated *MAPT* mutations that promote β sheet formation and aggregation, for example P301L or ΔK280, were used in some studies (Kfoury et al., 2012; Khlistunova et al., 2006; Vogelsberg-Ragaglia et al., 2000; Lu and Kosik, 2001).

In this study, a monoclonal, Dox-inducible and 2N4R Tau (P301L)-overexpressing SH-SY5Y cell line, referred to as Clone 4 cells, was established. The results confirmed that Dox treatment increased total Tau levels ~10-fold and ~16-fold after 2 or 4 days, respectively (Figure 3.3A), also leading to an increase in Tau degradation products (Figure 3.3C). However, Tau overexpression was not toxic to Clone 4 cells over these two time periods (Figure 3.4). This brings into question whether 2N4R Tau, and related Tau species, are in fact toxic. In this context, there are three major views to consider: a) insoluble NFTs are toxic and causative of AD, b) soluble hyperphosphorylated and/or oligomeric Tau that accumulate in non-axonal cellular compartments, including those capable of seeding transcellular Tau aggregation (the proteolysis-resistant core of PHFs), are toxic, whereas fibril formation acts as a sink to detoxify smaller aggregates or c) both soluble and insoluble Tau species are detrimental through varying mechanisms over different time scales (this is the most accepted opinion) (Kopeikina et al., 2012). Moreover, as elaborated in chapter 1.3.7, both loss of physiological function and gain-of-toxicity drive Tau-mediated neurodegeneration (Zhang et al., 2021a).

SH-SY5Y neuroblastoma cells show neuron-like characteristics, such as the expression of neuronal maturation markers, electrical synapse activity and, if differentiated, axonal outgrowth (Bell and Zempel, 2022a). Thus, SH-SY5Y cells are potentially more suitable to model the axonal (microtubule) and synaptic Tau pathologies compared to other non-neuronal cells, such as HEK293. In the context of neuron-specific toxicity, a study using SH-SY5Y cells demonstrated that the application of recombinant extracellular full-length 2N4R Tau (either native, hyperphosphorylated or mutant for G272V, P301L and R406W) triggered cell death by stimulating excessive muscarinic receptor-induced Ca^{2+} accumulation. Likewise, $Tau_{\Delta 306–311}$ (without the pro-aggregatory VQIVYK sequence, thus paralleling 3R Tau), ^{306}VQIVYK^{311} peptides and, with the weakest impact, pre-aggregated insoluble PHFs were toxic through the same mechanism (Gómez-Ramos et al., 2006). Under conditions of Tau overexpression, however, a different picture emerges. A cell culture study, using an inducible N2a cell model, demonstrated that the overexpression of pro-aggregatory Tau RD (ΔK280) accelerated cell death by ~ 10 %, as compared to uninduced controls or cells expressing inducible Tau RD or Tau

RD mutants that do not promote aggregation (Khlistunova et al., 2006). This suggests that Tau aggregation is harmful, whereas the overexpression of non-aggregating Tau species is not. Indeed, although toxicity was not assessed, another study showed that SH-SY5Y cells tolerated a 60-fold increase in total Tau levels. This constant increase in total Tau was achieved through stable transfection with 2N4R Tau under the control of a constitutive CMV promotor (Loffler et al., 2012). The suggestion that the aggregation of Tau (or oligomerisation-inducing Tau fragments) is toxic is supported by other cell culture studies (Wang et al., 2007b) and the fact that Tau propagation assessed via Braak staging correlates with cognitive decline in AD patients (Braak and Braak, 1991; Bancher et al., 1996; Grober et al., 1999; Duyckaerts et al., 1997; Geddes et al., 1996). In fact, the stable overexpression of 2N4R Tau by N2a and HEK293 cells rendered them resistant to multiple pro-apoptotic stimuli, such as the topoisomerase inhibitor camptothecin and hydrogen peroxide. Interestingly, accumulating Tau serves as a competitive substrate for phosphorylation by GSK-3β, preventing the inactivating phosphorylation of the survival-improving transcription factor beta-catenin (Li et al., 2007). Similar to the inability of native 2N4R Tau to self-oligomerise (Baum et al., 1995), a study using N2a cells overexpressing 2N4R Tau (ΔK280) or 2N4R Tau (P301L) verified that the co-presence of a seed, in this case a truncated fragment composed of the Tau RD (F3), was necessary to trigger aggregation and cell death (Wang et al., 2007b). Therefore, the induction of pathologic Tau aggregation, but not overexpression of Tau, is toxic in cells.

Because overexpressed 2N4R Tau is aggregation-incompetent (Lim et al., 2014; Chirita et al., 2005), the FTDP-17-associated P301L Tau mutation was employed to promote Tau β sheet and paired helical filament (PHF) formation in Clone 4 cells (Barghorn et al., 2000; von Bergen et al., 2001; Fischer et al., 2007). Furthermore, P301L-mutant Tau accumulates and oligomerises more effectively due to poorer association with microtubules, as compared to native Tau or other Tau mutants, such as V337M or R406W (Barghorn et al., 2000; Fischer et al., 2007; Dayanandan et al., 1999). In agreement with the increased aggregation propensity, i*n vivo* studies have demonstrated that only

2N4R Tau (P301L), but not 2N4R Tau, -transgenic mice developed NFTs in their brains (Terwel et al., 2005).

In the current study, predominantly soluble Tau could be detected in both non-Dox-treated SH-SY5Y (Figure 3.2B) and Clone 4 cells (Figure 3.3B). Importantly, despite the fact that soluble Tau formation was (non-significantly) decreased to ~65 % in response to 4 day-long Dox treatment (Figure 3.3B), there was no evidence of increased cell death of Clone 4 cells over this time period (Figure 3.4). The lack of a cytotoxic effect suggests that the overexpressed 2N4R Tau (P301L) in Clone 4 cells may not aggregate effectively into oligomers and insoluble inclusions. Given that polyclonal SH-SY5Y cells stably expressing 2N4R Tau or 2N4R Tau (P301L) displayed ~5 - 10 % insoluble Tau (Ott et al., 2011), this suggests that at least some Tau aggregates may form in Dox-induced Clone 4 cells. To confirm whether Tau inclusions are generated in Dox-treated Clone 4 cells, the Thioflavin S (ThS) or X-34 stains may be used in future experiments in order to investigate the presence of insoluble and β sheet-containing PHFs and NFTs via immunocytochemistry (Santa-Maria et al., 2006; Styren et al., 2000). Other studies suggest that the formation of insoluble Tau inclusions in Clone 4 cells is plausible. Although the more aggregation-prone Tau RD with another Tau mutation was overexpressed, (Khlistunova et al., 2006) observed ThS immunoreactivity following the 5 day-long Dox-induction of Tau RD (ΔK280) in N2a neuroblastoma cells (ThS reactivity in ~9% cells by day 9). Moreover, the group detected the accumulation of pelletable and sarkosyl-insoluble Tau from day 4, which continually increased to ~11 % by day 11 (Khlistunova et al., 2006).

In summary, overexpression of 2N4R Tau (P301L) by Clone 4 cells is not toxic for up to 4 days. Because Tau aggregation, but not overexpression, is reported to be cytotoxic, here may be limited Tau aggregation in Clone 4 cells. However, further studies are required to confirm if overexpressed 2N4R Tau (P301L) does indeed aggregate in these cells.

3.5.2. Variability of soluble Tau in Dox-induced Clone 4 cells

Despite the fact that there was no significant difference in the proportions of soluble Tau in Dox-induced Clone 4 cells across 7 days, there was a lot of variability in the dataset (Figure 3.3B). Curiously, Dox treatment for 1 day slightly increased soluble Tau in Clone 4 cells (to 100 %) relative to untreated controls. However, prolonged Dox-induction reduced soluble Tau until day 4 (64.98 ± 9.78 %), then heightened it back to 100 % on day 7 (Figure 3.3B). It is interesting to speculate what caused this bizarre pattern of insoluble Tau in Clone 4 under Dox-exposed conditions.

The application of Dox increased total Tau expression of Clone 4 cells 5.69-fold (Figure 3.3A). Considering the slow aggregation of full-length Tau (Lim et al., 2014; Chirita et al., 2005), it is possible that predominantly soluble 2N4R Tau (P301L) accumulated in the cytosol of Clone 4 cells following 1 day of Dox-induction. In comparison, non-Dox-treated Clone 4 cells displayed proportions of ~86.2 % (± 9.56 %) soluble and, thus, ~13.8 % insoluble Tau, whilst Dox-induced cells exhibited 100 % soluble and 0 % insoluble Tau at day 1 (Figure 3.3B). Because soluble 2N4R Tau (P301L) was overexpressed following Dox treatment, this could have masked the relatively small proportions of insoluble Tau present in Clone 4 cells on day 1, but also on day 7 and, partially, day 2.

It might be argued that Dox-based Tau cell models, such as Clone 4 cells, are limited in that it has previously been reported that Dox itself inhibits β sheet formation and the heparin-driven fibrillisation of recombinant 2N4R Tau and Tau RD (K18 fragment) with an IC_{50} of 29 µM (~12 µg/mL) (Medina et al., 2021). It was postulated that Dox is capable of interacting with the Tau RD, since the antibiotic prevented the incorporation of Tau monomers into fibrils. Furthermore, co-incubation of recombinant Tau and heparin with Dox for 24 h ablated the seeding capacity of Tau, fully rescuing the loss of cell viability when this pre-incubated Tau/heparin/Dox mixture was applied to SH-SY5Y cells. However, dose-response curves showed that ≤ 10 µM Dox (~4.14 µg/mL) had no impact on the aggregation of synthetic 2N4R Tau (Medina et al., 2021). The final Dox concentrations employed in the current experiments (500 ng/mL) were far below 10 µM / 4.14 µg/mL, which implies that Dox did

not influence Tau oligomerisation and insoluble Tau formation in Clone 4 cells. This is supported by the fact that Dox did not affect the proportions of soluble endogenous Tau in SH-SY5Y cells (Figure 3.2B).

On the other hand, it is unclear what caused the striking reduction in the relative proportions of soluble Tau to 64.99 ± 9.78 % specifically in 4 day-long treated Clone 4 cells (Figure 3.3B). Untransfected SH-SY5Y cells also showed varied soluble Tau proportions between 1 - 7 days in culture (Figure 3.2B), implying that there is a non-Dox-related and, rather, cell-associated variability in the quantities of soluble Tau. Another possibility is that the overexpressed 2N4R Tau (P301L) indeed aggregated by day 4, but cellular clearance mechanisms were co-activated on this day, thus evoking the degradation of insoluble Tau by day 7. This is potentially supported by the fact that Dox-induced total Tau expression in Clone 4 cells plateaued between day 4 and 7 (Figure 3.3A).

In any case, future experiments using ThS, X-34 or other amyloid stains are necessary to confirm the formation of β sheet-containing Tau inclusions in Clone 4 cells over, ideally, a time span of 2 weeks (Santa-Maria et al., 2006; Styren et al., 2000).

3.5.3. The RI-AG03-polyR-induced accumulation of Tau in Clone 4 cells

Interestingly, following the Dox-induced overexpression of 2N4R Tau (P301L) for 48 h, co-treatment of Clone 4 cells with either the scrambled peptide (10 nM, 100 nM or 5000 nM) or RI-AG03-polyR (10 nM, 1000 nM and 5000 nM) further elevated total Tau levels. These results suggest that the peptides elicit the accumulation of Tau in the cytoplasm when Tau is overexpressed. There could be two potential explanations for this phenomenon, as discussed below.

(i) Arginine-rich peptides, including polyR (4 - 10 arginine residues) and TAT, have been shown to block cathepsin D (Horn et al., 2000) and proteasomal function (Gao et al., 2000; Gaczynska et al., 2003; Kloss et al., 2009; Anbanandam et al., 2008; Karpowicz et al., 2015). Specifically, polyR (octaarginine; as present in RI-AG03-polyR and the scrambled peptide) blocked proteasome-

associated chymotrypsin or caspase-like activities with an IC_{50} of 100 nM or 200 nM, respectively, leading to the accumulation of ubiquitinated proteins in HeLa cells (Kloss et al., 2009). Thus, it is plausible the polyR sequence in the peptides enhanced the intracellular levels of overexpressed 2N4R Tau (P301L) by interfering with its degradation.

(ii) Previous experiments of our group showed that RI-AG03 interacts with the RD region of Tau through a combination of the peptide's Tau binding sequence as well as charge-associated effects, leading to the formation of ~36 nm spherical Tau structures *in vitro* (Aggidis A. et al., 2021). Since both the Tau RD and our retro-inverted peptides are proteolytically resistant (Taylor et al., 2010; Aggidis A. et al., 2021; Wischik et al., 2018), such peptide-bound Tau RD species might accumulate in cells. This is supported by the fact that the application of RI-AG03-polyR or the scrambled control peptide did not enhance the band of the overexpressed 2N4R Tau (P301L) (~68 kDa), but rather those of 2N4R Tau degradation products (20 - 40 kDa), in Dox-induced Clone 4 cells (Figure 3.5B). However, it is not known how the scrambled peptide could potentially interact with Tau.

Charge plays a role in mediating peptide-binding to Tau. Arginine residues, contained within the cell penetrating polyR sequence of both peptides in the current study, are positively charged, which could promote interactions with Tau. Indeed, our group previously found that the addition of multiple arginine residues significantly improved the anti-aggregatory effects of the initial peptide candidates in the ThT assay (Aggidis A. et al., 2021). Cationic arginine multimers, such as hexaarginine (R6), nonaarginine (R8) (Mamsa and Meloni, 2021), poly-l-arginine hydrochloride (Merck; between R32 - R96) (Nadimidla et al., 2017) or other arginine-rich peptides (reviewed in Mamsa and Meloni (2021)) have been shown to interact with negatively charged pathological Tau species or polyanionic co-factors (i.e. heparin) that stimulate the β sheet formation and aggregation of Tau. As such, even though octaarginine itself was not capable of inhibiting the heparin-induced aggregation of recombinant $Tau_{\Delta 1\text{-}250}$ (Aggidis A. et al., 2021), the polyR CPP in scrambled RI-AG03 might have bestowed it with some binding affinity towards Tau. This certainly warrants further characterisation, given the results seen in Clone 4 cells in the current study.

Moreover, in previous studies, we only confirmed that scrambled AG03, but not scrambled RI-AG03, had no effect on blocking the aggregation of recombinant $Tau_{\Delta 1\text{-}250}$ (Aggidis A. et al., 2021). Given that retro-inversion almost doubled the oligomerization-inhibiting effects on synthetic $Tau_{\Delta 1\text{-}250}$ (RI-AG03 (~94 %) compared to AG03 (~53 %) (Aggidis A. et al., 2021), it is possible that this improved the Tau affinity of scrambled AG03 in a similar manner. To confirm that the peptides interact with overexpressed Tau in Clone 4 cells, immunocytochemistry, using fluorophore-conjugated peptide versions and Tau-targeting antibodies could be employed. Moreover, the β sheet-inhibiting effects of scrambled RI-AG03 should be investigated with the ThT assay.

3.5.4. Potential methods to seed Tau aggregation and cell differentiation in future experiments

At least over the first 4 days, the data in the current study indicate that there was no cell death in response to the Dox-induced overexpression of 2N4R (P301L) Tau in Clone 4 cells (Figure 3.4). Moreover, the occurrence of Tau aggregation in these cells is questionable, as debated in section 3.5.2. Therefore, the cytoprotective and anti-aggregatory effects of RI-AG03-polyR might be investigated by seeding Tau aggregation in Clone 4 cells in the future.

A range of Tau seeding methods have been reported (Sanders et al., 2014; Iba et al., 2013; Xu et al., 2016; Tanaka et al., 1998; Boban et al., 2019; Ott et al., 2011; Bandyopadhyay et al., 2007; Nie et al., 2007; Takahashi et al., 2012). For example, it has been shown that the lipofectamine-mediated transfection of Tau-overexpressing cells with 400 nM recombinant, heparin-aggregated Tau seeds (consisting of either Tau RD or full-length Tau) (Sanders et al., 2014) or their injection into the brain of 1N4R (P301S) Tau-transgenic PS19 mice (2.5 mL of 2 µl/mL), induces Tau propagation (Iba et al., 2013). Notably, Tau seeding barriers have been reported. In this context, mutant Tau oligomers were incapable of stimulating native Tau or Tau with a different point mutation, whereas WT Tau fibrils could seed any form of Tau (Sanders et al., 2014; Xu et al., 2016). In the case of Clone 4 cells in the current study, recombinant WT or P301L-mutant 2N4R Tau or Tau RD could be used. Alternatively,

Tau seed-containing cell or brain lysate (~20 µg) could be added into the cell culture medium as a stimulus for Tau oligomerisation (Sanders et al., 2014; Xu et al., 2016). Unfortunately, the lysate of Clone 9 cells, which contains self-propagating Tau RD (P301L/V337M)-EYFP (chapter 4) (Sanders et al., 2014), would not be suitable to induce the aggregation of the 2N4R (P301L) Tau expressed by Clone 4 cells due to the aforementioned seeding barrier between P301L and P301S-mutant Tau (Xu et al., 2016). Similarly, the brain lysate of PS19 mice, transgenic for 1N4R Tau (P301S) (chapter 6), could not be used. However, brain homogenate from AD or Tauopathy patients (as previously carried out in SH-SY5Y cells (Tarutani et al., 2021)), or from Tau (P301L)-transgenic animals, might be employed.

In addition, Dox-induced Clone 4 cells could be exposed to okadaic acid (10 - 30 nM) which has been shown to inhibit the Tau-dephosphorylating PP-1 and PP-2A, whilst promoting the activity of mitogen-activated protein kinase, cyclin-dependent kinase 2 and cdk5 (Tanaka et al., 1998; Boban et al., 2019). As a consequence, okadaic acid triggered Tau hyperphosphorylation at multiple sites, Tau oligomerisation into high molecular weight species, microtubular disassembly and death in cultured SH-SY5Y cells (Tanaka et al., 1998; Boban et al., 2019). Finally, 2N4R Tau or 2N4R Tau (P301L)-overexpressing SH-SY5Y cells could be incubated with 10 µM pre-aggregated $A\beta_{1–42}$ peptides for 90 min, which has been shown to double insoluble phospho-Tau ($Ser^{199/202}$, Ser^{262} and Ser^{422}) levels and elicit the formation of intracellular Tau inclusions (Ott et al., 2011). The authors also demonstrated that the prolonged exposure of cells to $A\beta_{1–42}$ oligomers, for at least 48 h, induced cell lysis. Besides stimulating Tau aggregation upon Dox-induction, the co-application of Aβ would pose an excellent experiment to investigate the combinatorial treatment of RI-AG03 as well as our previously developed Aβ-aggregation inhibitor RI-OR2-TAT in Clone 4 cells (Taylor et al., 2010; Parthsarathy et al., 2013).

Besides the aforementioned methods, Tau aggregation in Dox-induced Clone 4 cells could also be stimulated by using congo red (10 µM) (Bandyopadhyay et al., 2007), formaldehyde (0.0002 - 0.0005 %) (Nie et al., 2007) or NO exposure, i.e. via applying DETA NONOate (Takahashi et al., 2012).

These seeding methods are not ideal to test RI-AG03, however. Disadvantages are that an external compound is used that generate non-physiological Tau aggregates (congo red and formaldehyde) (Bandyopadhyay et al., 2007; Nie et al., 2007), whilst NO exposure triggers non-specific side effects, including protein nitrosylation or mitochondrial impairment (Takahashi et al., 2012).

All experiments in this study have focused on using undifferentiated Clone 4 SH-SY5Y cells. However, these cells may be differentiated into neurons with e.g. BDNF or retinoic acid (Bell and Zempel, 2022a), leading to the maturation of both dendrites and axons, microtubule formation and a more balanced 3R:4R Tau isoform ratio (Bell and Zempel, 2022a; Agholme et al., 2010; Uberti et al., 1997). Once differentiated, the overexpression of 2N4R Tau (P301L), and the resulting impact on cell viability, Tau aggregation and morphology, may be investigated over a time period beyond 7 days.

3.6. Conclusion

Clone 4 SH-SY5Y cells are a Dox-inducible 2N4R Tau (P301L) overexpression model that shows a time-dependent increase in total Tau levels (up to ~16-fold) that plateaus after 4 days of Dox-induced 2N4R Tau (P301L) expression. An advantage is that Clone 4 cells exhibit endogenous Tau expression, similar to neurons. However, there is no Tau-associated cell death in this cell model. Moreover, over the assessed time course of 7 days, Clone 4 cells only produced soluble Tau following Dox-induced overexpression, with no evidence for the formation of insoluble aggregates.

The treatment of Clone 4 cells with the Tau aggregation inhibitor peptide RI-AG03-polyR or a scrambled control peptide had no effect on the levels of endogenous Tau. However, in comparison to Dox- and peptide-untreated Clone 4 cells, Dox-exposure led to a 6.47-fold increase in total Tau levels, whilst co-treatment with 10 nM, 1000 nM and 5000 nM RI-AG03-polyR and 10 nM, 100 nM and 5000 nM scrambled RI-AG03-polyR magnified this increase, resulting in 31.64-fold and 18.88-fold elevated total Tau levels at 5000 nM, respectively.

Because both peptides increased total Tau levels, but RI-AG03-polyR showed a stronger effect than the scrambled control peptide at 5000 nM, this implies that Tau accumulation was partly mediated by the intact Tau binding sequence in RI-AG03-polyR and the polyR CPP present in both peptides. In addition, earlier studies of our group suggest that potentially degradation-resistant, circular peptide-Tau species might form in the cytoplasm, which could subsequently accumulate. Despite strongly increasing total Tau levels in the presence of Dox, concentrations of up to 5000 nM RI-AG03-polyR or scrambled RI-AG03-polyR did not affect cell viability or death.

As this study has focused on using undifferentiated Clone 4 cells, these cells may be differentiated into neurons. In a differentiated state, the impact of 2N4R Tau (P301L) overexpression on the proportions of soluble vs. insoluble Tau, aggregate formation, cell morphology and viability over time may be investigated in Clone 4 cells. Given the poor toxicity of Tau overexpression and the possible absence of Tau aggregation, seeding the aggregation of overexpressed Tau may also be useful to investigate if RI-AG03-polyR can halt seed-induced Tau aggregation and cell death in undifferentiated or differentiated Clone 4 cells.

4. Assessment of RI-AG03 and RI-AG03-conjuated liposomes in Tau RD (P301L/V337M)-EYFP-overexpressing Clone 9 HEK293 cells

4.1. Introduction

Under physiological conditions, Tau binds to α-tubulin in microtubules via its R1 - R4 region (amino acids 244 - 372 of full-length 2N4R Tau_{1-441}), collectively referred to as the Tau repeat domain (RD; R1 - 4) hereafter. Notably, the Tau RD also drives pathology-associated β sheet formation and the aggregation of Tau (Kolarova et al., 2012). Tau aggregation was shown to be mediated by the ^{275}VQIINK^{280} sequence in R2 of 4R Tau species and ^{306}VQIVYK^{311} in R3 of all 6 Tau isoforms (von Bergen et al., 2000; von Bergen et al., 2001). It has been demonstrated that the absence of the ^{275}VQIINK^{280} motif in R2 (in both 3R and 4R Tau species) and ^{306}VQIVYK^{311} in R3 (present only in 4R Tau) reduce or fully abolish, respectively, the seeding capacity of Tau, implying that these sequences are key for both Tau aggregation and propagation (Falcon et al., 2015; von Bergen et al., 2001; von Bergen et al., 2000).

Using recombinant $Tau_{\Delta 1-250}$, we have previously demonstrated that our ^{306}VQIVYK^{311}-interacting peptide RI-AG03 inhibited ~94 % of heparin-induced Tau aggregation (β sheet formation) at equimolar concentrations. Additionally, RI-AG03 blocked $Tau_{\Delta 1-250}$ fibril formation in response to a synthetic Tau seeds (Aggidis A. et al., 2021). These results suggest that RI-AG03 might be able to prevent pathology-associated Tau oligomerisation and spread during AD.

The aim of the current chapter was to test RI-AG03 in a cell culture model showing intracellular Tau aggregation and transcellular propagation of these Tau inclusions (Kfoury et al., 2012; Simon et al., 2012; Santa-Maria et al., 2012; Sanders et al., 2014). The Dox-inducible 2N4R Tau (P301L) overexpression model developed in chapter 3 (undifferentiated Clone 4 SH-SY5Y cells) produced soluble Tau and did not show any evidence of Tau aggregation, however. Therefore, a monoclonal HEK293 cell line, known as Clone 9, was employed instead (Sanders et al., 2014). Unlike SH-SY5Y cells, HEK293 cells do not endogenously express Tau (Li et al., 2007). Instead, Clone 9 HEK293 cells

are stably transfected to constitutively overexpress a Tau RD (P301L/V337M)-EYFP fusion protein. In addition, perpetual Tau oligomerisation in these cells was initiated by lipofectamine-mediated transduction with heparin-aggregated, synthetic Tau RD (Sanders et al., 2014). Characterisation studies have shown that Clone 9 cells generate pronase-resistant Tau fragments of 20 - 25 kDa and 10 - 13 kDa (Sanders et al., 2014). Of these fragments, the smaller one (10 -13 kDa) represents the degradation-resistant, propagation-inducing and truncated Tau RD forming the core of Tau aggregates (either a 10 kDa or 12 kDa fragment) (Wischik et al., 2018). Although not directly assessed, the slow growth and Tau seeding-associated toxic effects of Clone 9 cell lysate on other Tau RD-overexpressing cells suggest that there is ongoing cell death (Sanders et al., 2014). Thus, Clone 9 cells represent a suitable cell line to investigate the anti-aggregatory and cytoprotective effects of RI-AG03-polyR treatment.

Tau is phosphorylated at Ser^{202}/Thr^{205} by the pathology-associated kinases JNK, p38 and ERK2 (Reynolds et al., 2000). Furthermore, phosphorylation at the AT8 epitope (Ser^{202}/Thr^{205}) is characteristically found in PHFs and, thus, serves as a measure of Tau aggregate formation (Malia et al., 2016). As such, in the current study, phosphorylation of Tau at the AT8 epitope was also assessed.

4.2. Experimental goals

- Confirm the reported presence of Tau aggregation in Clone 9 HEK293 cells
- Investigate the impact of RI-AG03-polyR, as compared to scrambled peptide treatment, on total Tau, soluble vs. insoluble Tau (Tau aggregation) and Ser^{202}/Thr^{205}-phosohorylated Tau (AT8) levels in Clone 9 cells
- Test whether RI-AG03-polyR can dissolve pre-formed Tau aggregates or slow the active process of intracellular Tau aggregation

- Examine the cytoprotective effects of RI-AG03, either containing a polyR or TAT CPP, and peptide-conjugated liposomes in Tau propagation-exhibiting Clone 9 HEK293 cells
- Verify that RI-AG03-polyR interacts with overexpressed Tau RD (P301L/V337M)-EYFP following uptake by Clone 9 cells

4.3. Effects of RI-AG03-polyR on total, soluble and phospho-Tau

Initially, the impact of RI-AG03-polyR and scrambled control peptides on total Tau levels in Tau (P301L/V337M)-EYFP-overexpressing Clone 9 HEK293 cells was investigated via immunoblotting using polyclonal $Tau_{243-441}$ antibodies. Because untransfected HEK293 cells do not endogenously express Tau, peptide-untreated Clone 9 cells were used as the control (Li et al., 2007). To normalise Tau or phospho-Tau levels in every sample and across blots, the same unprocessed and untreated IGC (Clone 9 cell lysate) was loaded on all gels in every western blot in this chapter.

Clone 9 cells treated with final concentrations of 10 nM - 5000 nM RI-AG03-polyR or scrambled RI-AG03-polyR peptide for 48 h showed no differences in their total Tau levels (Figure 4.1A). However, the peptide type and peptide concentration significantly interacted after a 96 h treatment period ($F(4, 20) = 8.53$, $p < 0.001$) (Figure 4.1B). In comparison to peptide-untreated Clone 9 cells, exposure to 5000 nM scrambled RI-AG03-polyR significantly elevated total Tau levels 4.13-fold ($p < 0.001$). Moreover, treatment with 5000 nM of the scrambled peptide significantly increased total Tau levels in comparison to the same concentration of RI-AG03-polyR ($p < 0.001$; Figure 4.1B). Neither the scramble peptide or RI-AG03-polyR significantly increased total Tau levels at concentrations lower than 5000 nM. As reported by Sanders et al (2014), $Tau_{243-441}$ antibody staining revealed a Tau band at ~30 kDa and ~40 kDa, which represent the overexpressed Tau (P301L/V337M)-EYFP (Figure 4.1C&D).

Thus, the data show that high concentrations of the scrambled RI-AG03-polyR peptide (5000 nM) increase total Tau levels in Clone 9 HEK293 cells. This effect is similar to that observed in Dox-

induced Clone 4 SH-SY5Y cells (section 3.4.1, Figure 3.5A). However, whilst RI-AG03-polyR also increased total Tau levels in Dox-treated Clone 4 cells, it did not in Clone 9 cells.

Preliminary toxicity assays (section 4.5) indicated that RI-AG03 treatment with concentrations ≤ 100 nM is protective in Clone 9 cells. Higher peptide concentrations were avoided since using 5000 nM of, at least, scrambled RI-AG03-polyR triggered Tau accumulation (Figure 4.1B). Therefore, the impact of 10 nM and 100 nM peptide on the proportions of soluble Tau in Clone 9 cells was investigated. Insoluble Tau in the samples was removed by ultracentrifugation and, using western blotting and total $Tau_{243-441}$ antibodies, the amounts of Tau in the unprocessed total fractions (containing total Tau) versus ultracentrifuged soluble fractions (containing soluble Tau) were compared to determine the proportions of soluble Tau (Sanders et al., 2014).

The presence of Tau aggregation and propagation in Clone 9 cells was demonstrated previously (Sanders et al., 2014). In agreement with these reports, my results indicated that ~36 % (48 h, Figure 4.1E) and ~72 % (96 h, Figure 4.1F) of Tau in Clone 9 cells was soluble. Notably, the 48 h time point showed half the amount of soluble Tau seen at 96 h, suggesting that there was twice as much insoluble Tau at 48 h. This temporal difference in the amount of soluble Tau might be related to the different cell densities prior to and during cell lysis in both experiments (more cells were seeded in the 48 h condition). Possibly, in a non-confluent flask, any Tau aggregates formed in an individual cell might be split in half whenever this cell divides, thus diluting the amount of aggregates per cell. In turn, Tau aggregates may accumulate in non-proliferating confluent cells.

This discrepancy in the proportion of Tau aggregates in Clone 9 cells provided the opportunity to test whether RI-AG03-polyR and its scrambled control version were capable of disintegrating pre-formed aggregates (48 h; low proportions of soluble Tau) or if the peptides influenced the process of Tau aggregation (96 h; high levels of soluble Tau). At 48 h, Tukey's post hoc test did not identify a significant impact of 10 nM and 100 nM RI-AG03-polyR or its scrambled version on the proportions of soluble Tau. When compared at the same concentration, both peptides did also did not show a

significantly different effect (Figure 4.1E). This suggests that RI-AG03-polyR and its scrambled peptide version cannot dissolve already formed Tau (P301L/V337M)-EYFP aggregates. This result is in agreement with the inability of RI-AG03-polyR to disintegrate recombinant $Tau_{\Delta 1\text{-}250}$ seeds (Aggidis A. et al., 2021).

By contrast, following a 96 h exposure, the peptide choice and peptide concentration showed a significant interaction ($F(2, 12) = 12.83$, $p = 0.001$) (Figure 4.1F). Curiously, treatment with 10 nM scrambled RI-AG03-polyR for 96 h significantly decreased the proportions of soluble Tau relative to that seen in untreated Clone 9 cells (control; $p < 0.001$), whilst 10 nM RI-AG03-polyR had no effect. Furthermore, at a concentration of 10 nM, scrambled RI-AG03-polyR reduced soluble Tau significantly more than RI-AG03-polyR ($p < 0.001$). Using 100 nM, both the scrambled peptide ($p < 0.001$) and RI-AG03-polyR ($p < 0.001$) significantly decreased the proportions of soluble Tau in Clone 9 cells compared to untreated control cells. The effects of both peptides at 100 nM were not significantly different (Figure 4.1F). As such, contrary to my expectations, both scrambled and unscrambled RI-AG03-polyR appeared to promote Tau aggregation.

In agreement with the results of Sanders et al (2014), the ~40 kDa, but not ~30 kDa, Tau band represented insoluble Tau that could be pelleted and removed from the total fraction (T compared to control in Figure 4.1G&H). Interestingly, at 96 h, the concentrations of RI-AG03-polyR and its scrambled version that lowered soluble Tau both appeared to reduce the insoluble ~40 kDa and also the initially soluble ~30 kDa Tau bands in the soluble fractions (control compared to 10 nM & 100 nM scrambled peptide and 100 nM RI-AG03-polyR; Figure 4.1H and Figure 4.1F). This suggests that the peptides interact with intracellular Tau RD (V337M/P301L)-EYFP and render the protein insoluble, as partially implied in earlier experiments of our group (Aggidis A. et al., 2021).

Supporting the presence of intracellular Tau aggregation in untreated Clone 9 cells, immunolabelling of the pellet fraction with anti-$Tau_{243\text{-}441}$ and nanogold-conjugated secondary antibody further revealed small Tau aggregates with a width of ~10 nm in the lysate of Clone 9 cells (arrows in

Figure 4.1I). Morphologically, normal HEK293 cells display a multangular body with short neurite-like processes (Figure 4.1J). While Clone 9 HEK293 cells partially retain these characteristics, they are often rounded and clump up more frequently (Figure 4.1J). Furthermore, unlike HEK293 cells, large clumps of Clone 9 cells regularly detach from their dishes during routine culture.

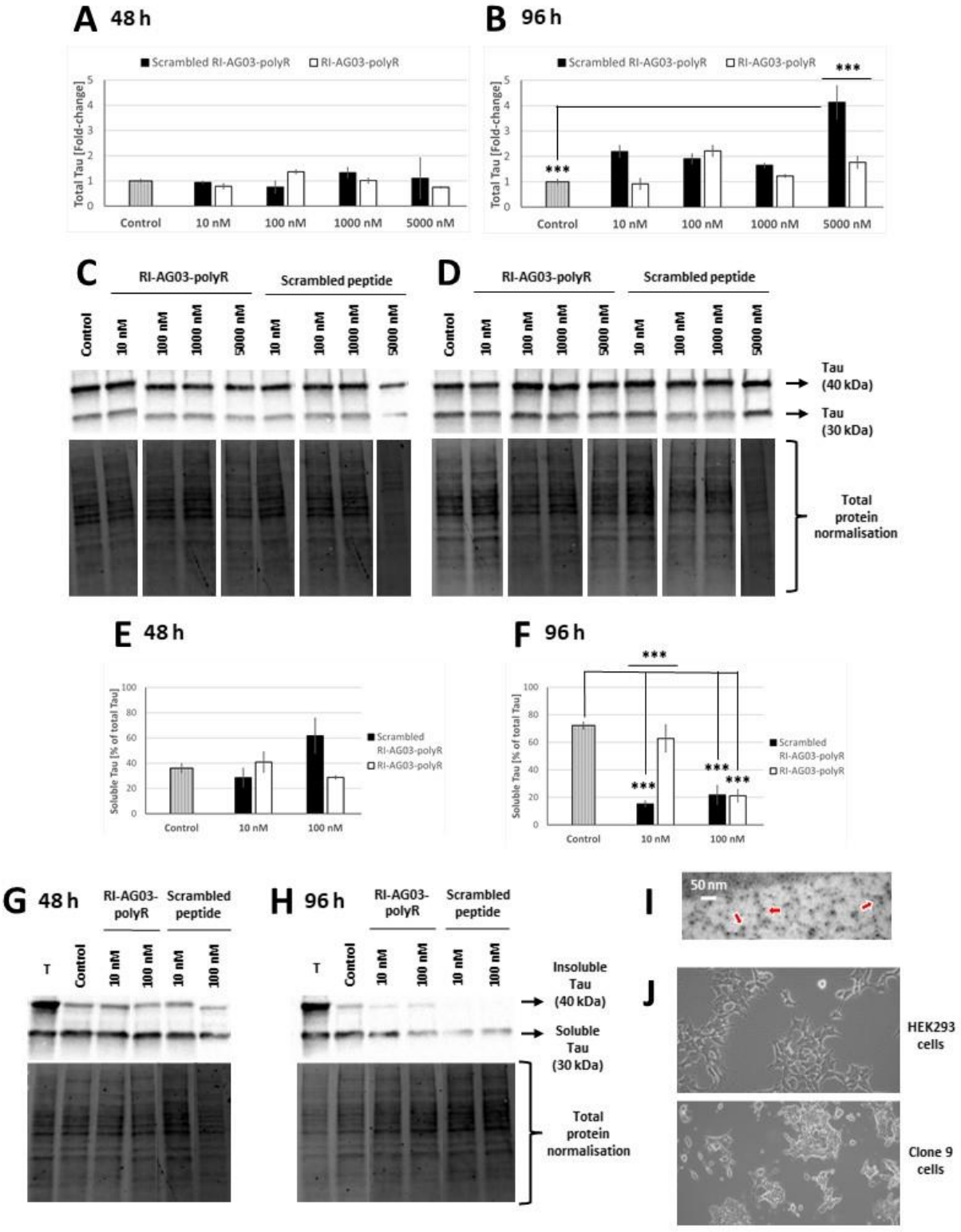

Figure 4.1: Effects of the RI-AG03-polyR and scrambled RI-AG03-polyR peptides on total and soluble Tau in Clone 9 cells. (A & B) mean ± SEM fold-change in total Tau levels after a 48 h or 96 h incubation period with the peptides (n = 3). Representative blots using total $Tau_{243-441}$ antibodies are shown in (C) for 48 h and (D) for 96 h incubations. (E & F) Proportions of soluble Tau (mean ± SEM % of total Tau, n = 3 technical replicates; separate cell wells/flasks treated at the same time) following a 48 h or 96 h-long peptide exposure. Representative immunoblots for $Tau_{243-441}$ in the total (T) and

soluble fractions of each sample are depicted in (G & H). For normalisation and comparison across all blots (A - H), the same untreated Clone 9 cell lysate was used on every gel (IGC). (I) TEM image of Tau RD (P301L/V337M)-EYFP aggregates (marked by arrows) that were purified from Clone 9 cells. Dots represent 10 nM nanogold-conjugated secondary antibodies bound to primary $Tau_{243-441}$ antibody. (J) Images of untransfected HEK293 and Clone 9 HEK293 cells. Western blots were normalised using total protein staining and data was analysed with two-way ANOVA followed by Tukey's post hoc test. *** = $p < 0.001$.

The impact of the peptides on the PHF-associated phosphorylation of Tau at Ser^{202} and Thr^{205} (AT8 epitope; (Malia et al., 2016)) over a 48 h and 96 h time period in Clone 9 cells was also evaluated. At peptide concentrations between 10 - 5000 nM, both RI-AG03-polyR and the scrambled peptide had no significant effect on (Ser^{202}/Thr^{205}) phospho-Tau levels in Clone 9 cells after a 48 h treatment period (Figure 4.2A). By contrast, when Clone 9 cells were incubated for 96 h, the peptide type and concentration significantly interacted ($F(4, 20) = 3.23$, $p = 0.034$; two-way ANOVA) (Figure 4.2B). However, two-way ANOVA did not reveal a significant effect of RI-AG03-polyR, nor the scrambled peptide, on the (Ser^{202}/Thr^{205}) phospho-Tau levels at any peptide concentration (Figure 4.2B). As seen in the representative immunoblot images, Clone 9 cell lysate probed with AT8 antibodies showed a phospho-Tau band at ~250 kDa and a few smaller smeary bands between ~100 - 150 kDa (Figure 4.2C&D). Therefore, the scrambled peptide and RI-AG03-polyR do not influence Tau RD (V337M/P301L)-EYFP phosphorylation at Ser^{202}/Thr^{205} in Clone 9 cells.

Similar to soluble total Tau, the proportions of soluble Ser^{202}/Thr^{205}-phosphorylated Tau in Clone 9 cells were determined by assessing total phospho-Tau levels in the total and ultracentrifuged soluble lysate fractions. A 96 h treatment time was chosen due to the earlier described Tau aggregation-stimulating effects of the peptides over this time period (Figure 4.1F).

Western blotting demonstrated only a small proportion of the Ser^{202}/Thr^{205}-phopshorylated Tau (~20 %) was soluble in Clone 9 cells (Figure 4.2E). Statistical analysis showed a significant interaction between the peptide type and concentration ($F(4, 20) = 9.76$, $p < 0.001$; two-way ANOVA). 96 h treatment with 10 nM scrambled peptide significantly increased the proportions of soluble

(Ser^{202}/Thr^{205}) phospho-Tau compared to untreated Clone 9 cells (p = 0.011). Additionally, cell exposure to 10 nM scrambled peptide led to higher proportions of soluble (Ser^{202}/Thr^{205}) phospho-Tau than the same concentration of RI-AG03-polyR (p = 0.005). By contrast, soluble (Ser^{202}/Thr^{205}) phospho-Tau levels were not significantly different from untreated control cells at any other peptide concentration, for either RI-AG03-polyR or the scrambled peptide (Figure 4.2E). Since total (Ser^{202}/Thr^{205}) phospho-Tau levels were unaltered in response to scrambled peptide treatment (Figure 4.2A&B), this suggests that 10 nM of this control peptide solubilised phospho-Tau (specifically the 250 kDa band; Figure 4.2F).

According to the manufacturer, AT8 antibodies (Invitrogen, #MN1020) recognise monomeric (Ser^{202}/Thr^{205}) phospho-Tau at a predicted molecular weight of ~79 kDa (as dependent on the form of Tau that is expressed and phosphorylation status). In Clone 9 cells, the overexpressed Tau RD (V337M/P301L)-EYFP showed molecular weights of 30 kDa (soluble) and 40 kDa (insoluble; Figure 4.1C,D,G&H). As seen in the uncropped representative blot in Figure 4.2G, (Ser^{202}/Thr^{205}) phospho-Tau bands only appeared between 100 - 250 kDa in Clone 9 cells. By contrast, when the earlier shown total $Tau_{243-441}$ blots (Figure 4.1) were exposed for a prolonged time, large MW bands of total Tau appeared at the same height as (Ser^{202}/Thr^{205}) phospho-Tau (e.g. see arrows showing 250 kDa species of Phospho-Tau (96 h) and Total Tau (96 h) in Figure 4.2G). This suggests that specifically larger and SDS-resistant Tau RD (V337M/P301L)-EYFP inclusions are phosphorylated at AT8 in Clone 9 cells (Sanders et al., 2014; Malia et al., 2016). In support of representing aggregated species, the amount of soluble (Ser^{202}/Thr^{205}) phospho-Tau was low in untreated Clone 9 cells (~20 %, Figure 4.2E) and all (Ser^{202}/Thr^{205}) phospho-Tau bands in the total cell fraction appeared to be partially pelletable (Figure 4.2F; T compared to control).

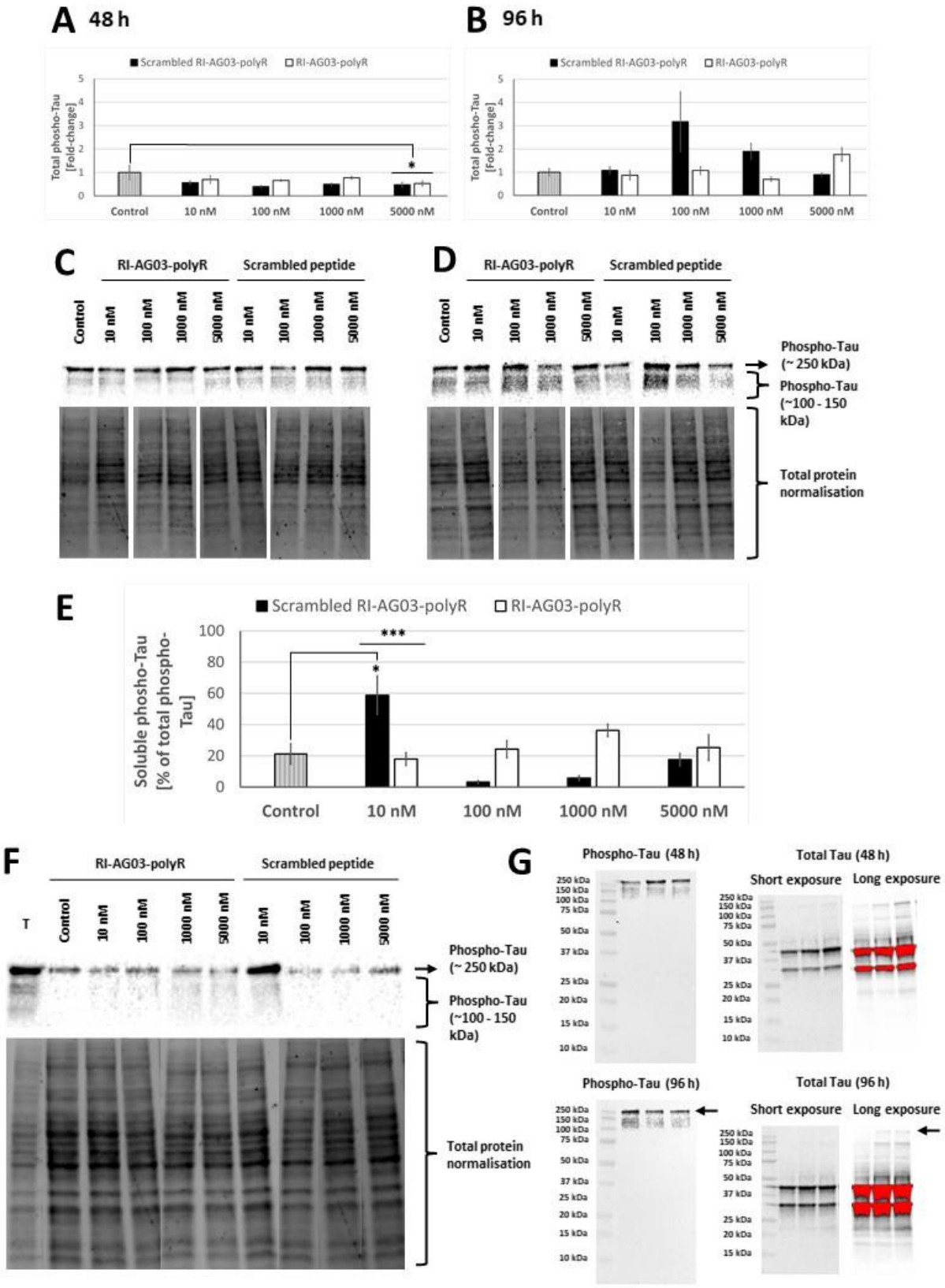

Figure 4.2: Total and soluble phospho-Tau levels in Clone 9 cells following peptide exposure.
(A & B) Mean ± SEM fold-change in (Ser^{202}/Thr^{205}) phospho-Tau levels (n = 3) in response to 48 h- or 96 h-long RI-AG03-polyR or scrambled peptide treatments, shown as fold-change relative to untreated Clone 9 cells (control). The corresponding representative blots using AT8 (Ser^{202}/Thr^{205})

phospho-Tau antibodies are depicted in (C) for 48 h and (D) for 96 h. (E) Proportions of soluble Ser^{202}/Thr^{205}-phopshorylated Tau (mean ± SEM % of total phospho-Tau, n = 3 technical replicates; separate cell wells/flasks treated at the same time) following 96 h. (F) Representative western blots showing AT8 phospho-Tau in the total (T) and soluble fractions. (G) Uncropped representative blots of untreated Clone 9 cell lysate (triplicates) stained with (Ser^{202}/Thr^{205}) phospho-Tau (long exposure) or total $Tau_{243-441}$ antibodies (short and long exposure) at 48 h and 96 h. Red bands are overexposed and arrows denote total Tau species at 250 kDa that match the MW of (Ser^{202}/Thr^{205}) phospho-Tau (at 96 h). Total protein normalisation was applied for immunoblots and Tau band intensities of the samples were normalised to that of the same IGC on all gels (unprocessed, untreated Clone 9 cell lysate). In order to calculate significant differences, two-way ANOVA and Tukey's post hoc test were used. * = $p < 0.05$ and *** = $p < 0.001$.

Finally, the relative ratio of total (Ser^{202}/Thr^{205}) phospho-Tau to total Tau was determined. RI-AG03-polyR and the scrambled peptide did not significantly alter the phospho-Tau/Tau ratio after a 48 h treatment period (Figure 4.3A). Following the 96 h-long peptide treatment in Clone 9 cells, there was a significant interaction between peptide type and concentration ($F(4, 20) = 5.92$, $p = 0.003$; two-way ANOVA) (Figure 4.3B). However, neither the scrambled peptide, nor RI-AG03-polyR, significantly altered the (Ser^{202}/Thr^{205}) phospho-Tau/Tau ratio relative to untreated cells. The effects of both peptides also were not significantly different at the same concentration (Figure 4.3B).

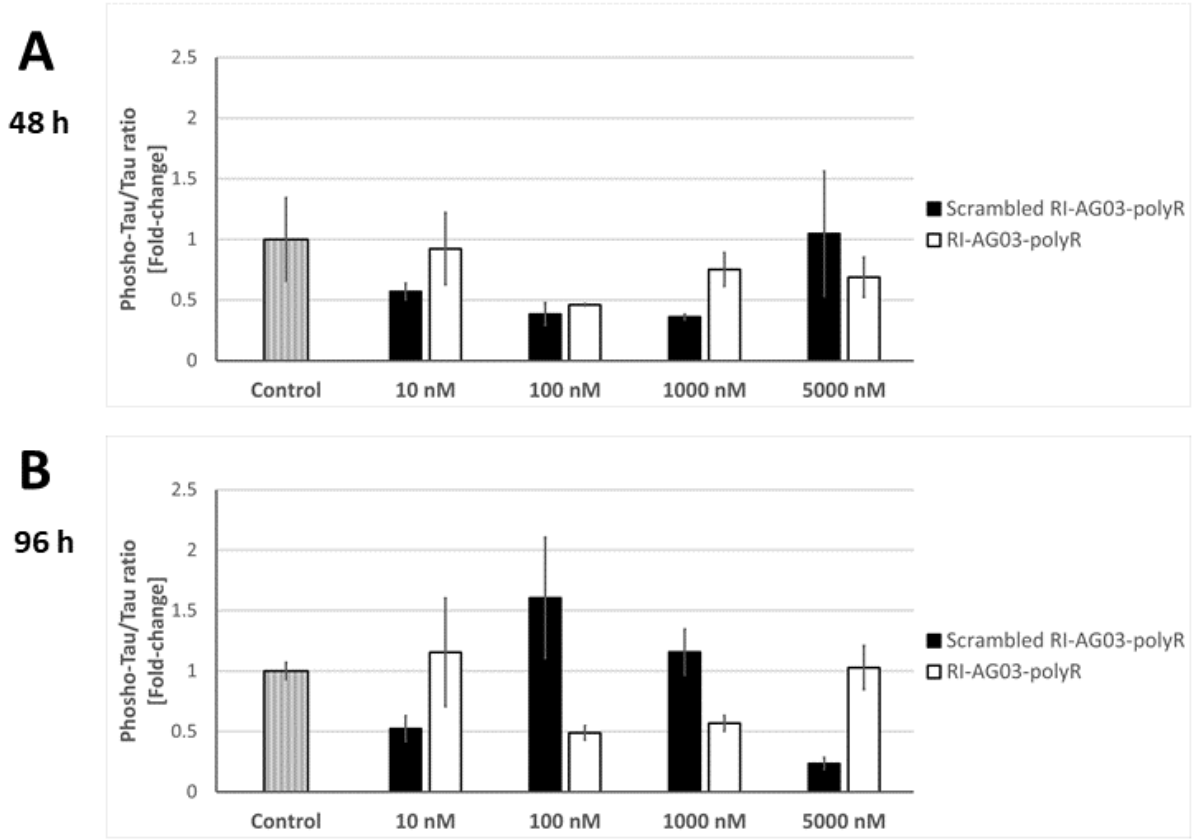

Figure 4.3: Impact of the RI-AG03-polyR and scrambled RI-AG03-polyR peptides on the phospho-Tau/Tau ratio. Shown are the mean ± SEM fold-change in the western blot ratio of AT8 (Ser^{202}/Thr^{205}) phospho-Tau and total Tau in the lysate of peptide-treated Clone 9 cells after 48 h (A) and 96 h (B) relative to untreated clone 9 cells (control; n = 3). Analysis of the data using two-way ANOVA and Tukey's post hoc test did not reveal any statistical differences.

4.4. Interaction of RI-AG03 and RI-AG03-linked liposomes with Tau

Because RI-AG03-polyR decreased the proportions of soluble Tau in Clone 9 cells, co-localisation of Cy-5-labelled RI-AG03-polyR peptide (red) with Tau RD (P301L/V337M)-EYFP (green) was monitored in Clone 9 cells (Figure 4.4). Co-localisation was additionally quantified using Pearson's correlation coefficient Rcoloc and Chan YH's interpretation (Table 4.1) (Akoglu, 2018). Notably, by conjugating RI-AG03-polyR to liposomes (characterised in chapter 5), we aim to administer these 'PINPs' across the nasal mucosa into the brain (Gregori et al., 2017). Thus, Cy-5-RI-AG03-polyR was additionally conjugated to liposomes (red) to investigate if this process affects the intracellular interaction with Tau RD (P301L/V337M)-EYFP. Drug concentrations of 5000 nM were used for better visualisation. 2

h and 16 h treatment periods were chosen to track potential changes in the subcellular localisation over time and because we have demonstrated that the cellular uptake of the peptides occurs within 10 min (Parthsarathy et al., 2013).

As shown in Figure 4.4A, Clone 9 cells display numerous large Tau RD (P301L/V337M)-EYFP aggregates in the cytoplasm and smaller inclusions in the nucleus, as reported previously (Sanders et al., 2014). This coincides with the fact that the proportions of soluble Tau RD (P301L/V337M)-EYFP in Clone 9 cells were modest (36 - 72 %; Figure 4.1E&F).

After a 2 h treatment period, there was a poor anti-correlation of Cy5-RI-AG03-polyR with Tau RD (P301L/V337M)-EYFP (Table 4.1), suggesting that the peptide and Tau RD (P301L/V337M)-EYFP were predominantly present in distinct intracellular locations. There was no intracellular co-localisation of the peptide with larger Tau RD (P301L/V337M)-EYFP inclusions (Figure 4.4B). However, the Cy5-peptide occasionally located in proximity to less aggregated Tau RD (P301L/V337M)-EYFP proteins (red arrow in Figure 4.4B). At 16 h, image analysis suggests that there was no co-localisation of Cy5-RI-AG03-polyR and Tau RD (P301L/V337M)-EYFP (Table 4.1). Marginal overlap of Cy5-RI-AG03-polyR with cytoplasmic Tau RD (P301L/V337M)-EYFP mono- or oligomers (red arrow) and aggregates (yellow arrow) could be observed (Figure 4.4B).

In the case of Cy5-RI-AG03-polyR-liposomes, quantification showed no co-localisation with Tau RD (P301L/V337M)-EYFP in Clone 9 cells following a 2 h or 16 h treatment period (Table 4.1). However, similar to the free Cy5-RI-AG03-polyR peptide, localisation of Cy5-RI-AG03-polyR-liposomes near Tau RD (P301L/V337M)-EYFP (red arrow), but no co-localisation with larger aggregates of this protein, was observed at 16 h (Figure 4.4C).

The average number and size of amyloid aggregates in Clone 9 cells, without and with Cy5-RI-AG03-polyR(-liposome) treatment, was also determined (Table 4.2). Statistical analysis revealed that drug treatment significantly affected the average number of Tau RD (P301L/V337M)-EYFP aggregates ($F(4, 7) = 5.21$, $p = 0.029$; one-way ANOVA). While missing significance at 2 h (~39 aggregates, p =

0.063), Cy5-RI-AG03-polyR significantly increased aggregate counts from ~8 (untreated) to ~42 per cell (p = 0.042) following a 16 h treatment period. On the other hand, the average size of Tau RD (P301L/V337M)-EYFP aggregates was not significantly altered. Notably, although non-significant, cell exposure to Cy5-RI-AG03-polyR lowered, or even halved, mean aggregate size relative to untreated Clone 9 cells (from 146.41 pixels to 74.79 pixels (49 % smaller) at 2 h and 92.38 pixels (37 % less) at 16 h).

Collectively, the results demonstrate that both RI-AG03-polyR and RI-AG03-polyR conjugated to liposomes poorly interact with Tau RD (P301L/V337M)-EYFP in Clone 9 cells. The lack of co-localisation with bigger Tau inclusions suggests that RI-AG03-polyR may not bind to these. Curiously, prolonged treatment with Cy5-RI-AG03-polyR for 16 h, but not 2 h, increased the number of Tau RD (P301L/V337M)-EYFP aggregates in Clone 9 cells, with a notable, but non-significant, reduction in aggregate size. Since RI-AG03-polyR reduced the proportions of soluble Tau in Clone 9 cells (Figure 4.1F), this might imply that RI-AG03-polyR stimulates the formation of smaller oligomeric Tau RD (P301L/V337M)-EYFP aggregates in these cells, as indicated in previous studies (Aggidis A. et al., 2021).

Table 4.1: Co-localisation of unconjugated or liposome-conjugated Cy5-RI-AG03-polyR with Tau (P301L/V337M)-EYFP in Clone 9 cells.

	Cy5-RI-AG03-polyR peptide (2 h)	Cy5-RI-AG03-polyR peptide (16 h)	Cy5-RI-AG03-polyR-liposomes (2 h)	Cy5-RI-AG03-polyR-liposomes (16 h)
Pearson's correlation coefficient (Rcoloc)	-0.2441 ± 0.1485	0.0145 ± 0.0702	0.0768 ± 0.0799	0
n	2	2	3	2
Interpretation co-localisation (Chan YH)	Poor	None	None	None

Table 4.2: Tau (P301L/V337M)-EYFP aggregate number and size in untreated or Cy5-RI-AG03-polyR(-liposome)-treated Clone 9 cells. Data was analysed using one-way ANOVA and Tukey's post hoc test. a = compared to untreated cells, $p < 0.05$.

	a. Untreated	b. Cy5-RI-AG03-polyR peptide (2 h)	c. Cy5-RI-AG03-polyR peptide (16 h)	d. Cy5-RI-AG03-polyR-liposomes (2 h)	e. Cy5-RI-AG03-polyR-liposomes (16 h)
Aggregates per cell (Average)	7.85 ± 0.28	38.51 ± 7.01	41.49 ± 5.77 a*	15.82 ± 2.23	27.81 ± 15.69
Aggregate size (Average pixels)	146.41 ± 15.50	74.79 ± 1.29	92.48 ± 14.65	116.55 ± 33.26	97.85 ± 21.91
n	3	2	2	3	2

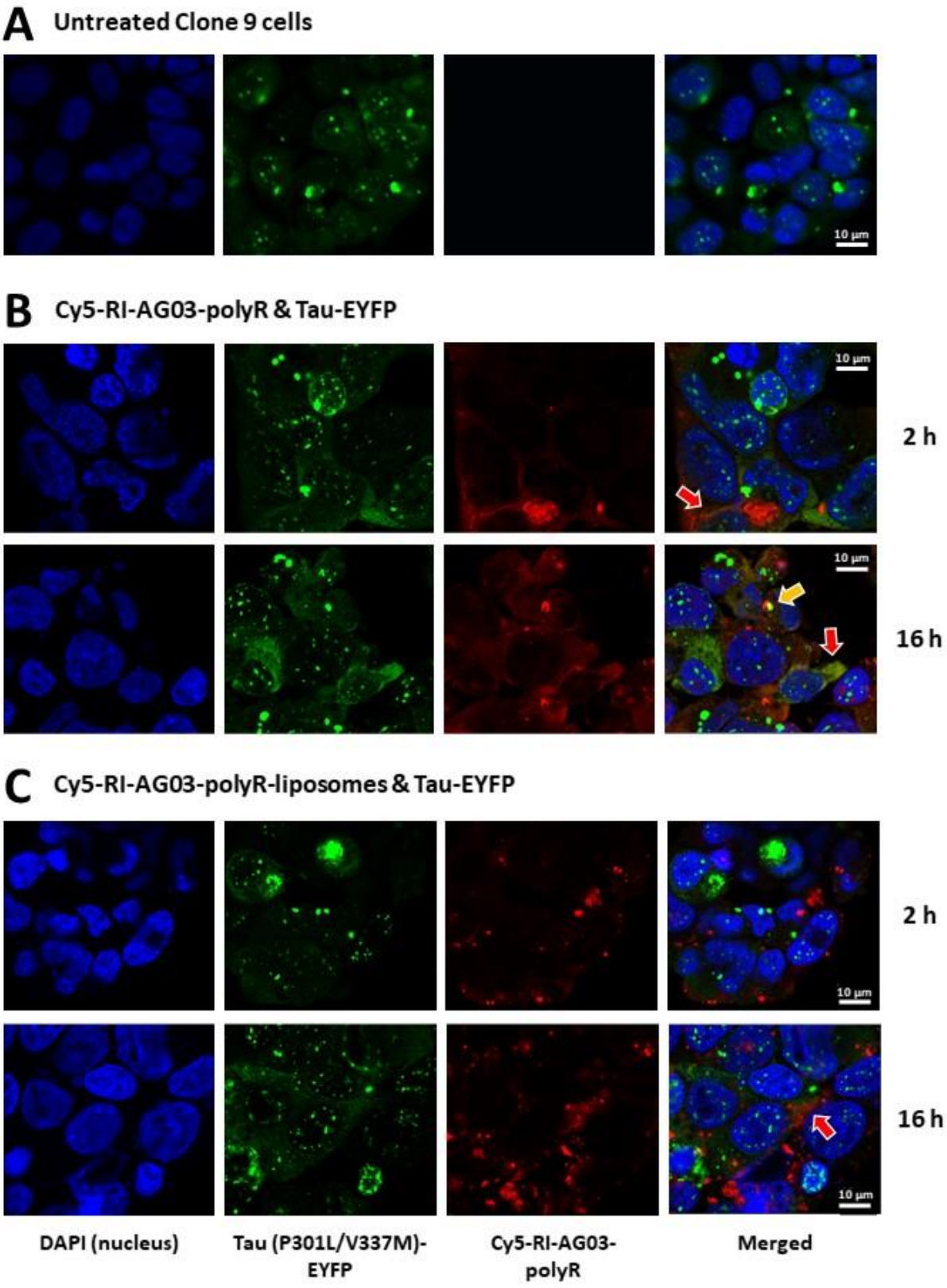

Figure 4.4: Co-localisation of RI-AG03-polyR and RI-AG03-conjugated liposomes with Tau RD (P301L/V337M)-EYFP in Clone 9 cells. Clone 9 was cultivated in the absence (A) or presence of Cy5-labelled RIAG03-polyR (B) or Cy5-RIAG03-polyR-liposomes (C) (peptide in red) for 2 h or 16 h. The confocal images depict Tau RD (P301L/V337M)-EYFP in green and the nucleus in blue (DAPI). Red

arrows imply co-localisation of the peptide or peptide-liposomes with putative monomeric or oligomeric Tau RD (P301L/V337M)-EYFP in the cytoplasm. The orange arrow highlights a potential (partial) interaction of Cy5-RIAG03-polyR with a large Tau RD (P301L/V337M)-EYFP inclusion.

4.5. The cytoprotective properties of RI-AG03 variants and RI-AG03-conjugated liposomes

Next, I investigated how the peptides affect cell viability, by observing the colorimetric conversion of MTT into formazans by living cells, and cell death, by characterising the membrane rupture-associated LDH release, in Clone 9 cells. A 48 h treatment was selected since this time period was sufficient to observe a drug effect (Figure 4.5).

In light of the cytoprotective effects of CPPs such as polyR and TAT (Mamsa and Meloni, 2021), and in order to ensure specificity, the effects of RI-AG03-polyR were compared to the previously used control peptide containing a scrambled Tau binding sequence and polyR. Because our previous Aβ aggregation inhibitor peptide, RI-OR2, contained TAT to promote cellular uptake (Parthsarathy et al., 2013), RI-AG03 was also synthesised with this CPP to compare it to the polyR sequence. In addition to testing the peptides in an unconjugated form, the effect of linking them to liposomes was assessed. Peptide and peptide-liposomes were initially used at 10 nM because, unlike 100 nM, this RI-AG03-polyR concentration did not reduce the proportions of soluble Tau in Clone 9 cells (Figure 4.1F).

Drug treatment significantly affected cell viability in MTT assays ($F(7, 42) = 4.64$, $p < 0.001$; one-way ANOVA). As expected, 10 nM of either scrambled RI-AG03-polyR, unconjugated liposomes or scrambled RI-AG03-polyR-conjugated liposomes did not influence cell viability (Figure 4.5A). However, treatment with 10 nM RI-AG03-polyR ($p = 0.014$) or RI-AG03-TAT peptide ($p = 0.029$) increased the cell viability of Clone 9 cells compared to untreated controls. A cell viability-enhancing effect was also observed when using 10 nM RI-AG03-polyR-linked liposomes ($p = 0.021$) and RI-AG03-TAT-conjugated liposomes ($p = 0.003$). In comparison to treatment with the scrambled peptide, RI-AG03-polyR and RI-AG03-TAT did not significantly enhance cell viability. On the other

hand, using RI-AG03-TAT-liposomes, but not RI-AG03-polyR-liposomes, improved cell viability significantly better than scrambled peptide-conjugated liposomes ($p = 0.044$; Figure 4.5A).

Peptide and peptide-liposome treatment also significantly influenced cell death, as measured via LDH release ($F(7, 42) = 5.58$, $p < 0.001$; one-way ANOVA). In agreement with the viability assays, neither the scrambled control peptide, unconjugated liposomes or scrambled RI-AG03-polyR-conjugated liposomes (at a concentration of 10 nM) reduced cell death (Figure 4.5B). On the other hand, the application of 10 nM RI-AG03-TAT ($p = 0.002$), RI-AG03-polyR-conjugated liposomes ($p = 0.010$) and RI-AG03-TAT-linked liposomes ($p = 0.006$) decreased LDH release relative to untreated Clone 9 cells. However, treatment with RI-AG03-polyR and RI-AG03-TAT did not significantly decrease membrane rupture relative to cells exposed to the scrambled control peptide. Similarly, using RI-AG03-polyR-liposomes or RI-AG03-TAT-liposomes did not significantly lower cell death compared to treatment with scrambled RI-AG03-polyR-liposomes (Figure 4.5B).

Collectively, unconjugated or liposome-conjugated RI-AG03 containing either CPP improved the viability of Clone 9 cells, whilst free RI-AG03-TAT peptide and RI-AG03-polyR/TAT-conjugated liposomes lowered cell death. Because the scrambled control peptide had no significant effect, this suggests that the Tau binding sequence in in RI-AG03, but not the polyR sequence, reduces toxicity in this Tauopathy cell model. Since we demonstrated that RI-AG03-polyR has no impact on LDH release in untransfected HEK293 cells ≤ 30 µM (Aggidis A. et al., 2021; Aggidis, 2019), this suggests that the peptide prevented Tau RD (P301L/V337M)-EYFP-induced cell death in Clone 9 cells.

Notably, when using peptide-liposomes, the concentration of 10 nM referred to the liposomes (lipids) rather than the peptide itself. The actual concentration of the liposome-conjugated peptide is theoretically ~40-fold lower, as elaborated in section 4.6.3. Therefore, in agreement with our previous *in vitro* studies using RI-OR2 or RI-AG03-polyR-conjugated liposomes (Gregori et al., 2017; Aggidis A. et al., 2021), my results suggest that RI-AG03-polyR/TAT-conjugated liposomes might be more effective in lowering Tau toxicity than the unconjugated form of the peptide.

Because peptide concentrations of 10 nM were protective in Clone 9 cells (Figure 4.5A&B), the impact of soluble Tau-lowering peptide concentrations (100 nM; Figure 4.1F) was also evaluated. Using a higher peptide concentration of 100 nM, RI-AG03-polyR and RI-AG03-TAT did not improve cell viability anymore (Figure 4.5C). As observed for 10 nM of the scrambled peptide (Figure 4.5A), using 100 nM of this peptide did not affect cell viability (Figure 4.5C). However, the peptides significantly influenced cell death ($F(3, 20) = 10.00$, $p < 0.001$; one-way ANOVA). Treatment with 100 nM RI-AG03-polyR ($p = 0.007$) and RI-AG03-TAT ($p = 0.003$) reduced LDH release in Clone 9 cells relative to untreated cells, whilst the scrambled peptide showed no effect. Moreover, cell exposure to either RI-AG03-polyR ($p = 0.008$) or RI-AG03-TAT ($p = 0.004$) significantly decreased membrane rupture compared to using the scrambled peptide (Figure 4.5D). Thus, these experiments indicate that Tau aggregation-enhancing RI-AG03-polyR/TAT concentrations still protect from Tau-induced death in Clone 9 cells.

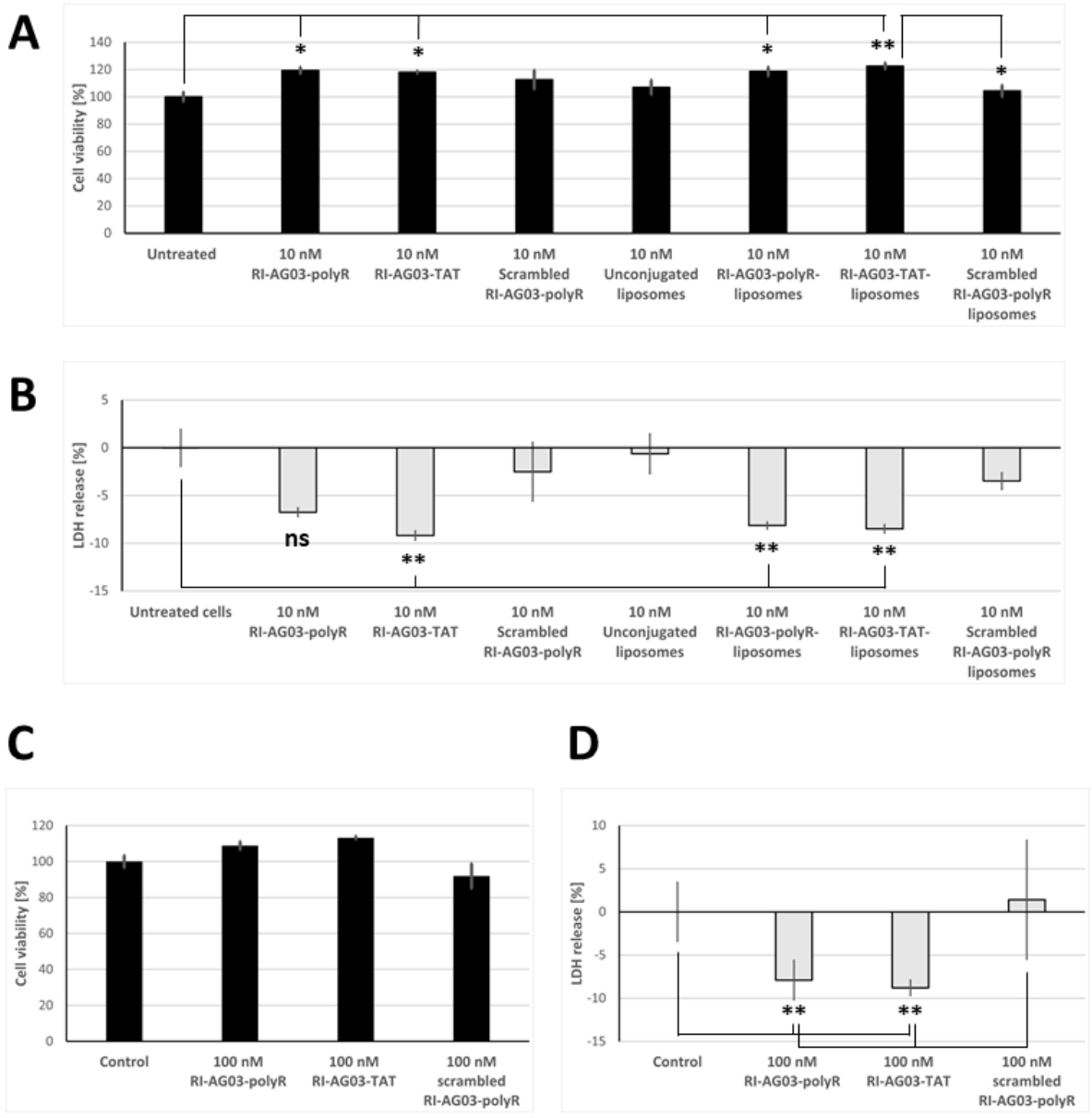

Figure 4.5: Cytoprotective effects of RI-AG03 peptide variants and peptide-conjugated liposomes in Tau RD (P301L/V337M)-EYFP-overexpressing Clone 9 cells. (A) Mean ± SEM % cell viability of Clone 9 cells following 48 h, as assessed with the colorimetric MTT assay relative to untreated cells (n = 6). (B) Cell death over 48 h, as evaluated by changes in LDH release relative to untreated control cells (data shown as Mean ± SEM; n = 6 technical replicates; separate cell wells/flasks treated at the same time). (C) MTT and (D) LDH assays using soluble Tau-reducing (aggregation-stimulating) peptide concentrations of 100 nM. Note that Clone 9 cells show continuous cell death in culture (Sanders et al., 2014), hence drug treatment generated negative LDH values. Statistically significant differences were analysed with one-way ANOVAs followed by Tukey's post hoc test. * = $p < 0.05$; ** = $p < 0.01$.

4.6. Discussion

4.6.1. Comparison of the total Tau-increasing effects of the peptides in Clone 9 HEK293 and Clone 4 SH-SY5Y cells

It was demonstrated that the 96 h, but not 48 h, treatment with 5000 nM scrambled RI-AG03-poly increased total Tau levels 4.13-fold in Tau RD (P301L/V337M)-EYFP-overexpressing Clone 9 cells (Figure 4.1B). Such effects were also observed in Dox-induced Clone 4 cells, in which 5000 nM of the scrambled control peptide increased total Tau levels 3.05-fold (from 6.17-fold (Dox) to 18.88-fold (Dox + scrambled peptide; Figure 3.5A) following a 48 h treatment period. Notably, whilst RI-AG03-polyR also raised total Tau levels in Dox-induced Clone 4 cells (Figure 3.5A), this peptide failed to affect total Tau levels in Clone 9 cells after a 96 h exposure (Figure 4.1B).

The different effects of the peptides in both Tauopathy cell models might be associated with the form of Tau that is overexpressed. Unlike the mostly soluble 2N4R Tau (P301L) expressed by Dox-induced Clone 4 cells (90 % soluble after 2 days of Dox-induction; Figure 3.3B), much less Tau RD (P301L/V337M)-EYFP in Clone 9 cells is soluble (between 36 % - 72 %; Figure 4.1E&F) and aggregated (Sanders et al., 2014). Moreover, immunocytochemistry indicated that RI-AG03-polyR does not bind to larger Tau RD (P301L/V337M)-EYFP aggregates in Clone 9 cells (Figure 4.4B). On the other hand, as discussed in section 3.5.3, potential reasons for peptide-induced Tau accumulation in cells include the inhibition of cathepsin D (Horn et al., 2000) and blockage of proteasomal Tau degradation by the polyR sequence in both peptides (Gao et al., 2000; Gaczynska et al., 2003; Kloss et al., 2009; Anbanandam et al., 2008; Karpowicz et al., 2015) and/or the formation of proteolytically resistant peptide-Tau species that might accumulate intracellularly (Taylor et al., 2010; Aggidis A. et al., 2021; Wischik et al., 2018). Due to weak peptide-binding to intracellular Tau RD (P301L/V337M)-EYFP (Figure 4.4B), it is unlikely that the scrambled peptide formed degradation-resistant Tau-peptide complexes in Clone 9 cells. Instead, 5000 nM scrambled peptide conceivably increased total Tau

levels in Clone 9 cells by inhibiting proteasomal degradation, as the polyR sequence is reported to inhibit this mechanism (IC_{50} = 100 - 200 nM in HeLa cells) (Kloss et al., 2009).

4.6.2. Impact of RI-AG03-polyR on Tau hyperphosphorylation

The experiments showed that neither RI-AG03-polyR, nor its scrambled version, affected (Ser^{202}/Thr^{205}) phospho-Tau levels in Clone 9 cells following a 48 h and 96 h incubation period. Curiously, although peptide treatment had no significant effect and whilst there was no interaction, the peptide concentration (10 - 5000 nM; $F(4, 20) = 3.00$; $p = 0.043$; two-way ANOVA) had a significant impact on (Ser^{202}/Thr^{205}) phospho-Tau levels at 48 h (Figure 4.2A). Specifically, Tukey's test revealed that a peptide concentration of 5000 nM approximately halved Tau phosphorylation at Ser^{202}/Thr^{205} ($p = 0.044$) (Figure 4.2A). Because there was no statistical difference in the effects of RI-AG03-polyR and its scrambled version (Figure 4.2A), this suggests that the arginine-rich polyR sequence in both peptides potentially inhibit Tau phosphorylation (Zhang et al., 2020; Kondo et al., 2021; Mamsa and Meloni, 2021).

Interestingly, with a similar design compared to RI-AG03-polyR, the Tau aggregation inhibitor peptides p-NH (D-nitmnsrrrrnh; also binds $^{306}VQIVYK^{311}$ in Tau) and TAT-7H (YGRKKRRQRRR-HHHHHHH; peptide details in Table 7.1, section 7.1) were reported to suppress Tau hyperphosphorylation in cells and *in vivo* (Zhang et al., 2020; Kondo et al., 2021). Nasal treatment of 1N4R Tau (P301S)-transgenic mice with 1 µM p-NH decreased cortical Thr^{231}- and Ser^{396}-phopsho-Tau levels without affecting kinase or phosphatase activities, suggesting that Tau hyperphosphorylation was inhibited by sterically hindering the access of kinases to Tau (Zhang et al., 2020). Moreover, treatment of 1N4R Tau (P301S)-expressing induced pluripotent stem cells (iPSCs) with 5 µM and 50 µM TAT-7H for 14 days suppressed Tau phosphorylation at the AT8 epitope (Ser^{202}/Thr^{205}) that was assessed in this study (Kondo et al., 2021). Notably, whilst TAT-7H was shown to inhibit the aggregation of recombinant R3 peptides ($Tau_{306-336}$), this peptide was not originally

designed to interact with Tau (Kondo et al., 2021). Thus, cationic and arginine-rich CPPs (TAT in 7H and polyR in RI-AG03) might both inhibit Tau aggregation and Tau hyperphosphorylation (Mamsa and Meloni, 2021).

Notably, in contrast to 48 h, the prolonged 96 h treatment with 5000 nM scrambled peptide had no effect on Tau phosphorylation at Ser^{202}/Thr^{205} (Figure 4.2A) in Clone 9 cells. Instead, the relative (Ser^{202}/Thr^{205}) phospho-Tau/Tau ratio was reduced by ~75 % (Figure 4.3B). However, the phospho-Tau/Tau ratio was lowered due to a scrambled peptide-evoked, concomitant increase in Tau levels, since 5000 nM scrambled peptide also quadrupled total Tau pools relative to untreated cells over 96 h (Figure 4.1A). This suggests higher (scrambled) peptide concentrations might only be useful to inhibit Tau phosphorylation at Ser^{202}/Thr^{205} across shorter time periods. Additionally, besides the AT8 epitope, Tau phosphorylation following peptide treatment at other AD-associated sites, such as Thr^{181}, Thr^{231}, Ser^{396} or Ser^{404} (reduced by p-NH in N2a cells in Zhang et al (2020)), should be investigated.

Curiously, the application of 10 nM scrambled RI-AG03-polyR significantly elevated the proportions of soluble (Ser^{202}/Thr^{205}) phospho-Tau in Clone 9 cells after 96 h (Figure 4.2E), but with decreased proportions of soluble Tau seen in Clone 9 cells (Figure 4.1F). This potentially suggests that low concentrations of scrambled RI-AG03-polyR induce the sequestration of non-phosphorylated Tau RD (P301L/V337M)-EYFP into inclusions, whilst reducing the aggregation of the phosphorylated protein. On the other hand, the detected (Ser^{202}/Thr^{205}) phospho-Tau bands ranged between 100 - 250 kDa, matching the size of high MW bands seen for total Tau (e.g. see arrows for 250 kDa total Tau and phospho-Tau species at 96 h in Figure 4.2G). Since (Ser^{202}/Thr^{205}) phospho-Tau also showed low solubility (20 %; Figure 4.2E), this suggests that these bands do not represent monomers, but rather already aggregated and phosphorylated Tau RD (V337M/P301L)-EYFP species. Since Clone 9 cell treatment with 10 nM scrambled peptide prevented the disappearance of the 250 kDa band in the soluble fraction after ultracentrifugation (Figure 4.2F), this implies that the scrambled peptide potentially had a solubilising effect on AT8-phosphorylated Tau aggregates. To further investigate

this peptide effect, future studies using less than 10 nM are necessary. Moreover, phosphatase treatment of the cell lysate could confirm if these high molecular weight bands (100 - 250 kDa) are indeed phospho-Tau species.

4.6.3. Cytoprotective properties of RI-AG03 variants and peptide-conjugated liposomes

Importantly, only the application of RI-AG03-polyR, but not its scrambled variant, in either an unconjugated or liposome-conjugated form, improved cell viability and decreased cell death in Clone 9 cells (Figure 4.5). In this context, it has been reported that the arginine-rich polyR and TAT CPPs are neuroprotective (reviewed in Mamsa and Meloni (2021)) and, at least conceptually, CPPs may prevent many previously discovered mechanisms of Tau toxicity (Ye et al., 2020; Yin et al., 2016; Diaz-Hernandez et al., 2010; Esteras et al., 2021; Esteras and Abramov, 2020; Quintanilla et al., 2009; Ittner et al., 2010; Miyamoto et al., 2017; Ozcelik et al., 2016; Manczak and Reddy, 2012; Perez et al., 2018; Li et al., 2016; Kovac et al., 2011; Laurent et al., 2018; Barron et al., 2017). Indeed, treatment of SH-SY5Y cells with poly-l-arginine hydrochloride (Merck, Feltham, UK; P4663; MW 5,000 - 15,000), a 32 - 96 residue-long arginine polypeptide, rescued loss of cell viability induced by the ^{275}VQIINK^{280}-containing peptide GKVQIINKLDL (Nadimidla et al., 2017). Because the polyR-containing scrambled control peptide had no effect in MTT and LDH assays in Clone 9 cells (Figure 4.5), this suggests that the survival-enhancing effects of RI-AG03-polyR were conveyed by its Tau binding sequence and not the polyR CPP.

Notably, my liposomes contained 5 % DSPE-PEG(2000)-Mal in order to conjugate the peptides. The direction of incorporated lipids is random, however, theoretically resulting in equal amounts of inwards and outwards-facing maleimide groups. Indeed, the pre-insert method I used to produce liposomes (without purification) resulted in ~63 % bioactive DSPE-PEG(2000)-Mal groups (Mason and Thordarson, 2016; Oswald et al., 2016). This suggests that approximately half of the DSPE-PEG(2000)-Mal groups in my liposomes (~2.5 %) are available for peptide-linkage. Using this

assumption, 10 nM peptide-liposomes, as used in the experiments (Figure 4.5), reflect actual conjugated peptide concentrations of ~0.25 nM. Since the treatment of Clone 9 cells with '10 nM' RI-AG03-polyR/TAT and RI-AG03-polyR/TAT-liposomes both reduced Tau toxicity, this implies that peptide-liposomes were ~40-fold more effective compared to the unconjugated peptides (Figure 4.5). However, to confirm this more potent effect of liposome-conjugated peptide compared to its unconjugated form, more experiments measuring both the peptide and liposome concentration in peptide-liposomes are required.

Peptide-liposomes might be more cytoprotective than free peptide due to inhibiting amyloid aggregation more potently. In this context, we have demonstrated that liposome-conjugation improved the $Tau_{\Delta 1\text{-}250}$ aggregation-inhibiting effects of R-AG03-polyR *in vitro* (Aggidis A. et al., 2021). Likewise, linking our previously developed Aβ aggregation inhibitor peptide RI-OR2-TAT to liposomes increased the $A\beta_{1\text{-}42}$ aggregation-blocking effects of RI-OR2 400-fold (Gregori et al., 2017). As likely applicable to RI-AG03-polyR/TAT-conjugated liposomes and their interaction with Tau, we hypothesised that RI-OR2-TAT-liposomes are more effective in blocking Aβ aggregation than unconjugated peptide due to a combination of effects (Gregori et al., 2017):

(i) Direct binding of Aβ by the ^{16}KLVFF^{20}-interacting sequence in RI-OR2-TAT.

(ii) Attraction of negatively charged Aβ peptides by the positively charged TAT sequence in the peptide.

(iii) Aβ monomers and oligomers sequestered by RI-OR2-TAT-liposomes might additionally capture nearby Aβ peptides.

(v) Aβ may also be incorporated into the lipid bilayer of RI-OR2-TAT-conjugated liposomes.

We expect that similar mechanisms may be relevant for the tau aggregation inhibitor, RI-AG03-PolyR, when conjugated to liposomes.

4.6.4. The link between the peptide-induced reduction in soluble Tau and cellular protection

As suggested by earlier studies of our group (Aggidis A. et al., 2021), my results reflected that RI-AG03-polyR treatment cannot disintegrate already formed Tau RD (P301L/V337M)-EYFP aggregates in Clone 9 cells (Figure 4.1E). However, when Clone 9 cells were seeded at a lower cell density to cultivate them for a longer time (96 h instead of 48 h), the proportions of soluble (unaggregated) Tau RD (P301L/V337M)-EYFP were higher (Figure 4.1F). In this scenario, exposure to RI-AG03-polyR (100 nM) or scrambled RI-AG03-polyR (10 & 100 nM) reduced the proportions of soluble Tau, suggesting that the peptides stimulated intracellular Tau aggregation (Figure 4.1F). In the presence of heparin, our earlier studies showed that RI-AG03-polyR blocked $Tau_{\Delta 1\text{-}250}$ fibrillisation and β-sheet formation by generating circular $Tau_{\Delta 1\text{-}250}$ oligomers with a diameter of 36 nm *in vitro* (Aggidis A. et al., 2021). My work indicates that RI-AG03-polyR does not appear to generate mature Tau fibrils in Clone 9 cells. This is supported by the fact that RI-AG03-polyR and RI-AG03-polyR-conjugated liposomes poorly co-localised with larger Tau RD (P301L/V337M)-EYFP inclusions in Clone 9 cells (Figure 4.4B&C). It is also implied that RI-AG03-polyR cannot bind to, and is not frequently incorporated into, bigger Tau aggregates. However, Cy5-RI-AG03-polyR treatment non-significantly elevated the average number of Tau RD (P301L/V337M)-EYFP aggregates per cell from ~8 (untreated) to ~39 at 2 h, while significantly increasing intracellular aggregate counts to ~42 at 16 h (Table 4.2). Although non-significant, these Cy5-peptide-exposed Clone 9 cells also showed smaller average aggregate sizes relative to untreated controls (49 % and 37 % smaller at 2 h and 16 h, respectively; Table 4.2). Considering the previous results of our group (Aggidis A. et al., 2021), my results suggest that peptide-induced Tau oligomer formation might occur in Tau-expressing cells. Generation of such peptide-Tau oligomers could have decreased the proportions of soluble Tau in Clone 9 cells because the bulky EYFP tag of Tau RD (P301L/V337M) likely promoted insolubility. These results indicate that more experimental work and the employment of other Tauopathy cell models, as suggested in section 4.6.5, are necessary to examine the potential anti- and pro-aggregatory interactions of RI-AG03-polyR with intracellular Tau.

Two other Tau aggregation inhibitor peptides similar to RI-AG03-polyR, including the ^{275}VQIINK^{280}-binding MD3/MMD3rev and ^{306}VQIVYK^{311}-interacting ISAD1/ISAD1rev, were shown to prevent heparin-induced fibril formation by recombinant Tau RD (ΔK280) (15 - 100 nm diameter) by, instead, generating β-sheet negative Tau oligomers of 3000 - 4000 nm or 2000 - 6000 nm in size, respectively (Malhis et al., 2021; Aillaud et al., 2022). Indeed, binding of MMD3/MMD3rev and ISAD1/ISAD1rev to Tau RD (ΔK280) increased the quantities of insoluble Tau (Malhis et al., 2021; Aillaud et al., 2022), similar to what was observed in RI-AG03-polyR- and scrambled peptide-treated Clone 9 cells (Figure 4.1F). As such, the RI-AG03-polyR and its scrambled variant likely decrease the proportions of soluble Tau in Clone 9 cells via the intracellular formation of circular peptide-Tau RD (P301L/V337M)-EYFP aggregates.

It is interesting to speculate how treatment with scrambled RI-AG03-polyR lowered soluble Tau in Clone 9 cells. This control peptide lacks the ^{306}VQIVYK^{31}-binding sequence of RI-AG03-polyR and we have confirmed that the non-retro-inverted version of the scrambled peptide did not inhibit heparin-induced $Tau_{\Delta 1\text{-}250}$ aggregation (Aggidis A. et al., 2021). However, because we only tested the anti-aggregatory effects of scrambled AG03-polyR, retro-inversion might have increased the binding affinity of the scrambled peptide for Tau (as it was the case for retro-inverting AG03-polyR into RI-AG03-polyR) (Aggidis A. et al., 2021).

Alternatively, the polyR CPP in the scrambled peptide could be involved in the observed reduction in soluble Tau. Cationic arginine-rich peptides, including polyR and TAT, were previously shown to block pathologic Tau aggregation by interfering with the aggregation-driving ^{275}VQIINK^{280} and ^{306}VQIVYK^{311} sequences in Tau (Mamsa and Meloni, 2021; von Bergen et al., 2001; von Bergen et al., 2000). Recently, it was suggested that cationic polyR peptides sequester polyanionic co-factors that induce Tau aggregation, such as heparin *in vitro* or heparan sulphate proteoglycans *in vivo* (Mamsa and Meloni, 2021). Specifically, hexaarginine (R6) and octaarginine (R8/polyR) peptides were shown to operate as β sheet-breakers, disintegrating pre-formed ^{306}VQIVYK^{311}-fibrils into smaller aggregates (Mamsa and Meloni, 2021), whilst poly-l-arginine hydrochloride (Merck; P4663; MW 5,000 - 15,000;

32 - 96 arginine residues) inhibited the heparin-induced aggregation of recombinant ^{306}VQIVYK^{311}, a ^{275}VQIINK^{280}-containing peptide (GKVQIINKLDL) and P301L-mutant 2N4R Tau in ThS assays (Nadimidla et al., 2017). In agreement with these studies, we also confirmed that a higher arginine content in the initial Tau aggregation inhibitor peptide candidates (AG01-03) slightly improved their anti-aggregatory effects in ThT assays (Aggidis A. et al., 2021). Interestingly, although in the context of another amyloid, pentaarginine (R5) (Gibson and Murphy, 2005) and the retro-inverted, arginine-rich 15 S.A. peptide (Ac-rklmqptrnrrnpnt-NH_2) (Barr et al., 2016) sequestered Aβ monomers into insoluble and oligomeric Aβ-peptide aggregates. Collectively, the findings in this study and other publications indicate that that the polyR CPP in the scrambled peptide may enable it to bind to Tau RD (P301L/V337M)-EYFP in Clone 9 cells, thus creating insoluble Tau in the process. Studies in Tauopathy cell models demonstrated that the overexpression of Tau is non-toxic, whereas the stimulation of Tau aggregation resulted in reduced cell viability (Khlistunova et al., 2006; Wang et al., 2007b). However, despite the fact that 100 nM RI-AG03-polyR lowered the proportions of soluble Tau RD (P301L/V337M)-EYFP in Clone 9 cells (Figure 4.1F), MTT and LDH assays show that Tau-driven cell death in these cells was reduced following treatment with 100 nM RI-AG03-polyR or RI-AG03-TAT (Figure 4.5D). This incongruence might be explained by the type of Tau aggregate that is formed. Specifically, the presence of non-phosphorylated, non-toxic, insoluble and β sheet-negative granular Tau oligomers (GTOs), which resemble RI-AG03-polyR-generated Tau oligomers (Aggidis A. et al., 2021), was demonstrated in Tauopathy *Drosophila* models (Cowan et al., 2015; Cowan and Mudher, 2013). Furthermore, feeding of RI-AG03-polyR to *Drosophila* overexpressing human transgenic 2N4R Tau locally in their eyes visibly improved their eye phenotype and lifespan, supporting the suggestion that RI-AG03-induced Tau oligomer formation protects from Tau toxicity (Aggidis A. et al., 2021). Similar to RI-AG03-polyR, the Tau aggregation inhibitor peptides ISAD1/ISAD1rev generated oligomers by binding to recombinant Tau RD (ΔK280), but lowered cell death and ROS production following the Dox-induced overexpression of Tau RD (ΔK280) or the external application of Tau RD (ΔK280) fibrils in N2a cells (Aillaud et al., 2022). Notably, in Tauopathy cell models, the current

evidence suggests that β sheet-containing and propagation-inducing Tau aggregates are the most toxic (Simic et al., 2016; Harrington et al., 2015; Wischik et al., 2018). Therefore, the sequestration of Tau into β sheet-negative aggregate conformations, which may occur in RI-AG03-polyR/TAT-treated Clone 9 cells, may rescue Tau toxicity.

The above discussion might also explain why the scrambled peptide, despite stimulating Tau aggregation similar to RI-AG03-polyR (Figure 4.1F), did not improve cell viability and LDH release in Clone 9 cells (Figure 4.5). Pathological Tau aggregation (β-sheet formation) and propagation are dependent on the ^{306}VQIVYK^{311} motif present in R3 in all six Tau isoforms and in the 10 or 12 kDa Tau fragments that form PHFs and SFs (Falcon et al., 2015; von Bergen et al., 2001; von Bergen et al., 2000; Wischik et al., 2018). RI-AG03-polyR contains an intact ^{306}VQIVYK^{311}-binding sequence that inhibits the aggregation of Tau into β sheet-containing aggregates (Aggidis A. et al., 2021). The scrambled peptide does not possess this ^{306}VQIVYK^{311}-interacting sequence, however, which likely explains the absence of cytoprotective effects in Clone 9 cells.

4.6.5. Study limitations and future experiments

For the assessment of soluble/insoluble Tau and phospho-Tau in response to peptide treatment (section 4.3), untreated Clone 9 cells were chosen as control because untransfected HEK293 cells do not endogenously express Tau (Li et al., 2007). However, using untreated Clone 9 cells as control, as opposed to a cell line that does not display increased cell death, was a weakness in the viability (MTT) and toxicity (LDH) assays (Figure 4.5). We previously confirmed that exposure to ≤ 30 μM RI-AG03-polyR did not cause cell death in HEK293 cells after, at least, a 24 h incubation period (Aggidis A. et al., 2021; Aggidis, 2019). On the other hand, the lack of control cells did not allow to assess the magnitude of Tau RD (P301L/V337M)-EYFP-triggered cell death in Clone 9 cells. Thus, future (repeat) toxicity experiments should also employ untransfected HEK293 cells. Moreover, cell viability and cell death in the presence or absence of RI-AG03-polyR/TAT and peptide-conjugated liposomes were

only evaluated over a 48 h, but not 96 h, time period. As such, a longer treatment time of 96 h might also be used.

When assessing co-localisation of Cy5-RI-AG03-polyR in its free or liposome-conjugated form with Tau RD (P301L/V337M)-EYFP in Clone 9 cells (Figure 4.4B&C), a Cy5-labelled scrambled peptide was not employed. Curiously, treatment with either RI-AG03-polyR or its scrambled variant decreased the proportions of soluble Tau in Clone 9 cells, which suggests that the peptides evoked Tau aggregation (Figure 4.1F), yet RI-AG03-polyR did not bind to (mostly already aggregated) Tau RD (P301L/V337M)-EYFP, as indicated by poor co-localisation (Table 4.1 and Figure 4.4B) (Sanders et al., 2014). The EYFP tag could also sterically hinder peptide-binding to Tau. To verify if an interaction with intracellular Tau occurs, a future study may assess co-localisation of fluorophore-tagged RI-AG03-polyR or scrambled peptide with soluble (endogenous) Tau in another cell line, such as SH-SY5Y or Clone 4 SH-SY5Y cells. Moreover, the group numbers for quantification of co-localisation and Tau RD (P301L/V337M)-EYFP aggregate number and size were low (n = 2 - 3, Table 4.2). Also, no z stacks were acquired to quantify aggregates across the entire cell body. A future study could repeat this quantification of amyloid aggregates in untreated, scrambled peptide- and RI-AG03-polyR-(liposome)-treated Clone 9 cells, using peptide concentrations that were found to not affect, or reduce, soluble Tau.

As indicated above, a shortcoming of this study was the incomplete characterisation of the anti- and pro-aggregatory effects of RI-AG03-polyR and its scrambled version in Clone 9 cells. In this context, employment of differentiated Clone 4 SH-SY5Y cells, with Dox-induced overexpression of 2N4R Tau (P301L) (chapter 3), could potentially be a suitable Tauopathy model to investigate the impact of the peptides on slower aggregating forms of Tau. Additional Tau seeding would also allow to assess whether RI-AG03-polyR can prevent Tau propagation. Moreover, to investigate if the peptides form GTOs in cells, and to assess whether these can seed Tau aggregation, Tau RD (P301S) Förster resonance energy transfer (FRET) Biosensor cells could be used (ATCC CRL-3275, Manassas, USA). This HEK293 cell line is frequently used to monitor Tau aggregation in response to Tau-seeding or

drugs (Lathuiliere and Hyman, 2021). Tau RD (P301S) FRET Biosensor cells co-express Tau RD (P301S)-cyan fluorescent protein (CFP) and Tau RD (P301S)-yellow fluorescent protein (YFP), which allows using FRET to assess intracellular Tau aggregation via flow cytometry (Lathuiliere and Hyman, 2021).

These Tau RD (P301S) FRET Biosensor cells could be exposed to RI-AG03-polyR, the scrambled peptide or peptide-conjugated liposomes to investigate if RI-AG03-polyR or scrambled RI-AG03-polyR form smaller Tau aggregates (an increased FRET signal would be observed in this case). Moreover, intracellular Tau aggregation could be seeded with one of the methods described in section 3.5.4, for example by applying the lysate of Clone 9 cells or via the lipofectamine-mediated transfection of the cells with pre (heparin)-aggregated Tau seeds. If the peptides or peptide-liposomes change the elevated FRET signal invoked by Tau seeding, it would imply that Tau aggregation and transcellular propagation were affected by the peptides. Using a green-fluorescent 6-FAM-RI-AG03-polyR peptide, intracellular binding to Tau RD (P301S)-CFP/YFP and potential peptide-induced Tau aggregate formation could be monitored. Finally, live cell counts or microplate-based viability assays that do not overlap with the fluorescence spectra of CFP or YFP (e.g. Cell Viability Assay Kit (Fluorometric – Blue), ab112120, Ex/Em = 360/450 nm) could show whether peptide-induced changes in Tau aggregation, if any, are protective or toxic in Biosensor cells.

4.7. Conclusion

Treatment of Clone 9 cells with 5000 nM scrambled RI-AG03-polyR, but not RI-AG03-polyR, increased total Tau levels. My results indicate that neither RI-AG03-polyR, nor its scrambled version, can disintegrate already formed Tau RD (P301L/V337M)-EYFP aggregates. In contrast to my initial expectations, both 100 nM RI-AG03-polyR and 10/100 nM scrambled RI-AG03-polyR reduced the proportions of soluble Tau in Clone 9 cells after a treatment period of 96 h, suggesting that Tau aggregation was accelerated by the peptides. However, poor co-localisation of unconjugated or

liposome-linked Cy5-RI-AG03-polyR with intracellular Tau RD (P301L/V337M)-EYFP and large Tau inclusions suggests that the peptide does neither interact with, nor generate, larger Tau aggregates *in vitro*. Because prolonged Cy5-RI-AG03-polyR treatment increased the number of Tau RD (P301L/V337M)-EYFP aggregates per cell (16 h), with non-significant aggregate size reductions of 49 % (2 h) and 37 % (16 h), this suggests that peptide-Tau oligomers might be formed in cells.

Both RI-AG03-polyR and the scrambled peptide did not affect the phosphorylation of Tau RD (P301L/V337M)-EYFP at Ser^{202}/Thr^{205} after 48 h. Interestingly, treatment with 10 nM of the scrambled peptide tripled the proportions of soluble (Ser^{202}/Thr^{205}) phospho-Tau in Clone 9 cells, but simultaneously reduced the amount of non-phosphorylated soluble Tau.

Congruent results in viability and LDH assays demonstrated that 10 nM RI-AG03-polyR or RI-AG03-TAT, either unconjugated or linked to liposomes, protected Clone 9 cells. By contrast, 10 nM unconjugated liposomes, scrambled RI-AG03-polyR and scrambled peptide-conjugated-liposomes had no effect. This suggests that the presence of an intact Tau (^{306}VQIVYK^{311})-binding sequence in RI-AG03-polyR, but not the polyR CPP in the peptide, was protective. Strikingly, although reducing the proportions of soluble Tau in Clone 9 cells, 100 nM RI-AG03-polyR and RI-AG03-TAT, but not the scrambled peptide, also decreased LDH release.

Collectively, these results suggest that RI-AG03-polyR/TAT and peptide-conjugated liposomes protect from Tau in a non-neuronal Tauopathy cell model. However, additional studies, possibly using differentiated Clone 4 cells, are needed to confirm the impact of RI-AG03-polyR on slower aggregating forms of Tau and Tau propagation.

5. Investigation of the endocytic mechanisms mediating the internalisation of liposomes and RI-AG03-conjugated liposomes

5.1. Introduction

Because Tau is an intracellular protein and predominantly propagates between interconnected neurons during AD (Vogel et al., 2021), RI-AG03-polyR has to both cross the BBB and be internalised by neurons. In this context, liposomes have emerged as drug nanocarriers in AD, allowing selective delivery of drugs, including RI-AG03, into the brain (Ross et al., 2018). By surface modification with polyR, TAT or other CPPs and the loading or linking of liposomes with therapeutic compounds, these nanoparticles can be designed for BBB penetration and cell-specific uptake via CME, CavME or macropinocytosis (Shi et al., 2014; Ross et al., 2018; Doherty and McMahon, 2009). Critical for the effectiveness of therapeutic nanocarriers, however, is the avoidance of intraorganellar entrapment or diffusion into degradative compartments of the cell (endosomes and lysosomes) following cellular internalisation (Sousa de Almeida et al., 2021; Dastpeyman et al., 2021; Pei and Buyanova, 2019). Translocation of the Tau aggregation inhibitor peptide RI-AG03 and peptide-conjugated liposomes into the neuronal cytoplasm is crucial in order to interact with pathologic Tau.

Notably, the TAT or polyR CPP sequences in the Aβ aggregation inhibitor RI-OR2 (Taylor et al., 2010) or Tau aggregation inhibitor RI-AG03 (Aggidis A. et al., 2021), respectively, were shown to mediate both cellular uptake and BBB penetration *in vivo* (Parthsarathy et al., 2013; Shi et al., 2014). Furthermore, using the previously developed Aβ aggregation inhibitor peptide RI-OR2-TAT, we showed that RI-OR2-TAT-conjugated liposomes (PINPs) crossed the BBB in an *in vitro* model and in Tg2576 mice *in vivo* (Gregori et al., 2017).

Following these initial results, this study aimed to characterise the internalisation mechanisms and subcellular trafficking of unconjugated and RI-AG03-conjugated liposomes in SH-SY5Y cells, which are a commonly used neuron-like cell model for AD and Tauopathies (Bell and Zempel, 2022a). In addition, the impact of conjugating liposomes to RI-AG03 with either a polyR or TAT CPP sequence

was studied. Finally, co-localisation with various cell organelles in SH-SY5Y cells was monitored to investigate potential entrapment in cell organelles.

To conduct the experiments, RI-AG03-polyR or RI-AG03-TAT peptides were synthesised with an additional cysteine for liposome-conjugation (see Figure 5.1A) (Mason and Thordarson, 2016), either with or without 6-FAM (green) or Cy5 (red) fluorophores. Fluorescent or non-fluorescent peptides were subsequently attached to liposomes or liposomes containing BODIPY-labelled cholesterol (green) via click chemistry between the cysteine residue of the peptide and DSPE-PEG(2000)-Mal chains of the liposomes (Figure 5.1B).

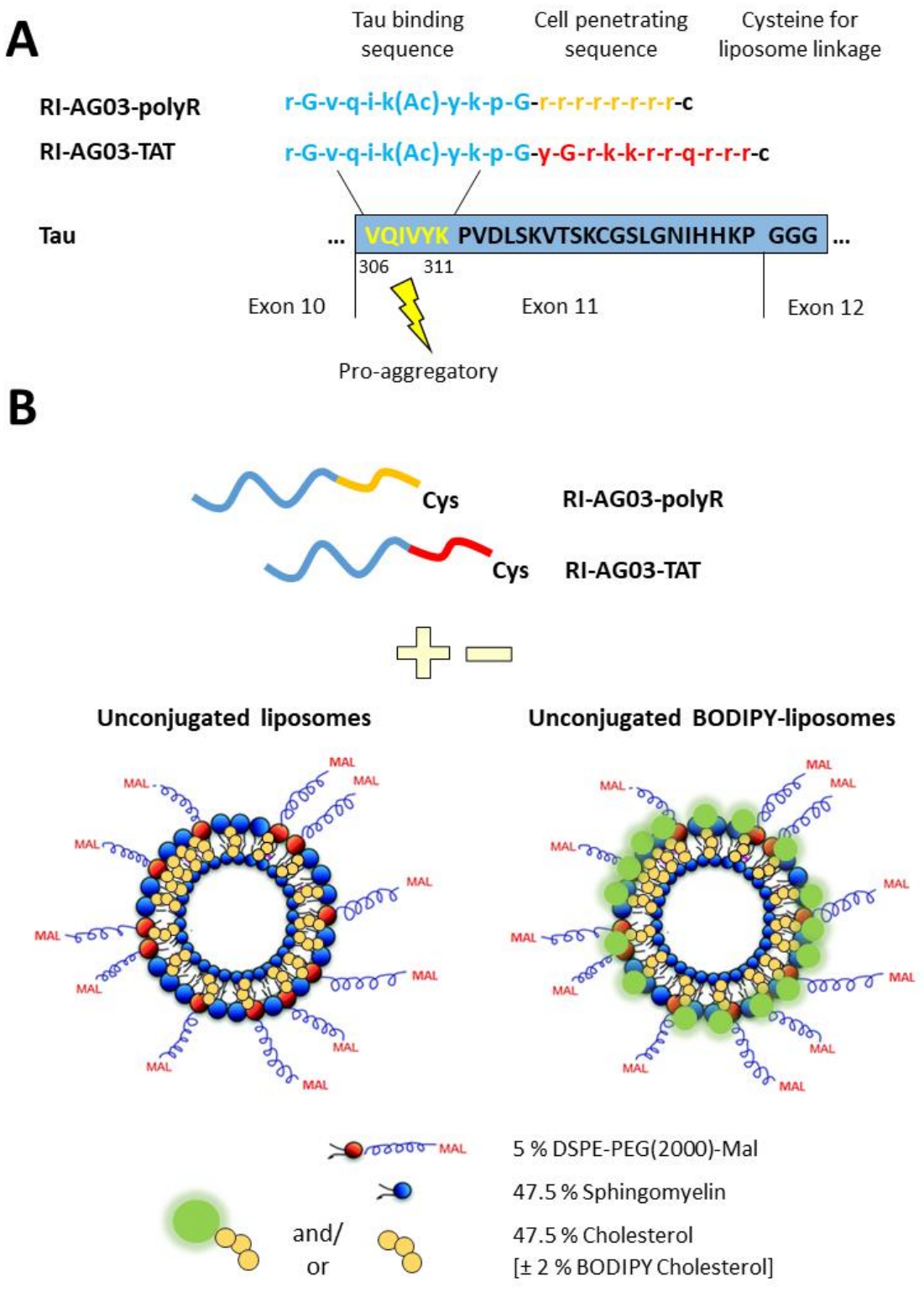

Figure 5.1: Design of RI-AG03 derivatives and liposome constructs to monitor subcellular trafficking. (A) Sequence of the Tau aggregation inhibitor peptide RI-AG03. The peptide consists of a Tau binding sequence that interacts with the pro-aggregatory 'VQIVYK' sequence in microtubule-binding repeat domain 3 (indicated by the blue box) that is present in all 6 isoforms of Tau. The positively charged cell penetrating sequences polyR (orange) or TAT (red) were attached to the peptide to facilitate cellular uptake. A cysteine was added to enable linkage of the peptide to

liposomes via click chemistry. For illustrative purposes, the retro-inverted sequences of RI-AG03-polyR (c-r-r-r-r-r-r-r-r-G-p-k-y-k(Ac)-i-q-v-G-r-NH_2) and RI-AG03-TAT (c-r-r-r-q-r-r-k-k-r-G-y-G-p-k-y-k(Ac)-i-q-v-G-r-NH_2) were depicted in opposite directions. (B) Composition of unconjugated liposomes and BODIPY-liposomes. RI-AG03 was attached through click chemistry between the cysteine residue of the peptide and protruding maleimide groups (Mal) of the liposomes. To create fluorescent liposomes, 2 % of cholesterol was replaced with BODIPY-labelled cholesterol. Partially modified from Chandrasekaran et al. (2014).

5.2. Experimental goals

- Compare the uptake of unconjugated and RI-AG03-polyR or RI-AG03-TAT-conjugated liposomes in SH-SY5Y cells
- Identify the primary endocytosis mechanism of unconjugated and peptide-conjugated liposomes
- Employ immunocytochemistry to monitor the intraorganellar trafficking of free RI-AG03-polyR or RI-AG03-TAT peptide, unconjugated liposomes and peptide-linked liposomes
- Following internalisation of peptide-conjugated liposomes by SH-SY5Y cells, determine if the subcellular localisation of the liposome vehicle and the conjugated peptide differ

5.3. Liposome uptake

5.3.1. Internalisation of liposomes and RI-AG03-conjugated liposomes by SH-SY5Y cells

Initially, it was investigated whether unconjugated BODIPY-liposomes or peptide-conjugated BODIPY-liposomes were taken up by SH-SY5Y neuroblastoma cells. The same experiment was repeated three independent times with fresh liposomes and cells (n = 3 technical replicates per experiment). Analysis of the average values from experiment 1 - 3 showed that BODIPY-liposome and peptide-conjugated BODIPY-liposome treatment significantly elevated median cell fluorescence compared to untreated cells ($F(3, 8) = 6.768$, $p = 0.014$; one-way ANOVA) (Figure 5.2A). Treatment of SH-SY5Y cells with unconjugated BODIPY-liposomes led to a 94-fold increase in median cell

fluorescence relative to untreated control cells, but this was not significant. However, the application of RI-AG03-polyR-BODIPY-liposomes resulted in a 309-fold increase in median cell fluorescence relative to untreated control cells ($p = 0.028$), whilst RI-AG03-TAT-BODIPY-liposomes elevated the median cell fluorescence 311-fold ($p = 0.027$). In comparison to unconjugated BODIPY-liposomes, the conjugation of either RI-AG03-polyR or RI-AG03-TAT to liposomes (non-significantly) heightened their uptake ~3-fold.

Notably, separate analysis of all data points via two-way ANOVA with 'liposome treatment' (untreated, unconjugated BODIPY-liposomes, RI-AG03-polyR-BODIPY-liposomes or RI-AG03-TAT-BODIPY-liposomes) and 'experimental run' (1, 2 or 3) as independent variables identified a significant interaction between both ($F(6, 24) = 31.24$, $p < 0.001$). Post hoc analysis revealed that the application of unconjugated liposomes significantly increased median cell fluorescence in run 1 ($p = 0.005$) and run 2 ($p = 0.003$), but not in run 3. This indicates that unconjugated liposomes, even without surface conjugation of RI-AG03-polyR or RI-AG03-TAT, are internalised by cells over a time period of 4 h. There appears to be some variability in the effectiveness of liposome uptake between experimental runs, however.

Confocal microscopy (Figure 5.2B) confirmed that both unconjugated BODIPY-liposomes and peptide-BODIPY-liposomes were internalised by SH-SY5Y cells, leading to a visible increase in green fluorescence throughout the cytoplasm. In agreement with the fact that the internalisation of peptide-liposomes, but not that of unconjugated liposomes, was significantly higher relative to untreated SH-SY5Y cells, RI-AG03-polyR-BODIPY-liposome and RI-AG03-TAT-BODIPY-liposome-treated cells exhibited greater cell fluorescence than unconjugated BODIPY-liposome-treated and untreated cells (Figure 5.2B).

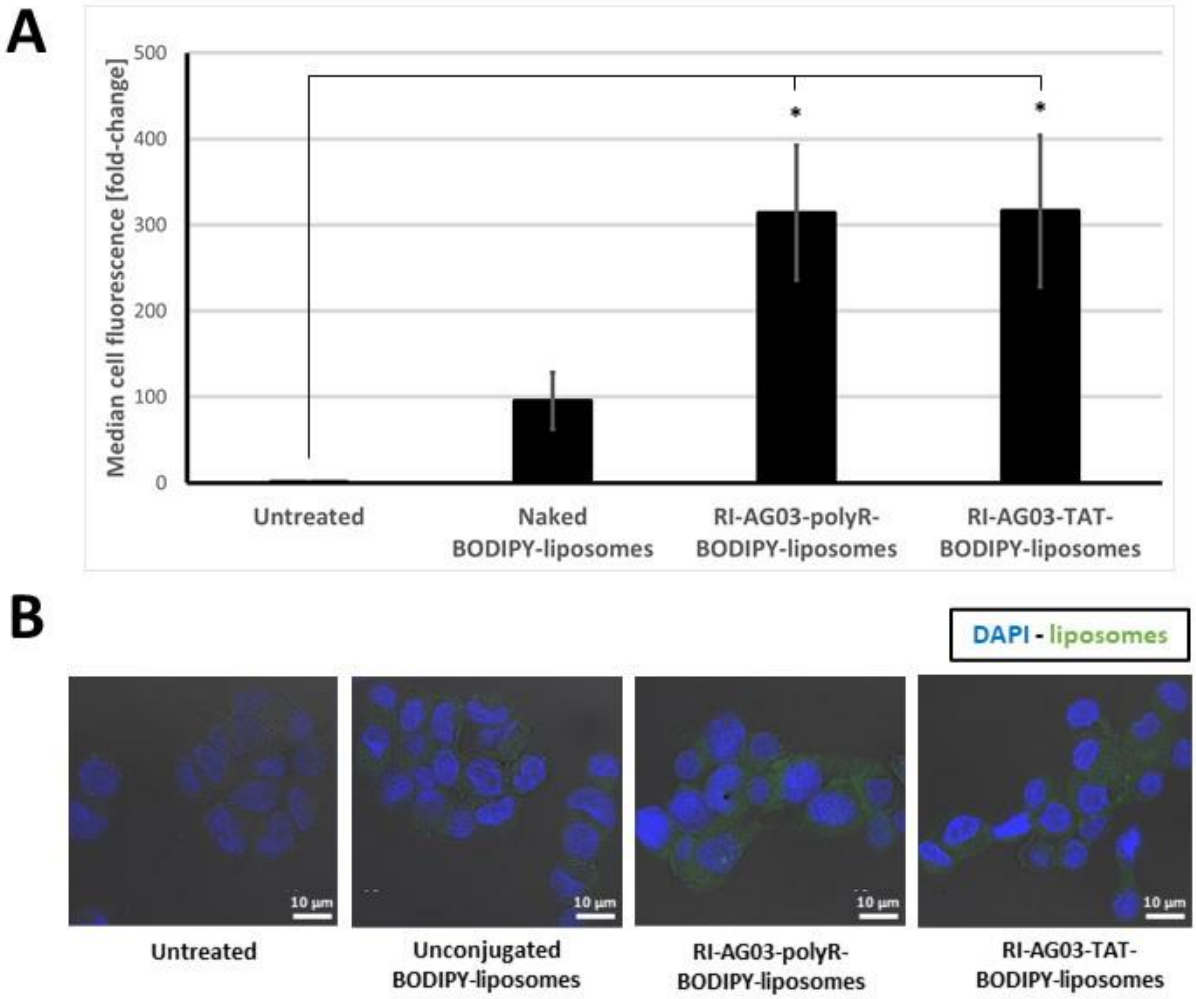

Figure 5.2: Cellular uptake of unconjugated BODIPY-liposomes and peptide-BODIPY-liposomes by SH-SY5Y cells. (A) Flow cytometry analysis of cells treated with 75 µM unconjugated BODIPY-liposomes, RI-AG03-PolyR-BODIPY-liposomes or RI-AG03-TAT-BODIPY-liposomes for 4 h. Data are shown as the Mean ± SEM median cell fluorescence of the average of three independent biological replicates (n = 3 technical replicates, or separate cell wells/flasks treated at the same time, per experiment, using freshly prepared liposome stocks and new cells in every experiment) relative to untreated controls. One-way ANOVA and Tukey's Post-Hoc test were applied to assess significant differences. * = $p < 0.05$. (B) Representative confocal images of untreated, unconjugated BODIPY-liposome and peptide-BODIPY-liposome-treated SH-SY5Y cells. For the green channel (intracellular fluorescence of internalised unconjugated or peptide-conjugated BODIPY-liposomes), consistent settings for the pinhole size, laser strength and gain were applied in all images.

5.3.2. Identification of the endocytosis pathways of unconjugated and peptide-linked liposomes

To reveal if the cellular uptake of unconjugated BODIPY-liposomes and peptide-BODIPY-liposomes is mediated by endocytosis or ATP-independent internalisation, SH-SY5Y cells were co-treated with the

pharmacological endocytosis inhibitors chlorpromazine, filipin, cytochalasin D or EIPA. These compounds are reported to block CME, CavME and macropinocytosis, respectively (Dutta and Donaldson, 2012; Ivanov, 2008). Chlorpromazine is a CME inhibitor that interferes with the characteristic clathrin-coating and AP2 adaptor complex on endosomal membranes. Filipin is a cholesterol-extracting agent that disturbs lipid rafts to block CavME. Cytochalasin D depolymerises F actin to impede phagocytosis and macropinocytosis, but is also thought to have nonspecific inhibitory effects on CME and some forms of clathrin-independent endocytosis. Finally, the Na^+/H^+ exchange inhibitor EIPA is considered to be one of the most effective and selective currently available macropinocytosis inhibitors (Dutta and Donaldson, 2012; Ivanov, 2008).

Notably, cationic CPPs are internalised in a direct manner by distorting the cellular plasma membrane, which includes inverted micelle, pore or carpet formation (Palm-Apergi et al., 2012; Shi et al., 2014). This process may be toxic to cells, however. Despite low toxicity of polyR and TAT *in vitro*, greater CPP concentrations may damage the cellular membrane and trigger cell lysis (Kilk et al., 2009; Saar et al., 2005; Tunnemann et al., 2008). Similarly, positively charged nanoparticles can elicit pore formation and cell death (Li and Malmstadt, 2013; Foroozandeh and Aziz, 2018). Thus, in my initial studies, I confirmed that the final concentrations of unconjugated liposomes, RI-AG03-polyR/TAT-liposomes and endocytosis inhibitors utilised were non-toxic to SH-SY5Y cells (Appendix, Figure 9.4A&B).

Endocytosis inhibitor treatment significantly altered unconjugated BODIPY-liposome uptake by SH-SY5Y cells ($F(4, 10) = 5.44$, $p = 0.014$; one-way ANOVA using the mean of three technical replicates from three independent experiments each) (Figure 5.3A). Post hoc-testing confirmed that the CME inhibitor chlorpromazine, CavME inhibitor filipin and macropinocytosis inhibitor EIPA had no effect on the uptake of unconjugated BODIPY-liposomes by SH-SY5Y cells. However, the mixed endocytosis inhibitor cytochalasin D ($p = 0.041$) significantly reduced the uptake of unconjugated liposomes, as indicated by reductions in the median cell-associated fluorescence by 19 %, relative to control cells without inhibitor treatment. Since cytochalasin D mainly restricts macropinocytosis (Dutta and

Donaldson, 2012; Ivanov, 2008), this suggests that unconjugated BODIPY-liposomes are not internalised by CME and CavME, but that they may be partially taken up via macropinocytosis. Because the effects of the endocytosis inhibitors were modest, this further suggests that most of the unconjugated BODIPY-liposomes entered SH-SY5Y cells through endocytosis-independent direct membrane fusion.

The cellular internalisation of RI-AG03-polyR-BODIPY-liposomes was not significantly affected by the endocytosis inhibitors (one-way ANOVA). Interestingly, despite being non-significant, EIPA-treated cells showed a notable (28 %) reduction in median cell fluorescence (Figure 5.3B). If all data points (9 instead of 3) are included in the analysis, there is a significant effect of the endocytosis inhibitors ($F(4, 30) = 5.58$, $p = 0.002$; two-way ANOVA), with EIPA treatment significantly reducing RI-AG03-polyR-BODIPY-liposome uptake ($p = 0.027$). These data suggest that RI-AG03-polyR-BODIPY-liposomes are not internalised by CME or CavME, but that macropinocytosis could be partly involved.

In the case of RI-AG03-TAT-BODIPY-liposomes (Figure 5.3C), statistical analysis showed that none of the endocytosis inhibitors significantly altered uptake of these peptide-liposomes. Thus, RI-AG03-TAT-BODIPY-liposomes are not internalised by CME, CavME and macropinocytosis, suggesting that alternative, and potentially energy-independent mechanisms, may be involved in their uptake.

Collectively, as typical for lipid-based and hydrophobic nanoparticles, these results demonstrate that unconjugated BODIPY-liposomes, RI-AG03-polyR-BODIPY-liposomes and RI-AG03-TAT-BODIPY-liposomes predominantly enter cultured SH-SY5Y cells through energy-independent plasma membrane fusion and translocation (Curtis et al., 2015; Foroozandeh and Aziz, 2018). Minor proportions of unconjugated BODIPY-liposomes, and potentially RI-AG03-polyR-conjugated BODIPY-liposomes, are internalised by macropinocytosis. The cellular uptake of RI-AG03-TAT-BODIPY-liposomes appears to be largely independent of endocytosis mechanisms.

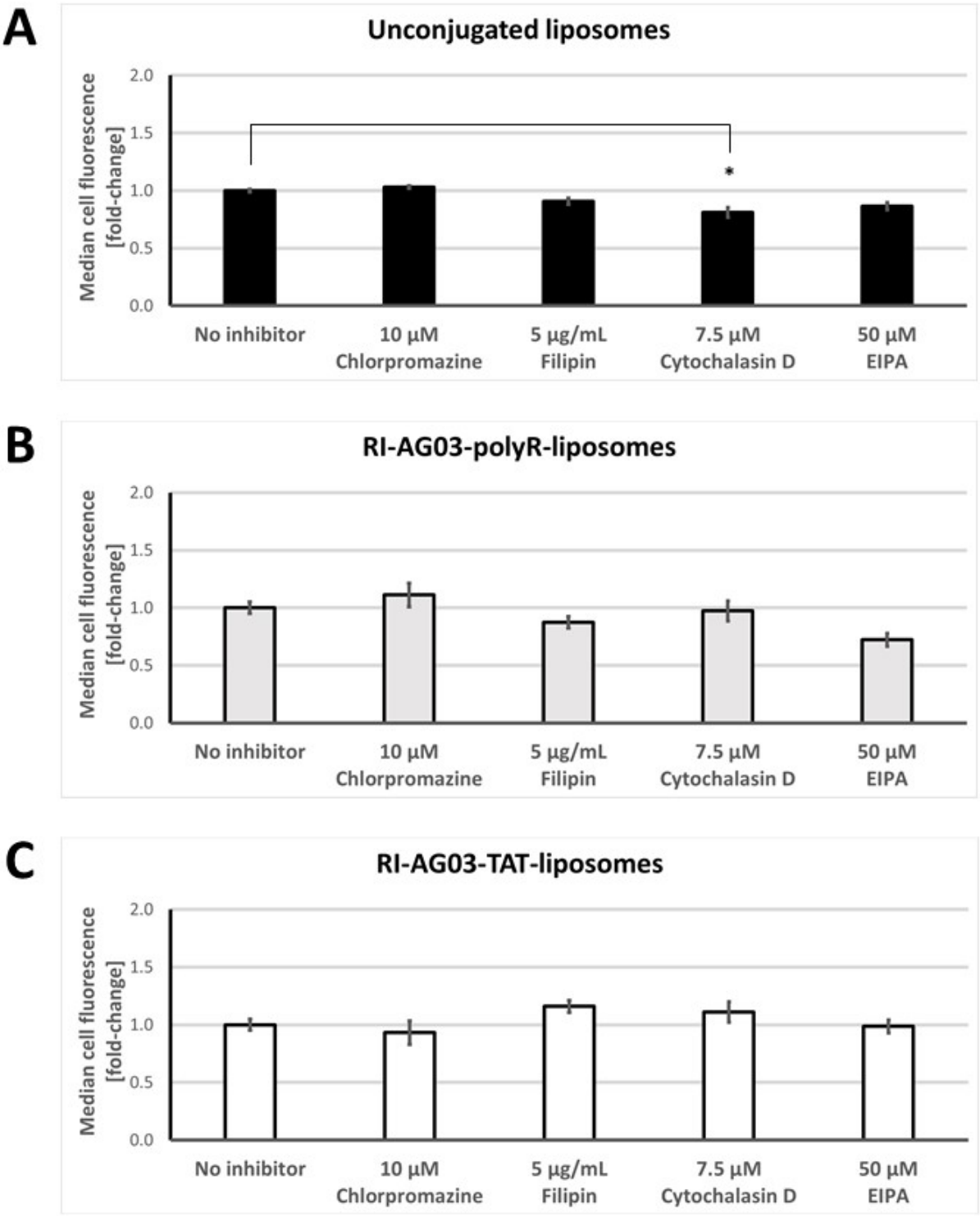

Figure 5.3: Effects of endocytosis inhibitors on the internalisation of unconjugated BODIPY liposomes (A), RI-AG03-polyR-BODIPY-liposomes (B) and RI-AG03-TAT-BODIPY-liposomes (C). SH-SY5Y cells were pre-treated with endocytosis inhibitors or vehicle solution (DMSO), then exposed to 75 µM BODIPY-liposomes or peptide-BODIPY-liposomes for 4 h. The graphs show the Mean ± SEM median cell fluorescence of the average of three independent biological replicates (n = 3 technical replicates, or separate cell wells/flasks treated at the same time, per experiment, with freshly prepared liposome stocks and new cells every time) in comparison to untreated controls, as

measured using Flow cytometry. One-way ANOVA followed by Tukey's Post-Hoc test was used to calculate significant differences. * = $p < 0.05$.

5.4. Co-localisation with cell organelles

5.4.1. Intracellular trafficking of BODIPY-liposomes and peptide-BODIPY-liposomes

In order to investigate subcellular trafficking of various fluorescent peptide and liposome constructs, co-localisation with multiple cell organelles was assessed in SH-SY5Y cells after a treatment period of 16 h. A longer treatment time than that in the previous experiments was chosen to allow the peptide and peptide-liposomes to reach their intracellular destination(s). Co-localisation was quantified by calculating Pearson's correlation coefficient (Rcoloc) and using Chan YH's interpretation style (none, poor, fair, moderate, very strong and perfect; Table 5.1) (Akoglu, 2018). Representative images with all individual channels (blue, green and red) are found in the appendix (Figure 9.5).

Initially, co-localisation unconjugated BODIPY-liposomes and RI-AG03-polyR or RI-AG03-TAT-conjugated BODIPY-liposomes (green fluorescent) with the fluorescent live cell organelle stains LysoTracker Deep Red (lysosomes) or pHrodo™ Red Dextran (macropinosomes) (both red fluorescent) was monitored following a 16 h treatment period (see Figure 5.4). To improve assessment of co-localisation with cholera toxin subunit B, a lipid raft marker (red fluorescent), cells were treated with the unconjugated and peptide-conjugated BODIPY-liposomes on ice for 30 min.

Unconjugated BODIPY-liposomes, RI-AG03-polyR-BODIPY-liposomes and RI-AG03-TAT-BODIPY-liposomes all showed fair co-localisation with LysoTracker Deep Red in lysosomes (Table 5.1 and Figure 5.4A). This implies that the liposomes and peptide-liposomes may be processed in degradative compartments, but also that a good proportion of them is not entrapped in lysosomes. Thus, peptide-liposomes are suitable for therapeutic use. Furthermore, unconjugated liposomes displayed moderate and RI-AG03-polyR- or RI-AG03-TAT-conjugated BODIPY-liposomes fair co-

localisation with macropinosome marker pHrodo™ Red Dextran (Table 5.1, Figure 5.4B and Appendix, Figure 9.5B, for more clarity). The stronger co-localisation of unconjugated BODIPY-liposomes with macropinosomes compared to RI-AG03-polyR/TAT-BODIPY-liposomes is in agreement with the fact that cytochalasin D (predominantly a macropinocytosis inhibitor) slightly lowered cellular internalisation (Figure 5.3A and Figure 5.3B).

As expected, all three liposome species co-localised fairly (BODIPY-liposomes, RI-AG03-TAT-BODIPY-liposomes) or moderately (RI-AG03-polyR-BODIPY-liposomes) with CellLight™ Plasma Membrane-RFP probes, suggesting that the liposome species were translocating across the cell membrane at the time of cell fixation (Table 5.1 and Figure 5.4C). There was poor co-localisation of unconjugated BODIPY-liposomes and peptide-BODIPY-liposomes with cholera toxin subunit B in lipid rafts (Table 5.1 and Figure 5.4D). Since the results showed that the cellular uptake of unconjugated or peptide-conjugated BODIPY-liposomes was not significantly mediated by CavME (Figure 5.3A-C), liposomes and peptide-liposomes might randomly fuse with the cell membrane and, thus, may co-localise with lipid rafts by chance, as seen in Figure 5.4D.

Table 5.1: Quantification of drug co-localisation with cell organelles. Rcoloc = Pearson's correlation coefficient.

		6-FAM-RI-AG03-polyR peptide	6-FAM-RI-AG03-TAT peptide	BODIPY-liposomes	RI-AG03-polyR-BODIPY-liposomes	RI-AG03-TAT-BODIPY-liposomes	6-FAM-RI-AG03-polyR-liposomes	6-FAM-RI-AG03-TAT-liposomes
Lysosomes	Rcoloc	0.3268 ± 0.0436	0.1432 ± 0.0663	0.3417 ± 0.0103	0.3918 ± 0.0599	0.3408 ± 0.0380	0.0786 ± 0.2547	-0.0284 ± 0.0382
	n	7	6	5	4	3	3	4
	Interpretation (Chan YH)	Fair	Poor	Fair	Fair	Fair	None	None
Macropinosomes	Rcoloc	0.5753 ± 0.0555	0.5414 ± 0.1651	0.7258 ± 0.0703	0.4734 ± 0.1210	0.4998 ± 0.1021	0.3273 ± 0.2096	-0.0227 ± 0.0480
	n	5	6	3	3	4	3	7
	Interpretation (Chan YH)	Fair	Fair	Moderate	Fair	Fair	Fair	None
Cell membrane	Rcoloc	0.5028 ± 0.0613	0.3014 ± 0.1129	0.4583 ± 0.0433	0.7484 ± 0.0507	0.5979 ± 0.0696	0.5399 ± 0.0715	0.3856 ± 0.0999
	n	3	4	6	4	4	4	4
	Interpretation (Chan YH)	Fair	Fair	Fair	Moderate	Fair	Fair	Fair

Lipid rafts	Rcoloc	-0.0360	0.5664 ± 0.0090	0.2536 ± 0.1387	0.2480 ± 0.0658	0.2213 ± 0.0305	0.3031 ± 0.0032	0.2884 ± 0.0557
	n	1	2	2	4	2	2	2
	Interpretation (Chan YH)	None	Fair	Poor	Poor	Poor	Fair	Poor
Early endosomes	Rcoloc	0.4277 ± 0.0441	0.1120 ± 0.0484	0.4693 ± 0.0707	0.2852 ± 0.0414	0.3071 ± 0.0562	-0.1390 ± 0.0740	0.0934 ± 0.0765
	n	3	4	5	4	6	3	5
	Interpretation (Chan YH)	Fair	Poor	Fair	Poor	Fair	None	None
Endoplasmic reticulum	Rcoloc	0.0405 ± 0.0595	0.1805 ± 0.1118	0.2748 ± 0.0582	0.2614 ± 0.0580	0.2580 ± 0.0922	-0.0986 ± 0.0326	0.1665 ± 0.0974
	n	6	6	3	3	5	5	3
	Interpretation (Chan YH)	None	Poor	Poor	Poor	Poor	None	Poor
Golgi	Rcoloc	-0.0286 ± 0.0609	-0.1339 ± 0.0513	0.3688 ± 0.0897	0.1120 ± 0.1233	0.2366 ± 0.0870	-0.0827 ± 0.0617	-0.0313 ± 0.0956
	n	4	3	3	3	3	4	4
	Interpretation (Chan YH)	None	None	Fair	Poor	Poor	None	None

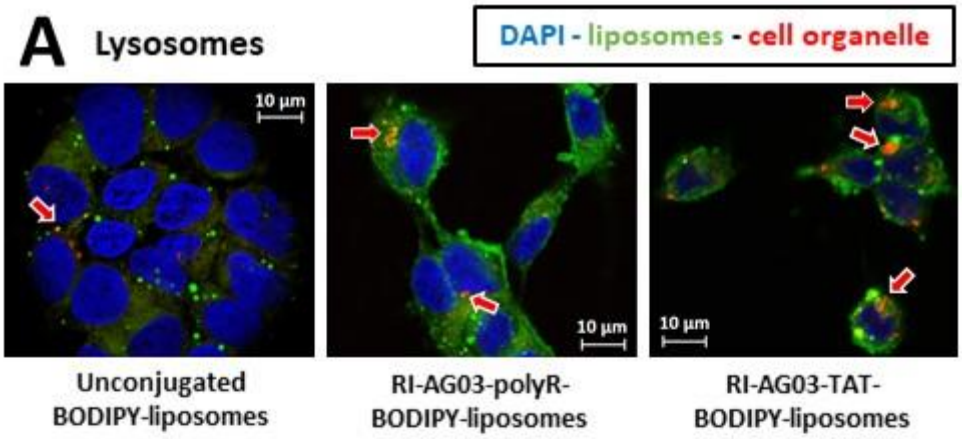
A Lysosomes
DAPI - liposomes - cell organelle
10 µm
Unconjugated BODIPY-liposomes
RI-AG03-polyR-BODIPY-liposomes
RI-AG03-TAT-BODIPY-liposomes

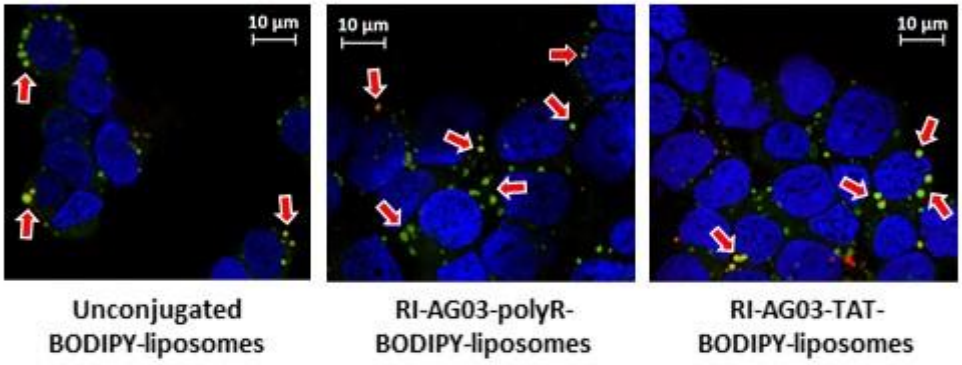
B Macropinosomes
10 µm
Unconjugated BODIPY-liposomes
RI-AG03-polyR-BODIPY-liposomes
RI-AG03-TAT-BODIPY-liposomes

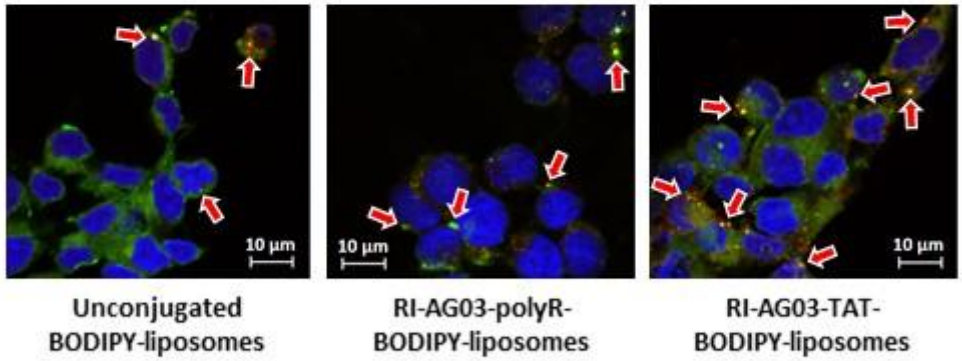
C Cell Membrane
10 µm
Unconjugated BODIPY-liposomes
RI-AG03-polyR-BODIPY-liposomes
RI-AG03-TAT-BODIPY-liposomes

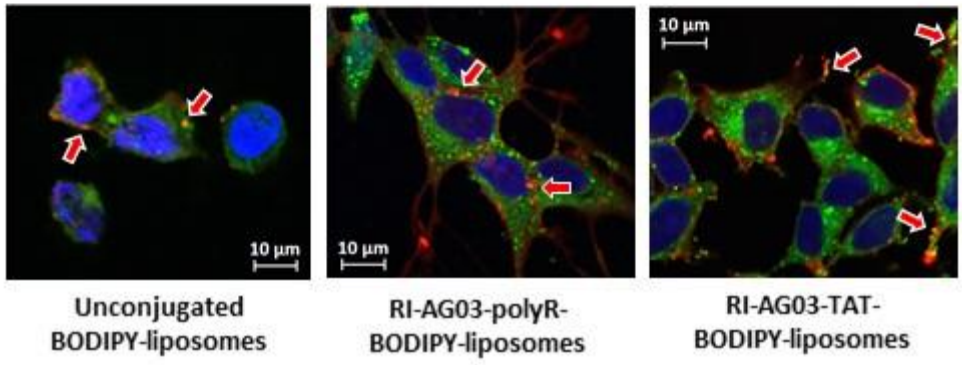
D Lipid Rafts
10 µm
Unconjugated BODIPY-liposomes
RI-AG03-polyR-BODIPY-liposomes
RI-AG03-TAT-BODIPY-liposomes

Figure 5.4: Co-localisation of unconjugated BODIPY-liposomes and peptide-conjugated BODIPY-liposomes with lysosomes (A), macropinosomes (B), the cell membrane (C) or lipid rafts (D) in SH-SY5Y cells. Cells were co-incubated with the indicated BODIPY-liposome constructs (green) and a live cell organelle marker (red), including either LysoTracker Deep Red, pHrodo™ Red Dextran or CellLight™ Plasma Membrane-RFP, for 16 h. For lipid rafts (D), cells were treated with BODIPY-liposome species in the presence of Cholera Toxin Subunit B (Recombinant), Alexa Fluor™ 594 Conjugates on ice for 30 min. Blue indicates the nucleus (DAPI) and arrows highlight co-localisation.

In addition to macropinocytosis-related cell organelles, trafficking into other cell compartments was examined (Figure 5.5). Interestingly, even though the CME inhibitor chlorpromazine did not affect their uptake (Figure 5.3A-C), unconjugated BODIPY-liposomes and RI-AG03-TAT-BODIPY-liposomes showed fair, but RI-AG03-polyR-BODIPY-liposomes poor, co-localisation with Rab5a-RFP in early endosomes (Table 5.1 and Figure 5.5A). Potential reasons for this observation are debated in section 5.5.4. Regarding the ER, three BODIPY-liposome constructs showed poor trafficking into this cell organelle, as evidenced by the lack of co-localisation with CellLight™ ER-RFP probes (Table 5.1 and Figure 5.5B). Interestingly, while RI-AG03-polyR-BODIPY-liposomes and RI-AG03-TAT-BODIPY-liposomes had poor co-localisation, there was fair co-localisation of unconjugated BODIPY-liposomes with N-acetylgalactosaminyltransferase-RFP in the Golgi (Figure 5.5C). In this context, CavME may deliver internalised cargo to the Golgi (Le and Nabi, 2003). However, as the CavME inhibitor filipin did not significantly inhibit the cellular uptake of unconjugated BODIPY-liposomes (Figure 5.3A), the co-localisation of these liposomes with the Golgi may be random or is mediated by other transport mechanisms.

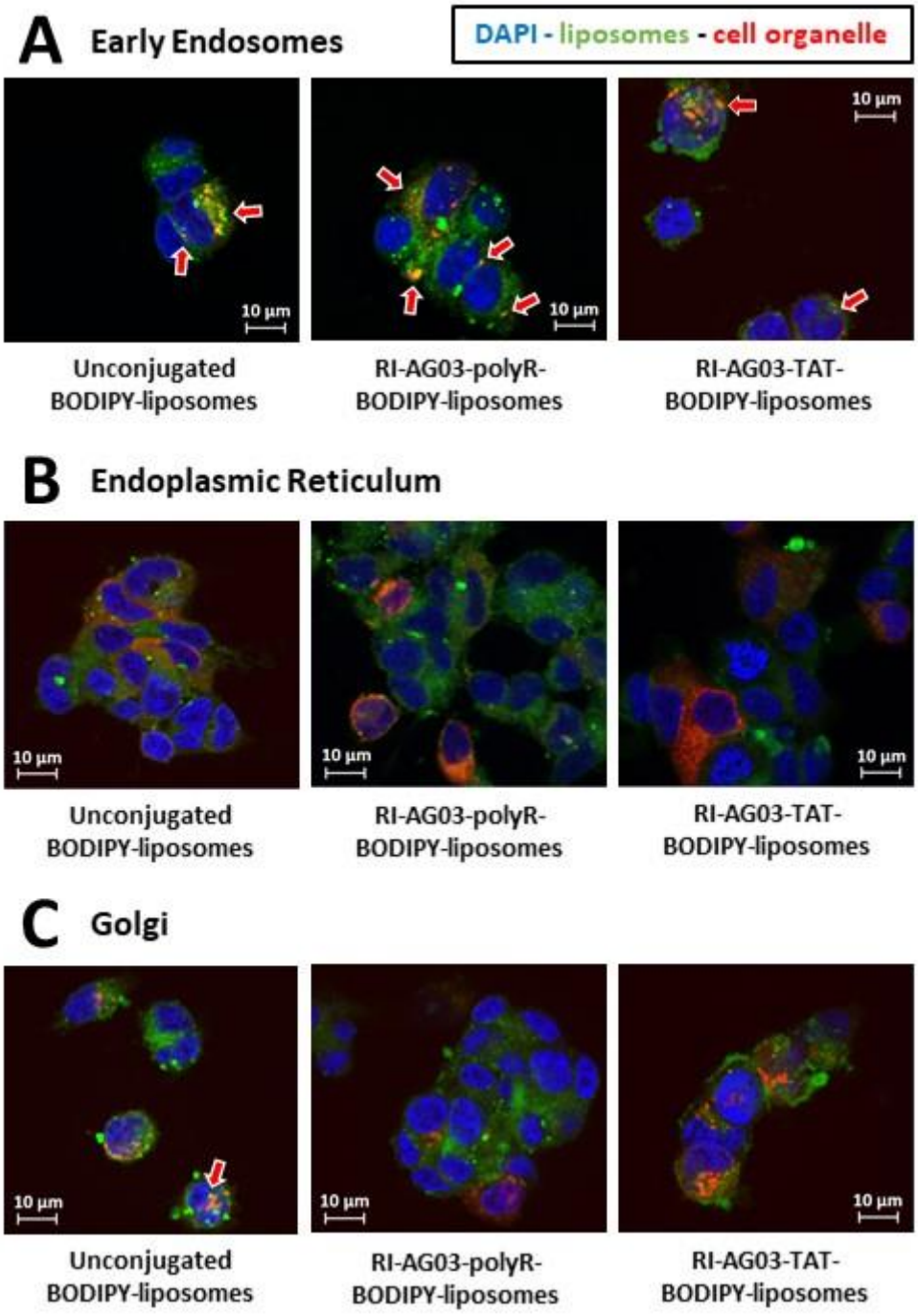

Figure 5.5: Trafficking of unconjugated BODIPY-liposomes and peptide-linked BODIPY-liposomes into early endosomes (A), the ER (B) or Golgi (C) in SH-SY5Y cells. For a duration of 16 h, cells were co-exposed to unconjugated BODIPY-liposomes, RI-AG03-polyR-BODIPY-liposomes or RI-AG03-TAT-BODIPY-liposomes (green) and a live cell organelle stain (red) that was either Rab5a-RFP (CellLight™ Early Endosomes-RFP), CellLight™ ER-RFP probes or N-acetylgalactosaminyltransferase-RFP (CellLight™ Golgi-RFP). Blue in the confocal images indicates the cellular nucleus (DAPI), while arrows emphasise co-localisation.

5.4.2. Distinct intraorganellar co-localisation of 6-FAM-RI-AG03 and 6-FAM-peptide-liposomes relative to BODIPY-labelled liposomes

In the previous section, BODIPY-labelled cholesterol was incorporated into liposomes to track their subcellular distribution. However, there remained the possibility that the trafficking of the liposomes did not necessarily reflect the distribution of the conjugated peptide. Therefore, instead of using BODIPY-cholesterol, RI-AG03-polyR and RI-AG03-TAT were synthesised with a 6-FAM moiety to monitor the whereabouts of these green fluorescent peptides in their free and liposome-conjugated forms.

As visualised in Figure 5.6A, free 6-FAM-RI-AG03-polyR showed fair and 6-FAM-RI-AG03-TAT poor co-localisation with LysoTracker Deep Red in SH-SY5Y cells, indicating that the free peptide mostly evades entrapment and degradation in lysosomes (Table 5.1). Retro-inversion additionally renders the peptides resistant to proteolysis (Taylor et al., 2010; Aggidis A. et al., 2021). Curiously, in contrast to the fair co-localisation observed for RI-AG03-polyR-BODIPY-liposomes and RI-AG03-TAT-BODIPY-liposomes (Table 5.1 and Figure 5.4A), the 6-FAM-labelled peptides showed no co-localisation with lysosomes anymore when conjugated to liposomes (Table 5.1 and Figure 5.6A).

Regarding trafficking into macropinosomes, unconjugated 6-FAM-RI-AG03-polyR and 6-FAM-RI-AG03-TAT exhibited fair co-localisation with pHrodo™ Red Dextran (Table 5.1 and Figure 5.6B). Interestingly, while 6-FAM-RI-AG03-polyR-liposomes also showed fair co-localisation, there was no co-localisation of 6-FAM-RI-AG03-TAT-liposomes with macropinosomes (Table 5.1 and Figure 5.6B). By contrast, earlier results indicated that both RI-AG03-polyR- BODIPY-liposomes and RI-AG03-TAT-BODIPY-liposomes had fair co-localisation with this organelle (Table 5.1 and Figure 5.6B).

Both free 6-FAM-RI-AG03-polyR and 6-FAM-RI-AG03-TAT peptides also fairly co-localised with CellLight™ Plasma Membrane-RFP (Table 5.1 and Figure 5.6C), suggesting that the peptide was in transit through the cell membrane at the moment of fixation. No (6-FAM-RI-AG03-polyR) and fair (6-FAM-RI-AG03-TAT) co-localisation with the lipid raft marker cholera toxin subunit B was observed

(Table 5.1 and Figure 5.6D). Because polyR or TAT CPPs are capable of energy-independent cell membrane penetration (Palm-Apergi et al., 2012; Shi et al., 2014), this may occur randomly at any location on the cell membrane (including at lipid rafts). Moreover, depending on the experimental conditions, these CPPs may be internalised by CavME occurring at lipid rafts (Shi et al., 2014; Duchardt et al., 2007; Allolio et al., 2018). Comparable to the free 6-FAM peptides, 6-FAM-RI-AG03-polyR- and 6-FAM-RI-AG03-TAT-conjugated liposomes both co-localised fairly with the cell membrane (Table 5.1 and Figure 5.6C). Co-localisation with lipid rafts was fair or poor for 6-FAM-RI-AG03-polyR-liposomes and 6-FAM-RI-AG03-TAT-liposomes, respectively, but both peptide-liposome constructs had almost identically low Rcoloc values (Table 5.1 and Figure 5.6D).

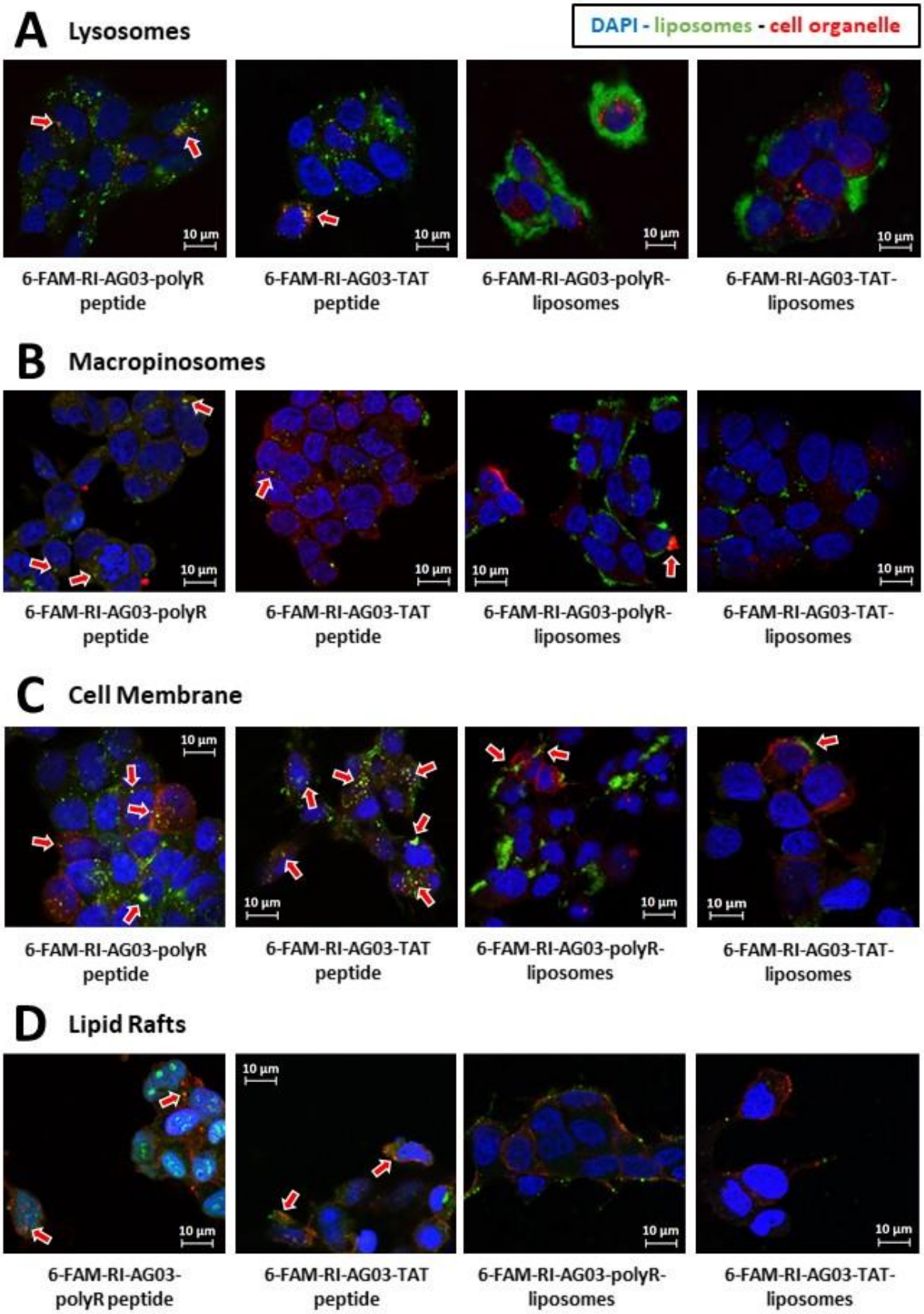

Figure 5.6: Co-localisation of unconjugated or liposome-conjugated 6-FAM-RI-AG03 peptides with lysosomes (A), macropinosomes (B), the cell membrane (C) or lipid rafts (D) in SH-SY5Y cells. For a

total of 16 h, cells were co-incubated with unconjugated or liposome-conjugated fluorescent RI-AG03 peptide and a live cell organelle stain, which was either LysoTracker Deep Red (lysosomes), pHrodo™ Red Dextran (macropinosomes) or CellLight™ Plasma Membrane-RFP (cell membrane). To visualise lipid rafts in (D), Cholera Toxin Subunit B (Recombinant), Alexa Fluor™ 594 Conjugates and an incubation time of 30 min on ice were used. In the confocal images, green represents the 6-FAM fluorophore of the peptide, red the cell organelle stain and blue the nucleus (DAPI). Arrows indicate co-localisation.

Given that 6-FAM-peptides conjugated to liposomes mostly showed no co-localisation with macropinosomes and lysosomes (Table 5.1), trafficking into other cell compartments was investigated (Figure 5.7). Unbound 6-FAM-RI-AG03-polyR and 6-FAM-RI-AG03-TAT peptides showed fair and poor co-localisation, respectively, with the early endosome marker Rab5a-RFP (Table 5.1 and Figure 5.7A). However, the 6-FAM-RI-AG03-polyR nor 6-FAM-RI-AG03-TAT peptide bound to liposomes displayed no co-localisation with early endosomes (Table 5.1 and Figure 5.7A). Using CellLight™ ER-RFP probes as an ER marker, there was no co-localisation with free or liposome-conjugated 6-FAM-RI-AG03-polyR and poor co-localisation with unconjugated or liposome-linked 6-FAM-RI-AG03-TAT (Table 5.1 and Figure 5.7B). Similarly, there was no co-localisation of any of the 6-FAM peptides with N-acetylgalactosaminyltransferase-RFP proteins in the Golgi, independent of whether these were free or conjugated to liposomes (Table 5.1 and Figure 5.7C).

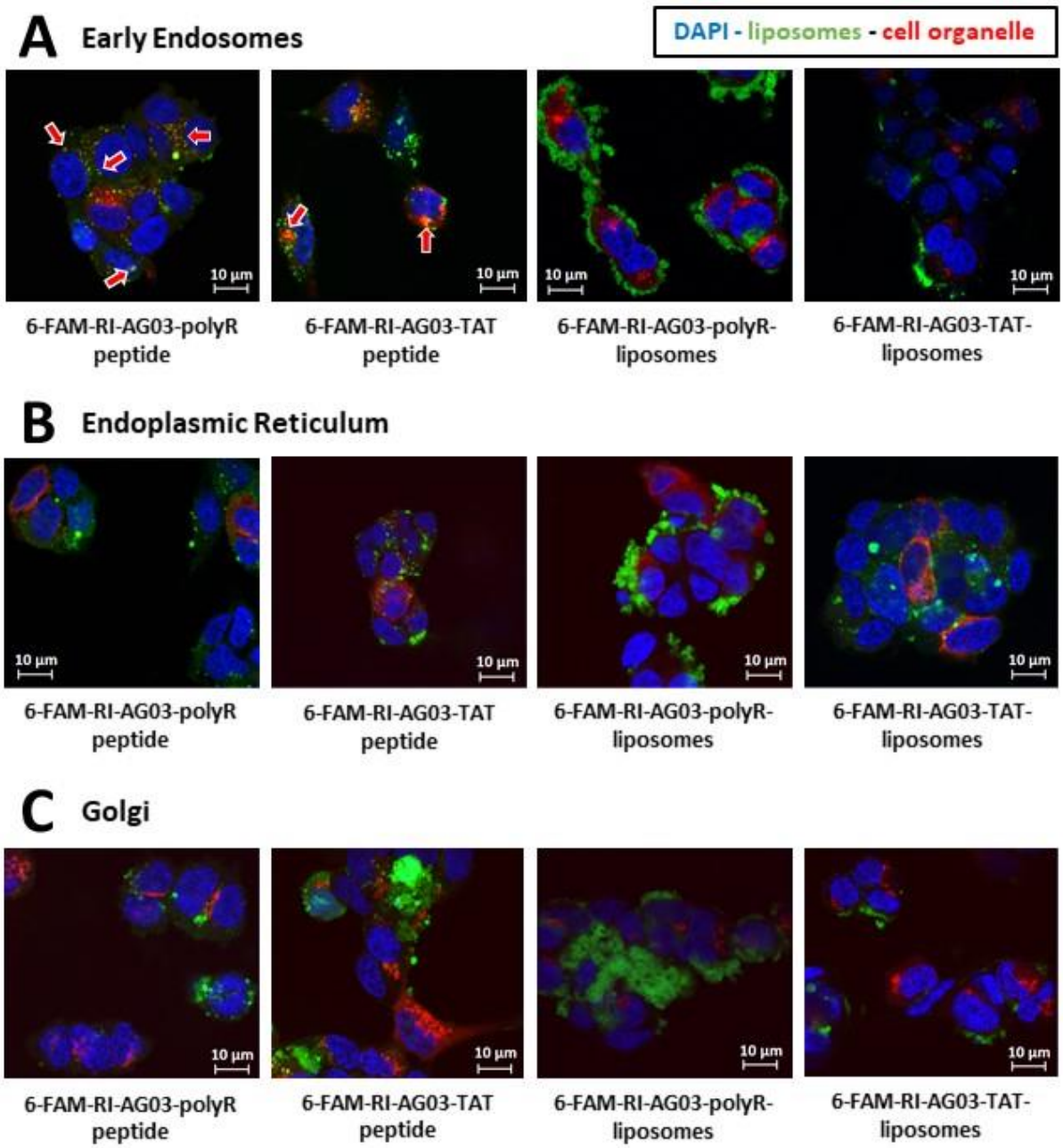

Figure 5.7: Trafficking of 6-FAM-RI-AG03 peptides and 6-FAM-RI-AG03-liposomes into early endosomes (A), the ER (B) or Golgi (C) in SH-SY5Y cells. Prior to confocal microscopy, cells were co-treated with unconjugated 6-FAM-RIAG03-polyR/TAT or 6-FAM-peptide-linked liposomes (green) and a live cell organelle stain (red) that was either Rab5a-RFP (CellLight™ Early Endosomes-RFP), CellLight™ ER-RFP or N-acetylgalactosaminyltransferase-RFP (CellLight™ Golgi-RFP) for 16 h. Blue indicates the nucleus (DAPI) and arrows show co-localisation.

In summary, the above data suggest that the liposome vehicle and the initially conjugated peptides undergo a distinct intracellular trafficking pattern after their internalisation by SH-SY5Y cells. In

contrast to the mostly fair co-localisation observed for peptide-conjugated BODIPY-liposomes, 6-FAM-RI-AG03-polyR- or 6-FAM-RI-AG03-TAT- conjugated liposomes showed no co-localisation with lysosomes, macropinosomes (6-FAM-RI-AG03-TAT-liposomes only) and early endosomes anymore. Trafficking into the ER and Golgi was generally poor or absent. This suggests that the initially liposome-coupled 6-FAM peptides potentially traffic into the cytoplasm.

5.4.3. Dissociation of RI-AG03 from its liposome vehicle following cellular uptake

In light of the disparate co-localisation of liposome-conjugated 6-FAM-peptides and peptide-BODIPY-liposomes with cell organelles, I investigated whether the peptide detaches from its liposome vehicle before moving to an alternative cellular destination. As such, a novel construct consisting of a Cy5-labelled RI-AG03-polyR peptide (red fluorescence) that was linked to BODIPY-liposomes (green fluorescence) was employed to simultaneously monitor the subcellular distribution of the peptide and liposome carrier in SH-SY5Y cells following a 2 h and 16 h incubation (Figure 5.8).

As seen in Figure 5.8A, after a 2 h treatment with Cy5-RI-AG03-polyR-BODIPY-liposomes, co-localisation of the peptide and liposome vehicle was fair (Rcoloc = 0.5962) and still observed close to the cell membrane. However, following a 16 h incubation period, there was no co-localisation anymore (Rcoloc = -0.0186, Figure 5.8B). At this time point, Cy5-RI-AG03-polyR (red) remained localised at the periphery of the cells, whilst the BODIPY-liposomes (green) had dispersed throughout the cytoplasm (Figure 5.8B). Therefore, following membrane fusion and the cellular uptake of peptide-liposomes, the peptide appears to dissociate from its liposome carrier.

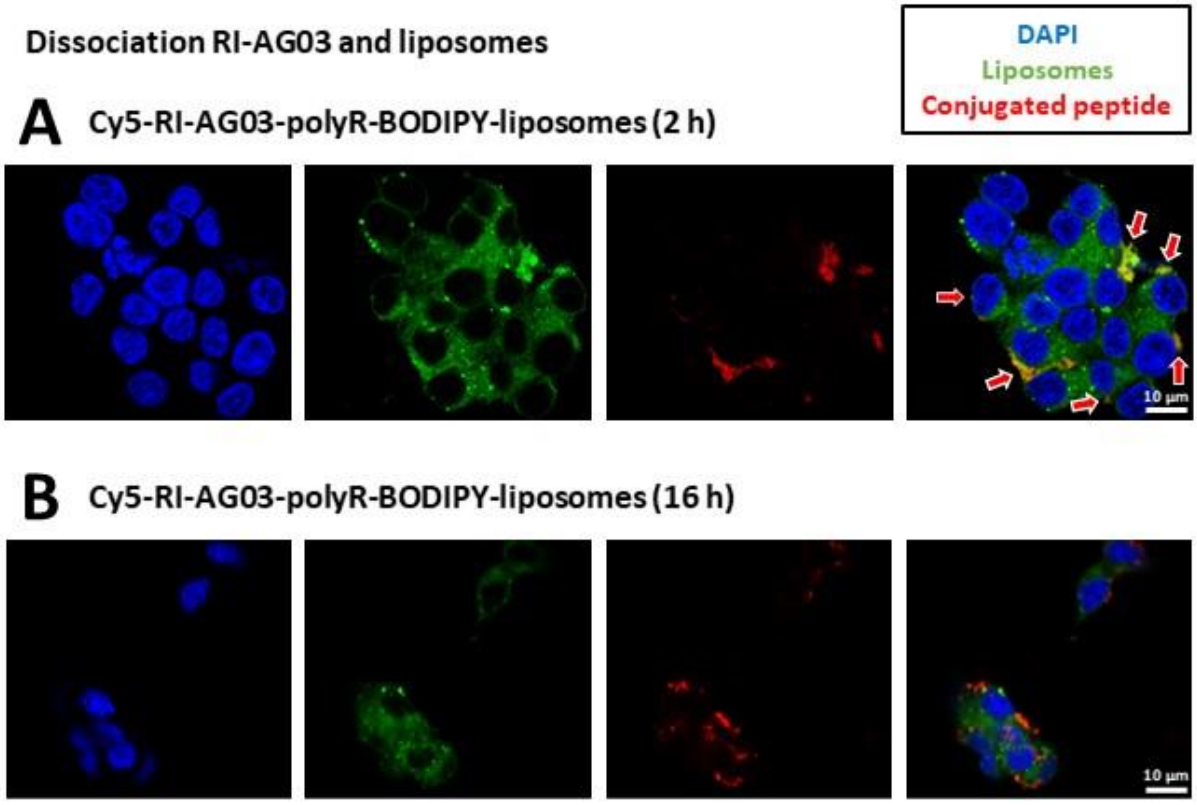

Figure 5.8: Dissociation of RI-AG03 from its liposome vehicle following fusion with cells. SH-SY5Y cells were treated with Cy5-RI-AG03-polyR-BODIPY-liposomes for 2 h (A) or 16 h (B) and images were acquired with confocal microscopy. Red represents the Cy5 peptide, green BODIPY-liposomes and blue the nucleus (DAPI). Arrows show co-localisation.

5.5. Discussion

5.5.1. Factors influencing the uptake efficiency of liposomes

This study demonstrated that, especially, RI-AG03-polyR- or RI-AG03-TAT-conjugated BODIPY-liposomes are readily taken up by SH-SY5Y cells (Figure 5.2). Because my liposomes contain a high proportion of cholesterol (47.5 %) (Figure 5.1B), this likely facilitated their internalisation. It has previously been shown that incorporating cholesterol into liposomes resulted in 8-fold, 11-fold and 5-fold-improved uptake by SH-SY5Y cells, BBB-associated brain microvascular endothelial cells and glia-like Schwann cells, respectively, relative to liposomes without cholesterol (Lee et al., 2013). Cholesterol incorporation did not heighten liposome uptake by skeletal muscle-like NIH-3T3 fibroblasts, however. This possibly suggests that the composition of my liposomes might favour BBB translocation and fusion with both Tau-containing neurons and oligodendrocytes (the CNS counterpart of peripheral Schwann cells) (Vogel et al., 2021; Narasimhan et al., 2020; Zareba-Paslawska et al., 2020; Higuchi et al., 2005), with lesser uptake by skeletal muscle cells.

The surface charge of the liposomes, which can be modified by the conjugation of CPPs, also impacts their cellular uptake (Foroozandeh and Aziz, 2018). *In vitro*, cationic nanoparticles were shown to be electrostatically attracted to anionic bilipid membranes, independent of the lipid composition of the membrane (Li and Malmstadt, 2013). Although we have not characterised the zeta potential of unconjugated liposomes, earlier studies of our group and the charge characteristics of cholesterol (47.5 %; negative), SM (47.5 %; positive) and DSPE-PEG(2000)-Mal (5 %; negative) suggest that unconjugated liposomes exhibit negative surface charge (Magarkar et al., 2014; Rye et al., 1996; Oswald et al., 2016; Taylor et al., 2011). In contrast, PolyR and TAT are positively charged CPPs (net charge +8) (Juliano et al., 2008). Interestingly, it has been demonstrated that an initially anionic liposome formulation acquired a positive zeta charge following surface coating with polyR CPPs (Opanasopit et al., 2011). Thus, linkage of RI-AG03-polyR or RI-AG03-TAT to liposomes potentially imparts a positive surface charge that, in turn, promotes fusion of the peptide-liposomes with the

negatively charged cellular plasma membrane (El-Sayed et al., 2009). This charge effect presumably contributed to the 3-fold enhanced uptake of RI-AG03-polyR- or RI-AG03-TAT-conjugated BODIPY-liposomes compared to unconjugated BODIPY-liposomes (Figure 5.2A).

In agreement with this suggestion, it was shown that cationic gold beads (+ 20 mV) were internalised 5 to 10-fold faster than neutral (- 4 mV) and anionic (- 10 mV) gold nanospheres (Cho et al., 2009). In addition, similar to RI-AG03-polyR-liposomes, the surface conjugation of polyR to PEG(2000)-containing liposomes loaded with siRNA resulted in more effective gene silencing in cells compared to Lipofectamine (Zhang et al., 2006a; Kim et al., 2010). Comparable to RI-AG03-TAT-liposomes, coating polyethylenimine/PEG-liposomes with TAT peptides also improved the transfection efficiency of SH-SY5Y cells by 14-fold (Suk et al., 2006). Collectively, the results of these experiments and other studies demonstrate that the cellular uptake of liposomes is greater if their zeta charge is positive and polyR or TAT CPPs are conjugated to the liposome surface.

Notably, the cysteine used for click chemistry-mediated conjugation of RI-AG03 to liposomes was added at the end of the polyR or TAT CPP in the peptide (Figure 5.1) (Mason and Thordarson, 2016). This decision was made to ensure that, when conjugated to liposomes, the Tau binding sequence of RI-AG03 faces outwards in order to bind Tau, whilst the CPP is orientated inwards. However, only BODIPY-liposomes with surface conjugation of RI-AG03-polyR or RI-AG03-TAT, but not unconjugated BODIPY-liposomes, showed a statistically significant uptake by SH-SY5Y cells. The internalisation of peptide-BODIPY-liposomes was also 3-fold higher relative to unconjugated BODIPY-liposomes (Figure 5.2A). Thus, despite the fact that the polyR or TAT sequence in RI-AG03 faces inwards following conjugation to liposomes, this does not appear to impair the uptake-enhancing function of these CPPs (Parthsarathy et al., 2013; Shi et al., 2014).

5.5.2. Inconsistencies between the cellular uptake mechanism and cell organelle trafficking

Using various endocytosis inhibitors and immunocytochemistry, it was revealed the uptake of unconjugated BODIPY-liposomes was reduced by cytochalasin D (-19 %, Figure 5.3A), which is predominantly a macropinocytosis inhibitor (Curtis et al., 2015; Foroozandeh and Aziz, 2018). Despite a 28 % reduction in the internalisation of RI-AG03-polyR-BODIPY-liposomes in response to EIPA treatment (a macropinocytosis inhibitor) (Curtis et al., 2015; Foroozandeh and Aziz, 2018), this was not significant. However, an alternative analysis of all nine data points, as opposed to using the average of experimental run 1 - 3 (n = 3 technical replicates per run), a significant effect is seen (section 5.3.2 and Figure 5.3B). The uptake of RI-AG03-TAT-BODIPY-liposomes was independent of macropinocytosis (Figure 5.3C). The latter endocytic pathway involves the ruffling of the cellular membrane and the formation of protrusions (lamellipodia) that unselectively engulf large volumes of extracellular fluid. This mechanism enables the uptake of compounds that are too large for other endocytosis pathways. The internalised macropinosomes range from 0.5 - 10 μm in diameter and are delivered to lysosomes (Lim and Gleeson, 2011; Foroozandeh and Aziz, 2018). In agreement with uptake inhibition by cytochalasin D, unconjugated BODIPY-liposomes showed (higher) moderate co-localisation with macropinosomes (pHrodo™ Red Dextran), while internalisation of RI-AG03-polyR/TAT-conjugated BODIPY-liposomes was only fair (Table 5.1 and Figure 5.4A). Co-localisation with lysosomes (LysoTracker) was fair for all three BODIPY-liposome species (Table 5.1 and Figure 5.4B).

The cellular internalisation of the three BODIPY-liposome constructs used was not mediated by CavME, which occurs at lipid rafts (Figure 5.3A-C) (Lajoie and Nabi, 2010). Congruently, there was poor co-localisation of unconjugated or peptide-conjugated BODIPY liposomes with lipid raft marker Cholera Toxin Subunit B (Table 5.1 and Figure 5.4D). Because unconjugated BODIPY-liposomes (fair), RI-AG03-polyR-BODIPY-liposomes (moderate) and RI-AG03-TAT-BODIPY-liposomes (fair) showed co-localisation with CellLight™ Plasma Membrane-RFP (Table 5.1 and Figure 5.4C), this suggests that

these liposomes may randomly fuse with lipid rafts for direct cell membrane penetration (Curtis et al., 2015; Foroozandeh and Aziz, 2018).

Although the internalisation of RI-AG03-TAT-liposomes was independent of macropinocytosis in SH-SY5Y cells (Figure 5.3C), they displayed fair co-localisation with macropinosome and lysosome markers (Table 5.1 and Figure 5.4A&B). It is plausible that random membrane fusion led to unspecific internalisation by macropinocytosis and trafficking into macropinocytosis-associated cell organelles. In support of this suggestion, unconjugated BODIPY-liposomes, whose uptake was partially dependent on macropinocytosis (Figure 5.3A), co-localised more strongly with macropinosomes than RI-AG03-TAT-BODIPY-liposomes (Table 5.1 and Figure 5.4B).

Notably, early glucose hypometabolism in neurons during the prodromal mild cognitive impairment (MCI) stage, caused by the development of cerebral insulin resistance, is a clinical feature of AD (Mosconi et al., 2008; Neth and Craft, 2017). The presence of bioenergetic impairments in neurons suggests that ATP-dependent endocytosis might be impaired. As such, the energy-independent uptake of, particularly, TAT-conjugated liposomes might be advantageous to deliver RI-AG03 into Tau-burdened neurons.

5.5.3. The impact of liposome characteristics and CPP conjugation on cellular endocytosis

Multiple characteristics, including concentration, cargo type, material choice, size, shape, surface charge, hydrophobicity and surface modifications determine the preferred cellular uptake pathway of nanoparticles (Foroozandeh and Aziz, 2018; Shi et al., 2014). The impact of these characteristics and CPPs on the cellular internalisation mechanisms of unconjugated and peptide-conjugated liposomes is discussed below.

The size of liposomes affects their endocytic uptake in cells (Foroozandeh and Aziz, 2018). Nanoparticles ranging from a few to several hundred nm in size and displaying positive surface charge are commonly internalised by macropinocytosis. By contrast, negatively charged particles

ranging from 120 - 150 nm, with a maximum diameter of 200 nm, are preferentially taken up via CME or CavME (Foroozandeh and Aziz, 2018). Although extruded with 100 nm pores, our earlier studies showed that SM:cholesterol:DSPE-PEG(2000)-Mal liposomes, due to the incorporated PEG groups, display an average diameter of 180 nm (Ross, 2020). Moreover, surface conjugation of the Aβ-binding peptide RI-OR2-TAT, which has a similar length to RI-AG03-TAT and RI-AG03-polyR peptides, expanded the liposome size to around 280 nm (Ross, 2020). Thus, the size of unconjugated liposomes and peptide-liposomes is likely at the upper limit or too large for CME- and CavME-mediated uptake that is selective for cargo sizes between, ideally, 120 - 150 nm (Foroozandeh and Aziz, 2018). This is in agreement with the fact that macropinocytosis partially mediated the internalisation of unconjugated BODIPY-liposomes (Figure 5.3A).

The liposome composition also possibly influences endocytosis. In this context, the plasma membrane extraction of cholesterol has been shown to prevent the recruitment of RAS-related C3 botulinum toxin substrate 1 (Rac1), a protein that induces macropinocytosis by evoking membrane ruffling and the formation of macropinosomes at the plasma membrane (Grimmer et al., 2002). Given the high molar amounts of cholesterol in the liposomes used in the current study (47.5 %), it could be possible that the cholesterol in membrane-fused unconjugated liposomes served as a macropinocytosis-triggering recruitment signal for Rac1.

The surface charge of liposomes also affects endocytosis (Foroozandeh and Aziz, 2018). Earlier studies of our group and other publications evaluating the characteristics of cholesterol, SM and DSPE-PEG(2000)-Mal imply that unconjugated liposomes likely display negative surface charge (Taylor et al., 2011; Magarkar et al., 2014; Rye et al., 1996; Oswald et al., 2016). On the other hand, both polyR and TAT are positively charged CPPs (Juliano et al., 2008) that, when conjugated to the surface of liposomes, impart positive zeta charge (Opanasopit et al., 2011). Although non-significant (depending on the applied data analysis method), this positive surface charge could be involved in the uptake of RI-AG03-polyR-BODIPY-liposomes by macropinocytosis (28 % inhibition by EIPA, Figure 5.3B) (Foroozandeh and Aziz, 2018). Since unconjugated BODIPY-liposomes only showed a

13 % reduction in their cellular uptake following EIPA treatment (Figure 5.3A), this indicates that the conjugation of RI-AG03-polyR to liposomes could potentially increase the relative proportion of macropinocytosis-mediated uptake.

Finally, the choice of the nanocarrier-conjugated CPP might affect the endocytosis pathway. CPPs may be taken up by direct membrane translocation, CME, CavME or macropinocytosis, as dependent on a range of conditions (reviewed in Shi et al. (2014)). For example, by increasing the CPP concentrations from 10 to 40 μM, nonaarginine and TAT became less dependent on CME and were gradually more internalised by direct membrane penetration, CavME and macropinocytosis in HeLa cells (Duchardt et al., 2007). Therefore, how linkage of a CPP to liposomes alters their cellular uptake is presumably also context-dependent. Hypothetically, CPP conjugation to liposomes could:

(i) Enhance ATP-independent membrane fusion and translocation of the peptide-liposomes.

(ii) Accelerate uptake by the primary endocytosis mechanism of the unconjugated liposomes.

(iii) Improve uptake by both of the above mechanisms.

(iv) Alter the main endocytosis pathway entirely.

Studies have shown that nonaarginine peptides induce membrane multilamellarity, resulting in their energy-independent cellular uptake (Allolio et al., 2018). Additionally, surface conjugation of cationic polyR CPPs to liposomes was suggested to enhance the apposition and, hence, fusion of CPP-conjugated liposomes with lipid bilayers (El-Sayed et al., 2009; Pei and Buyanova, 2019). This suggests that the coating of liposomes with polyR or TAT CPPs may enhance direct cell membrane translocation. Such an increase in direct membrane translocation was observed for RI-AG03-polyR- or RI-AG03-TAT-conjugated liposomes, whose internalisation was 3-fold, but non-significantly, increased in an endocytosis-independent manner (Figure 5.3C) compared to unconjugated liposomes (Figure 5.2A). Therefore, CPPs magnify the cellular liposome uptake by enhancing energy-independent uptake. On the other hand, the conjugation of RI-AG03-polyR to liposomes elevated the proportion of macropinocytosis-mediated uptake from 13 % to 28 % (EIPA-treated groups in

Figure 5.3A compared to Figure 5.3B). Although EIPA failed to significantly lower the internalisation or RI-AG03-polyR-BODIPY-liposomes (Figure 5.3B), this suggests that CPPs could also boost endocytosis-mediated uptake.

5.5.4. Limitations of the experimental design for the assessment of endocytosis pathways

The experimental design in the current study has several caveats in relation to the study of the main endocytosis pathways of unconjugated or peptide-conjugated BODIPY-liposomes in SH-SY5Y cells.

First, other less characterised endocytosis mechanisms exist, such as CLIC/GEEC-driven endocytosis, flotillin-mediated endocytosis, circular dorsal ruffles and more (see Doherty and McMahon (2009)), yet inhibitors for these endocytic pathways are lacking (Dutta and Donaldson, 2012; Ivanov, 2008). Thus, it cannot be ruled out that unconjugated liposomes and peptide-liposome were internalised by these alternative endocytosis mechanisms in SH-SY5Y cells.

My study showed that there was poor (RI-AG03-polyR-BODIPY-liposomes) or fair (unconjugated BODIPY-liposomes and RI-AG03-TAT-BODIPY-liposomes) co-localisation of some liposome constructs with early endosomes, a CME-associated cell organelle (Table 5.1 and Figure 5.5A) (McMahon and Boucrot, 2011). The literature supports that the used endocytosis inhibitor concentrations for filipin (CavME: 5 µg/mL) (Cuddy et al., 2014), cytochalasin D (macropinocytosis and partially CME plus CavMe: 7.5 µM) (Nara et al., 2010) and EIPA (macropinocytosis: 50 µM) (Kim et al., 2016) were sufficient to block endocytosis in SH-SY5Y cells, whilst being non-toxic in MTT assays (Appendix, Figure 9.4B). Chlorpromazine is typically used in the range of 50 - 100 µM to inhibit CME in cells (Ivanov, 2008), with an IC_{50} of 17.4 µM (Daniel et al., 2015). Similar to my study, 10 µM chlorpromazine has previously been used to block CME in SH-SY5Y cells (Wang et al., 2019). Notably, using higher concentrations was not possible in this study because 12.5 µM chlorpromazine provoked the detachment of SH-SY5Y cells from their cultivation dishes, whilst concentrations ≥ 15 µM were highly toxic (Appendix, Figure 9.4C). It was also recently reported that chlorpromazine

and another CME inhibitor, trifluoperazine, were toxic to undifferentiated SH-SY5Y cells (LC_{50} values of 5 µM and 6 µM, respectively) (Hakeem et al., 2020). Therefore, CME might not have been totally blocked in these experiments because the inhibition of CME itself could be toxic to SH-SY5Y cells, serving as an explanation for the fair co-localisation of unconjugated BODIPY-liposomes and RI-AG03-TAT-BODIPY-liposomes with early endosomes (Table 5.1 and Figure 5.5A). Since chlorpromazine and trifluoperazine were less toxic in differentiated SH-SY5Y cells or COS-7 fibroblasts (Hakeem et al., 2020), other (ideally neuronal) cell lines might be more appropriate to investigate CME-conveyed liposome uptake.

Related to the previous paragraph, despite using chlorpromazine, cytochalasin D, filipin and EIPA concentrations shown to inhibit endocytosis in SH-SY5Y cells (Wang et al., 2019; Nara et al., 2010; Cuddy et al., 2014; Kim et al., 2016), it has not been determined whether endocytosis was indeed blocked in the experiments. To do so, a control experiment could assess the uptake of an endocytosis pathway-specific, fluorescent substrate in the presence of different concentrations of the respective endocytosis inhibitor. For example, cells may be exposed to fluorescent dextran with or without EIPA treatment, followed by the quantification of cell fluorescence (Le and Machesky, 2022).

Notably, although the CavME-inhibitor filipin did not reduce the cellular internalisation of unconjugated BODIPY-liposomes (Figure 5.3A), there was fair co-localisation with the Golgi (Table 5.1 and Figure 5.5C), which is a CavME-associated cell organelle (Le and Nabi, 2003). In this study, co-localisation of unconjugated and peptide-conjugated BODIPY-liposomes with CavME-associated caveosomes was not assessed, however, because SH-SY5Y cells do not express the typical caveosome marker caveolin-1 (Parkin et al., 1997). Moreover, live cell fluorescent dyes, such as the HCS LipidTOX™ Deep Red Neutral Lipid Stain (Invitrogen/Thermo Fisher Scientific, Loughborough, UK), stained internalised liposomes in the cytosol (Appendix, Figure 9.6). Therefore, although it could not be confirmed experimentally, minor co-localisation of unconjugated BODIPY-liposomes with caveosomes is plausible.

5.5.5. Discrepant intracellular trafficking of the liposome vehicle and the initially conjugated RI-AG03 peptide following cellular uptake

A major challenge for drug-conjugated or -containing nanocarriers is to avoid entrapment in cell or degradative cell compartments, such as endosomes and lysosomes (Pei and Buyanova, 2019). The current study demonstrated that RI-AG03-polyR-BODIPY-liposomes and RI-AG03-TAT-BODIPY-liposomes showed fair co-localisation with fluorescent probes in lysosomes (Figure 5.4A) and macropinosomes (Figure 5.4B) and poor or fair co-localisation, respectively, with early endosomes (Figure 5.5A) following uptake by SH-SY5Y cells. However, when 6-FAM-labelled RI-AG03-polyR and RI-AG03-TAT were conjugated to non-fluorescent liposomes (the conjugated 6-FAM peptide was tracked instead of BODIPY-cholesterol in the liposomes), there was no co-localisation with lysosomes (Figure 5.6A), macropinosomes (only 6-FAM-RI-AG03-TAT-liposomes, Figure 5.6B) and early endosomes (Figure 5.7A) anymore (Table 5.1). 6-FAM-RI-AG03-polyR- and 6-FAM-RI-AG03-TAT-conjugated liposomes also showed no, or poor, co-localisation with the ER and Golgi (Table 5.1 and Figure 5.7B&C). Further research revealed that the initially conjugated 6-FAM-RI-AG03-polyR peptide detached from BODIPIY-labelled liposomes after fusing with the SH-SY5Y cell membrane (Figure 5.8). Therefore, following the cellular uptake of peptide-liposomes, the conjugated peptide escaped entrapment in cell organelles, whilst the liposome vehicle did not.

Since both RI-AG03-polyR- and RI-AG03-TAT-linked liposomes were predominantly internalised in an endocytosis-independent manner (Figure 5.3B&C), direct membrane translocation presumably prevented trafficking into cell organelles in the first place. In agreement with this suggestion, the initially conjugated 6-FAM-RI-AG03-polyR peptide detached from BODIPIY-labelled liposomes after fusing with the SH-SY5Y cell membrane (Figure 5.8). Therefore, peptide-conjugation to liposomes might change peptide trafficking, potentially in favour of cytoplasmic delivery. Compared to RI-AG03-polyR/TAT-BODIPY-liposomes, co-localisation of 6-FAM-RI-AG03-polyR or 6-FAM-RI-AG03-TAT conjugated to liposomes with CellLight™ Plasma Membrane-RFP was similar or slightly weaker (Table 5.1 and Figure 5.6C). This suggests that the initially conjugated peptide does not remain within the

cell membrane. On the other hand, whilst the liposome vehicle visibly disperses through the intracellular space after internalisation (green fluorescence in Figure 5.8), some images imply that the initially conjugated peptide might localise in proximity to the cell membrane. At least 16 h post treatment, it could be possible that the initially conjugated peptide is still stuck to, or protrudes from, the extracellular part of the cell membrane (e.g. distinct localisation of fluorescent 6-FAM-RI-AG03-polyR/TAT peptide conjugated to liposomes in green with cytoplasmic lysosomes or early endosomes in red in Figure 5.6A and 5.7A). To confirm that RI-AG03-polyR and RI-AG03-TAT peptides do not remain anchored to the cell membrane after detaching from their liposome vehicle, co-localisation with other cell membrane markers could be assessed. Additionally, to investigate if the initially liposome-conjugated peptide indeed travels into the cytoplasm following cellular uptake, co-localisation of 6-FAM-RI-AG03-liposomes with endogenous Tau (stained with $Tau_{243-441}$ antibodies and a fluorophore-coupled secondary antibody) may be examined in SH-SY5Y cells.

Interestingly, unlike their 6-FAM-RI-AG03-TAT-conjugated counterparts, 6-FAM-RI-AG03-polyR-liposomes displayed fair co-localisation with macropinosomes (Table 5.1). In this context, despite being non-significant, EIPA reduced the uptake of 6-FAM-RI-AG03-polyR-liposomes by 28 %, suggesting that a notable proportion of RI-AG03-polyR-linked liposomes is internalised by macropinocytosis. Indeed, polyR peptides can be internalised by macropinocytosis (Duchardt et al., 2007) and both the unconjugated 6-FAM-RI-AG03-polyR peptide and RI-AG03-polyR-liposomes showed fair co-localisation with macropinosomes (Table 5.1). This suggests that 6-FAM-RI-AG03-polyR-liposomes possibly exhibited co-localisation with macropinosomes due to minor uptake by macropinocytosis.

Notably, it is also possible that the incorporated CPP in the initially conjugated 6-FAM-RI-AG03-polyR/TAT peptide promoted escape from cell organelles. It has been proposed that the linkage of polyR, TAT or other CPPs to liposomes facilitates fusion with the endolysosomal membrane, leading to the ejection of liposome-encapsulated cargo into the cytoplasm (El-Sayed et al., 2009). However, this does not necessarily imply that the liposomes or surface-conjugated molecules, in this case RI-

AG03, also translocate through the endosomal/lysosomal membrane into the cytoplasm. For example, Ruan et al (2007) demonstrated that their TAT-conjugated quantum dots were internalised by macropinocytosis and transported along microtubules in macropinosomes. However, the TAT-quantum dots remained trapped in the inner macropinosome membranes (Ruan et al., 2007). Thus, linking a CPP to a nanocarrier does not necessarily improve cell organelle escape, and the utility of additional endosomal escape strategies might be necessary (El-Sayed et al., 2009).

5.6. Conclusion

Only uptake of RI-AG03-polyR- or RIAG03-TAT-conjugated, but not unconjugated, BODIPY-liposomes was significant in SH-SY5Y cells after a 4 h treatment period. Furthermore, surface conjugation of either RI-AG03-polyR or RI-AG03-TAT to BODIPY-liposomes elevated their cellular internalisation 3-fold, although this was not significant. Due to the modest endocytosis-inhibiting effects of various pharmacological inhibitors, uptake of unconjugated, RI-AG03-polyR- or RI-AG03-TAT-BODIPY-liposomes mainly ensued by energy-independent membrane fusion and translocation. However, unconjugated BODIPY-liposomes, and possibly RI-AG03-polyR-BODIPY-liposomes, were partially internalised through macropinocytosis. In agreement with their partial uptake via macropinocystosis, unconjugated BODIPY-liposomes and RI-AG03-polyR-BODIPY-liposomes displayed moderate and fair, respectively, co-localisation with macropinosomes and fair co-localisation with lysosomes. On the other hand, despite endocytosis-independent internalisation, RI-AG03-TAT-liposomes also showed fair co-localisation with these macropinocytosis-associated cell organelles.

Using Cy5-RI-AG03-polyR-BODIPY-liposomes, it was shown that the initially conjugated Cy5-peptide dissociated from its BODIPY-liposome vehicle after fusing with the cell membrane. Because no or poor co-localisation of 6-FAM-RI-AG03-polyR or Cy5-RI-AG03-TAT peptides conjugated to liposomes with lysosomes, macropinosomes (6-FAM-RI-AG03-TAT-liposomes only), early endosomes, the ER

and the Golgi was observed, this suggests that linking RI-AG03-polyR or RI-AG03-TAT to liposomes prevents intraorganellar entrapment of the peptide and potentially promotes cytosolic peptide delivery. An exception was that 6-FAM-RI-AG03-polyR-liposomes had fair co-localisation with macropinosomes, possibly due to macropinocytosis-mediated uptake.

In summary, due to their effective and mostly energy-independent uptake by cells, in combination with improved cytoplasmic peptide delivery, RI-AG03-polyR- and RI-AG03-TAT-conjugated liposomes are promising constructs to prevent the pathologic aggregation of Tau in neurons.

6. Pilot study to assess the impact of RI-AG03-polyR on the Tau pathology in human 1N4R Tau (P301S)-transgenic PS19 mice

6.1. Introduction

In order to advance RI-AG03 into human clinical trials, the biochemical effects and safety of the peptide have to be tested in a suitable Tauopathy animal model. Over 100 genetically engineered rodent lines that model pathologic aspects of AD are available, each with their own advantages and drawbacks (reviewed in Jankowsky and Zheng (2017). Notably, *MAPT* point mutations do not lead to the development of AD, but Tau-exclusive frontotemporal lobar degeneration. For example, Tau (P301L)- or (P301S)-transgenic animals replicate the pathology of FTDP-17 (Jankowsky and Zheng, 2017; Goedert and Jakes, 2005).

The most frequently employed *MAPT* rodent models are rTg4510 and PS19 (Jankowsky and Zheng, 2017). Due to their diverse pathology, PS19 animals were chosen for the *in vivo* experiments. Whilst showing a milder Tau phenotype than rTg4510PS19 mice, PS19 mice exhibit a ~5-fold-increase in the expression of human 1N4R Tau (P301S), as regulated by a constitutive mouse prion promoter (Jankowsky and Zheng, 2017). The pathology reported in these animals includes microglial and astroglial activation in brain regions such as the hippocampus, entorhinal cortex and spinal cord (3 months) and presynaptic atrophy (at 3 - 6 months) prior to phospho-Tau and NFT accumulation in the neocortex, hippocampus, brainstem, amygdala and spinal cord (at 6 months) (Yoshiyama et al., 2007; Takeuchi et al., 2011; Lasagna-Reeves et al., 2016; Maruyama et al., 2013). Furthermore, impairments in hippocampal long-term potentiation (LTP) and spatial and contextual fear memory (6 months), hindlimb paralysis (beginning at 7 months), cortical and hippocampal neurodegeneration (from 9 months) and death (at 10 - 12 months) follow.

I used our previous *in vivo* studies with the Aβ aggregation inhibitor peptide RI-OR2-TAT to inform the design of this initial pilot *in* vivo study. RI-OR2-TAT crossed the BBB in biodistribution studies *in vivo* (Parthsarathy et al., 2013). Moreover, daily i.p. administrations of 100 nmol/kg RI-OR2-TAT for a

total of 21 days improved the Aβ pathology, microgliosis, oxidative stress and neurogenesis in APPswe/PSEN1ΔE9 AD mice (Parthsarathy et al., 2013). Similarly, we demonstrated that RI-OR2-TAT-conjugated liposomes (PINPs) entered the brain. Using the aforementioned injection schedule, 100 nmol/kg PINPs also preserved object recognition memory in Tg2576 mice that overexpress human APP_{695} with the Swedish mutation (KM670/671NL) resulting in elevated Aβ levels and amyloid plaques (Gregori et al., 2017). Notably, we added a TAT sequence to RI-OR2 (Parthsarathy et al., 2013), but we have not assessed the BBB-penetrating ability of the polyR sequence in the lead RI-AG03 peptide. However, polyR CPPs, with a length of 6 or more arginine residues, have previously been shown to penetrate cells and diffuse from the blood into the brain *in vivo* (Mitchell et al., 2000; Gotanda et al., 2014; Pham et al., 2005).

Based on the promising results with RI-OR2-TAT, it was decided to adopt a similar experimental design to test the Tau aggregation inhibitor peptide RI-AG03-polyR in a pilot *in vivo* study. Both WT and PS19 mice were injected (i.p) with 100 nmol/kg RI-AG03-polyR or a scrambled RI-AG03 peptide control every other day for a total duration of 44 days, starting at 6 months of age. By extending the injection schedule, it was hoped to achieve a stronger therapeutic effect. At a final age of ~7.5 months, Tau, phospho-Tau and other AD-associated markers were examined in the brain homogenates of vehicle- or peptide-treated WT and PS19 mice via immunoblotting. As detailed below, this includes markers related to synapses (synaptophysin and PSD-95), apoptosis (caspase 3), autophagy (Beclin-1, LC3 and p62) and inflammation-associated glial activation (IBA1 and GFAP).

In AD, synapse loss and neuronal degeneration are well-established features and have been reproduced in AD animal models (Wirths and Zampar, 2020; Pozueta et al., 2013). Reductions in dendritic (presynaptic) synaptophysin, other pre- and postsynaptic markers, and synaptic density have been reported in the hippocampus of 3 - 6 month-old PS19 mice (Yoshiyama et al., 2007; Di et al., 2021). On the other hand, PSD-95 is localised to axonal postsynaptic terminals in neurons, and its expression is abnormally altered in a brain region-specific manner during aging and AD (Savioz et al., 2014). Given that PS19 mice show marked synapse loss (up to ~50 %) in areas such as the

hippocampal CA3 region (Yoshiyama et al., 2007; Di et al., 2021), both synaptophysin and PSD-95 were evaluated to assess the integrity of dendritic and axonal synaptic terminals, respectively, in these mice. Notably, in AD patients, expression of both the inactive procaspase 3 and active caspase 3 forms were shown to be enriched in postsynaptic areas, suggesting a link to synaptic atrophy (Louneva et al., 2008). Caspase 3 is a commonly used apoptosis marker that is activated in the brains of AD patients, for example in neurons and astrocytes, co-localizing with NFTs and plaques (Su et al., 2001; Rohn and Head, 2008). Caspase 3 also cleaves Tau at multiple sites to generate a variety of neurotoxic or aggregation-inducing Tau fragments (Zhang et al., 2021a; Kolarova et al., 2012). Although there are no reports on cerebral caspase 3 activation in PS19 mice, it was chosen to investigate this synapse-associated apoptosis marker.

As impaired in AD, autophagy is a lysosome and autophagosome co-mediated, cellular waste removal process involved in the degradation of pathologic Tau and other amyloids (Uddin et al., 2018). There are multiple forms of autophagy and, of these, Tau is predominantly degraded by macroautophagy, but also CMA. Beclin-1, LC3 and p62 act in concert to initiate macroautophagy by inducing phagophore formation, autophagosome maturation and the recognition of ubiquitinated cargo requiring degradation (Gorantla and Chinnathambi, 2021). Beclin-1 is part of the class III phosphatidylinositol 3-kinase complex that modulates phagophore assembly and maturation along with the fusion with endolysosomes (Sun et al., 2009). It has been shown that the expression of Beclin-1 is downregulated during the prodromal MCI stage of AD (Pickford et al., 2008). LC3-I is modified with PE to generate LC3-II, then incorporated into the membrane of assembling autophagosomes. Since LC3-II correlates with the amount of autophagosomes, LC3 conversion is a popular measure of autophagy (Tanida et al., 2008). The LC3-II/LC3-I ratio was shown to be elevated in AD patients, indicating impaired autophagosome degradation (Jaeger et al., 2010). Finally, p62 serves as a receptor for LC3 and is also degraded by autophagy. Therefore, p62 accumulation suggests impaired, whereas p62 reductions indicate enhanced, autophagic flux (Bjorkoy et al., 2009). However, p62 levels may also be affected by autophagy-independent mechanisms (Mizushima and

Yoshimori, 2007; Nakaso et al., 2004; Kuusisto et al., 2001b; Bardag-Gorce et al., 2005). Collectively, these autophagy markers have been investigated in other Tau (P301S)-transgenic mouse and 3x Tg AD animal models (Schaeffer et al., 2012; Villamil-Ortiz and Cardona-Gomez, 2015), but not in PS19 mice. For example, 3xTg mice displayed an initial increase in Beclin-1 levels and LC3-II/LC3-I ratio at 6 months, followed by a gradual decline of these autophagy markers in the cerebral cortex at 12 and 18 months (Villamil-Ortiz and Cardona-Gomez, 2015). The number of LC3-puncta also increased at 6 months, but stayed elevated at a higher age, suggesting that autophagy defects manifest in this AD animal model. Although p62 levels were unaltered to WT littermates, another study demonstrated that P301S Tau-transgenic mice exhibited co-localisation of p62 with Tau aggregates in their brains (Schaeffer et al., 2012). Treatment of P301S-transgenic mice with trehalose stimulated LC3-I conversion into LC3-II, increased LC3 puncta, lowered p62 levels and decreased insoluble Tau, supporting a link between autophagy and Tau clearance.

Microglia and astrocytes represent the two main immune cells in the CNS, but chronic activation of these glial cells are hallmarks of AD. For instance, in their anti-inflammatory M2 state, microglia defend the brain from infections, phagocytose accumulating amyloids, modulate synaptic function and secrete growth factors, whilst astrocytes release lactate and eliminate glutamate in synaptic terminals to aid nearby neurons (Morales et al., 2014; Xu et al., 2021; Smith et al., 2012). In AD, however, amyloid amassment, oxidative stress, neuronal death and other pathologic events trigger chronic switching of glial cells into a pro-inflammatory state. This state is characterised by increased IBA1 expression in microglia and GFAP in astrocytes. Activated glial cells then secrete a range of pro-inflammatory cytokines, for example IL-1β, IL-6 or TNF-α, ROS and NO that damage neurons (Morales et al., 2014; Xu et al., 2021; Cortes et al., 2018). There is also a mutual relationship between neuroinflammation and the Tau pathology in neurons. Pathologic Tau species released by neurons mobilize microglia and astroglia, leading to the secretion of pro-inflammatory cytokines. The latter act on their respective pro-inflammatory cytokine receptors on neurons to induce kinase activity (e.g. p38, cdk5 and JNK) and Tau hyperphosphorylation (Laurent et al., 2018; Morales et al.,

2013; Cortes et al., 2018). PS19 mice display age-dependent abnormalities in IBA1 and GFAP immunoreactivity in brain areas such as the hippocampus, spinal cord, entorhinal cortex or amygdala (Yoshiyama et al., 2007; Sun et al., 2020). Thus, characterisation of these markers allows to assess the impact of RI-AG03-polyR on glial inflammation.

6.2. Experimental goals

- Compare the Tau pathology in PS19 mice to age-matched WT littermates
- Investigate the effects of RI-AG03-polyR and scrambled peptide administrations on total, soluble and Ser^{202}/Thr^{205}-phosohorylated Tau in the brains of PS19 and WT mice
- Evaluate changes in presynaptic synaptophysin, postsynaptic PSD-95 and caspase 3-associated apoptosis in the CNS *in vivo* in scrambled control and RI-AG03-polyR-treated PS19 and WT mice
- Assess Beclin-1, LC3 and p62 as indicators of autophagy function in scrambled control and RI-AG03-polyR-treated PS19 and WT mice
- Examine the brain homogenate of PBS, scrambled peptide or RI-AG03-polyR-injected PS19 and WT mice for pro-inflammatory microglial (IBA-1) and astrocyte (GFAP) activation

6.3. Effect of RI-AG03-polyR treatment on Tau and phospho-Tau in PS19 mice

WT and PS19 mice were injected (i.p.) with PBS, RI-AG03-polyR or scrambled RI-AG03-polyR and the impact on total Tau in the mouse brain homogenates was determined via immunoblotting (Figure 6.1). In this preliminary study, the animal numbers of each treatment group were n = 6 (PBS) and n = 4 (RI-AG03-polyR) in WT mice and n = 6 (PBS), n = 4 (RI-AG03-polyR) and n = 3 (scrambled RI-AG03-polyR) in PS19 mice. Notably, because (Ser^{202}/Thr^{205}) phospho-Tau was undetectable in WT animals, all western blots in chapter 6 were normalised and plotted relative to the brain lysate of a PBS-treated PS19 mouse (inter-gel control; IGC) that was run on the same gel.

Probing of the brain homogenates with $Tau_{243-441}$ antibodies demonstrated a significant difference in total Tau levels between the groups ($F(4, 17) = 5.71$, $p = 0.004$; one-way ANOVA) (Figure 6.1A). Whilst PS19 mice treated with PBS exhibited approximately twice as much total Tau in their brains compared to WT rodents treated with PBS, this was not significant. Treatment of WT animals with RI-AG03-polyR had no effect on total Tau levels. Similarly, the administration of RI-AG03-polyR and the scrambled control peptide did not change total Tau levels in PS19 mice when compared to PBS-treated PS19 animals. However, in comparison to PBS-administered WT animals, total Tau levels were significantly elevated in RI-AG03-polyR- ($p = 0.018$) and scrambled RI-AG03-polyR-injected ($p = 0.021$) PS19 animals (Figure 6.1A).

Next, soluble Tau was quantified by assessing Tau levels in total and ultracentrifuged soluble homogenate fractions (Figure 6.1B) (Sanders et al., 2014). Both PBS-treated PS19 transgenic and WT mice displayed mostly soluble Tau in the CNS, accounting for 90.70 % and 94.64 % of total Tau, respectively. There was no significant difference in the proportions of soluble Tau between WT and transgenic mice. Administration of RI-AG03-polyR and scrambled RI-AG03-polyR also did not alter the amount of soluble Tau in WT or PS19 mice (Figure 6.1B).

Notably, adult mice do not express 3R Tau isoforms (Hernandez et al., 2020). Congruent with this fact, adult WT mice endogenously expressed the three mouse 4R Tau isoforms, including 0N4R (~50 kDa), 1N4R (~60 kDa) and 2N4R Tau (~70 kDa), in their brains (Figure 6.1C). Additionally, a band at ~37 kDa was observed, which likely represents a Tau degradation fragment. By contrast, PS19 mice showed a more pronounced band of 1N4R Tau at ~60 kDa due to knock in and overexpression of one allele of the human 1N4R *MAPT* (P301S) transgene (Jankowsky and Zheng, 2017). Moreover, PS19 mice display additional degradation products derived from human 1N4R Tau (P301S) that are between ~25 - 35 kDa in size (Figure 6.1C).

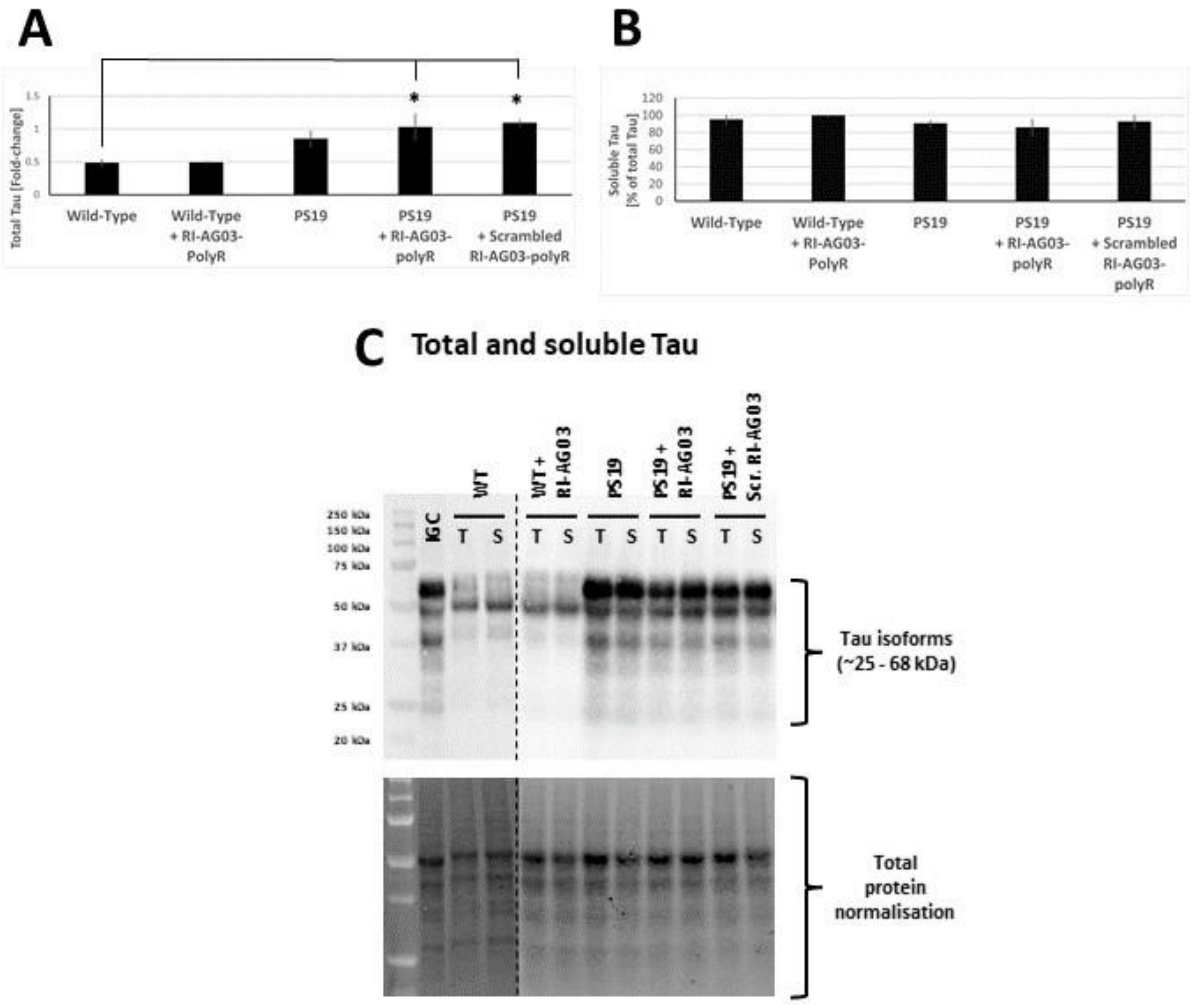

Figure 6.1: Effect of peptide treatment on total and soluble Tau in the PS19 mouse model. (A) Mean ± SEM fold-change of total Tau levels in the brain homogenate of WT and PS19 mice (n = 3 - 6). Total Tau was assessed using polyclonal $Tau_{243-441}$ antibodies. (B) Mean ± SEM % proportions of soluble Tau, as determined through the difference of total $Tau_{243-441}$ in total versus soluble fractions. (C) Immunoblots representing $Tau_{243-441}$ in the total (T) and ultracentrifuged soluble fractions (S), with the corresponding total proteins used for normalisation. Dotted lines separate different blots. IGC (inter-gel control) was the total brain lysate fraction of a PS19 mouse and all measurements (Y-axis) of total and soluble Tau were normalised to and plotted relative to this sample. Significant differences were calculated using one-way ANOVA and Tukey's post-hoc test. * = $p < 0.05$. Animal numbers were n = 6 (PBS/WT), n = 4 (RI-AG03-polyR/WT), n = 6 (PBS/PS19), n = 4 (RI-AG03-polyR/PS19) and n = 3 (scrambled RI-AG03-polyR/PS19).

In addition, the amount of Ser^{202}/Thr^{205}-phosphorylated Tau in the mouse brain lysate was investigated using AT8 antibodies. (Ser^{202}/Thr^{205}) phospho-Tau was almost entirely absent in both PBS- and RI-AG03-polyR-treated WT mice (Figure 6.2A), whilst Ser^{202}/Thr^{205}-phosphorylated Tau was

present in the brains of PS19 mice. Although the administration of the scrambled RI-AG03-polyR peptide more than halved Ser^{202}/Thr^{205}-phospho-Tau levels in PS19 mice, treatment with RI-AG03-polyR or scrambled RI-AG03-polyR had no significant effect on (Ser^{202}/Thr^{205}) phospho-Tau levels in these animals (Figure 6.2A).

Finally, the proportion of soluble and PHF-associated Ser^{202}/Thr^{205}-phosphorylated Tau was quantified (Figure 6.2B), as described for soluble Tau above. Due to lacking phospho-Tau, soluble phospho-Tau could not be assessed in PBS- or RI-AG03-polyR-injected WT mice (not shown). In PS19 rodents, 84.69 % of phospho-Tau was soluble. Both the scrambled peptide and RI-AG03-polyR had no significant effect on the proportions of soluble (Ser^{202}/Thr^{205}) phospho-Tau in PS19 mice compared to PBS-treated PS19 littermates (Figure 6.2B). As seen in Figure 6.2C, PS19, but not WT, mice showed a pronounced (Ser^{202}/Thr^{205}) phospho-Tau band at ~68 kDa in their total (T) and soluble (S) brain homogenate fractions (Figure 6.2C).

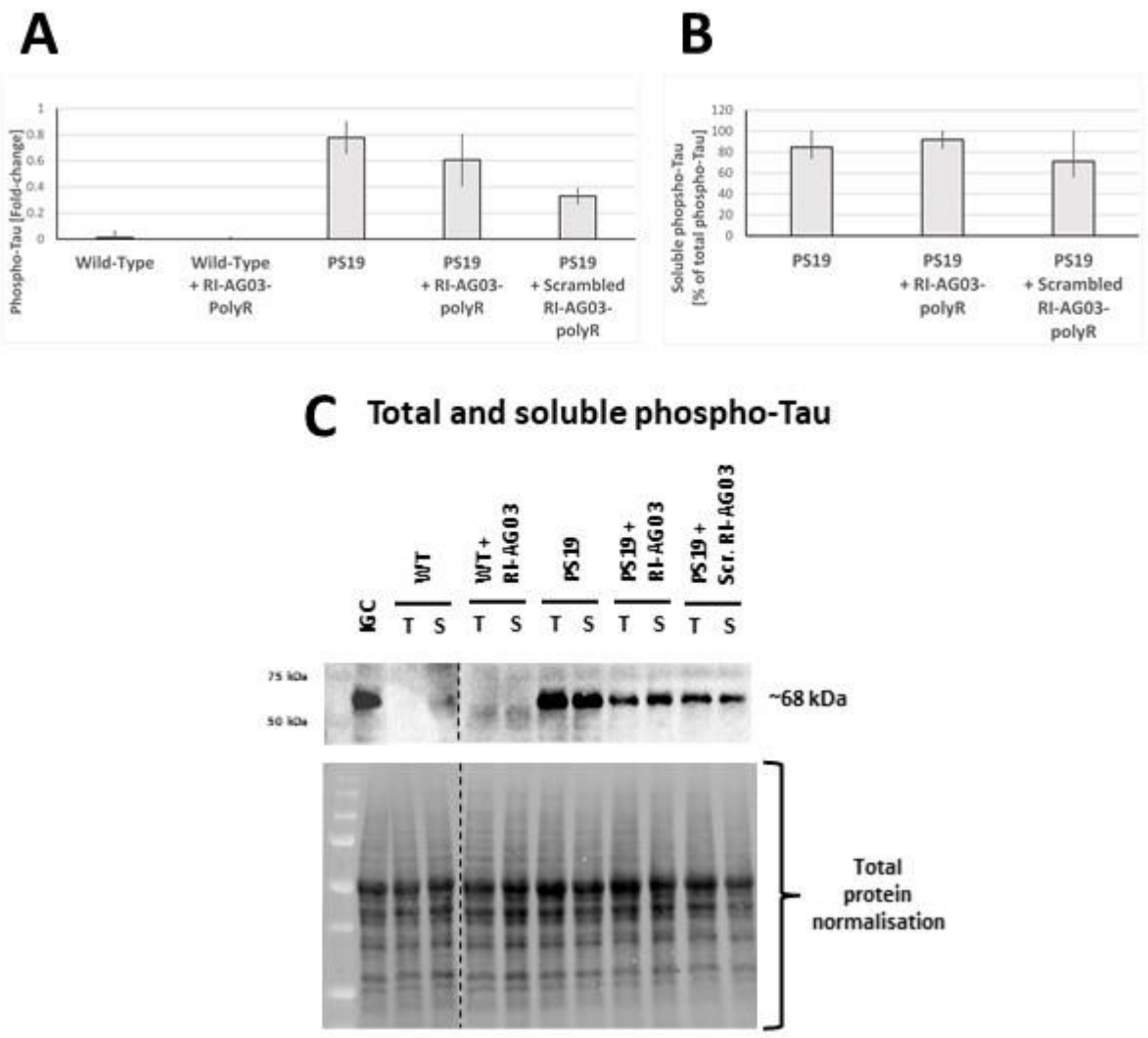

Figure 6.2: Resulting Ser^{202}/Thr^{205}-phosphorylated Tau levels following peptide administration *in vivo*. (A) Mean ± SEM fold-change in total Ser^{202}/Thr^{205}-phosphorylated Tau levels in the mouse brains (n = 3 - 6). AT8 antibodies were applied. (B) Mean ± SEM % of soluble (Ser^{202}/Thr^{205}) phospho-Tau. The latter was calculated based on (Ser^{202}/Thr^{205}) phospho-Tau levels in total fractions compared to ultracentrifuged (insoluble phospho-Tau-depleted) soluble fractions. (C) Representative blots illustrating the total (T) and soluble (S) homogenate fractions plus total protein normalisation. Dotted lines indicate different blots. IGC (inter-gel control) was the brain lysate of a PS19 mouse (total fraction) that was run on every gel. Data were normalised to the IGC on the corresponding blot, plotted and analysed with one-way ANOVA and Tukey's post hoc test. Animal numbers were n = 6 (PBS/WT), n = 4 (RI-AG03-polyR/WT), n = 6 (PBS/PS19), n = 4 (RI-AG03-polyR/PS19) and n = 3 (scrambled RI-AG03-polyR/PS19).

Collectively, the absence of statistical differences in total and soluble Tau and (Ser^{202}/Thr^{205}) phospho-Tau levels in the brains of PS19 and WT animals suggest that the Tau pathology in transgenic rodents was not fully developed. Therefore, the effect of the peptides could not be

assessed. However, RI-AG03-polyR and the scrambled control peptide modestly increased total Tau levels in the CNS of PS19 mice, rendering Tau significantly increased relative to PBS-injected WT mice (Figure 6.1A).

6.4. Impact of RI-AG03 administration on markers of synaptic degeneration and apoptosis *in vivo*

Synaptic degeneration in the brain lysate of PS19 and WT littermates was evaluated using monoclonal antibodies recognising presynaptic synaptophysin (Ala_{230})- and postsynaptic PSD-95 (Gln_{53}). No differences in synaptophysin levels were observed between PS19 and WT mice treated with PBS (Figure 6.3A). The administration of RI-AG03-polyR to WT mice and either RI-AG03-polyR or the scrambled peptide to PS19 mice also did not affect synaptophysin levels (Figure 6.3A).

In contrast to synaptophysin, PSD-95 levels were significantly different across groups ($F(4, 17) = 6.11$, $p = 0.003$; one-way ANOVA) (Figure 6.3B). PSD-95 expression levels were comparable between PS19 and WT rodents treated with PBS. However, intriguingly, the application of RI-AG03-polyR significantly elevated PSD-95 levels in the brains of WT mice ($p = 0.025$). Likewise, RI-AG03-polyR, but not its scrambled variant, significantly increased PSD-95 levels in PS19 mice compared to PBS-treated transgenic littermates ($p = 0.045$). In PS19 mice, treatment with RI-AG03-polyR did not significantly increase PSD-95 levels compared to administration of the scrambled peptide, however (Figure 6.3B).

In light of the unexpected postsynaptic effects of RI-AG03-polyR, the mouse brain extracts were additionally probed with anti-caspase 3 (p20 subunit) antibodies to assess apoptosis. Statistical analysis revealed a significant difference in the expression levels of (inactive) procaspase 3 amongst all groups ($F(4, 17) = 3.54$, $p = 0.028$; one-way ANOVA) (Figure 6.3C). However, procaspase 3 levels were not different in PBS-injected PS19 mice compared to equally treated WT mice. Administering RI-AG03-polyR to WT animals did not affect procaspase 3 levels. The injection of RI-AG03-polyR or

the scrambled RI-AG03-polyR peptide into PS19 animals also had no effect on procaspase 3 levels (Figure 6.3C).

Similar to procaspase 3, the levels of active caspase 3 were significantly different between groups ($F(4, 17) = 3.75$, $p = 0.023$; one-way ANOVA) (Figure 6.3C). While PS19 mice treated with PBS had slightly higher CNS levels of active caspase 3, but they were not significantly different from those of PSB-treated WT mice. The application of RI-AG03-polyR to WT mice or RI-AG03-polyR and the scrambled peptide to PS19 mice did not change the quantities of active caspase 3 compared to their respective PBS-treated littermates (Figure 6.3C).

As another measure of cellular apoptosis, the active caspase 3:procaspase 3 apoptosis ratio was found to be significantly different amongst the animal groups ($F(4, 17) = 5.98$, $p = 0.003$; one-way ANOVA) (Figure 6.3D). In agreement with the individual assessment of both markers, the active caspase 3:procaspase 3 apoptosis ratio was similar in PBS-injected PS19 and WT mice treated with PBS. Surprisingly, the injection of RI-AG03-polyR significantly increased the caspase 3:procaspase ratio in WT mice ($p = 0.038$). On the other hand, the administration of scrambled RI-AG03-polyR and RI-AG03-polyR did not affect the active caspase 3:procaspase 3 ratio in the CNS of PS19 mice (Figure 6.3D).

Collectively, the results in PS19 and WT rodents show that RI-AG03-polyR treatment increased postsynaptic PSD-95 levels beyond their baseline in the animal brain. This effect on PSD-95 is not necessarily caused by the Tau binding sequence in RI-AG03-polyR, however, because there is no statistical difference compared to scrambled peptide treatment in PS19 mice. Contrary to what was expected, both RI-AG03-polyR and scrambled RI-AG03-polyR may demonstrate apoptosis-promoting effects in the brains of WT and PS19 rodents. It is not clear which type of cells, for example neurons, microglia, astrocytes or oligodendrocytes, were harmed by peptide administration, however.

Notably, neuronal death would elicit a decrease in both pre- and postsynaptic markers, yet this was not observed in peptide-treated rodents. Considering the PSD-95-increasing effects of RI-AG03-polyR

(Figure 6.3B) and the fact that caspase 3 activation is associated with postsynaptic degeneration (Louneva et al., 2008), the peptides might promote a recently proposed excitotoxic interaction between Tau, PSD-95 and Fyn *in vivo* (Ittner and Ittner, 2018). This is further debated in section 6.7.2.

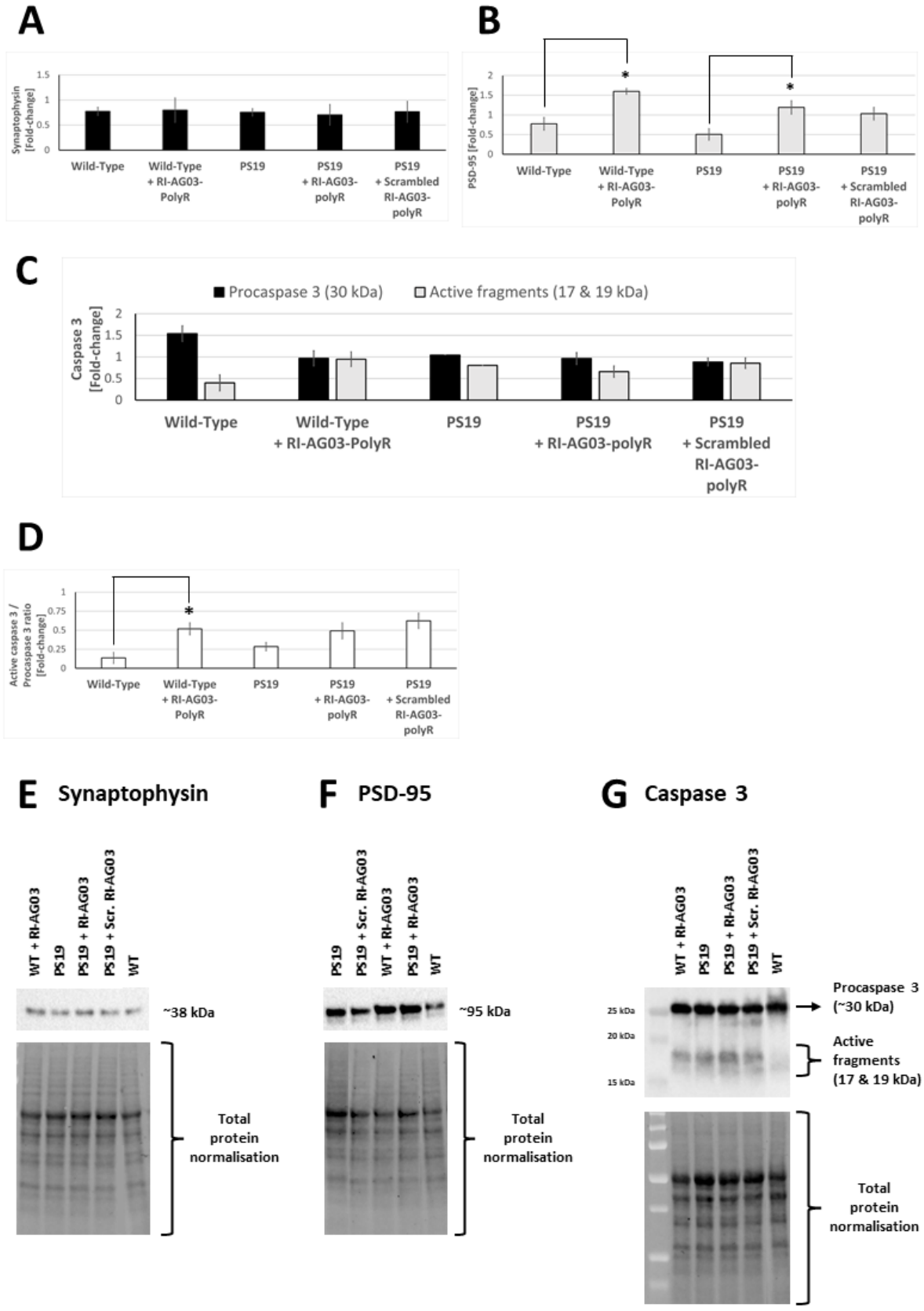

Figure 6.3: Synaptic alterations and apoptosis in RI-AG03-polyR-treated mice. Graphs illustrate the mean ± SEM fold-changes in presynaptic synaptophysin (A), postsynaptic PSD-95 (B), inactive

procaspase 3 and active caspase 3 levels (C). (D) shows active caspase 3:procaspase 3 apoptosis induction ratios. For immunoblotting, anti-Ala_{23} synaptophysin, anti-Gln_{53} PSD-95 and anti-p20 subunit caspase 3 antibodies were applied. All samples in these graphs (n = 3 - 6) were normalised to an inter-gel control (brain lysate of a PS19 mouse) on every blot, then plotted. (E - G) Representative western blots and total protein stains used for normalisation. Significant differences were calculated via one-way ANOVA followed by Tukey's post -hoc test. * = $p < 0.05$ and ** = $p < 0.01$. Animal numbers were n = 6 (PBS/WT), n = 4 (RI-AG03-polyR/WT), n = 6 (PBS/PS19), n = 4 (RI-AG03-polyR/PS19) and n = 3 (scrambled RI-AG03-polyR/PS19).

6.5. Alterations in autophagy markers in mice following RI-AG03-polyR administration

In order to explore whether peptide treatment evokes CNS autophagy *in vivo*, the total brain lysate was evaluated using western blotting and antibodies targeting Beclin 1 (Thr_{72}), LC3A/B (Leu_{44}) and p62 (C-terminus) (Figure 6.4). The CNS levels of the macroautophagy-initiating protein Beclin 1 were similar between PS19 and WT mice treated with PBS. The application of RI-AG03-polyR to WT mice had no effect. Similarly, injection of RI-AG03-polyR or scrambled RI-AG03-polyR into PS19 rodents did not alter protein levels of Beclin 1 (Figure 6.4A).

In agreement with the unchanged levels of Beclin 1, PS19 and WT rodents treated with PBS showed no differences in total LC3 levels (Figure 6.4B). RI-AG03-polyR administration in WT mice, and both RI-AG03-polyR and scrambled RI-AG03-polyR administration in PS19 mice, also had no effect on the levels of total LC3 (Figure 6.4B). Identical results to those described for total LC3 were observed for the LC3-II/LC3-I ratio, which is a relative measurement of autophagosome generation (Figure 6.4C).

Interestingly, the levels of the LC3-interacting protein p62 were significantly different between treatment groups ($F(4, 14) = 5.09$, $p = 0.010$; one-way ANOVA) (Figure 6.4D). Similar to Beclin 1 and LC3, PS19 and WT mice treated with PBS displayed comparable p62 levels. However, the injection of RI-AG03-polyR into WT mice significantly increased p62 levels two-fold compared to PBS-treated WT mice ($p = 0.021$). On the other hand, the administration of RI-AG03-polyR or scrambled RI-AG03-polyR to PS19 mice did not influence p62 levels (Figure 6.4D).

In summary, the results show that autophagy was similar between mice with a mutant Tau genotype (PS19 mice) and their WT littermates, suggesting that there was no autophagy impairment in PS19 mice at ~7.5 months old. However, the administration of RI-AG03-polyR in WT mice, but not their transgenic littermates, elevated p62 levels in the brain. Because other markers of autophagy were unaffected, peptide-induced p62 accumulation might be related to apoptosis (Figure 6.3D) or proteasomal inhibition in WT mice (Nakaso et al., 2004; Kuusisto et al., 2001b; Bardag-Gorce et al., 2005).

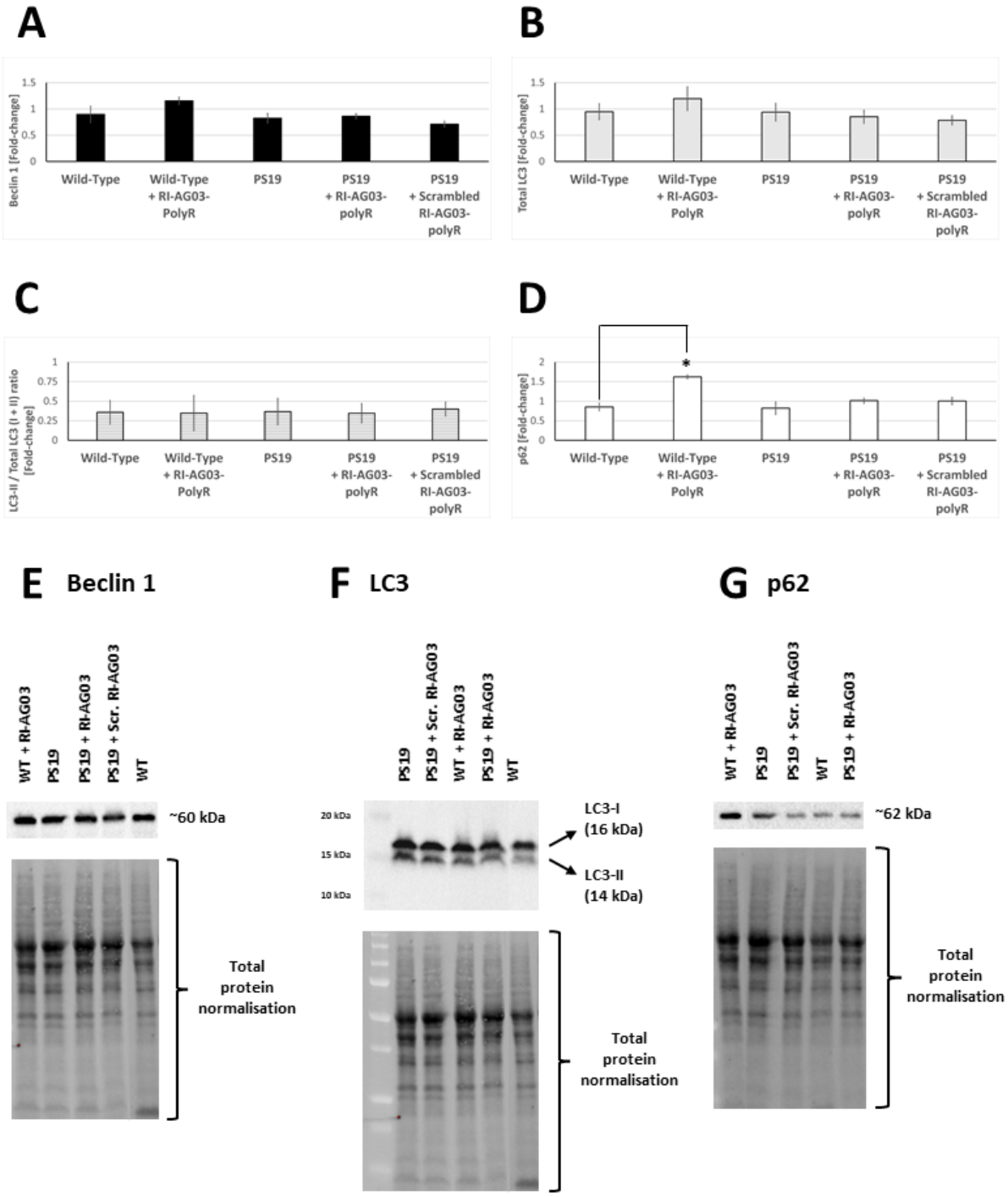

Figure 6.4: Impact of RI-AG03-polyR administrations on cerebral autophagy *in vivo*. Mouse brain extracts (n = 3 - 6) were probed with antibodies recognising Thr_{72} of Beclin 1, Leu_{44} of LC3 and the C-terminus of p62. Depicted are the mean ± SEM fold-change in Beclin 1 (A), total LC3 (LC3-I + LC3-II) (B), LC3-II/LC3-I ratios (C) and p62 (D) relative to an inter-gel control on the same blot (a PBS-treated PS19 mouse). (E - G) Representative immunoblots and respective total protein normalisation stains. Data was assessed for significant differences using one-way ANOVA and Tukey's post-hoc correction. * = $p < 0.05$ and ** = $p < 0.01$. Animal numbers were n = 6 (PBS/WT), n = 4 (RI-AG03-polyR/WT), n = 6 (PBS/PS19), n = 4 (RI-AG03-polyR/PS19) and n = 3 (scrambled RI-AG03-polyR/PS19).

6.6. Impact of the Tau genotype and RI-AG03-polyR treatment on cerebral microgliosis and astrogliosis

The effects of the Tau genotype and the peptide on glial inflammation were investigated by subjecting the mouse brain homogenate to immunoblotting with anti-ionized calcium binding adaptor molecule 1 (IBA1; Ala_{139}) and anti-glial fibrillary acidic protein (GFAP; Asp_{395}) antibodies.

Indicative of activated and pro-inflammatory microglia, the levels of IBA1 were not different in PS19 and WT mice treated with PBS (Figure 6.5A). The administration of RI-AG03-polyR had no effect on microgliosis in WT animals. Likewise, treatment with RI-AG03-polyR and scrambled RI-AG03-polyR did not alter IBA1 levels in PS19 mice (Figure 6.5A).

Identical to IBA1, levels of the astrogliosis marker GFAP were similar in PS19 and WT rodents (Figure 6.5B). RI-AG03-polyR did not affect GFAP levels in WT mice. Likewise, the administration of RI-AG03-polyR or scrambled RI-AG03-polyR did not alter GFAP levels in PS19 mice (Figure 6.5B).

In accordance with the weak Tau pathology in ~7.5 month-old PS19 mice (Figure 6.1 & 6.2), no evidence for pro-inflammatory microglial and astrocyte activation was found in the brain homogenate of these animals. Furthermore, the results indicate that RI-AG03-polyR and the scrambled peptide do not trigger neuroinflammation *in vivo*.

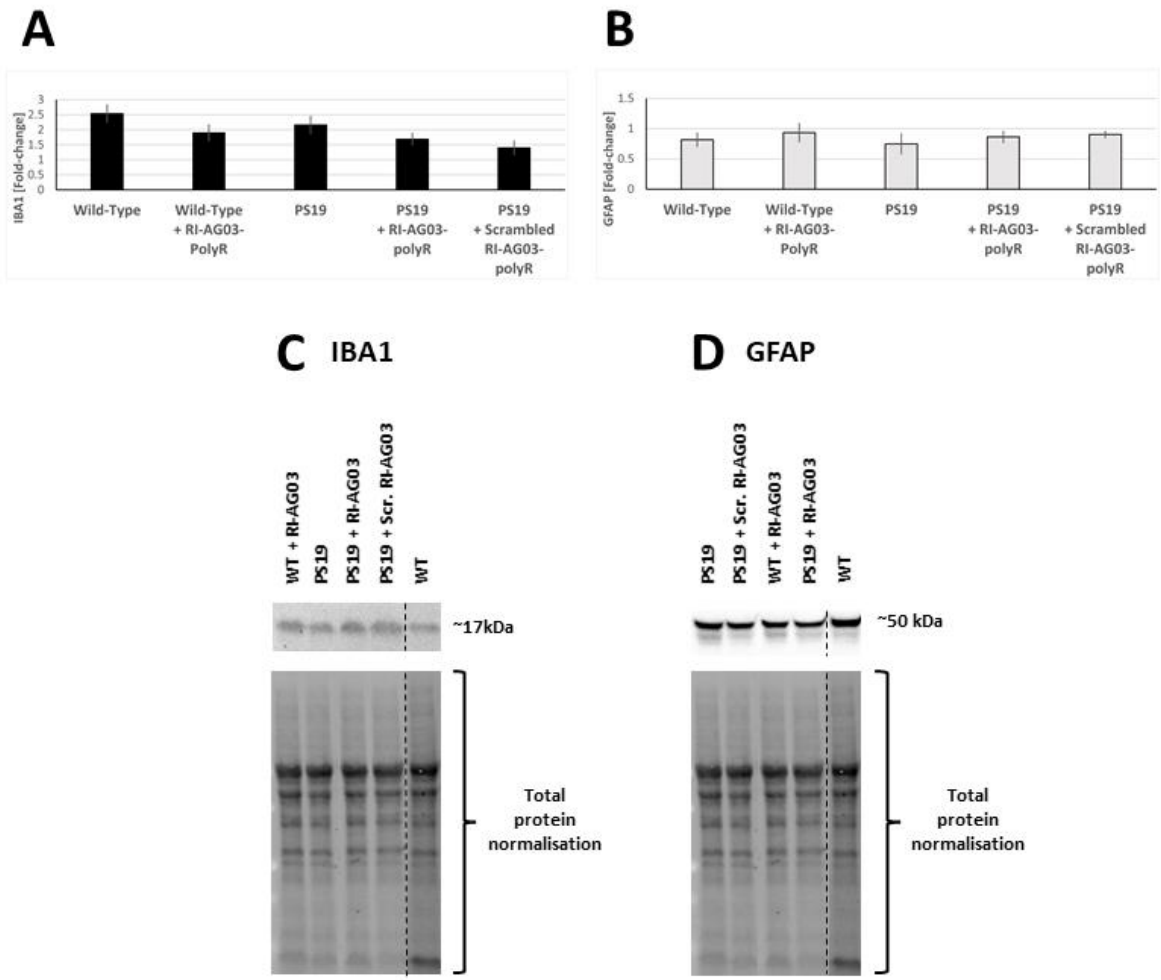

Figure 6.5: Assessment of microgliosis and astrogliosis after peptide treatment in control and PS19 mice. Shown are the mean ± SEM fold-change in microglial IBA1 (A) and astrocyte GFAP (B) levels in the mouse brain (n = 3 - 6). Antibodies recognising Ala_{139} of IBA1 and Asp_{395} of GFAP were used. All samples were normalised and plotted relative to an inter-gel control (PS19 brain homogenate) on the same blot. (C & D) Representative immunoblots and total protein normalisation stains, with dotted lines indicating separate blots. Statistical analysis with one-way ANOVA and Tukey's post hoc test revealed that there are no significant differences between groups. Animal numbers were n = 6 (PBS/WT), n = 4 (RI-AG03-polyR/WT), n = 6 (PBS/PS19), n = 4 (RI-AG03-polyR/PS19) and n = 3 (scrambled RI-AG03-polyR/PS19).

6.7. Power analysis

A potential limitation of this *in vivo* pilot study was the limited group sizes, which may result in insufficient power to detect significant differences. Therefore, using G*Power, power was determined for every western blot analysis in this chapter (Table 6.1). The results show that the power of most analyses was above 80 % (0.8), suggesting that their power was sufficient. The only

exception was the analysis of GFAP, which had a medium power of 50.95 %. The effect size (Cohen's f) of GFAP (0.6064) is still large (≥ 0.4), but also the lowest of all analyses. In this context, increasing treatment group sizes to n = 6 each would increase power of the GFAP analysis to 65.11 %, while using n = 8 would result in a sufficiently powered 81.43 %.

Therefore, higher group sizes would be useful to determine differences in GFAP levels in the brains of PBS- and peptide-treated WT and PS19 mice. Greater group sizes could also be useful to investigate more subtle peptide effects.

Table 6.1: Power analysis of the *in vivo* experiments. G*Power and an α error probability of 0.05 were used for the calculations.

	Pooled S.E.M (across groups)	**Effect size (Cohen's f)**	**Calculated power (1 - β error probability)**
Total Tau	0.0887	2.8022	1
Soluble Tau	5.3283	0.8332	0.8133
Synaptophysin	0.1637	0.1788	0.0805
PSD-95	0.1439	2.6290	1.0000
Procaspase 3	0.1160	2.1657	1.0000
Active caspase 3 fragments	0.1211	1.6583	1.0000
Beclin 1	0.0855	1.5561	0.9999
LC3	0.1521	0.8279	0.8078
p62	0.0948	2.9912	1.0000
IBA1	0.2519	1.5212	0.9998
GFAP	0.1114	0.6064	0.5095

6.8. Discussion

6.8.1. Assessment of total and soluble Tau *in vivo* and associated experimental limitations

PS19 mice have previously been characterised by other groups (Yoshiyama et al., 2007; Takeuchi et al., 2011; Maruyama et al., 2013). It was shown that PS19 animals show five-fold increased Tau expression in the CNS compared to control mice (Yoshiyama et al., 2007). Moreover, the proportions of insoluble Tau in PS19 mouse brain extracts rose in an age-dependent manner from 5 % at 1 month to 15 % at 3 months and 30 % at 6 months of age. At an age of 6 months, these insoluble Tau fractions were also hyperphosphorylated at Ser^{202}/Thr^{205} (AT8) and other positions (Yoshiyama et al., 2007; Takeuchi et al., 2011).

By contrast, the results in this study demonstrated that the CNS total Tau levels in the used ~7.5-month-old PS19 mice appeared to be elevated, but not significantly different, in comparison to age-matched WT mice (Figure 6.1A). Whilst 90.07 % of Tau in the brain lysate of PS19 mice was soluble, suggesting the presence of aggregated Tau, this was also not statistically different from age-matched WT mice (Figure 6.1B). Likewise, despite potentially increased total (Ser^{202}/Thr^{205}) phospho-Tau and reduced soluble Ser^{202}/Thr^{205}-phosphorylated Tau in the CNS of PS19 mice, this was not statistically different from WT mice either (Figure 6.2A&B). Some research groups reported a 3 - 6 month delay in the onset of the Tau phenotype in PS19 mice (Zhang et al., 2012; Iba et al., 2013; Alzforum), which also could have affected this study. As an alternative to PS19 mice, 0N4R Tau (P301L)-transgenic rTg4510mice, which display rapid severe Tau pathology and neuronal degeneration (Jankowsky and Zheng, 2017), might be used to investigate the biochemical effects of RI-AG03-polyR.

Interestingly, treatment of PS19 mice with 100 nmol/kg RI-AG03-polyR or scrambled RI-AG03-polyR slightly enhanced total Tau levels, rendering them significantly increased compared to WT mice (Figure 6.1A). RI-AG03-polyR-injected PS19 mice did not show increased total Tau levels compared to PBS-administered PS19 mice, however, and the same applied to PBS- vs. RI-AG03-polyR-treated WT mice. On the other hand, i*n vitro*, RI-AG03-polyR and scrambled RI-AG03-polyR (10, 1000 and

5000 nM) enhanced total Tau levels in 2N4R Tau (P301L)-overexpressing (Dox-induced) Clone 4 SH-SY5Y cells (Figure 3.5A), whilst the scrambled peptide (5000 nM) did so in 1N4R Tau RD (P301L/V337M)-EYFP-overexpressing Clone 9 HEK293 cells (Figure 4.1B). These *in vitro* results imply that peptide treatment might promote the intracellular accumulation of Tau, but using older PS19 mice with greater Tau accumulation are likely necessary to confirm this effect *in vivo*.

Unlike in 1N4R Tau RD (P301L/V337M)-EYFP-overexpressing Clone 9 HEK293 cells (Figure 4.1F), RI-AG03-polyR or scrambled RI-AG03-polyR peptide administration did not lower the proportions of soluble Tau *in vivo* (Figure 6.1B). Whilst this demonstrates that the injected peptide dose of 100 nmol/kg does not stimulate Tau aggregation in WT or PS19 mice, the *in vitro* experiments imply that the impact of higher drug concentrations on the proportion of soluble Tau *in vivo* need to be tested.

It has previously been reported that the arginine-rich and ^{306}VQIVYK^{311}-binding peptide p-NH (NITMNSRRRRNH), which features a similar design to RI-AG03, and N7-TAT (YGRKKRRQRRR-HHHHHHH) blocked Tau hyperphosphorylation at various pathology-associated sites in cells and PS19 mice *in vivo*, including Ser^{202}/Thr^{205} (AT8), but also Thr^{181}, Thr^{231}, Ser^{396} and Ser^{404} (Zhang et al., 2020; Kondo et al., 2021). Unfortunately, the effects of RI-AG03-polyR and its scrambled variant need to be re-assessed in future studies, since the levels of total and soluble Ser^{202}/Thr^{205}-phosphorylated Tau detected here were not statistically different in WT and PS19 mice (Figure 6.2A&B).

Notably, the western blots evaluated soluble Tau and (Ser^{202}/Thr^{205}) phospho-Tau levels in the entire mouse brain, as opposed to specific brain areas. In this context, ~7 - 7.5 month old PS19 mice, comparable to the final mouse age used in the experiments, displayed (Ser^{202}/Thr^{205}) phospho-Tau (AT8) staining (11.2 ± 6.7% of the region) and Gallyas Silver-positive Tau inclusions specifically in the CA3 region of the hippocampus (Di et al., 2021). Additionally, hippocampal, but not cortical, cerebellar or midbrain/brainstem-derived, lysate from these animals contained TOC-1-positive Tau

oligomers. In agreement with this regional Tau pathology, another study also observed increased soluble (Ser^{202}/Thr^{205}) phospho-Tau levels in 9-month old male PS19 mice, followed by aggregation into insoluble (Ser^{202}/Thr^{205}) phospho-Tau at 12 months, across the hippocampus (Sun et al., 2020). Notably, female PS19 mice showed a comparably weaker Tau pathology that was characterised by increasing amounts of soluble (3 months) and insoluble (6 months) Ser^{396}/Ser^{404}-phosphorylated Tau. Thus, in future studies, hippocampal lysate and tissue slices from ideally 9 - 12 month-old and peptide-treated PS19 mice of both sexes should be collected and subjected to western blotting and immunohistochemistry using AT8 (Ser^{202}/Thr^{205}) phospho-Tau antibodies. Alternatively, NFTs in brain sections could be stained and counted using ThS or Gallyas Silver staining (i.e. PK 301/301A, FD NeuroSilver™ Kit II, FD, NeuroTechnologies, Inc, Laisves, Lithuania), which would allow more systematic characterisation of discrete brain regions (Santa-Maria et al., 2006; Styren et al., 2000).

6.8.2. Indication of potential postsynaptic neuronal toxicity following RI-AG03-polyR administration *in vivo*

Yoshiyama et al. (2007) demonstrated that PS19 mice show progressive reductions in presynaptic synaptophysin at 3 - 6 months and postsynaptic glutamate receptor 2/3 between 6 - 9 months of age in the hippocampal CA3 area, suggesting early onset of synaptic degeneration. Another study detected decreases in Bassoon- (presynaptic) and Homer- (postsynaptic) positive puncta, with an approximate 50 % reduction in CA3 synapses, in ~7 - 7.5-month-old PS19 animals (Di et al., 2021). However, evaluating synaptophysin (Figure 6.3A) and PSD-95 (Figure 6.3B) levels in the brain lysate of 7.5 month-old PS19 mice showed no evidence of pre- or postsynaptic degeneration in PS19 mice compared to WT animals. Notably, synaptic damage was specifically observed in the hippocampal CA3 area in PS19 mice (Yoshiyama et al., 2007; Di et al., 2021), whilst the Tau pathology was generally the most severe in this brain region (Yoshiyama et al., 2007; Takeuchi et al., 2011; Maruyama et al., 2013; Di et al., 2021; Sun et al., 2020). This suggests that synapse loss does not

occur widely across the CNS in PS19 mice by 7.5 months of age, but that it develops locally in brain regions affected by Tau toxicity. Considering the weak Tau pathology identified in whole brain lysates in PS19 mice (Figure 6.1 & 6.2), this might also explain the unaltered synaptophysin and PSD-95 levels relative to WT littermates in this study (Figure 6.3A&B). On the other hand, Zhang et al. (2012) did not find any significant reductions in synaptophysin in the hippocampus of PS19 mice, despite detecting hippocampal neuronal death at 12 months of age. Therefore, brain-wide synapse loss might be minor in PS19 mice. Since an early study reported that synapse loss preceded neuronal death in PS19 mice (Yoshiyama et al., 2007), synapse loss in this study could have not occurred due to a temporal delay in the onset of Tau pathology, as implied in some studies (Zhang et al., 2012; Iba et al., 2013; Alzforum).

In PS19 mice, age-dependent reductions in hematoxylin or NeuN staining (neuronal markers) were shown to occur from an age of 8 months, substantially affecting the hippocampus, but also entorhinal and neocortical regions and the amygdala. In another study, hippocampal neuronal degeneration was apparent at an age of 12 months and could be rescued via weekly administrations of the microtubule-stabilizer EpoD from the age of 9 months (Zhang et al., 2012). Because the number of PHF-burdened neurons initially increased, but subsequently decreased in older PS19 mice, this implies that the Tau pathology eventually leads to neuronal loss (Yoshiyama et al., 2007). Total and soluble Tau, synaptophysin and PSD-95 levels as well as pro-apoptotic caspase 3 activation were not different in the brain lysate of ~7.5-month-old PS19 mice relative to age-matched WT controls, however (Figure 6.1A&B and Figure 6.3A,B&D). As elaborated elsewhere (section 6.7.1), the absence of synaptic degeneration and apoptosis in the employed ~7.5 month-old PS19 mice is likely a consequence of a delayed Tau phenotype and the presence of regional, as opposed to global, pathology.

Interestingly, RI-AG03-polyR administration doubled PSD-95 levels in both WT and PS19 mice (Figure 6.3B). PSD-95 mediates neuronal plasticity and was shown to both increase and stabilise activity (AMPAR)-dependent postsynaptic transmission (Beique and Andrade, 2003; Ehrlich et al.,

2007). Greater PSD-95 levels were also shown to promote synapse formation between dendrites (postsynaptic site) and axons of adjacent neurons (presynaptic site) (Nikonenko et al., 2008). Due to the well-established deficits in hippocampal synaptic plasticity in MCI and AD patients, which involves the downregulation of PSD-95 (Counts et al., 2014), the PSD-95-enhancing effects of RI-AG03-polyR *in vivo* (Figure 6.3B) might benefit learning and memory (Mufson et al., 2015). However, it is concerning that the peptide abnormally raised PSD-95 levels above baseline in both WT and PS19 animals, as discussed further below.

In addition to affecting PSD-95 levels, RI-AG03-polyR-administration resulted in increased pro-apoptotic caspase 3 activation in WT mice (Figure 6.3D). It is possible that caspase 3 activation was induced by the CPP in the peptide. At least *in vitro*, some CPPs may induce cell lysis at high concentrations (Kilk et al., 2009; Saar et al., 2005; Tunnemann et al., 2008). High intravenous concentrations of polyR (nonaarginine; 2.5 µmol/kg), as present in RI-AG03 and its scrambled version, also caused acute blood vessel dilation and respiratory failure in nude mice (Aguilera et al., 2009). On the other hand, the adverse effects of, specifically, polyR and TAT in cultivated cells were weak (Kilk et al., 2009; Saar et al., 2005; Tunnemann et al., 2008). The polyR dose triggering systemic toxicity (2.5 µmol/kg i.v.) (Aguilera et al., 2009) was also far beyond that of RI-AG03-polyR in these experiments (100 nmol/kg i.p.). Finally, i.p. injection of 100 nmol/kg of the TAT-containing Aβ aggregation inhibitor peptide RI-OR2-TAT was neuroprotective in APP/PSEN1 mice (Parthsarathy et al., 2013). Thus, treatment of WT mice with the same dose of a scrambled RI-AG03-polyR peptide is necessary to confirm if the CPP caused caspase 3 activation in the brain.

Alternatively, increased caspase 3 expression was shown to be associated with postsynaptic damage in AD patients (Louneva et al., 2008). RI-AG03-polyR could potentially interact with Tau in a toxic manner, resulting in the observed increases in postsynaptic PSD-95 levels and apoptosis in WT mice (Figure 6.3B&D). In this context, an excitotoxic interaction of Tau with Fyn and PSD-95 in dendritic postsynaptic terminals of neurons has been proposed (Ittner and Ittner, 2018). Under normal conditions, post-translational modifications, protein interactions and a diffusion barrier (axonal

initial segment) ensure that Tau is sorted into axons. On the other hand, pathologic Tau hyperphosphorylation evokes microtubule detachment and the re-distribution of Tau into cytosolic and dendritic (postsynaptic) compartments (Ittner and Ittner, 2018). In AD, oligomeric Aβ was demonstrated to accelerate Tau hyperphosphorylation and missorting of the protein into dendrites, followed by the Tau-mediated recruitment of Fyn to the postsynaptic space (Ittner et al., 2010; Li and Gotz, 2017). The Tyr^{18}-phopshorylation of Tau, dephosphorylation of the protein at certain residues and some Tau point mutations (e.g. P301L) also promote the association of Tau with Fyn (Usardi et al., 2011; Bhaskar et al., 2005; Pooler et al., 2012). This, inversely, results in the dendritic spine delivery of Tau by Fyn (Xia et al., 2015; Miller et al., 2014; Sohn et al., 2016). Tau and Fyn then interact with PSD-95 at postsynaptic sites, leading to excessive phosphorylation of NR2-NMDARs at Tyr^{1472} by Fyn and, thus, excitotoxicity in neurons (reviewed in Ittner and Ittner (2018)).

In this context, our group showed that RI-AG03-polyR formed circular Tau structures (GTO-like) by binding to recombinant $Tau_{\Delta 1\text{-}250}$ in the presence of heparin (Aggidis A. et al., 2021). Peptide-driven Tau oligomer formation in cells is support by the fact that treatment of Clone 9 cells with RI-AG03-polyR decreased the proportions of soluble Tau (Figure 4.1F). Importantly, soluble Tau oligomers are not confined by the axonal initial segment that restricts Tau to axons (Kopeikina et al., 2012; Xia et al., 2015; Sohn et al., 2016; Thies and Mandelkow, 2007; Ittner and Ittner, 2018). Therefore, hypothetically, peptide-generated Tau oligomers might mislocalise to somatodendritic compartments in neurons, similar to pathology-associated Tau species (Ittner and Ittner, 2018), resulting in the recruitment of Fyn and PSD-95 and excitotoxicity (Xia et al., 2015; Ittner and Ittner, 2018). Further studies in cultivated primary neurons, Clone 4 SH-SY5Y cells differentiated into a neuronal phenotype or in animals are necessary to investigate whether RI-AG03-polyR stimulates Fyn activity, Tyr^{1472}-phosphorylation of NR2-NMDARs, Tau missorting into dendrites and/or postsynaptic toxicity (Chen et al., 2014; Bell and Zempel, 2022a).

Notably, besides neurons, oligodendrocytes also express Tau (Ksiezak-Reding et al., 2003). Moreover, these cells were shown to display separate intracellular Tau hyperphosphorylation,

followed by Tau aggregation and propagation, in Tauopathy rodent models (Zareba-Paslawska et al., 2020; Higuchi et al., 2005; LoPresti, 2018). As such, the peptide-induced increase in caspase 3 *in vivo* (Figure 6.3D) could have occurred in oligodendrocytes. Thus, death of oligodendrocytes in fixed brain tissue could be evaluated with antibodies, such as myelin basic protein #78896, (Cell Signaling Technology; a marker of mature, myelinating oligodendrocytes and the myelin sheath (Baumann and Pham-Dinh, 2001)) or Olig-2 (#65915, Cell Signaling Technology; an oligodendrocyte marker). This may be differentiated from neuronal death markers, for instance neuron-specific Nissl stains (Kadar et al., 2009) or antibodies recognising nuclear NeuN (e.g. #62994, NeuN (D4G4O) XP® Rabbit mAb (Alexa Fluor® 647 Conjugate); Cell Signaling Technology, Danvers, USA).

6.8.3. Inconclusive effects of RI-AG03-polyR administrations on cerebral autophagy in WT animals

Although Tau pathology has been extensively characterised in PS19 mice (Yoshiyama et al., 2007; Takeuchi et al., 2011; Maruyama et al., 2013; Zhang et al., 2012; Iba et al., 2013; Sun et al., 2020; Di et al., 2021), there are no reports concerning autophagy or proteasomal markers. However, in a 0N4R Tau (P301S)-transgenic animal model similar to PS19 mice, despite the presence of insoluble Tau inclusions, LC3-II was undetectable and p62 levels were comparable to WT mice (Schaeffer et al., 2012). This suggests that Tau pathology does not necessarily trigger autophagy *in vivo*. In agreement with this study, there were no changes in the macroautophagy-initiator Beclin-1 (Figure 6.4A), LC3-associated autophagosome formation (Figure 6.4B&C) and the complementary factor p62 (Figure 6.4D) in the brain homogenate of PBS-treated PS19 mice relative to PBS-injected WT mice.

RI-AG03-polyR and scrambled RI-AG03-polyR administrations had no effect on Beclin-1 (Figure 6.4A) and LC3 (Figure 6.4B&C) levels, suggesting that the peptides do not affect the rate of macroautophagy. Interestingly, RI-AG03-polyR administration induced a two-fold increase in p62 levels in the brains of WT, but not PS19, mice (Figure 6.4D). p62 is implicated in the proteasomal and

macroautophagy-conducted elimination of Tau (Babu et al., 2005; Pankiv et al., 2007). Autophagy inhibition was shown to enhance cellular p62 expression (Bjorkoy et al., 2005), and increase the accumulation of p62-bound phospho-Tau inclusions in primary cortical neurons (Inoue et al., 2012). In turn, inducing autophagy with trehalose was demonstrated to lower p62 levels in the brains of Tau (P301S)-transgenic rodents (Schaeffer et al., 2012). Since autophagy (Beclin-1 (Figure 6.4A) and LC3 (Figure 6.4B&C)) was unaffected by RI-AG03-polyR or scrambled peptide *in vivo* injections in this study, the RI-AG03-polyR-induced doubling in p62 levels in the brains of WT mice (Figure 6.4D) was likely not caused by autophagy inhibition.

Besides autophagy, p62 was shown to be upregulated in response to apoptosis and proteasome inhibition (Nakaso et al., 2004; Kuusisto et al., 2001b; Bardag-Gorce et al., 2005). Given that pro-apoptotic caspase 3 activation was increased in RI-AG03-polyR-treated WT mice, but not in RI-AG03-polyR-injected PS19 littermates (Figure 6.3D), peptide-induced apoptosis could be responsible for the observed increase in p62 levels (Figure 6.4D). As another potential mechanism, polyR peptides were shown to inhibit proteasomal activity in HeLa cells (Kloss et al., 2009; Meloni et al., 2020). Thus, the CPP in RI-AG03-polyR might have elevated p62 levels by inhibiting proteasomal activity (Nakaso et al., 2004; Kuusisto et al., 2001b; Bardag-Gorce et al., 2005). Notably, PHFs present in the frontal lobe of AD patients were shown to decrease proteasomal activity by 56 % (Keck et al., 2003), whilst experiments of our group showed that RI-AG03-polyR generates spherical oligomers when binding to recombinant $Tau_{\Delta 1\text{-}250}$ (Aggidis A. et al., 2021). Peptide-induced Tau oligomer formation likely occurred in this study as well, since RI-AG03-polyR treatment reduced the proportions of soluble Tau in Clone 9 cells (Figure 4.1F). It cannot be ruled out that such peptide-Tau complexes could form in mouse neurons *in vivo* (by binding to endogenous Tau) and inhibit the proteasome, similar to PHFs. Alternatively, p62 was shown to co-localise with Tau aggregates in the brains of AD and Tauopathy patients (Kuusisto et al., 2001a; Kuusisto et al., 2002). Because RI-AG03-polyR is proteolytically resistant (Taylor et al., 2010; Aggidis A. et al., 2021), RI-AG03-polyR-bound Tau may accumulate in the cytoplasm, resulting in p62-binding to these peptide-Tau complexes and, thus,

p62 accumulation. Considering the prominent autophagy defects in AD (Liu and Li, 2019), future studies need to assess whether peptide-bound Tau is degraded and if RI-AG03-polyR treatment impairs proteasomal activity in neurons.

6.8.4. Neuroinflammatory assessments *in vivo* and possible improvements in future studies

Age-associated neuroinflammation in the employed PS19 mice has been documented (Yoshiyama et al., 2007; Sun et al., 2020). Immunohistological antibody staining and use of a radiotracer ([^{3}H]DAA1106) confirmed that microgliosis occurs and precedes astroglial activation (Yoshiyama et al., 2007). Microgliosis was demonstrated to commence in the hippocampus of 3 month-old PS19 mice, which progressively worsened in an age-dependent manner and affected further brain regions (Yoshiyama et al., 2007). Another study using IBA-1 antibodies confirmed this age-associated increase in local hippocampal microgliosis in PS19 mice from an age of 6 months (Sun et al., 2020). However, curiously, the CNS IBA1 levels in PS19 mice were shown to be lower compared to age-matched WT animals between 3 - 12 months of age. It was proposed that microglia were suppressed across the CNS in PS19 animals, but stimulated by the regional development of Tau pathology in the hippocampus. In this study, IBA1 levels (Figure 6.5A) were similar in the brains of 7.5 month-old WT and PS19 animals treated with PBS. Thus, the aforementioned microglial suppression (Sun et al., 2020) was not observed in this study.

Astrocyte GFAP immunoreactivity was observed in the white matter and spinal cord of PS19 mice from an early age of three months (Yoshiyama et al., 2007). Astrogliosis then gradually aggravated and spread across other regions, such as the hippocampus, entorhinal cortex or amygdala, in 6 month-old transgenic mice. Astrocyte immunoreactivity further co-localised with NFT deposits and the projections of Tau tangle-burdened neurons in the white matter (Yoshiyama et al., 2007). It was also reported that hippocampal GFAP immunoreactivity became more severe when compared to WT mice from an age of 9 months (Sun et al., 2020). By contrast, in the brain lysate of PS19 mice, the

same group detected a biphasic activation pattern, with increased GFAP levels at 3 months, comparable to WT mice at 6 months, and then enhanced again between 9 - 12 months of age. It was postulated that GFAP increased as a consequence of, predominantly, (Ser^{202}/Thr^{205}) phospho-Tau accumulation in the brains of PS19 animals. Similar to the unaltered GFAP levels in 6 month-old PS19 mice in Sun et al (2020), the experiments demonstrated that GFAP pools (Figure 6.5B) were comparable in the brain homogenates of WT and PS19 animals. In light of the weak Tau pathology in the brains of PS19 mice (Figure 6.1A&B and Figure 6.2A&B), it is no surprise that there is no astrocyte inflammation. However, in contrast to all other western blots in chapter 6, it must be noted that the analysis of GFAP was mildly underpowered due to too low group sizes (50.91 % instead of the desired ≥ 80 % power; Table 6.1). As such, significant differences might have been missed.

Whilst RI-AG03-polyR or scrambled peptide injections dosed at 100 nmol/kg did not stimulate microgliosis (IBA-1; Figure 6.5A) or astrogliosis (GFAP; Figure 6.5B) *in vivo*, the lack of neuroinflammation in PS19 mice did not allow the evaluation of potential anti-inflammatory effects of the peptides. A positive effect of RI-AG03-polyR on inflammation is probable, however, due to the mutually aggravating link between Tau pathology and neuroinflammation that has also been observed in PS19 mice (Yoshiyama et al., 2007; Laurent et al., 2018). In addition, it was demonstrated that IBA1, but not GFAP, immunoreactivity and the production of various pro-inflammatory cytokines and chemokines were heightened in the hippocampal CA3 area, but unaltered across the brain, in ~7 month (+)-old PS19 mice compared to WT littermates (Di et al., 2021; Sun et al., 2020; Yoshiyama et al., 2007). Thus, there is poor CNS-wide, and more brain region-specific, inflammation in PS19 rodents.

Collectively, a future full-scale *in vivo* study would benefit from using older PS19 animals with more a severe CNS pathology in order to evaluate potential inflammation-suppressing effects of RI-AG03-polyR. Furthermore, immunohistochemistry using IBA1 and GFAP antibodies and hippocampal tissue may be employed. Immunoblot analysis of pro-inflammatory modulators in hippocampal lysate, such

as IL-1β or chemokine cyclooxygenease-2 (increased at 4 and 12 months (Yoshiyama et al., 2007)), or the activation of the transcription factor NF-κB that drives pro-inflammatory cytokine expression in AD (Jha et al., 2019), would also be suitable.

6.9. Conclusion

Despite a suggested two-fold increase in total Tau levels and the presence of Ser^{202}/Thr^{205}-phopshorylated Tau in the brains of 7.5-month-old PS19 mice, there was no statistical difference when compared to age-matched WT littermates. Similarly, the proportions of soluble Tau and (Ser^{202}/Thr^{205}) phospho-Tau, pre- (synaptophysin) and post-synaptic (PSD-95) markers, apoptosis (caspase 3), autophagy (Beclin-1, LC3 and p62) and glial inflammation (IBA1 and GFAP) were unaltered.

Similar to what was observed *in vitro*, a mild total Tau-increasing effect was observed in RI-AG03-polyR or scrambled peptide-injected PS19 mice. Interestingly, RI-AG03-polyR doubled the baseline PSD-95 levels in both WT and PS19 mice, suggesting that the peptide affects postsynaptic function *in vivo.* However, by an unknown mechanism, RI-AG03-polyR administration promoted pro-apoptotic caspase 3 activity in control and PS19 animals, whilst the scrambled peptide increased caspase 3-mediated apoptosis in PS19 mice. WT, but not PS19, mice treated with RI-AG03-polyR also showed two-fold-elevated p62 levels, but no changes in the macroautophagy-associated markers Beclin-1 or LC3-I/II. This may indicate that peptide-bound, endogenous mouse Tau is labelled by p62 for degradation, or that the proteasome is inhibited by RI-AG03-polyR, thus resulting in the accumulation of p62-tagged proteins. Whilst PS19 mice did not exhibit microgliosis and astrogliosis, the administration of RI-AG03-polyR and its scrambled variant did not stimulate neuroinflammation *in vivo*.

Collectively, the use of too young PS19 animals in this *in vivo* study prevented the detection of significant differences between mouse genotypes and treatment groups. In order to fully evaluate

the neuroprotective and potential adverse effects of RI-AG03-polyR, future studies older PS19 mice, different drug dosages and ideally higher animal numbers, focusing on the impact of RI-AG03-polyR on Tau pathology and neuroinflammation, neuronal death, proteasomal function and the intracellular removal of peptide-bound Tau.

7. Overall discussion

7.1. Comparison of RI-AG03 with other Tau aggregation inhibitor peptides

7.1.1. Recombinant Tau and in cells *in vitro*

Previous studies of our group showed that RI-AG03-polyR inhibits the heparin-induced aggregation of recombinant $Tau_{\Delta 1\text{-}250}$ at equimolar concentrations (IC_{50} = 7.83 µM) *in vitro* (Aggidis A. et al., 2021). The presence of RI-AG03-polyR also prevented $Tau_{\Delta 1\text{-}250}$ aggregation in response to adding a preformed Tau seed. Similar to RI-AG03-polyR, other peptide-based aggregation inhibitors that bind the pro-aggregatory ^{275}VQIINK^{280} (R2) or ^{306}VQIVYK^{311} (R3) sequence in Tau have been developed and tested by other researchers, as summarised in Table 7.1. The aggregation-inhibiting properties of these competitor peptides were tested using recombinant Tau or Tau fragments *in vitro*, both with and without heparin, and the reported IC_{50} values range between 1.1 µM - 182.8 µM. When ranked for their efficacy, the most potent Tau aggregation inhibitor peptide is W-MINK and the weakest KNT (Dammers et al., 2016; Malhis et al., 2021; Aillaud et al., 2022; Seidler et al., 2018). Although the peptide TLKIVW blocked VQIVYK, $Tau_{244\text{ - }394}$ (K12) and $Tau_{244 - 372}$ (K19) aggregation (Sievers et al., 2011), an IC_{50} value is not available. TLKIVW also failed to inhibit the heparin-induced aggregation of Tau RD (ΔK280) (Malhis et al., 2021). Compared to the IC_{50} of other reported Tau aggregation inhibitor peptides (Table 7.1), the aggregation-inhibiting effects of RI-AG03-polyR (7.83 µM) are similar. However, whilst we have not determined the IC_{50} of RI-AG03-polyR-conjugated liposomes, our group previously showed that RI-AG03-polyR-liposomes block $Tau_{\Delta 1\text{-}250}$ aggregation at a ~40-fold lower peptide concentration relative to using the unconjugated peptide (Aggidis A. et al., 2021). Thus, *in vitro*, RI-AG03-polyR-liposomes might be the most effective Tau aggregation inhibitor that is currently available.

Table 7.1: Overview of reported peptide-based Tau aggregation inhibitors. Rev = retro-inverted.

Name	Details	Results	References
APT (D-aptllrlhslga) KNT (D-kntpqhrklrls) TD28 (D-ttslqmrlyypp) TD28rev (D-ppyylrmqlstt)	Mirror image phage display-mediated identification of Tau (PHF6 / ^{306}VQIVYK^{311})-binding and proteolytically-resistant D-peptides	• VQIVYK and arachidonic acid-induced 2N4R Tau aggregation inhibited (1:1 and 1:10 ratio Tau:peptide). • The latter peptides were superior to TLKIVW by (Sievers et al., 2011) • IC_{50} of inhibiting K19 Tau aggregation: TD28 = 7.9 µM > TD28rev = 96.2 µM > APT 139.6 µM > KNT = 182.8 µM • Preferential peptide binding to Tau monomers, but also fibrils • FAM-labelled APT, KNT, TD28 & TD28rev internalised by N2a cells after 2 h and 4 day incubations. Localisation to membrane, cytosol and nuclei.	(Dammers et al., 2016)
MMD3 (dplkarhtsvwy) MMD3rev (ywvsthraklpd)	Mirror image phage display identification of PHF6* / ^{275}VQIINK^{280}-based D-peptides	• Aggregation of ^{275}VQIINK^{280}, but not ^{306}VQIVYK^{311}, peptides blocked (1:10 ^{275}VQIINK^{280}:peptide ratio). • Interaction of the peptides with ^{275}VQIINK^{280}, 2N4R Tau monomers and Tau fibrils confirmed • Heparin-induced PHF-formation of Tau RD (ΔK280) prevented by MMD3/MMD3rev. The peptides sequestered Tau RD (ΔK280) into oligomers/amorphous aggregates (3000 - 4000 nm diameter), leading to increased insoluble Tau levels in the pellet fraction. • Alexa 647-labelled MMD3/MMD3rev entered N2a cells following 2 days. • IC_{50} of inhibiting heparin-induced Tau RD (ΔK280) aggregation: W-MINK = 1.1 µM (Seidler et al., 2018) > MMD3 = 4.6 µM > MMD3rev = 5.2 µM > APT = 5.9 µM (Dammers et al., 2016) > TLKIVW (Sievers et al., 2011)	(Malhis et al., 2021)
D1 (D-lyiwvq) D1b (D-lyiwiwrt) D1d (D-lyiwiqkt)	Rosetta and structure-based design of (proteolytically-stable) D-peptide inhibitors of Aβ aggregation. Screened for the ability to bind the pro-aggregatory ^{16}KLVFFAE^{22} motif in Aβ. Peptides co-tested for their ability to prevent Tau aggregation.	• 1 h treatment of Aβ aggregates with D1, D1d and, especially, D1b, abolished the Tau cross-seeding ability of the Aβ oligomers in EYFP-Tau RD (P301S)-expressing HEK293 biosensor cells. • Heparin-mediated aggregation of 2N4R Tau inhibited by D1 (1:1 Tau:peptide), D1d (10:1) and, best, D1b (10:1) • 2N4R Tau pre-incubated with heparin and the peptides, then 250 nm added to Tau K18CY biosensor cells: IC_{50} of D1b to suppress cellular Tau seeding = 4.5 µM. Superior to D1 (from 50 µM) and D1d (from 75 µM). • D1b prevented seeding by ^{275}VQIINK^{280}- and/or ^{306}VQIVYK^{311}-containing, pre-aggregated Tau species in biosensor cells. Structural similarities between the pathologic Aβ and Tau cores were suggested. • Treatment of brain lysate of AD/PSP patients with D1b and, partially, D1 and D1d inhibited Tau seeding in biosensor cells.	(Griner et al., 2019)

ISAD1 (D-svfklsltdaas) ISAD1rev (D-saadtlslkfvs)	Development of a D-peptide Tau aggregation inhibitor, as identified using 2N4R Tau and phage display screening.	• Peptide-binding to 2N4R Tau monomers and fibrils. EC_{50}: ISAD1 = 2.2 µM & ISAD1rev = 2.7 µM • Interaction of ISAD1 and TLKIVW (Sievers et al., 2011), with the ^{306}VQIVYK^{311} motif in Tau. • Heparin-induced aggregation of 2N4R Tau or Tau RD (ΔK280) blocked by ISAD1. IC_{50} for 2N4R Tau/ Tau RD (ΔK280) were 2.91/2.90 µM (ISAD1) and 20.96/17.8 µM (ISAD1rev). • ISAD1 dose-dependently inhibited the heparin-mediated aggregation of mutant 2N4R Tau (ΔK280, P301L or A152T): ~25% (Tau ΔK280), ~80 % (Tau A152T) and ~45 % (Tau P301L) inhibition at equimolar concentrations. • Tau RD (ΔK280) formed aggregates of 30 - 90 nm in size in the presence of heparin. Co-incubation with ISAD1/ISAD1rev led to the generation of even larger Tau inclusions (2000 - 6000 nm) and higher amounts of insoluble, pelletable Tau. Peptide-formed Tau species were non-fibrillar, since ThT-negative. • Formation of 1000 - 8000 nm aggregates of mutant Tau (ΔK280, P301L or A152T) upon heparin and ISAD1, but not ISAD1rev, co-treatment. • Both FAM-labelled peptides were taken up by N2a cells, entering the cytosol (24 h incubation). • External pre-incubation of Tau RD (ΔK280) with ISAD1/ISAD1rev prevented Tau-induced loss of cell viability, membrane damage and ROS production in N2a cells. • Improved viability (MTT) and membrane leakage (LDH) in Dox-inducible, Tau RD (ΔK280)-expressing N2a cells following 24 h treatment with the peptides (from 100 µM).	(Aillaud et al., 2022)
p-NH (D-nitmnsrrrrnh)	Screening and identification of PHF6 (^{306}VQIVYK^{311})-interacting high affinity peptides via mirror phage image display.	• p-NH dose-dependently inhibited VQIVYK peptide fibrillisation (ThT assay): ~50 % inhibition at equimolar concentrations and ~70 % inhibition at 8-fold molar excess compared to VQIVYK. • The peptide prevented fibril formation (TEM) and could disassemble pre-formed VQIVYK fibrils at a 1:4 molar ratio (fibril:p-NH) • FAM-labelled p-NH was internalised, then exocytosed, by N2a cells (between 5 min - 48h). • Okadaic acid (PP1 and PP2A inhibitor)-induced Tau hyperphosphorylation at Thr^{181}, Ser^{202}, Thr^{231}, Ser^{396} and Ser^{404} in N2a cells was suppressed by 1 µM p-NH. • Modest inhibition of NFT formation by p-NH treatment in response to the transfection of N2a cells with EGFP-Tau (P301S) • FAM-labelled p-NH detectable in the mouse brain following intranasal delivery (from 30 min and until 24 h post administration). • 3 month-long nasal application of p-NH in Tau (P301S)-transgenic PS19 mice, starting at an age of 3 months, led to: modestly lowered NFTs levels, reduction in NFT-burdened hippocampal and cortical neurons (~43 - 44 %), decreased Thr^{231} and Ser^{396}-phosphorylated Tau in the cortex and improved performance in MWM and nest construction tests. No change in Tau kinases or phosphatases.	(Zhang et al., 2020)

TAT-7H (YGRKKRRQRRR-HHHHHHH)	Investigation of the Tau aggregation-inhibiting effects of (TAT)-7H. The latter peptide was originally designed to inhibit pathology-associated Ku70 and mutant huntingtin interactions in Huntington's disease.	• 7H dose-dependently blocked, but could not resolve, the aggregation and fibrillisation of R3 Tau peptides (amino acids 306 - 336). 7H:R3 molar ratios from 0.2:1 were effective. • Using the modified fragment TauF4Δ (amino acids 225 - 324), NMR revealed weak interactions of 7H with Tau residues 240-250 (N-terminal region of R1) and 280 (PHF* / ^{275}VQIINK^{280} motif in R2). • FITC-labelled TAT-7H translocated into the cytoplasm of HeLa cells after 1.5 and 6 h incubations. • Phosphorylation of Tau at Ser^{202}/Thr^{205} (AT8) decreased in Tau (P301S)-expressing, differentiated pan neurons following 14 day treatment with 5 µM or 50 µM TAT-7H. • 14 day incubation with 5 µM or 50 µM TAT-7H was non-toxic and did not adversely affect neurite length of human iPSCs.	(Kondo et al., 2021)
TLKIVW (D-tlkivw)	Computation (Rosetta software)-based design of structural D-amino acid Tau aggregation inhibitor peptides that bind the ^{306}VQIVYK^{311} segment of Tau.	• Co-incubation of VQIVYK peptides, K12 Tau (amino acids 244 - 394, without R2/^{275}VQIINK^{280} motif) or K19 Tau (amino acids 244 – 372, also excluding R2) with TLKIVW blocked K19 fibrillisation (TEM) and delayed Tau aggregation in a concentration-dependent manner for multiple days (ThT).	(Sievers et al., 2011)
Phase 1: MINK (DVQMINKKRK) WINK (DVQWINKKRK) Phase 2: W-MINK (DVWMINKKRK) M4W39 (DVWMINKKWK)	Design of various phase 1 and 2 Tau aggregation inhibitors informed by the crystal structure of VQIINK fibrils.	• 1:2 molar ratios of 2N4R Tau:peptide (MINK or WINK) approximately halved heparin-induced Tau aggregation. MINK was slightly more effective than WINK, but exhibited mild self-aggregation. • Seeding of Tau aggregation via heparin-assembled 2N4R Tau fibrils in 1N4R Tau (P301S)-YFP-expressing HEK293 biosensor cells was blocked by the external co-incubation of Tau/heparin mixtures with MINK (IC_{50} = 22.6 µM), WINK (IC_{50} = 28.9 µM), W-MINK (IC_{50} = 1.1 µM) or M4W39 (IC_{50} = 2.9 µM). TLKIVW (see Sievers et al. (2011) above) failed to inhibit Tau seeding, while combining TLKIVW with MINK gave IC_{50} = 52.2 µM.	(Seidler et al., 2018)

As previously demonstrated by our group (Aggidis A. et al., 2021) and further characterised by my work in chapter 5, polyR- or TAT-containing versions of free RI-AG03, unconjugated liposomes and peptide-conjugated liposomes were all internalised by SH-SY5Y and HEK293 cells. Compared to unconjugated liposomes, the surface conjugation of RI-AG03-polyR or RI-AG03-TAT to liposomes (non-significantly) increased liposome uptake by SH-SY5Y cells three-fold (Figure 5.2A). Also, only uptake of peptide-conjugated, but not unconjugated, BODIPY-liposomes by SH-SY5Y cells was significant (Figure 5.2A). This supports the concept that the surface conjugation of a CPP-containing peptide to a lipid nanoparticle results in greater cellular uptake, as previously reported by others (Shi et al., 2014; Ross et al., 2018). Interestingly, while other Tau aggregation inhibitor peptides were shown to be internalised by cultured cells, such as ISAD1 or ISAD1rev, not all of these peptides included a CPP (Table 7.1) (Dammers et al., 2016; Malhis et al., 2021; Aillaud et al., 2022; Zhang et al., 2020). The lack of a CPP potentially limits cellular uptake and, thus, the therapeutic effect of these peptides. For example, over 100 µM of the ^{306}VQIVYK^{311}-interacting peptides ISAD1 or ISAD1rev were necessary to promote the survival of Tau RD (ΔK280)-overexpressing N2a cells (Aillaud et al., 2022). By contrast, although in another Tauopathy cell model, both RI-AG03-polyR and RI-AG03-TAT were cytoprotective at a considerably lower peptide concentration of 10 nM in Tau RD (V337M/P301L)-EYFP-overexpressing Clone 9 HEK293 cells (Figure 4.5). Interestingly, RI-AG03-polyR exhibited better protective effects in Tauopathy cells despite an inferior IC_{50} for Tau aggregation *in vitro*; 7.83 µM for heparin-$Tau_{\Delta 1\text{-}250}$ mixtures (Aggidis A. et al., 2021)), as compared to ISAD1 (2.90 µM for heparin-aggregated 2N4R Tau and 2.91 µM for Tau RD (ΔK280) (Aillaud et al., 2022)). This suggests that the presence of a CPP in Tau aggregation inhibitor peptides, such as polyR or TAT in RI-AG03, can further promote peptide efficacy by improving peptide internalisation and, thus, the therapeutic interaction with pathologic, intracellular Tau.

The subcellular trafficking studies in chapter 5 demonstrate that both polyR- or TAT-containing versions of RI-AG03 display either fair or poor co-localisation with lysosomes, macropinosomes and early endosomes (Table 5.1, Figure 5.6 and Figure 5.7). On the other hand, peptide Tau aggregation

inhibitors by other research groups have been shown to localise to the membrane, cytoplasm and nucleus, whilst co-localisation with cell organelles was not investigated (Table 7.1) (Dammers et al., 2016; Malhis et al., 2021; Aillaud et al., 2022; Zhang et al., 2020). Tau-interacting peptides must not be entrapped in cell organelles or the nucleus in order to ensure access to cytosolic Tau following cellular internalisation (El-Sayed et al., 2009). As most of the peptides listed in Table 7.1 are proteolytically-resistant, retro-inverted D-peptides, similar to RI-AG03, lysosomal degradation may not be a prominent mechanism of peptide degradation. In this context, following the uptake of peptide-conjugated liposomes by SH-SY5Y cells, it was shown that RI-AG03-polyR detached from the initially conjugated liposome vehicle at the cell membrane (Figure 5.8), preventing subsequent entrapment of the peptide in cell organelles (section 5.6). Thus, conjugating RI-AG03 to liposomes might allow for the more selective delivery of the peptide into the cytoplasm to bind pathologic cytosolic Tau, which could be an advantage relative to non-conjugated peptides (Table 7.1).

A possible weakness of RI-AG03 is that the peptide does not dissociate already formed, recombinant Tau fibrils (Aggidis A. et al., 2021). I have also made this observation in Clone 9 cells because RI-AG03-polyR had no effect when the proportions of soluble Tau in these cells were low initially (Figure 4.1E). Moreover, at least in Clone 9 HEK293 cells, my results suggest that unconjugated or liposome-conjugated RI-AG03-polyR does not bind larger Tau inclusions (Figure 4.4B&C). Given that smaller Tau oligomers drive Tau propagation and toxicity, whereas mature NFTs are hypothesised to act as a sink for these more detrimental Tau species (de Calignon et al., 2009; de Calignon et al., 2010; Wischik et al., 2018; Kolarova et al., 2012), the inability of RI-AG03 to interact with large Tau fibrils is not necessarily problematic. On the other hand, various Tau aggregation-inhibiting peptides developed by other groups were shown to bind both monomeric and fibrillated Tau (Table 7.1) (Dammers et al., 2016; Malhis et al., 2021; Aillaud et al., 2022). Moreover, p-NH, which targets ^{306}VQIVYK^{311} similar to RI-AG03-polyR, was capable of disintegrating Tau inclusions consisting of VQIVYK peptides (Zhang et al., 2020). It is not clear why p-NH can interact with, and disassemble, Tau fibrils. Since RI-AG03-polyR and p-NH consist of D-amino acids and exhibit positive charge (~5.09

for p-NH and ~10.95 for RI-AG03-polyR at pH 7), the specific amino acid composition of p-NH might allow it to bind to and extract Tau monomers from pre-formed Tau fibrils. Unlike p-NH, my data suggests that, unlike Tau antibodies, vaccines or p-NH (Sandusky-Beltran and Sigurdsson, 2020; Zhang et al., 2020), RI-AG03 will presumably not be able to clear already formed NFTs in the brain (Aggidis A. et al., 2021). Instead, early treatment with RI-AG03-polyR will hopefully prevent, or halt ongoing, Tau propagation and deposition in the brain.

In previous studies our group showed that RI-AG03-polyR can prevent the oligomerisation and β sheet formation of recombinant $Tau_{\Delta 1\text{-}250}$ in response to a Tau seed (Aggidis A. et al., 2021). Several Tau aggregation inhibitor peptides developed by other groups have also been shown to block Tau seeding in cell models. For example, pre-incubation with ISAD1 or ISAD1rev interfered with the formation of Tau seeds and suppressed cell death and ROS production in N2a cells exposed to recombinant Tau RD (ΔK280) (Aillaud et al., 2022). Likewise, heparin-generated 2N4R Tau seeds were detoxified by the addition of MINK, WINK, W-MINK and M4W39, as investigated in biosensor cells (Seidler et al., 2018). Therefore, future experiments assessing the ability of RI-AG03-polyR or peptide-conjugated liposomes to prevent seed-induced Tau aggregation in suitable cell models would be of interest.

As discussed in section 4.6.4, our group noticed that RI-AG03 generated circular structures (GTO-like) in the presence of heparin and $Tau_{\Delta 1\text{-}250}$ (Aggidis A. et al., 2021). These peptide-Tau complexes (~36 nm in diameter) possibly accounted for the reduction in soluble Tau seen in Clone 9 HEK293 cells exposed to 100 nM RI-AG03-polyR (Figure 4.1). As additional evidence for peptide-induced Tau oligomer formation, treatment of Clone 9 cells with 5000 nM Cy5-RI-AG03-polyR elevated the mean number of Tau RD (P301L/V337M)-EYFP aggregates per cell from ~8 to ~42, seemingly with a (non-significant) decrease in aggregate size (-49 % at 2 h and -37 % at 16 h) (Table 4.2). Similar to RI-AG03-polyR, the ^{306}VQIVYK^{311}-binding ISAD1/ISAD1rev generated 2000 - 6000 nm aggregates with recombinant Tau RD (ΔK280) (Aillaud et al., 2022). Moreover, the ^{275}VQIINK^{280}-interacting peptides MMD3/MMD3rev formed non-fibrillar, β sheet-negative and amorphous Tau-peptide aggregates

(3000 - 4000 nm in diameter) and increased the proportion of insoluble recombinant Tau RD (ΔK280) (Malhis et al., 2021). These results suggest that Tau aggregation inhibitor peptides can prevent pathologic Tau aggregation by sequestering the protein into peptide-Tau species instead.

Curiously, treatment of Clone 9 cells with an aggregation-stimulating concentration of 100 nM RI-AG03-polyR decreased cell death (Figure 4.5). Similarly, Tau RD (ΔK280)-overexpressing N2a cells exposed to the Tau aggregation-inducing peptides ISAD1 and ISAD1rev showed increased cell survival (Aillaud et al., 2022). It is debatable whether the generation of peptide-Tau complexes is beneficial or detrimental, however. It has been proposed that the formation of specific non-phosphorylated, β sheet-negative and insoluble Tau species (GTOs), which resemble RI-AG03-polyR-Tau oligomers, are neuroprotective (Cowan et al., 2015; Cowan and Mudher, 2013; Aggidis A. et al., 2021). Studies of our group and others indicate that inclusions formed by the binding of aggregation inhibitor peptides to Tau cannot seed further Tau aggregation and propagation, which may protect cells from Tau toxicity (Aggidis A. et al., 2021; Aillaud et al., 2022; Malhis et al., 2021). Although peptide-binding to Tau can result in increased proportions of the insoluble form of the protein, such peptide-Tau complexes do not exhibit β sheet conformation and are thus not detected by ThT assays. By contrast, a recent study speculated that methylene blue (or its improved variant LMTX) failed in a phase 3 clinical trial for AD patients because the drug specifically inhibits NFT formation, but promotes Tau aggregation into GTOs (Soeda et al., 2019). GTOs, with a molecular weight of 1800 kDa and a diameter of 20 - 50 nm, have also been shown to accumulate in the prefrontal cortex in Braak stage I at an early stage during AD. Accumulation of these GTOs was postulated to precede clinical symptoms and initiate Tau deposition in the brain (Maeda et al., 2006; Maeda et al., 2007). As such, the peptide-induced generation of GTO-like structures, as in the case of RI-AG03-polyR (Aggidis A. et al., 2021), could also be harmful. Further studies are necessary to both confirm RI-AG03-polyR-induced Tau oligomer formation in neurons and whether this event is protective in neurons *in vivo*.

7.1.2. *In vivo*

My pilot *in vivo* study suggests that i.p. injections of RI-AG03-polyR on every other day for 44 days in total had a limited effect on total Tau, soluble Tau and Ser^{202}/Thr^{205}-phosphorylated Tau levels in PS19 mice (Figure 6.1 and Figure 6.2). The ^{306}VQIVYK^{311}-binding peptide p-NH has previously also been tested in PS19 mice (Zhang et al., 2020). It was confirmed that the intranasal application of p-NH, a route used to circumvent the BBB, successfully delivered the peptide into the brain. Furthermore, the 3 month-long intranasal peptide treatment of PS19 mice lowered cortical and hippocampal NFT burden, diminished Tau hyperphosphorylation and enhanced performance in hippocampus-dependent behavioural tests.

While p-NH improved the Tau pathology in PS19 mice (Zhang et al., 2020), an advantage of RI-AG03-polyR is that it contains the BBB-crossing CPP polyR, which allows peptide administration via injection (Pham et al., 2005; Gotanda et al., 2014). However, the initial *in vivo* pilot experiments with RI-AG03 suggest that the peptide potentially displays a few potential concerns:

(i) RI-AG03-polyR doubled p62 levels in the brains of WT mice (Figure 6.4). This could indicate that peptide-bound endogenous Tau is tagged by p62 for macroautophagy or proteasome-mediated removal (Gorantla and Chinnathambi, 2021). Alternatively, the proteasome might be inhibited by RI-AG03-polyR-Tau structures and/or the polyR sequence in the peptide (Gao et al., 2000; Gaczynska et al., 2003; Kloss et al., 2009; Anbanandam et al., 2008; Karpowicz et al., 2015), leading to the accumulation of non-degraded peptide-Tau-p62 species (Gorantla and Chinnathambi, 2021). Proteasomal inhibition by RI-AG03-polyR is also a plausible explanation for the peptide-induced increase in total Tau levels that was observed *in vitro* (Figure 3.5).

(ii) Elevated pro-apoptotic caspase 3 activation and a two-fold increase in baseline PSD-95 levels were detected in the brain lysate of RI-AG03-polyR-treated PS19 and/or WT mice (Figure 6.3). This possibly suggests that the peptide exerts detrimental effects in the postsynaptic space *in vivo* (section 6.7.2) (Xia et al., 2015; Ittner and Ittner, 2018; Louneva et al., 2008).

Future *in vivo* studies are necessary to investigate the effects of RI-AG03-polyR in a suitable Tauopathy animal model. Whilst we have demonstrated that the Aβ aggregation inhibitor peptide RI-OR2-TAT crossed the BBB *in vivo* (Gregori et al., 2017), and polyR peptides were also shown to do so (Futaki et al., 2001; Mitchell et al., 2000; Gotanda et al., 2014; Pham et al., 2005), biodistribution studies are also needed to confirm BBB-crossing of RI-AG03-polyR.

7.2. Final summary and conclusion

In summary, I demonstrated that the Tau aggregation inhibitor peptide RI-AG03 had beneficial effects in Tauopathy cell models. In Tau RD (P301L/V337M)-EYFP-overexpressing Clone 9 HEK293 cells, treatment with either 10 nM RI-AG03-polyR or RI-AG03-TAT and peptide-conjugated liposomes improved cell viability and decreased cell death, indicating that RI-AG03 may have therapeutic merit. Surprisingly, higher concentrations of RI-AG03-polyR (100 nM) lowered the proportions of soluble Tau in Clone 9 cells, yet still decreased cell death. Prolonged Cy5-RI-AG03-polyR also treatment increased the average number of Tau RD (P301L/V337M)-EYFP aggregates in Clone 9 cells, potentially with a concomitant reduction in aggregate size. In alignment with previous studies, this suggests that RI-AG03 might sequester intracellular pathologic Tau into non-toxic conformations. These peptide-Tau complexes are likely oligomeric because there was no co-localisation of RI-AG03-polyR with large Tau inclusions.

Interestingly, conjugating RI-AG03-polyR or RI-AG03-TAT to liposomes might enhance the Tau toxicity-reducing effects of RI-AG03, in part by enhancing cellular uptake mediated by alternative uptake mechanisms. My results suggest that RI-AG03-polyR-conjugated liposomes might be partially internalised by macropinocytosis, but that most of the uptake of RI-AG03-polyR- or RI-AG03-TAT-liposomes occurs through endocytosis-independent membrane translocation. After uptake, the peptide dissociates from its liposome vehicle, thus leading to the avoidance of peptide entrapment in cell organelles and potentially promoting cytosolic localisation. Therefore, lipid conjugation of RI-

AG03, containing either the polyR or TAT CPP, may promote the therapeutic potential of the peptide.

The *in vivo* pilot study showed that RI-AG03-polyR-injections doubled p62 levels in the brain, but autophagy markers were unaffected, suggesting that the peptide may interfere with proteasomal degradation. RI-AG03-polyR also elevated PSD-95 levels and caspase 3 activity in the CNS, possibly indicating a toxic effect *in vivo*. However, additional *in vivo* experiments are necessary to verify these effects, and an effective, yet safe, dose of RI-AG03-polyR that improves Tau pathology in PS19 mice must be determined. Although further research is necessary, these results raise hope that RI-AG03 may be used therapeutically in AD.

8. References

Abcam. (2020) *Ab228554 – Cell Counting Kit 8 (WST-8) Protocol* [Online]. Available at: https://www.abcam.com/cell-counting-kit-8-wst-8--cck8-ab228554.html. Accessed 02.10.22.

Abra, R. M. & Hunt, C. A. (1981) Liposome disposition in vivo. III. Dose and vesicle-size effects. *Biochim Biophys Acta,* 666(3)**,** 493-503.

Adamec, E., Vonsattel, J. P. & Nixon, R. A. (1999) DNA strand breaks in Alzheimer's disease. *Brain Res,* 849(1-2)**,** 67-77.

Aggidis, A. (2019) *The development of peptide-based inhibitors for Tau aggregation as a potential therapeutic for Alzheimer's disease.* [Online]. Doctoral Thesis, Biomedical and Life Sciences, Lancaster University, Lancaster. Available at: http://www.research.lancs.ac.uk/portal/en/publications/the-development-of-peptidebased-inhibitors-for-tau-aggregation-as-a-potential-therapeutic-for-alzheimers-disease(e9be4377-1da8-447d-8fad-9a00fadb574e).html.

Aggidis A., Chatterjee S., Townsend D., Fullwood N.J., Ortega E. R., Tarutani A., Hasegawa M., Lucas H., A., M. & D., A. (2021) Peptide-based inhibitors of Tau aggregation as a potential therapeutic for Alzheimer's disease and other Tauopathies. *bioRxiv, doi: https://doi.org/10.1101/2021.06.04.447069*.

Agholme, L., Lindstrom, T., Kagedal, K., Marcusson, J. & Hallbeck, M. (2010) An in vitro model for neuroscience: differentiation of SH-SY5Y cells into cells with morphological and biochemical characteristics of mature neurons. *J Alzheimers Dis,* 20(4)**,** 1069-82.

Aguilera, T. A., Olson, E. S., Timmers, M. M., Jiang, T. & Tsien, R. Y. (2009) Systemic in vivo distribution of activatable cell penetrating peptides is superior to that of cell penetrating peptides. *Integr Biol (Camb),* 1(5-6)**,** 371-81.

Aillaud, I. & Funke, S. A. (2022) Tau Aggregation Inhibiting Peptides as Potential Therapeutics for Alzheimer Disease. *Cell Mol Neurobiol*.

Aillaud, I., Kaniyappan, S., Chandupatla, R. R., Ramirez, L. M., Alkhashrom, S., Eichler, J., Horn, A. H. C., Zweckstetter, M., Mandelkow, E., Sticht, H. & Funke, S. A. (2022) A novel D-amino acid peptide with therapeutic potential (ISAD1) inhibits aggregation of neurotoxic disease-relevant mutant Tau and prevents Tau toxicity in vitro. *Alzheimers Res Ther,* 14(1)**,** 15.

Aizenstein, H. J., Nebes, R. D., Saxton, J. A., Price, J. C., Mathis, C. A., Tsopelas, N. D., Ziolko, S. K., James, J. A., Snitz, B. E., Houck, P. R., Bi, W., Cohen, A. D., Lopresti, B. J., Dekosky, S. T., Halligan, E. M. & Klunk, W. E. (2008) Frequent amyloid deposition without significant cognitive impairment among the elderly. *Arch Neurol,* 65(11)**,** 1509-17.

Akhtar, A. & Sah, S. P. (2020) Insulin signaling pathway and related molecules: Role in neurodegeneration and Alzheimer's disease. *Neurochem Int,* 135**,** 104707.

Akoglu, H. (2018) User's guide to correlation coefficients. *Turk J Emerg Med,* 18(3)**,** 91-93.

Akoury, E., Pickhardt, M., Gajda, M., Biernat, J., Mandelkow, E. & Zweckstetter, M. (2013) Mechanistic basis of phenothiazine-driven inhibition of Tau aggregation. *Angew Chem Int Ed Engl,* 52(12)**,** 3511-5.

Al-Hilaly, Y. K., Pollack, S. J., Rickard, J. E., Simpson, M., Raulin, A. C., Baddeley, T., Schellenberger, P., Storey, J. M. D., Harrington, C. R., Wischik, C. M. & Serpell, L. C. (2018) Cysteine-Independent

Inhibition of Alzheimer's Disease-like Paired Helical Filament Assembly by Leuco-Methylthioninium (LMT). *J Mol Biol,* 430(21)**,** 4119-4131.

Allolio, C., Magarkar, A., Jurkiewicz, P., Baxova, K., Javanainen, M., Mason, P. E., Sachl, R., Cebecauer, M., Hof, M., Horinek, D., Heinz, V., Rachel, R., Ziegler, C. M., Schrofel, A. & Jungwirth, P. (2018) Arginine-rich cell-penetrating peptides induce membrane multilamellarity and subsequently enter via formation of a fusion pore. *Proc Natl Acad Sci U S A,* 115(47)**,** 11923-11928.

Alonso, A. C., Grundke-Iqbal, I. & Iqbal, K. (1996) Alzheimer's disease hyperphosphorylated tau sequesters normal tau into tangles of filaments and disassembles microtubules. *Nat Med,* 2(7)**,** 783-7.

Alonso, A. C., Zaidi, T., Grundke-Iqbal, I. & Iqbal, K. (1994) Role of abnormally phosphorylated tau in the breakdown of microtubules in Alzheimer disease. *Proc Natl Acad Sci U S A,* 91(12)**,** 5562-6.

Alonso, A. D., Grundke-Iqbal, I., Barra, H. S. & Iqbal, K. (1997) Abnormal phosphorylation of tau and the mechanism of Alzheimer neurofibrillary degeneration: sequestration of microtubule-associated proteins 1 and 2 and the disassembly of microtubules by the abnormal tau. *Proc Natl Acad Sci U S A,* 94(1)**,** 298-303.

Alonso Adel, C., Li, B., Grundke-Iqbal, I. & Iqbal, K. (2006) Polymerization of hyperphosphorylated tau into filaments eliminates its inhibitory activity. *Proc Natl Acad Sci U S A,* 103(23)**,** 8864-9.

Alonso Adel, C., Mederlyova, A., Novak, M., Grundke-Iqbal, I. & Iqbal, K. (2004) Promotion of hyperphosphorylation by frontotemporal dementia tau mutations. *J Biol Chem,* 279(33)**,** 34873-81.

Alquezar, C., Arya, S. & Kao, A. W. (2020) Tau Post-translational Modifications: Dynamic Transformers of Tau Function, Degradation, and Aggregation. *Front Neurol,* 11**,** 595532.

Alzforum. *Research Models - Tau P301S (Line PS19)* [Online]. Available at: https://www.alzforum.org/research-models/tau-p301s-line-ps19. Accessed 18.07.22.

Alzforum. *Therapeutics* [Online]. Available at: https://www.alzforum.org/therapeutics/search?fda_statuses=&target_types%5B%5D=177&therapy_types=&conditions=&keywords-entry=&keywords=#results. Accessed 20.07.22.

Alzforum. *Therapeutics - LMTM* [Online]. Available at: https://www.alzforum.org/therapeutics/lmtm. Accessed 12.07.22

Alzforum. (2019) *Mutations* [Online]. Available at: https://www.alzforum.org/mutations. Accessed 04.07.2022.

Alzforum. (2021) *Field Loses David Allsop, First to Isolate Amyloid* [Online]. Available at: https://www.alzforum.org/news/community-news/field-loses-david-allsop-first-isolate-amyloid. Accessed 15.07.22.

Anbanandam, A., Albarado, D. C., Tirziu, D. C., Simons, M. & Veeraraghavan, S. (2008) Molecular basis for proline- and arginine-rich peptide inhibition of proteasome. *J Mol Biol,* 384(1)**,** 219-27.

Andorfer, C., Kress, Y., Espinoza, M., De Silva, R., Tucker, K. L., Barde, Y. A., Duff, K. & Davies, P. (2003) Hyperphosphorylation and aggregation of tau in mice expressing normal human tau isoforms. *J Neurochem,* 86(3)**,** 582-90.

Andreadis, A. (2005) Tau gene alternative splicing: expression patterns, regulation and modulation of function in normal brain and neurodegenerative diseases. *Biochim Biophys Acta,* 1739(2-3)**,** 91-103.

Andreadis, A. (2012) Tau splicing and the intricacies of dementia. *J Cell Physiol,* 227(3)**,** 1220-5.

Andreadis, A., Brown, W. M. & Kosik, K. S. (1992) Structure and novel exons of the human tau gene. *Biochemistry,* 31(43)**,** 10626-33.

Arakhamia, T., Lee, C. E., Carlomagno, Y., Duong, D. M., Kundinger, S. R., Wang, K., Williams, D., Deture, M., Dickson, D. W., Cook, C. N., Seyfried, N. T., Petrucelli, L. & Fitzpatrick, A. W. P. (2020) Posttranslational Modifications Mediate the Structural Diversity of Tauopathy Strains. *Cell,* 180(4)**,** 633-644 e12.

Arnsten, A. F. T., Datta, D., Del Tredici, K. & Braak, H. (2021) Hypothesis: Tau pathology is an initiating factor in sporadic Alzheimer's disease. *Alzheimers Dement,* 17(1)**,** 115-124.

Arrasate, M., Perez, M., Armas-Portela, R. & Avila, J. (1999) Polymerization of tau peptides into fibrillar structures. The effect of FTDP-17 mutations. *FEBS Lett,* 446(1)**,** 199-202.

Arriagada, P. V., Growdon, J. H., Hedley-Whyte, E. T. & Hyman, B. T. (1992) Neurofibrillary tangles but not senile plaques parallel duration and severity of Alzheimer's disease. *Neurology,* 42(3 Pt 1)**,** 631-9.

Asai, H., Ikezu, S., Tsunoda, S., Medalla, M., Luebke, J., Haydar, T., Wolozin, B., Butovsky, O., Kugler, S. & Ikezu, T. (2015) Depletion of microglia and inhibition of exosome synthesis halt tau propagation. *Nat Neurosci,* 18(11)**,** 1584-93.

Austen, B. M., Paleologou, K. E., Ali, S. A., Qureshi, M. M., Allsop, D. & El-Agnaf, O. M. (2008) Designing peptide inhibitors for oligomerization and toxicity of Alzheimer's beta-amyloid peptide. *Biochemistry,* 47(7)**,** 1984-92.

Avila, J., Lucas, J. J., Perez, M. & Hernandez, F. (2004) Role of tau protein in both physiological and pathological conditions. *Physiol Rev,* 84(2)**,** 361-84.

Baas, P. W. & Black, M. M. (1990) Individual microtubules in the axon consist of domains that differ in both composition and stability. *J Cell Biol,* 111(2)**,** 495-509.

Baas, P. W., Black, M. M. & Banker, G. A. (1989) Changes in microtubule polarity orientation during the development of hippocampal neurons in culture. *J Cell Biol,* 109(6 Pt 1)**,** 3085-94.

Baas, P. W., Deitch, J. S., Black, M. M. & Banker, G. A. (1988) Polarity orientation of microtubules in hippocampal neurons: uniformity in the axon and nonuniformity in the dendrite. *Proc Natl Acad Sci U S A,* 85(21)**,** 8335-9.

Baas, P. W., Rao, A. N., Matamoros, A. J. & Leo, L. (2016) Stability properties of neuronal microtubules. *Cytoskeleton (Hoboken),* 73(9)**,** 442-60.

Babu, J. R., Geetha, T. & Wooten, M. W. (2005) Sequestosome 1/p62 shuttles polyubiquitinated tau for proteasomal degradation. *J Neurochem,* 94(1)**,** 192-203.

Ballatore, C., Brunden, K. R., Huryn, D. M., Trojanowski, J. Q., Lee, V. M. & Smith, A. B., 3rd (2012) Microtubule stabilizing agents as potential treatment for Alzheimer's disease and related neurodegenerative tauopathies. *J Med Chem,* 55(21)**,** 8979-96.

Bancher, C., Jellinger, K., Lassmann, H., Fischer, P. & Leblhuber, F. (1996) Correlations between mental state and quantitative neuropathology in the Vienna Longitudinal Study on Dementia. *Eur Arch Psychiatry Clin Neurosci,* 246(3)**,** 137-46.

Bandyopadhyay, B., Li, G., Yin, H. & Kuret, J. (2007) Tau aggregation and toxicity in a cell culture model of tauopathy. *J Biol Chem,* 282(22)**,** 16454-64.

Bardag-Gorce, F., Francis, T., Nan, L., Li, J., He Lue, Y., French, B. A. & French, S. W. (2005) Modifications in P62 occur due to proteasome inhibition in alcoholic liver disease. *Life Sci,* 77(20)**,** 2594-602.

Barghorn, S., Zheng-Fischhofer, Q., Ackmann, M., Biernat, J., Von Bergen, M., Mandelkow, E. M. & Mandelkow, E. (2000) Structure, microtubule interactions, and paired helical filament aggregation by tau mutants of frontotemporal dementias. *Biochemistry,* 39(38)**,** 11714-21.

Barr, R. K., Verdile, G., Wijaya, L. K., Morici, M., Taddei, K., Gupta, V. B., Pedrini, S., Jin, L., Nicolazzo, J. A., Knock, E., Fraser, P. E. & Martins, R. N. (2016) Validation and Characterization of a Novel Peptide That Binds Monomeric and Aggregated beta-Amyloid and Inhibits the Formation of Neurotoxic Oligomers. *J Biol Chem,* 291(2)**,** 547-59.

Barron, M., Gartlon, J., Dawson, L. A., Atkinson, P. J. & Pardon, M. C. (2017) A state of delirium: Deciphering the effect of inflammation on tau pathology in Alzheimer's disease. *Exp Gerontol,* 94**,** 103-107.

Baum, L., Seger, R., Woodgett, J. R., Kawabata, S., Maruyama, K., Koyama, M., Silver, J. & Saitoh, T. (1995) Overexpressed tau protein in cultured cells is phosphorylated without formation of PHF: implication of phosphoprotein phosphatase involvement. *Brain Res Mol Brain Res,* 34(1)**,** 1-17.

Baumann, N. & Pham-Dinh, D. (2001) Biology of oligodendrocyte and myelin in the mammalian central nervous system. *Physiol Rev,* 81(2)**,** 871-927.

Beique, J. C. & Andrade, R. (2003) PSD-95 regulates synaptic transmission and plasticity in rat cerebral cortex. *J Physiol,* 546(Pt 3)**,** 859-67.

Bell, M., Bachmann, S., Klimek, J., Langerscheidt, F. & Zempel, H. (2021) Axonal TAU Sorting Requires the C-terminus of TAU but is Independent of ANKG and TRIM46 Enrichment at the AIS. *Neuroscience,* 461**,** 155-171.

Bell, M. & Zempel, H. (2022a) SH-SY5Y-derived neurons: a human neuronal model system for investigating TAU sorting and neuronal subtype-specific TAU vulnerability. *Rev Neurosci,* 33(1)**,** 1-15.

Bell, M. & Zempel, H. (2022b) A simple human cell model for TAU trafficking and tauopathy-related TAU pathology. *Neural Regen Res,* 17(4)**,** 770-772.

Benlimame, N., Le, P. U. & Nabi, I. R. (1998) Localization of autocrine motility factor receptor to caveolae and clathrin-independent internalization of its ligand to smooth endoplasmic reticulum. *Mol Biol Cell,* 9(7)**,** 1773-86.

Berger, Z., Roder, H., Hanna, A., Carlson, A., Rangachari, V., Yue, M., Wszolek, Z., Ashe, K., Knight, J., Dickson, D., Andorfer, C., Rosenberry, T. L., Lewis, J., Hutton, M. & Janus, C. (2007) Accumulation of pathological tau species and memory loss in a conditional model of tauopathy. *J Neurosci,* 27(14)**,** 3650-62.

Berriman, J., Serpell, L. C., Oberg, K. A., Fink, A. L., Goedert, M. & Crowther, R. A. (2003) Tau filaments from human brain and from in vitro assembly of recombinant protein show cross-beta structure. *Proc Natl Acad Sci U S A,* 100(15)**,** 9034-8.

Bhaskar, K., Yen, S. H. & Lee, G. (2005) Disease-related modifications in tau affect the interaction between Fyn and Tau. *J Biol Chem,* 280(42)**,** 35119-25.

Bhowmik, A., Khan, R. & Ghosh, M. K. (2015) Blood brain barrier: a challenge for effectual therapy of brain tumors. *Biomed Res Int,* 2015**,** 320941.

Biernat, J. & Mandelkow, E. M. (1999) The development of cell processes induced by tau protein requires phosphorylation of serine 262 and 356 in the repeat domain and is inhibited by phosphorylation in the proline-rich domains. *Mol Biol Cell,* 10(3)**,** 727-40.

Biernat, J., Wu, Y. Z., Timm, T., Zheng-Fischhofer, Q., Mandelkow, E., Meijer, L. & Mandelkow, E. M. (2002) Protein kinase MARK/PAR-1 is required for neurite outgrowth and establishment of neuronal polarity. *Mol Biol Cell,* 13(11)**,** 4013-28.

Bio-Rad. (2022) *RC DC Protein Assay Instruction Manual* [Online]. Available at: https://www.bio-rad.com/en-uk/sku/5000122-rc-dc-protein-assay-kit-ii?ID=5000122. Accessed 01.10.22.

Bjorkoy, G., Lamark, T., Brech, A., Outzen, H., Perander, M., Overvatn, A., Stenmark, H. & Johansen, T. (2005) p62/SQSTM1 forms protein aggregates degraded by autophagy and has a protective effect on huntingtin-induced cell death. *J Cell Biol,* 171(4)**,** 603-14.

Bjorkoy, G., Lamark, T., Pankiv, S., Overvatn, A., Brech, A. & Johansen, T. (2009) Monitoring autophagic degradation of p62/SQSTM1. *Methods Enzymol,* 452**,** 181-97.

Boban, M., Babic Leko, M., Miskic, T., Hof, P. R. & Simic, G. (2019) Human neuroblastoma SH-SY5Y cells treated with okadaic acid express phosphorylated high molecular weight tau-immunoreactive protein species. *J Neurosci Methods,* 319**,** 60-68.

Boyarko, B. & Hook, V. (2021) Human Tau Isoforms and Proteolysis for Production of Toxic Tau Fragments in Neurodegeneration. *Front Neurosci,* 15**,** 702788.

Braak, H. & Braak, E. (1991) Neuropathological stageing of Alzheimer-related changes. *Acta Neuropathol,* 82(4)**,** 239-59.

Breijyeh, Z. & Karaman, R. (2020) Comprehensive Review on Alzheimer's Disease: Causes and Treatment. *Molecules,* 25(24).

Brelstaff, J., Tolkovsky, A. M., Ghetti, B., Goedert, M. & Spillantini, M. G. (2018) Living Neurons with Tau Filaments Aberrantly Expose Phosphatidylserine and Are Phagocytosed by Microglia. *Cell Rep,* 24(8)**,** 1939-1948 e4.

Briuglia, M. L., Rotella, C., Mcfarlane, A. & Lamprou, D. A. (2015) Influence of cholesterol on liposome stability and on in vitro drug release. *Drug Deliv Transl Res,* 5(3)**,** 231-42.

Buee, L., Bussiere, T., Buee-Scherrer, V., Delacourte, A. & Hof, P. R. (2000) Tau protein isoforms, phosphorylation and role in neurodegenerative disorders. *Brain Res Brain Res Rev,* 33(1)**,** 95-130.

Busija, A. R., Patel, H. H. & Insel, P. A. (2017) Caveolins and cavins in the trafficking, maturation, and degradation of caveolae: implications for cell physiology. *Am J Physiol Cell Physiol,* 312(4)**,** C459-C477.

Butner, K. A. & Kirschner, M. W. (1991) Tau protein binds to microtubules through a flexible array of distributed weak sites. *J Cell Biol,* 115(3)**,** 717-30.

Cai, Z., Hussain, M. D. & Yan, L. J. (2014) Microglia, neuroinflammation, and beta-amyloid protein in Alzheimer's disease. *Int J Neurosci,* 124(5)**,** 307-21.

Cao, T. T., Mays, R. W. & Von Zastrow, M. (1998) Regulated endocytosis of G-protein-coupled receptors by a biochemically and functionally distinct subpopulation of clathrin-coated pits. *J Biol Chem,* 273(38)**,** 24592-602.

Carlomagno, Y., Chung, D. C., Yue, M., Castanedes-Casey, M., Madden, B. J., Dunmore, J., Tong, J., Deture, M., Dickson, D. W., Petrucelli, L. & Cook, C. (2017) An acetylation-phosphorylation

switch that regulates tau aggregation propensity and function. *J Biol Chem,* 292(37)**,** 15277-15286.

Carroll, T., Guha, S., Nehrke, K. & Johnson, G. V. W. (2021) Tau Post-Translational Modifications: Potentiators of Selective Vulnerability in Sporadic Alzheimer's Disease. *Biology (Basel),* 10(10).

Castillo-Carranza, D. L., Guerrero-Munoz, M. J., Sengupta, U., Hernandez, C., Barrett, A. D., Dineley, K. & Kayed, R. (2015) Tau immunotherapy modulates both pathological tau and upstream amyloid pathology in an Alzheimer's disease mouse model. *J Neurosci,* 35(12)**,** 4857-68.

Chandrasekaran, S., Mcguire, M. J. & King, M. R. (2014) Sweeping lymph node micrometastases off their feet: an engineered model to evaluate natural killer cell mediated therapeutic intervention of circulating tumor cells that disseminate to the lymph nodes. *Lab Chip,* 14(1)**,** 118-27.

Chen, J., Kanai, Y., Cowan, N. J. & Hirokawa, N. (1992) Projection domains of MAP2 and tau determine spacings between microtubules in dendrites and axons. *Nature,* 360(6405)**,** 674-7.

Chen, Q., Zhou, Z., Zhang, L., Xu, S., Chen, C. & Yu, Z. (2014) The cellular distribution and Ser262 phosphorylation of tau protein are regulated by BDNF in vitro. *PLoS One,* 9(3)**,** e91793.

Cheng, Y. & Bai, F. (2018) The Association of Tau With Mitochondrial Dysfunction in Alzheimer's Disease. *Front Neurosci,* 12**,** 163.

Chirita, C. N., Congdon, E. E., Yin, H. & Kuret, J. (2005) Triggers of full-length tau aggregation: a role for partially folded intermediates. *Biochemistry,* 44(15)**,** 5862-72.

Cho, E. C., Xie, J., Wurm, P. A. & Xia, Y. (2009) Understanding the role of surface charges in cellular adsorption versus internalization by selectively removing gold nanoparticles on the cell surface with a I2/KI etchant. *Nano Lett,* 9(3)**,** 1080-4.

Chun, W. & Johnson, G. V. (2007) Activation of glycogen synthase kinase 3beta promotes the intermolecular association of tau. The use of fluorescence resonance energy transfer microscopy. *J Biol Chem,* 282(32)**,** 23410-7.

Chun, W., Waldo, G. S. & Johnson, G. V. (2007) Split GFP complementation assay: a novel approach to quantitatively measure aggregation of tau in situ: effects of GSK3beta activation and caspase 3 cleavage. *J Neurochem,* 103(6)**,** 2529-39.

Clavaguera, F., Akatsu, H., Fraser, G., Crowther, R. A., Frank, S., Hench, J., Probst, A., Winkler, D. T., Reichwald, J., Staufenbiel, M., Ghetti, B., Goedert, M. & Tolnay, M. (2013) Brain homogenates from human tauopathies induce tau inclusions in mouse brain. *Proc Natl Acad Sci U S A,* 110(23)**,** 9535-40.

Clavaguera, F., Bolmont, T., Crowther, R. A., Abramowski, D., Frank, S., Probst, A., Fraser, G., Stalder, A. K., Beibel, M., Staufenbiel, M., Jucker, M., Goedert, M. & Tolnay, M. (2009) Transmission and spreading of tauopathy in transgenic mouse brain. *Nat Cell Biol,* 11(7)**,** 909-13.

Clift, D., So, C., Mcewan, W. A., James, L. C. & Schuh, M. (2018) Acute and rapid degradation of endogenous proteins by Trim-Away. *Nat Protoc,* 13(10)**,** 2149-2175.

Cohen, T. J., Friedmann, D., Hwang, A. W., Marmorstein, R. & Lee, V. M. (2013) The microtubule-associated tau protein has intrinsic acetyltransferase activity. *Nat Struct Mol Biol,* 20(6)**,** 756-62.

Cohen, T. J., Guo, J. L., Hurtado, D. E., Kwong, L. K., Mills, I. P., Trojanowski, J. Q. & Lee, V. M. (2011) The acetylation of tau inhibits its function and promotes pathological tau aggregation. *Nat Commun,* 2**,** 252.

Congdon, E. E. & Sigurdsson, E. M. (2018) Tau-targeting therapies for Alzheimer disease. *Nat Rev Neurol,* 14(7)**,** 399-415.

Congdon, E. E., Wu, J. W., Myeku, N., Figueroa, Y. H., Herman, M., Marinec, P. S., Gestwicki, J. E., Dickey, C. A., Yu, W. H. & Duff, K. E. (2012) Methylthioninium chloride (methylene blue) induces autophagy and attenuates tauopathy in vitro and in vivo. *Autophagy,* 8(4)**,** 609-22.

Cortes, N., Andrade, V., Guzman-Martinez, L., Estrella, M. & Maccioni, R. B. (2018) Neuroimmune Tau Mechanisms: Their Role in the Progression of Neuronal Degeneration. *Int J Mol Sci,* 19(4).

Counts, S. E., Alldred, M. J., Che, S., Ginsberg, S. D. & Mufson, E. J. (2014) Synaptic gene dysregulation within hippocampal CA1 pyramidal neurons in mild cognitive impairment. *Neuropharmacology,* 79**,** 172-9.

Cowan, C. M. & Mudher, A. (2013) Are tau aggregates toxic or protective in tauopathies? *Front Neurol,* 4**,** 114.

Cowan, C. M., Quraishe, S., Hands, S., Sealey, M., Mahajan, S., Allan, D. W. & Mudher, A. (2015) Rescue from tau-induced neuronal dysfunction produces insoluble tau oligomers. *Sci Rep,* 5**,** 17191.

Crowe, A., James, M. J., Lee, V. M., Smith, A. B., 3rd, Trojanowski, J. Q., Ballatore, C. & Brunden, K. R. (2013) Aminothienopyridazines and methylene blue affect Tau fibrillization via cysteine oxidation. *J Biol Chem,* 288(16)**,** 11024-37.

Crowther, R. A. (1991a) Straight and Paired Helical Filaments in Alzheimer-Disease Have a Common Structural Unit. *Proceedings of the National Academy of Sciences of the United States of America,* 88(6)**,** 2288-2292.

Crowther, R. A. (1991b) Straight and paired helical filaments in Alzheimer disease have a common structural unit. *Proc Natl Acad Sci U S A,* 88(6)**,** 2288-92.

Cruz, A., Verma, M. & Wolozin, B. (2019) The Pathophysiology of Tau and Stress Granules in Disease. *Adv Exp Med Biol,* 1184**,** 359-372.

Cuchillo-Ibanez, I., Seereeram, A., Byers, H. L., Leung, K. Y., Ward, M. A., Anderton, B. H. & Hanger, D. P. (2008) Phosphorylation of tau regulates its axonal transport by controlling its binding to kinesin. *FASEB J,* 22(9)**,** 3186-95.

Cuddy, L. K., Winick-Ng, W. & Rylett, R. J. (2014) Regulation of the high-affinity choline transporter activity and trafficking by its association with cholesterol-rich lipid rafts. *J Neurochem,* 128(5)**,** 725-40.

Curtis, E. M., Bahrami, A. H., Weikl, T. R. & Hall, C. K. (2015) Modeling nanoparticle wrapping or translocation in bilayer membranes. *Nanoscale,* 7(34)**,** 14505-14.

Dammers, C., Yolcu, D., Kukuk, L., Willbold, D., Pickhardt, M., Mandelkow, E., Horn, A. H., Sticht, H., Malhis, M. N., Will, N., Schuster, J. & Funke, S. A. (2016) Selection and Characterization of Tau Binding -Enantiomeric Peptides with Potential for Therapy of Alzheimer Disease. *PLoS One,* 11(12)**,** e0167432.

Daniel, J. A., Chau, N., Abdel-Hamid, M. K., Hu, L., Von Kleist, L., Whiting, A., Krishnan, S., Maamary, P., Joseph, S. R., Simpson, F., Haucke, V., Mccluskey, A. & Robinson, P. J. (2015)

Phenothiazine-derived antipsychotic drugs inhibit dynamin and clathrin-mediated endocytosis. *Traffic,* 16(6)**,** 635-54.

Dastpeyman, M., Sharifi, R., Amin, A., Karas, J. A., Cuic, B., Pan, Y., Nicolazzo, J. A., Turner, B. J. & Shabanpoor, F. (2021) Endosomal escape cell-penetrating peptides significantly enhance pharmacological effectiveness and CNS activity of systemically administered antisense oligonucleotides. *Int J Pharm,* 599**,** 120398.

Dayanandan, R., Van Slegtenhorst, M., Mack, T. G., Ko, L., Yen, S. H., Leroy, K., Brion, J. P., Anderton, B. H., Hutton, M. & Lovestone, S. (1999) Mutations in tau reduce its microtubule binding properties in intact cells and affect its phosphorylation. *FEBS Lett,* 446(2-3)**,** 228-32.

De Anda-Hernández, M. A., Lira-De León, K. I., Mena, R., Campos-Peña, V. & Meraz-Ríos, M. A. (2012) *Chapter 15: Tau and Amyloid-ß Conformational Change to ß-Sheet Structures as Effectors in the Development of Alzheimer's Disease*. [In: Contreras, C.M. (Ed) Neursoscience - Dealing with Frontiers], InTech, Rijeka; Croatia.

De Calignon, A., Fox, L. M., Pitstick, R., Carlson, G. A., Bacskai, B. J., Spires-Jones, T. L. & Hyman, B. T. (2010) Caspase activation precedes and leads to tangles. *Nature,* 464(7292)**,** 1201-4.

De Calignon, A., Spires-Jones, T. L., Pitstick, R., Carlson, G. A. & Hyman, B. T. (2009) Tangle-bearing neurons survive despite disruption of membrane integrity in a mouse model of tauopathy. *J Neuropathol Exp Neurol,* 68(7)**,** 757-61.

De La-Rocque, S., Moretto, E., Butnaru, I. & Schiavo, G. (2021) Knockin' on heaven's door: Molecular mechanisms of neuronal tau uptake. *J Neurochem,* 156(5)**,** 563-588.

Decker, J. M., Kruger, L., Sydow, A., Dennissen, F. J., Siskova, Z., Mandelkow, E. & Mandelkow, E. M. (2016) The Tau/A152T mutation, a risk factor for frontotemporal-spectrum disorders, leads to NR2B receptor-mediated excitotoxicity. *EMBO Rep,* 17(4)**,** 552-69.

Di, J., Siddique, I., Li, Z., Malki, G., Hornung, S., Dutta, S., Hurst, I., Ishaaya, E., Wang, A., Tu, S., Boghos, A., Ericsson, I., Klarner, F. G., Schrader, T. & Bitan, G. (2021) Correction to: The molecular tweezer CLR01 improves behavioral deficits and reduces tau pathology in P301S-tau transgenic mice. *Alzheimers Res Ther,* 13(1)**,** 88.

Diaz-Hernandez, M., Gomez-Ramos, A., Rubio, A., Gomez-Villafuertes, R., Naranjo, J. R., Miras-Portugal, M. T. & Avila, J. (2010) Tissue-nonspecific alkaline phosphatase promotes the neurotoxicity effect of extracellular tau. *J Biol Chem,* 285(42)**,** 32539-48.

Dixit, R., Ross, J. L., Goldman, Y. E. & Holzbaur, E. L. (2008) Differential regulation of dynein and kinesin motor proteins by tau. *Science,* 319(5866)**,** 1086-9.

Doherty, G. J. & Mcmahon, H. T. (2009) Mechanisms of endocytosis. *Annu Rev Biochem,* 78**,** 857-902.

Dorval, V. & Fraser, P. E. (2006) Small ubiquitin-like modifier (SUMO) modification of natively unfolded proteins tau and alpha-synuclein. *J Biol Chem,* 281(15)**,** 9919-24.

Dubey, M., Chaudhury, P., Kabiru, H. & Shea, T. B. (2008) Tau inhibits anterograde axonal transport and perturbs stability in growing axonal neurites in part by displacing kinesin cargo: neurofilaments attenuate tau-mediated neurite instability. *Cell Motil Cytoskeleton,* 65(2)**,** 89-99.

Dubois, B., Villain, N., Frisoni, G. B., Rabinovici, G. D., Sabbagh, M., Cappa, S., Bejanin, A., Bombois, S., Epelbaum, S., Teichmann, M., Habert, M. O., Nordberg, A., Blennow, K., Galasko, D., Stern, Y., Rowe, C. C., Salloway, S., Schneider, L. S., Cummings, J. L. & Feldman, H. H. (2021)

Clinical diagnosis of Alzheimer's disease: recommendations of the International Working Group. *Lancet Neurol,* 20(6)**,** 484-496.

Duchardt, F., Fotin-Mleczek, M., Schwarz, H., Fischer, R. & Brock, R. (2007) A comprehensive model for the cellular uptake of cationic cell-penetrating peptides. *Traffic,* 8(7)**,** 848-66.

Duncan, M. J., Shin, J. S. & Abraham, S. N. (2002) Microbial entry through caveolae: variations on a theme. *Cell Microbiol,* 4(12)**,** 783-91.

Dupont-Wallois, L., Sautiere, P. E., Cocquerelle, C., Bailleul, B., Delacourte, A. & Caillet-Boudin, M. L. (1995) Shift from fetal-type to Alzheimer-type phosphorylated Tau proteins in SKNSH-SY 5Y cells treated with okadaic acid. *FEBS Lett,* 357(2)**,** 197-201.

Dutta, D. & Donaldson, J. G. (2012) Search for inhibitors of endocytosis: Intended specificity and unintended consequences. *Cell Logist,* 2(4)**,** 203-208.

Duyckaerts, C., Bennecib, M., Grignon, Y., Uchihara, T., He, Y., Piette, F. & Hauw, J. J. (1997) Modeling the relation between neurofibrillary tangles and intellectual status. *Neurobiol Aging,* 18(3)**,** 267-73.

Ebneth, A., Godemann, R., Stamer, K., Illenberger, S., Trinczek, B. & Mandelkow, E. (1998) Overexpression of tau protein inhibits kinesin-dependent trafficking of vesicles, mitochondria, and endoplasmic reticulum: implications for Alzheimer's disease. *J Cell Biol,* 143(3)**,** 777-94.

Ehrlich, I., Klein, M., Rumpel, S. & Malinow, R. (2007) PSD-95 is required for activity-driven synapse stabilization. *Proc Natl Acad Sci U S A,* 104(10)**,** 4176-81.

El-Sayed, A., Futaki, S. & Harashima, H. (2009) Delivery of macromolecules using arginine-rich cell-penetrating peptides: ways to overcome endosomal entrapment. *AAPS J,* 11(1)**,** 13-22.

Espindola, S. L., Damianich, A., Alvarez, R. J., Sartor, M., Belforte, J. E., Ferrario, J. E., Gallo, J. M. & Avale, M. E. (2018) Modulation of Tau Isoforms Imbalance Precludes Tau Pathology and Cognitive Decline in a Mouse Model of Tauopathy. *Cell Rep,* 23(3)**,** 709-715.

Esteras, N. & Abramov, A. Y. (2020) Mitochondrial Calcium Deregulation in the Mechanism of Beta-Amyloid and Tau Pathology. *Cells,* 9(9).

Esteras, N., Kundel, F., Amodeo, G. F., Pavlov, E. V., Klenerman, D. & Abramov, A. Y. (2021) Insoluble tau aggregates induce neuronal death through modification of membrane ion conductance, activation of voltage-gated calcium channels and NADPH oxidase. *FEBS J,* 288(1)**,** 127-141.

Falcon, B., Cavallini, A., Angers, R., Glover, S., Murray, T. K., Barnham, L., Jackson, S., O'neill, M. J., Isaacs, A. M., Hutton, M. L., Szekeres, P. G., Goedert, M. & Bose, S. (2015) Conformation determines the seeding potencies of native and recombinant Tau aggregates. *J Biol Chem,* 290(2)**,** 1049-65.

Faul, F., Erdfelder, E., Lang, A. G. & Buchner, A. (2007) G*Power 3: a flexible statistical power analysis program for the social, behavioral, and biomedical sciences. *Behav Res Methods,* 39(2)**,** 175-91.

Ferreira, I. L., Bajouco, L. M., Mota, S. I., Auberson, Y. P., Oliveira, C. R. & Rego, A. C. (2012) Amyloid beta peptide 1-42 disturbs intracellular calcium homeostasis through activation of GluN2B-containing N-methyl-d-aspartate receptors in cortical cultures. *Cell Calcium,* 51(2)**,** 95-106.

Fillebeen, C., Descamps, L., Dehouck, M. P., Fenart, L., Benaissa, M., Spik, G., Cecchelli, R. & Pierce, A. (1999) Receptor-mediated transcytosis of lactoferrin through the blood-brain barrier. *J Biol Chem,* 274(11)**,** 7011-7.

Fischer, D., Mukrasch, M. D., Von Bergen, M., Klos-Witkowska, A., Biernat, J., Griesinger, C., Mandelkow, E. & Zweckstetter, M. (2007) Structural and microtubule binding properties of tau mutants of frontotemporal dementias. *Biochemistry,* 46(10)**,** 2574-82.

Fitzpatrick, A. W. P., Falcon, B., He, S., Murzin, A. G., Murshudov, G., Garringer, H. J., Crowther, R. A., Ghetti, B., Goedert, M. & Scheres, S. H. W. (2017) Cryo-EM structures of tau filaments from Alzheimer's disease. *Nature,* 547(7662)**,** 185-190.

Foroozandeh, P. & Aziz, A. A. (2018) Insight into Cellular Uptake and Intracellular Trafficking of Nanoparticles. *Nanoscale Res Lett,* 13(1)**,** 339.

Frost, B., Hemberg, M., Lewis, J. & Feany, M. B. (2014) Tau promotes neurodegeneration through global chromatin relaxation. *Nat Neurosci,* 17(3)**,** 357-66.

Frost, B., Jacks, R. L. & Diamond, M. I. (2009) Propagation of tau misfolding from the outside to the inside of a cell. *J Biol Chem,* 284(19)**,** 12845-52.

Funk, K. E., Thomas, S. N., Schafer, K. N., Cooper, G. L., Liao, Z., Clark, D. J., Yang, A. J. & Kuret, J. (2014) Lysine methylation is an endogenous post-translational modification of tau protein in human brain and a modulator of aggregation propensity. *Biochem J,* 462(1)**,** 77-88.

Futaki, S., Ohashi, W., Suzuki, T., Niwa, M., Tanaka, S., Ueda, K., Harashima, H. & Sugiura, Y. (2001) Stearylated arginine-rich peptides: a new class of transfection systems. *Bioconjug Chem,* 12(6)**,** 1005-11.

Gaczynska, M., Osmulski, P. A., Gao, Y., Post, M. J. & Simons, M. (2003) Proline- and arginine-rich peptides constitute a novel class of allosteric inhibitors of proteasome activity. *Biochemistry,* 42(29)**,** 8663-70.

Gaillard, P. J., Appeldoorn, C. C., Dorland, R., Van Kregten, J., Manca, F., Vugts, D. J., Windhorst, B., Van Dongen, G. A., De Vries, H. E., Maussang, D. & Van Tellingen, O. (2014) Pharmacokinetics, brain delivery, and efficacy in brain tumor-bearing mice of glutathione pegylated liposomal doxorubicin (2B3-101). *PLoS One,* 9(1)**,** e82331.

Gandy, S. (2005) The role of cerebral amyloid beta accumulation in common forms of Alzheimer disease. *J Clin Invest,* 115(5)**,** 1121-9.

Gandy, S. & Dekosky, S. T. (2013) Toward the treatment and prevention of Alzheimer's disease: rational strategies and recent progress. *Annu Rev Med,* 64**,** 367-83.

Ganguly, P., Do, T. D., Larini, L., Lapointe, N. E., Sercel, A. J., Shade, M. F., Feinstein, S. C., Bowers, M. T. & Shea, J. E. (2015) Tau assembly: the dominant role of PHF6 (VQIVYK) in microtubule binding region repeat R3. *J Phys Chem B,* 119(13)**,** 4582-93.

Gao, Y., Lecker, S., Post, M. J., Hietaranta, A. J., Li, J., Volk, R., Li, M., Sato, K., Saluja, A. K., Steer, M. L., Goldberg, A. L. & Simons, M. (2000) Inhibition of ubiquitin-proteasome pathway-mediated I kappa B alpha degradation by a naturally occurring antibacterial peptide. *J Clin Invest,* 106(3)**,** 439-48.

Garuti, R., Jones, C., Li, W. P., Michaely, P., Herz, J., Gerard, R. D., Cohen, J. C. & Hobbs, H. H. (2005) The modular adaptor protein autosomal recessive hypercholesterolemia (ARH) promotes low density lipoprotein receptor clustering into clathrin-coated pits. *J Biol Chem,* 280(49)**,** 40996-1004.

Gasparini, L., Terni, B. & Spillantini, M. G. (2007) Frontotemporal dementia with tau pathology. *Neurodegener Dis,* 4(2-3)**,** 236-53.

Geddes, J. W., Snowdon, D. A., Soultanian, N. S., Tekirian, T. L., Riley, K. P., Ashford, J. W., Davis, D. G. & Markesbery, W. R. (1996) Braak stages III-IV of Alzheimer-related neuropathology are associated with mild memory loss, stages V-VI are associated with dementia: Findings from the nun study. *J Neuropath Exp Neur,* 55(5)**,** 48.

Giannakopoulos, P., Herrmann, F. R., Bussiere, T., Bouras, C., Kovari, E., Perl, D. P., Morrison, J. H., Gold, G. & Hof, P. R. (2003) Tangle and neuron numbers, but not amyloid load, predict cognitive status in Alzheimer's disease. *Neurology,* 60(9)**,** 1495-500.

Gibson, T. J. & Murphy, R. M. (2005) Design of peptidyl compounds that affect beta-amyloid aggregation: importance of surface tension and context. *Biochemistry,* 44(24)**,** 8898-907.

Goedert, M. & Jakes, R. (2005) Mutations causing neurodegenerative tauopathies. *Biochim Biophys Acta,* 1739(2-3)**,** 240-50.

Goedert, M., Masuda-Suzukake, M. & Falcon, B. (2017) Like prions: the propagation of aggregated tau and alpha-synuclein in neurodegeneration. *Brain,* 140(2)**,** 266-278.

Goedert, M. & Spillantini, M. G. (2017) Propagation of Tau aggregates. *Mol Brain,* 10(1)**,** 18.

Goedert, M., Spillantini, M. G., Jakes, R., Rutherford, D. & Crowther, R. A. (1989) Multiple isoforms of human microtubule-associated protein tau: sequences and localization in neurofibrillary tangles of Alzheimer's disease. *Neuron,* 3(4)**,** 519-26.

Gomez-Isla, T., Hollister, R., West, H., Mui, S., Growdon, J. H., Petersen, R. C., Parisi, J. E. & Hyman, B. T. (1997) Neuronal loss correlates with but exceeds neurofibrillary tangles in Alzheimer's disease. *Ann Neurol,* 41(1)**,** 17-24.

Gómez-Ramos, A., Díaz-Hernández, M., Cuadros, R., Hernández, F. & Avila, J. (2006) Extracellular tau is toxic to neuronal cells. *FEBS Letters,* 580(20)**,** 4842-50.

Gong, C. X., Singh, T. J., Grundke-Iqbal, I. & Iqbal, K. (1993) Phosphoprotein phosphatase activities in Alzheimer disease brain. *J Neurochem,* 61(3)**,** 921-7.

Goode, B. L., Denis, P. E., Panda, D., Radeke, M. J., Miller, H. P., Wilson, L. & Feinstein, S. C. (1997) Functional interactions between the proline-rich and repeat regions of tau enhance microtubule binding and assembly. *Mol Biol Cell,* 8(2)**,** 353-65.

Goode, B. L. & Feinstein, S. C. (1994) Identification of a novel microtubule binding and assembly domain in the developmentally regulated inter-repeat region of tau. *J Cell Biol,* 124(5)**,** 769-82.

Gorantla, N. V. & Chinnathambi, S. (2018) Tau Protein Squired by Molecular Chaperones During Alzheimer's Disease. *J Mol Neurosci,* 66(3)**,** 356-368.

Gorantla, N. V. & Chinnathambi, S. (2021) Autophagic Pathways to Clear the Tau Aggregates in Alzheimer's Disease. *Cell Mol Neurobiol,* 41(6)**,** 1175-1181.

Gotanda, Y., Wei, F. Y., Harada, H., Ohta, K., Nakamura, K. I., Tomizawa, K. & Ushijima, K. (2014) Efficient transduction of 11 poly-arginine peptide in an ischemic lesion of mouse brain. *J Stroke Cerebrovasc Dis,* 23(8)**,** 2023-2030.

Goto, Y., Duthie, M. S., Kawazu, S., Inoue, N. & Carter, D. (2011) Biased cellular locations of tandem repeat antigens in African trypanosomes. *Biochem Biophys Res Commun,* 405(3)**,** 434-8.

Gregori, M., Taylor, M., Salvati, E., Re, F., Mancini, S., Balducci, C., Forloni, G., Zambelli, V., Sesana, S., Michael, M., Michail, C., Tinker-Mill, C., Kolosov, O., Sherer, M., Harris, S., Fullwood, N. J., Masserini, M. & Allsop, D. (2017) Retro-inverso peptide inhibitor nanoparticles as potent inhibitors of aggregation of the Alzheimer's Abeta peptide. *Nanomedicine,* 13(2)**,** 723-732.

Grimmer, S., Van Deurs, B. & Sandvig, K. (2002) Membrane ruffling and macropinocytosis in A431 cells require cholesterol. *J Cell Sci,* 115(Pt 14)**,** 2953-62.

Griner, S. L., Seidler, P., Bowler, J., Murray, K. A., Yang, T. P., Sahay, S., Sawaya, M. R., Cascio, D., Rodriguez, J. A., Philipp, S., Sosna, J., Glabe, C. G., Gonen, T. & Eisenberg, D. S. (2019) Structure-based inhibitors of amyloid beta core suggest a common interface with tau. *Elife,* 8.

Grober, E., Dickson, D., Sliwinski, M. J., Buschke, H., Katz, M., Crystal, H. & Lipton, R. B. (1999) Memory and mental status correlates of modified Braak staging. *Neurobiol Aging,* 20(6)**,** 573-9.

Grundke-Iqbal, I., Iqbal, K., Tung, Y. C., Quinlan, M., Wisniewski, H. M. & Binder, L. I. (1986) Abnormal phosphorylation of the microtubule-associated protein tau (tau) in Alzheimer cytoskeletal pathology. *Proc Natl Acad Sci U S A,* 83(13)**,** 4913-7.

Gu, J., Xu, W., Jin, N., Li, L., Zhou, Y., Chu, D., Gong, C. X., Iqbal, K. & Liu, F. (2020) Truncation of Tau selectively facilitates its pathological activities. *J Biol Chem,* 295(40)**,** 13812-13828.

Guerrero-Munoz, M. J., Gerson, J. & Castillo-Carranza, D. L. (2015) Tau Oligomers: The Toxic Player at Synapses in Alzheimer's Disease. *Front Cell Neurosci,* 9**,** 464.

Guillozet-Bongaarts, A. L., Garcia-Sierra, F., Reynolds, M. R., Horowitz, P. M., Fu, Y., Wang, T., Cahill, M. E., Bigio, E. H., Berry, R. W. & Binder, L. I. (2005) Tau truncation during neurofibrillary tangle evolution in Alzheimer's disease. *Neurobiol Aging,* 26(7)**,** 1015-22.

Guo, C., Jeong, H. H., Hsieh, Y. C., Klein, H. U., Bennett, D. A., De Jager, P. L., Liu, Z. & Shulman, J. M. (2018) Tau Activates Transposable Elements in Alzheimer's Disease. *Cell Rep,* 23(10)**,** 2874-2880.

Guo, J. L. & Lee, V. M. (2011) Seeding of normal Tau by pathological Tau conformers drives pathogenesis of Alzheimer-like tangles. *J Biol Chem,* 286(17)**,** 15317-31.

Gupta, A., Bisht, B. & Dey, C. S. (2011) Peripheral insulin-sensitizer drug metformin ameliorates neuronal insulin resistance and Alzheimer's-like changes. *Neuropharmacology,* 60(6)**,** 910-20.

Haigler, H. T., Mckanna, J. A. & Cohen, S. (1979) Rapid stimulation of pinocytosis in human carcinoma cells A-431 by epidermal growth factor. *J Cell Biol,* 83(1)**,** 82-90.

Hakeem, I. J., Hodges, N. J. & Michelangeli, F. (2020) Cytotoxicity of SH-SY5Y Neuroblastoma Cells to the Antipsychotic Drugs, Chlorpromazine and Trifluoperazine, is via a Ca2+-Mediated Apoptosis Process and Differentiation of These Cells with Retinoic Acid Makes Them More Resistant to Cell Death. *Clin Oncol Res*.

Hamilton, J. (2023) *An experimental Alzheimer's drug outperforms one just approved by the FDA (news report)* [Online]. Available at: https://www.npr.org/sections/health-shots/2023/07/17/1188075646/donanemab-experimental-alzheimers-drug-outperforms-lecanemab-leqembi [acessed 20.08.23].

Hampel, H., Hardy, J., Blennow, K., Chen, C., Perry, G., Kim, S. H., Villemagne, V. L., Aisen, P., Vendruscolo, M., Iwatsubo, T., Masters, C. L., Cho, M., Lannfelt, L., Cummings, J. L. & Vergallo, A. (2021) The Amyloid-beta Pathway in Alzheimer's Disease. *Mol Psychiatry,* 26(10)**,** 5481-5503.

Hanger, D. P., Anderton, B. H. & Noble, W. (2009) Tau phosphorylation: the therapeutic challenge for neurodegenerative disease. *Trends Mol Med,* 15(3)**,** 112-9.

Harashima, H. & Kiwada, H. (1996) Liposomal targeting and drug delivery: kinetic consideration. *Advanced Drug Delivery Reviews,* 19(3)**,** 425-444.

Hardy, J. & Allsop, D. (1991) Amyloid deposition as the central event in the aetiology of Alzheimer's disease. *Trends Pharmacol Sci,* 12(10)**,** 383-8.

Hardy, J. & Selkoe, D. J. (2002) The amyloid hypothesis of Alzheimer's disease: progress and problems on the road to therapeutics. *Science,* 297(5580)**,** 353-6.

Hardy, J. A. & Higgins, G. A. (1992) Alzheimer's disease: the amyloid cascade hypothesis. *Science,* 256(5054)**,** 184-5.

Harrington, C. R., Louwagie, J., Rossau, R., Vanmechelen, E., Perry, R. H., Perry, E. K., Xuereb, J. H., Roth, M. & Wischik, C. M. (1994) Influence of apolipoprotein E genotype on senile dementia of the Alzheimer and Lewy body types. Significance for etiological theories of Alzheimer's disease. *Am J Pathol,* 145(6)**,** 1472-84.

Harrington, C. R., Storey, J. M., Clunas, S., Harrington, K. A., Horsley, D., Ishaq, A., Kemp, S. J., Larch, C. P., Marshall, C., Nicoll, S. L., Rickard, J. E., Simpson, M., Sinclair, J. P., Storey, L. J. & Wischik, C. M. (2015) Cellular Models of Aggregation-dependent Template-directed Proteolysis to Characterize Tau Aggregation Inhibitors for Treatment of Alzheimer Disease. *J Biol Chem,* 290(17)**,** 10862-75.

Hayer, A., Stoeber, M., Ritz, D., Engel, S., Meyer, H. H. & Helenius, A. (2010) Caveolin-1 is ubiquitinated and targeted to intralumenal vesicles in endolysosomes for degradation. *J Cell Biol,* 191(3)**,** 615-29.

He, Z., Guo, J. L., Mcbride, J. D., Narasimhan, S., Kim, H., Changolkar, L., Zhang, B., Gathagan, R. J., Yue, C., Dengler, C., Stieber, A., Nitla, M., Coulter, D. A., Abel, T., Brunden, K. R., Trojanowski,

J. Q. & Lee, V. M. (2018) Amyloid-beta plaques enhance Alzheimer's brain tau-seeded pathologies by facilitating neuritic plaque tau aggregation. *Nat Med,* 24(1)**,** 29-38.

Helzner, E. P., Scarmeas, N., Cosentino, S., Tang, M. X., Schupf, N. & Stern, Y. (2008) Survival in Alzheimer disease: a multiethnic, population-based study of incident cases. *Neurology,* 71(19)**,** 1489-95.

Henry, A. G., Hislop, J. N., Grove, J., Thorn, K., Marsh, M. & Von Zastrow, M. (2012) Regulation of endocytic clathrin dynamics by cargo ubiquitination. *Dev Cell,* 23(3)**,** 519-32.

Hernandez, F., Merchan-Rubira, J., Valles-Saiz, L., Rodriguez-Matellan, A. & Avila, J. (2020) Differences Between Human and Murine Tau at the N-terminal End. *Front Aging Neurosci,* 12**,** 11.

Higuchi, M., Zhang, B., Forman, M. S., Yoshiyama, Y., Trojanowski, J. Q. & Lee, V. M. (2005) Axonal degeneration induced by targeted expression of mutant human tau in oligodendrocytes of transgenic mice that model glial tauopathies. *J Neurosci,* 25(41)**,** 9434-43.

Hirokawa, N., Niwa, S. & Tanaka, Y. (2010) Molecular motors in neurons: transport mechanisms and roles in brain function, development, and disease. *Neuron,* 68(4)**,** 610-38.

Holmes, B. B., Devos, S. L., Kfoury, N., Li, M., Jacks, R., Yanamandra, K., Ouidja, M. O., Brodsky, F. M., Marasa, J., Bagchi, D. P., Kotzbauer, P. T., Miller, T. M., Papy-Garcia, D. & Diamond, M. I. (2013) Heparan sulfate proteoglycans mediate internalization and propagation of specific proteopathic seeds. *Proc Natl Acad Sci U S A,* 110(33)**,** E3138-47.

Holscher, C. (2019) Insulin Signaling Impairment in the Brain as a Risk Factor in Alzheimer's Disease. *Front Aging Neurosci,* 11**,** 88.

Hong, M. & Lee, V. M. (1997) Insulin and insulin-like growth factor-1 regulate tau phosphorylation in cultured human neurons. *J Biol Chem,* 272(31)**,** 19547-53.

Hooper, C., Killick, R. & Lovestone, S. (2008) The GSK3 hypothesis of Alzheimer's disease. *J Neurochem,* 104(6)**,** 1433-9.

Horn, M., Pavlik, M., Doleckova, L., Baudys, M. & Mares, M. (2000) Arginine-based structures are specific inhibitors of cathepsin C. Application of peptide combinatorial libraries. *Eur J Biochem,* 267(11)**,** 3330-6.

Hu, Y., Gaillard, P. J., De Lange, E. C. M. & Hammarlund-Udenaes, M. (2019) Targeted brain delivery of methotrexate by glutathione PEGylated liposomes: How can the formulation make a difference? *Eur J Pharm Biopharm,* 139**,** 197-204.

Hu, Y., Rip, J., Gaillard, P. J., De Lange, E. C. M. & Hammarlund-Udenaes, M. (2017) The Impact of Liposomal Formulations on the Release and Brain Delivery of Methotrexate: An In Vivo Microdialysis Study. *J Pharm Sci,* 106(9)**,** 2606-2613.

Huang, L. K., Chao, S. P. & Hu, C. J. (2020) Clinical trials of new drugs for Alzheimer disease. *J Biomed Sci,* 27(1)**,** 18.

Huseby, C. J., Hoffman, C. N., Cooper, G. L., Cocuron, J. C., Alonso, A. P., Thomas, S. N., Yang, A. J. & Kuret, J. (2019) Quantification of Tau Protein Lysine Methylation in Aging and Alzheimer's Disease. *J Alzheimers Dis,* 71(3)**,** 979-991.

Iba, M., Guo, J. L., Mcbride, J. D., Zhang, B., Trojanowski, J. Q. & Lee, V. M. (2013) Synthetic tau fibrils mediate transmission of neurofibrillary tangles in a transgenic mouse model of Alzheimer's-like tauopathy. *J Neurosci,* 33(3)**,** 1024-37.

Ingelson, M., Vanmechelen, E. & Lannfelt, L. (1996) Microtubule-associated protein tau in human fibroblasts with the Swedish Alzheimer mutation. *Neurosci Lett,* 220(1)**,** 9-12.

Inoue, K., Rispoli, J., Kaphzan, H., Klann, E., Chen, E. I., Kim, J., Komatsu, M. & Abeliovich, A. (2012) Macroautophagy deficiency mediates age-dependent neurodegeneration through a phospho-tau pathway. *Mol Neurodegener,* 7**,** 48.

Iqbal, K., Alonso Adel, C. & Grundke-Iqbal, I. (2008) Cytosolic abnormally hyperphosphorylated tau but not paired helical filaments sequester normal MAPs and inhibit microtubule assembly. *J Alzheimers Dis,* 14(4)**,** 365-70.

Iqbal, K. & Grundke-Iqbal, I. (2010) Alzheimer's disease, a multifactorial disorder seeking multitherapies. *Alzheimers Dement,* 6(5)**,** 420-4.

Iqbal, K., Grundke-Iqbal, I., Smith, A. J., George, L., Tung, Y. C. & Zaidi, T. (1989) Identification and localization of a tau peptide to paired helical filaments of Alzheimer disease. *Proc Natl Acad Sci U S A,* 86(14)**,** 5646-50.

Irwin, D. J., Cohen, T. J., Grossman, M., Arnold, S. E., Xie, S. X., Lee, V. M. & Trojanowski, J. Q. (2012) Acetylated tau, a novel pathological signature in Alzheimer's disease and other tauopathies. *Brain,* 135(Pt 3)**,** 807-18.

Ittner, A. & Ittner, L. M. (2018) Dendritic Tau in Alzheimer's Disease. *Neuron,* 99(1)**,** 13-27.

Ittner, L. M., Ke, Y. D., Delerue, F., Bi, M., Gladbach, A., Van Eersel, J., Wolfing, H., Chieng, B. C., Christie, M. J., Napier, I. A., Eckert, A., Staufenbiel, M., Hardeman, E. & Gotz, J. (2010) Dendritic function of tau mediates amyloid-beta toxicity in Alzheimer's disease mouse models. *Cell,* 142(3)**,** 387-97.

Ittner, L. M., Ke, Y. D. & Gotz, J. (2009) Phosphorylated Tau interacts with c-Jun N-terminal kinase-interacting protein 1 (JIP1) in Alzheimer disease. *J Biol Chem,* 284(31)**,** 20909-16.

Ivanov, A. I. (2008) Pharmacological inhibition of endocytic pathways: is it specific enough to be useful? *Methods Mol Biol,* 440**,** 15-33.

Jabr-Milane, L. S., Van Vlerken, L. E., Yadav, S. & Amiji, M. M. (2008) Multi-functional nanocarriers to overcome tumor drug resistance. *Cancer Treat Rev,* 34(7)**,** 592-602.

Jaeger, P. A., Pickford, F., Sun, C. H., Lucin, K. M., Masliah, E. & Wyss-Coray, T. (2010) Regulation of amyloid precursor protein processing by the Beclin 1 complex. *PLoS One,* 5(6)**,** e11102.

Jankowsky, J. L. & Zheng, H. (2017) Practical considerations for choosing a mouse model of Alzheimer's disease. *Mol Neurodegener,* 12(1)**,** 89.

Janning, D., Igaev, M., Sundermann, F., Bruhmann, J., Beutel, O., Heinisch, J. J., Bakota, L., Piehler, J., Junge, W. & Brandt, R. (2014) Single-molecule tracking of tau reveals fast kiss-and-hop interaction with microtubules in living neurons. *Mol Biol Cell,* 25(22)**,** 3541-51.

Jantrapirom, S., Nimlamool, W., Chattipakorn, N., Chattipakorn, S., Temviriyanukul, P., Inthachat, W., Govitrapong, P. & Potikanond, S. (2020) Liraglutide Suppresses Tau Hyperphosphorylation, Amyloid Beta Accumulation through Regulating Neuronal Insulin Signaling and BACE-1 Activity. *Int J Mol Sci,* 21(5).

Jeganathan, S., Von Bergen, M., Brutlach, H., Steinhoff, H. J. & Mandelkow, E. (2006) Global hairpin folding of tau in solution. *Biochemistry,* 45(7)**,** 2283-93.

Jha, N. K., Jha, S. K., Kar, R., Nand, P., Swati, K. & Goswami, V. K. (2019) Nuclear factor-kappa beta as a therapeutic target for Alzheimer's disease. *J Neurochem,* 150(2)**,** 113-137.

Juhairiyah, F. & De Lange, E. C. M. (2021) Understanding Drug Delivery to the Brain Using Liposome-Based Strategies: Studies that Provide Mechanistic Insights Are Essential. *AAPS J,* 23(6)**,** 114.

Juliano, R., Alam, M. R., Dixit, V. & Kang, H. (2008) Mechanisms and strategies for effective delivery of antisense and siRNA oligonucleotides. *Nucleic Acids Res,* 36(12)**,** 4158-71.

Jun, S. R., Wassenaar, T. M., Wanchai, V., Patumcharoenpol, P., Nookaew, I. & Ussery, D. W. (2017) Suggested mechanisms for Zika virus causing microcephaly: what do the genomes tell us? *BMC Bioinformatics,* 18(Suppl 14)**,** 471.

Kadar, A., Wittmann, G., Liposits, Z. & Fekete, C. (2009) Improved method for combination of immunocytochemistry and Nissl staining. *J Neurosci Methods,* 184(1)**,** 115-8.

Kadavath, H., Hofele, R. V., Biernat, J., Kumar, S., Tepper, K., Urlaub, H., Mandelkow, E. & Zweckstetter, M. (2015) Tau stabilizes microtubules by binding at the interface between tubulin heterodimers. *Proc Natl Acad Sci U S A,* 112(24)**,** 7501-6.

Kahana, M., Weizman, A., Gabay, M., Loboda, Y., Segal-Gavish, H., Gavish, A., Barhum, Y., Offen, D., Finberg, J., Allon, N. & Gavish, M. (2021) Liposome-based targeting of dopamine to the brain: a novel approach for the treatment of Parkinson's disease. *Mol Psychiatry,* 26(6)**,** 2626-2632.

Kametani, F. & Hasegawa, M. (2018) Reconsideration of Amyloid Hypothesis and Tau Hypothesis in Alzheimer's Disease. *Front Neurosci,* 12**,** 25.

Kanaan, N. M., Morfini, G. A., Lapointe, N. E., Pigino, G. F., Patterson, K. R., Song, Y., Andreadis, A., Fu, Y., Brady, S. T. & Binder, L. I. (2011) Pathogenic forms of tau inhibit kinesin-dependent axonal transport through a mechanism involving activation of axonal phosphotransferases. *J Neurosci,* 31(27)**,** 9858-68.

Karch, C. M., Jeng, A. T. & Goate, A. M. (2012) Extracellular Tau levels are influenced by variability in Tau that is associated with tauopathies. *J Biol Chem,* 287(51)**,** 42751-62.

Karpowicz, P., Osmulski, P. A., Witkowska, J., Sikorska, E., Gizynska, M., Belczyk-Ciesielska, A., Gaczynska, M. E. & Jankowska, E. (2015) Interplay between Structure and Charge as a Key to Allosteric Modulation of Human 20S Proteasome by the Basic Fragment of HIV-1 Tat Protein. *PLoS One,* 10(11)**,** e0143038.

Keck, S., Nitsch, R., Grune, T. & Ullrich, O. (2003) Proteasome inhibition by paired helical filament-tau in brains of patients with Alzheimer's disease. *J Neurochem,* 85(1)**,** 115-22.

Kfoury, N., Holmes, B. B., Jiang, H., Holtzman, D. M. & Diamond, M. I. (2012) Trans-cellular propagation of Tau aggregation by fibrillar species. *J Biol Chem,* 287(23)**,** 19440-51.

Khan, I. U., Khan, R. U., Asif, H., Alamgeer, Khalid, S. H., Asghar, S., Saleem, M., Shah, K. U., Shah, S. U., Rizvi, S. a. A. & Shahzad, Y. (2017) Co-delivery strategies to overcome multidrug resistance in ovarian cancer. *Int J Pharm,* 533(1)**,** 111-124.

Khatoon, S., Grundke-Iqbal, I. & Iqbal, K. (1992) Brain levels of microtubule-associated protein tau are elevated in Alzheimer's disease: a radioimmuno-slot-blot assay for nanograms of the protein. *J Neurochem,* 59(2)**,** 750-3.

Khatoon, S., Grundke-Iqbal, I. & Iqbal, K. (1994) Levels of normal and abnormally phosphorylated tau in different cellular and regional compartments of Alzheimer disease and control brains. *FEBS Lett,* 351(1)**,** 80-4.

Khlistunova, I., Biernat, J., Wang, Y., Pickhardt, M., Von Bergen, M., Gazova, Z., Mandelkow, E. & Mandelkow, E. M. (2006) Inducible expression of Tau repeat domain in cell models of

tauopathy: aggregation is toxic to cells but can be reversed by inhibitor drugs. *J Biol Chem,* 281(2)**,** 1205-14.

Khurana, V., Merlo, P., Duboff, B., Fulga, T. A., Sharp, K. A., Campbell, S. D., Gotz, J. & Feany, M. B. (2012) A neuroprotective role for the DNA damage checkpoint in tauopathy. *Aging Cell,* 11(2)**,** 360-2.

Kilk, K., Mahlapuu, R., Soomets, U. & Langel, U. (2009) Analysis of in vitro toxicity of five cell-penetrating peptides by metabolic profiling. *Toxicology,* 265(3)**,** 87-95.

Kim, H. K., Davaa, E., Myung, C. S. & Park, J. S. (2010) Enhanced siRNA delivery using cationic liposomes with new polyarginine-conjugated PEG-lipid. *Int J Pharm,* 392(1-2)**,** 141-7.

Kim, J. A., Casalini, T., Brambilla, D. & Leroux, J. C. (2016) Presumed LRP1-targeting transport peptide delivers beta-secretase inhibitor to neurons in vitro with limited efficiency. *Sci Rep,* 6**,** 34297.

Kim, Y., Hwang, O. & Kim, D. J. (2012) *Pathology of neurodegenerative diseases*. [In: D.A. Gonzalez-Quevedo (Ed.) Brain damage - bridging between basic research and clinics], InTech.

Kizuka, Y., Kitazume, S. & Taniguchi, N. (2017) N-glycan and Alzheimer's disease. *Biochim Biophys Acta Gen Subj,* 1861(10)**,** 2447-2454.

Kloss, A., Henklein, P., Siele, D., Schmolke, M., Apcher, S., Kuehn, L., Sheppard, P. W. & Dahlmann, B. (2009) The cell-penetrating peptide octa-arginine is a potent inhibitor of proteasome activities. *Eur J Pharm Biopharm,* 72(1)**,** 219-25.

Ko, L. W., Ko, E. C., Nacharaju, P., Liu, W. K., Chang, E., Kenessey, A. & Yen, S. H. (1999) An immunochemical study on tau glycation in paired helical filaments. *Brain Res,* 830(2)**,** 301-13.

Kolarova, M., Garcia-Sierra, F., Bartos, A., Ricny, J. & Ripova, D. (2012) Structure and pathology of tau protein in Alzheimer disease. *Int J Alzheimers Dis,* 2012**,** 731526.

Kolata, G. (1985) Down syndrome--Alzheimer's linked. *Science,* 230(4730)**,** 1152-3.

Kondo, K., Ikura, T., Tanaka, H., Fujita, K., Takayama, S., Yoshioka, Y., Tagawa, K., Homma, H., Liu, S., Kawasaki, R., Huang, Y., Ito, N., Tate, S. I. & Okazawa, H. (2021) Hepta-Histidine Inhibits Tau Aggregation. *ACS Chem Neurosci,* 12(16)**,** 3015-3027.

Kopeikina, K. J., Hyman, B. T. & Spires-Jones, T. L. (2012) Soluble forms of tau are toxic in Alzheimer's disease. *Transl Neurosci,* 3(3)**,** 223-233.

Kopke, E., Tung, Y. C., Shaikh, S., Alonso, A. C., Iqbal, K. & Grundke-Iqbal, I. (1993) Microtubule-associated protein tau. Abnormal phosphorylation of a non-paired helical filament pool in Alzheimer disease. *J Biol Chem,* 268(32)**,** 24374-84.

Koren, S. A., Galvis-Escobar, S. & Abisambra, J. F. (2020) Tau-mediated dysregulation of RNA: Evidence for a common molecular mechanism of toxicity in frontotemporal dementia and other tauopathies. *Neurobiol Dis,* 141**,** 104939.

Kosik, K. S., Orecchio, L. D., Bakalis, S. & Neve, R. L. (1989) Developmentally regulated expression of specific tau sequences. *Neuron,* 2(4)**,** 1389-97.

Kovac, A., Zilka, N., Kazmerova, Z., Cente, M., Zilkova, M. & Novak, M. (2011) Misfolded truncated protein tau induces innate immune response via MAPK pathway. *J Immunol,* 187(5)**,** 2732-9.

Ksiezak-Reding, H., Farooq, M., Yang, L. S., Dickson, D. W. & Lopresti, P. (2003) Tau protein expression in adult bovine oligodendrocytes: functional and pathological significance. *Neurochem Res,* 28(9)**,** 1385-92.

Kuusisto, E., Salminen, A. & Alafuzoff, I. (2001a) Ubiquitin-binding protein p62 is present in neuronal and glial inclusions in human tauopathies and synucleinopathies. *Neuroreport,* 12(10)**,** 2085-90.

Kuusisto, E., Salminen, A. & Alafuzoff, I. (2002) Early accumulation of p62 in neurofibrillary tangles in Alzheimer's disease: possible role in tangle formation. *Neuropathol Appl Neurobiol,* 28(3)**,** 228-37.

Kuusisto, E., Suuronen, T. & Salminen, A. (2001b) Ubiquitin-binding protein p62 expression is induced during apoptosis and proteasomal inhibition in neuronal cells. *Biochem Biophys Res Commun,* 280(1)**,** 223-8.

Lajoie, P. & Nabi, I. R. (2010) Lipid rafts, caveolae, and their endocytosis. *Int Rev Cell Mol Biol,* 282**,** 135-63.

Lamaze, C., Dujeancourt, A., Baba, T., Lo, C. G., Benmerah, A. & Dautry-Varsat, A. (2001) Interleukin 2 receptors and detergent-resistant membrane domains define a clathrin-independent endocytic pathway. *Mol Cell,* 7(3)**,** 661-71.

Lapointe, N. E., Morfini, G., Pigino, G., Gaisina, I. N., Kozikowski, A. P., Binder, L. I. & Brady, S. T. (2009) The amino terminus of tau inhibits kinesin-dependent axonal transport: implications for filament toxicity. *J Neurosci Res,* 87(2)**,** 440-51.

Lasagna-Reeves, C. A., Castillo-Carranza, D. L., Guerrero-Muoz, M. J., Jackson, G. R. & Kayed, R. (2010) Preparation and characterization of neurotoxic tau oligomers. *Biochemistry,* 49(47)**,** 10039-41.

Lasagna-Reeves, C. A., De Haro, M., Hao, S., Park, J., Rousseaux, M. W., Al-Ramahi, I., Jafar-Nejad, P., Vilanova-Velez, L., See, L., De Maio, A., Nitschke, L., Wu, Z., Troncoso, J. C., Westbrook, T. F.,

Tang, J., Botas, J. & Zoghbi, H. Y. (2016) Reduction of Nuak1 Decreases Tau and Reverses Phenotypes in a Tauopathy Mouse Model. *Neuron,* 92(2)**,** 407-418.

Lasagna-Reeves, C. A., Sengupta, U., Castillo-Carranza, D., Gerson, J. E., Guerrero-Munoz, M., Troncoso, J. C., Jackson, G. R. & Kayed, R. (2014) The formation of tau pore-like structures is prevalent and cell specific: possible implications for the disease phenotypes. *Acta Neuropathol Commun,* 2**,** 56.

Lathuiliere, A. & Hyman, B. T. (2021) Quantitative Methods for the Detection of Tau Seeding Activity in Human Biofluids. *Front Neurosci,* 15**,** 654176.

Laurent, C., Buee, L. & Blum, D. (2018) Tau and neuroinflammation: What impact for Alzheimer's Disease and Tauopathies? *Biomed J,* 41(1)**,** 21-33.

Le, A. H. & Machesky, L. M. (2022) Image-based Quantification of Macropinocytosis Using Dextran Uptake into Cultured Cells. *Bio Protoc,* 12(7)**,** e4367.

Le, P. U. & Nabi, I. R. (2003) Distinct caveolae-mediated endocytic pathways target the Golgi apparatus and the endoplasmic reticulum. *J Cell Sci,* 116(Pt 6)**,** 1059-71.

Ledesma, M. D., Medina, M. & Avila, J. (1996) The in vitro formation of recombinant tau polymers: effect of phosphorylation and glycation. *Mol Chem Neuropathol,* 27(3)**,** 249-58.

Lee, S., Ashizawa, A. T., Kim, K. S., Falk, D. J. & Notterpek, L. (2013) Liposomes to target peripheral neurons and Schwann cells. *PLoS One,* 8(11)**,** e78724.

Lefebvre, T., Ferreira, S., Dupont-Wallois, L., Bussiere, T., Dupire, M. J., Delacourte, A., Michalski, J. C. & Caillet-Boudin, M. L. (2003) Evidence of a balance between phosphorylation and O-GlcNAc glycosylation of Tau proteins--a role in nuclear localization. *Biochim Biophys Acta,* 1619(2)**,** 167-76.

Levin, H. L. & Moran, J. V. (2011) Dynamic interactions between transposable elements and their hosts. *Nat Rev Genet,* 12(9)**,** 615-27.

Li, C. & Gotz, J. (2017) Somatodendritic accumulation of Tau in Alzheimer's disease is promoted by Fyn-mediated local protein translation. *EMBO J,* 36(21)**,** 3120-3138.

Li, H. L., Wang, H. H., Liu, S. J., Deng, Y. Q., Zhang, Y. J., Tian, Q., Wang, X. C., Chen, X. Q., Yang, Y., Zhang, J. Y., Wang, Q., Xu, H., Liao, F. F. & Wang, J. Z. (2007) Phosphorylation of tau antagonizes apoptosis by stabilizing beta-catenin, a mechanism involved in Alzheimer's neurodegeneration. *Proc Natl Acad Sci U S A,* 104(9)**,** 3591-6.

Li, S. & Malmstadt, N. (2013) Deformation and poration of lipid bilayer membranes by cationic nanoparticles. *Soft Matter,* 9(20)**,** 4969-4976.

Li, W. & Lee, V. M. (2006) Characterization of two VQIXXK motifs for tau fibrillization in vitro. *Biochemistry,* 45(51)**,** 15692-701.

Li, W., Prazak, L., Chatterjee, N., Gruninger, S., Krug, L., Theodorou, D. & Dubnau, J. (2013) Activation of transposable elements during aging and neuronal decline in Drosophila. *Nat Neurosci,* 16(5)**,** 529-31.

Li, X., Kumar, Y., Zempel, H., Mandelkow, E. M., Biernat, J. & Mandelkow, E. (2011) Novel diffusion barrier for axonal retention of Tau in neurons and its failure in neurodegeneration. *EMBO J,* 30(23)**,** 4825-37.

Li, X. C., Hu, Y., Wang, Z. H., Luo, Y., Zhang, Y., Liu, X. P., Feng, Q., Wang, Q., Ye, K., Liu, G. P. & Wang, J. Z. (2016) Human wild-type full-length tau accumulation disrupts mitochondrial dynamics and the functions via increasing mitofusins. *Sci Rep,* 6**,** 24756.

Lim, J. P. & Gleeson, P. A. (2011) Macropinocytosis: an endocytic pathway for internalising large gulps. *Immunol Cell Biol,* 89(8)**,** 836-43.

Lim, S., Haque, M. M., Kim, D., Kim, D. J. & Kim, Y. K. (2014) Cell-based Models To Investigate Tau Aggregation. *Comput Struct Biotechnol J,* 12(20-21)**,** 7-13.

Lin, H. P., Singla, B., Ghoshal, P., Faulkner, J. L., Cherian-Shaw, M., O'connor, P. M., She, J. X., Belin De Chantemele, E. J. & Csanyi, G. (2018) Identification of novel macropinocytosis inhibitors using a rational screen of Food and Drug Administration-approved drugs. *Br J Pharmacol,* 175(18)**,** 3640-3655.

Lindqvist, A., Rip, J., Gaillard, P. J., Bjorkman, S. & Hammarlund-Udenaes, M. (2013) Enhanced brain delivery of the opioid peptide DAMGO in glutathione pegylated liposomes: a microdialysis study. *Mol Pharm,* 10(5)**,** 1533-41.

Lindqvist, A., Rip, J., Van Kregten, J., Gaillard, P. J. & Hammarlund-Udenaes, M. (2016) In vivo Functional Evaluation of Increased Brain Delivery of the Opioid Peptide DAMGO by Glutathione-PEGylated Liposomes. *Pharm Res,* 33(1)**,** 177-85.

Lipids, A. P. *Mini-Extruder Extrusion Technique* [Online]. Available at: https://avantilipids.com/divisions/equipment-products/mini-extruder-extrusion-technique. Accessed 30.05.22.

Liu, A. P., Aguet, F., Danuser, G. & Schmid, S. L. (2010) Local clustering of transferrin receptors promotes clathrin-coated pit initiation. *J Cell Biol,* 191(7)**,** 1381-93.

Liu, F., Iqbal, K., Grundke-Iqbal, I., Hart, G. W. & Gong, C. X. (2004a) O-GlcNAcylation regulates phosphorylation of tau: a mechanism involved in Alzheimer's disease. *Proc Natl Acad Sci U S A,* 101(29)**,** 10804-9.

Liu, F., Zaidi, T., Iqbal, K., Grundke-Iqbal, I., Merkle, R. K. & Gong, C. X. (2002) Role of glycosylation in hyperphosphorylation of tau in Alzheimer's disease. *FEBS Lett,* 512(1-3)**,** 101-6.

Liu, J. & Li, L. (2019) Targeting Autophagy for the Treatment of Alzheimer's Disease: Challenges and Opportunities. *Front Mol Neurosci,* 12**,** 203.

Liu, S. J., Zhang, J. Y., Li, H. L., Fang, Z. Y., Wang, Q., Deng, H. M., Gong, C. X., Grundke-Iqbal, I., Iqbal, K. & Wang, J. Z. (2004b) Tau becomes a more favorable substrate for GSK-3 when it is prephosphorylated by PKA in rat brain. *J Biol Chem,* 279(48)**,** 50078-88.

Lo, C. H., Lim, C. K., Ding, Z., Wickramasinghe, S. P., Braun, A. R., Ashe, K. H., Rhoades, E., Thomas, D. D. & Sachs, J. N. (2019) Targeting the ensemble of heterogeneous tau oligomers in cells: A novel small molecule screening platform for tauopathies. *Alzheimers Dement,* 15(11)**,** 1489-1502.

Lobie, P. E., Sadir, R., Graichen, R., Mertani, H. C. & Morel, G. (1999) Caveolar internalization of growth hormone. *Exp Cell Res,* 246(1)**,** 47-55.

Loffler, T., Flunkert, S., Taub, N., Schofield, E. L., Ward, M. A., Windisch, M. & Hutter-Paier, B. (2012) Stable mutated tau441 transfected SH-SY5Y cells as screening tool for Alzheimer's disease drug candidates. *J Mol Neurosci,* 47(1)**,** 192-203.

Lopresti, P. (2018) Tau in Oligodendrocytes Takes Neurons in Sickness and in Health. *Int J Mol Sci,* 19(8).

Louneva, N., Cohen, J. W., Han, L. Y., Talbot, K., Wilson, R. S., Bennett, D. A., Trojanowski, J. Q. & Arnold, S. E. (2008) Caspase-3 is enriched in postsynaptic densities and increased in Alzheimer's disease. *Am J Pathol,* 173(5)**,** 1488-95.

Lu, M. & Kosik, K. S. (2001) Competition for microtubule-binding with dual expression of tau missense and splice isoforms. *Mol Biol Cell,* 12(1)**,** 171-84.

Luo, H. B., Xia, Y. Y., Shu, X. J., Liu, Z. C., Feng, Y., Liu, X. H., Yu, G., Yin, G., Xiong, Y. S., Zeng, K., Jiang, J., Ye, K., Wang, X. C. & Wang, J. Z. (2014) SUMOylation at K340 inhibits tau degradation through deregulating its phosphorylation and ubiquitination. *Proc Natl Acad Sci U S A,* 111(46)**,** 16586-91.

Ly, P. T., Wu, Y., Zou, H., Wang, R., Zhou, W., Kinoshita, A., Zhang, M., Yang, Y., Cai, F., Woodgett, J. & Song, W. (2013) Inhibition of GSK3beta-mediated BACE1 expression reduces Alzheimer-associated phenotypes. *J Clin Invest,* 123(1)**,** 224-35.

M.M.A.B.W.C. (2023) *What the FDA Approval of Lecanemab Means for Patients and Families: A Q&A with MBWC Clinicians (news report)* [Online]. Available at: https://depts.washington.edu/mbwc/news/article/lecanemab#:~:text=What%20is%20the%20controversy%20about,of%20ARIA%20are%20not%20clear [accessed 20.08.23].

Maccioni, R. B., Farias, G., Morales, I. & Navarrete, L. (2010) The revitalized tau hypothesis on Alzheimer's disease. *Arch Med Res,* 41(3)**,** 226-31.

Madabhushi, R., Pan, L. & Tsai, L. H. (2014) DNA damage and its links to neurodegeneration. *Neuron,* 83(2)**,** 266-282.

Maeda, S., Sahara, N., Saito, Y., Murayama, M., Yoshiike, Y., Kim, H., Miyasaka, T., Murayama, S., Ikai, A. & Takashima, A. (2007) Granular tau oligomers as intermediates of tau filaments. *Biochemistry,* 46(12)**,** 3856-61.

Maeda, S., Sahara, N., Saito, Y., Murayama, S., Ikai, A. & Takashima, A. (2006) Increased levels of granular tau oligomers: an early sign of brain aging and Alzheimer's disease. *Neurosci Res,* 54(3)**,** 197-201.

Magarkar, A., Dhawan, V., Kallinteri, P., Viitala, T., Elmowafy, M., Rog, T. & Bunker, A. (2014) Cholesterol level affects surface charge of lipid membranes in saline solution. *Sci Rep,* 4**,** 5005.

Majd, S., Koblar, S. & Power, J. (2018) Compound C enhances tau phosphorylation at Serine(396) via PI3K activation in an AMPK and rapamycin independent way in differentiated SH-SY5Y cells. *Neurosci Lett,* 670**,** 53-61.

Malhis, M., Kaniyappan, S., Aillaud, I., Chandupatla, R. R., Ramirez, L. M., Zweckstetter, M., Horn, A. H. C., Mandelkow, E., Sticht, H. & Funke, S. A. (2021) Potent Tau Aggregation Inhibitor D-Peptides Selected against Tau-Repeat 2 Using Mirror Image Phage Display. *Chembiochem,* 22(21)**,** 3049-3059.

Malia, T. J., Teplyakov, A., Ernst, R., Wu, S. J., Lacy, E. R., Liu, X., Vandermeeren, M., Mercken, M., Luo, J., Sweet, R. W. & Gilliland, G. L. (2016) Epitope mapping and structural basis for the recognition of phosphorylated tau by the anti-tau antibody AT8. *Proteins,* 84(4)**,** 427-34.

Mamsa, S. S. A. & Meloni, B. P. (2021) Arginine and Arginine-Rich Peptides as Modulators of Protein Aggregation and Cytotoxicity Associated With Alzheimer's Disease. *Front Mol Neurosci,* 14**,** 759729.

Manczak, M. & Reddy, P. H. (2012) Abnormal interaction between the mitochondrial fission protein Drp1 and hyperphosphorylated tau in Alzheimer's disease neurons: implications for mitochondrial dysfunction and neuronal damage. *Hum Mol Genet,* 21(11)**,** 2538-47.

Mandelkow, E., Von Bergen, M., Biernat, J. & Mandelkow, E. M. (2007) Structural principles of tau and the paired helical filaments of Alzheimer's disease. *Brain Pathol,* 17(1)**,** 83-90.

Mandell, J. W. & Banker, G. A. (1996) A spatial gradient of tau protein phosphorylation in nascent axons. *J Neurosci,* 16(18)**,** 5727-40.

Marciniak, E., Leboucher, A., Caron, E., Ahmed, T., Tailleux, A., Dumont, J., Issad, T., Gerhardt, E., Pagesy, P., Vileno, M., Bournonville, C., Hamdane, M., Bantubungi, K., Lancel, S., Demeyer, D., Eddarkaoui, S., Vallez, E., Vieau, D., Humez, S., Faivre, E., Grenier-Boley, B., Outeiro, T. F., Staels, B., Amouyel, P., Balschun, D., Buee, L. & Blum, D. (2017) Tau deletion promotes brain insulin resistance. *J Exp Med,* 214(8)**,** 2257-2269.

Margolis, R. L., Rauch, C. T., Pirollet, F. & Job, D. (1990) Specific association of STOP protein with microtubules in vitro and with stable microtubules in mitotic spindles of cultured cells. *EMBO J,* 9(12)**,** 4095-102.

Markesbery, W. R. (1997) Neuropathological criteria for the diagnosis of Alzheimer's disease. *Neurobiol Aging,* 18(4 Suppl)**,** S13-9.

Martini-Stoica, H., Cole, A. L., Swartzlander, D. B., Chen, F., Wan, Y. W., Bajaj, L., Bader, D. A., Lee, V. M. Y., Trojanowski, J. Q., Liu, Z., Sardiello, M. & Zheng, H. (2018) TFEB enhances astroglial uptake of extracellular tau species and reduces tau spreading. *J Exp Med,* 215(9)**,** 2355-2377.

Maruyama, M., Shimada, H., Suhara, T., Shinotoh, H., Ji, B., Maeda, J., Zhang, M. R., Trojanowski, J. Q., Lee, V. M., Ono, M., Masamoto, K., Takano, H., Sahara, N., Iwata, N., Okamura, N., Furumoto, S., Kudo, Y., Chang, Q., Saido, T. C., Takashima, A., Lewis, J., Jang, M. K., Aoki, I., Ito, H. & Higuchi, M. (2013) Imaging of tau pathology in a tauopathy mouse model and in Alzheimer patients compared to normal controls. *Neuron,* 79(6)**,** 1094-108.

Mason, A. F. & Thordarson, P. (2016) Synthesis of Protein Bioconjugates via Cysteine-maleimide Chemistry. *J Vis Exp*(113).

Maxwell, P. H., Burhans, W. C. & Curcio, M. J. (2011) Retrotransposition is associated with genome instability during chronological aging. *Proc Natl Acad Sci U S A,* 108(51)**,** 20376-81.

Mcclean, P. L. & Holscher, C. (2014) Liraglutide can reverse memory impairment, synaptic loss and reduce plaque load in aged APP/PS1 mice, a model of Alzheimer's disease. *Neuropharmacology,* 76 Pt A**,** 57-67.

Mcewan, W. A., Falcon, B., Vaysburd, M., Clift, D., Oblak, A. L., Ghetti, B., Goedert, M. & James, L. C. (2017) Cytosolic Fc receptor TRIM21 inhibits seeded tau aggregation. *Proc Natl Acad Sci U S A,* 114(3)**,** 574-579.

Mcmahon, H. T. & Boucrot, E. (2011) Molecular mechanism and physiological functions of clathrin-mediated endocytosis. *Nat Rev Mol Cell Biol,* 12(8)**,** 517-33.

Medina, L., Gonzalez-Lizarraga, F., Dominguez-Meijide, A., Ploper, D., Parrales, V., Sequeira, S., Cima-Omori, M. S., Zweckstetter, M., Del Bel, E., Michel, P. P., Outeiro, T. F., Raisman-Vozari, R., Chehin, R. & Socias, S. B. (2021) Doxycycline Interferes With Tau Aggregation and Reduces Its Neuronal Toxicity. *Front Aging Neurosci,* 13**,** 635760.

Melis, V., Magbagbeolu, M., Rickard, J. E., Horsley, D., Davidson, K., Harrington, K. A., Goatman, K., Goatman, E. A., Deiana, S., Close, S. P., Zabke, C., Stamer, K., Dietze, S., Schwab, K., Storey, J. M., Harrington, C. R., Wischik, C. M., Theuring, F. & Riedel, G. (2015) Effects of oxidized and reduced forms of methylthioninium in two transgenic mouse tauopathy models. *Behav Pharmacol,* 26(4)**,** 353-68.

Meloni, B. P., Mastaglia, F. L. & Knuckey, N. W. (2020) Cationic Arginine-Rich Peptides (CARPs): A Novel Class of Neuroprotective Agents With a Multimodal Mechanism of Action. *Front Neurol,* 11**,** 108.

Merck. (2022) *MTT Assay Protocol for Cell Viability and Proliferation* [Online]. Available at: https://www.sigmaaldrich.com/GB/en/technical-documents/protocol/cell-culture-and-cell-culture-analysis/cell-counting-and-health-analysis/cell-proliferation-kit-i-mtt. Accessed 02.10.22.

Mettlen, M., Chen, P. H., Srinivasan, S., Danuser, G. & Schmid, S. L. (2018) Regulation of Clathrin-Mediated Endocytosis. *Annu Rev Biochem,* 87**,** 871-896.

Michel, C. H., Kumar, S., Pinotsi, D., Tunnacliffe, A., St George-Hyslop, P., Mandelkow, E., Mandelkow, E. M., Kaminski, C. F. & Kaminski Schierle, G. S. (2014) Extracellular monomeric tau protein is sufficient to initiate the spread of tau protein pathology. *J Biol Chem,* 289(2)**,** 956-67.

Miller, E. C., Teravskis, P. J., Dummer, B. W., Zhao, X., Huganir, R. L. & Liao, D. (2014) Tau phosphorylation and tau mislocalization mediate soluble Abeta oligomer-induced AMPA glutamate receptor signaling deficits. *Eur J Neurosci,* 39(7)**,** 1214-24.

Min, S. W., Cho, S. H., Zhou, Y., Schroeder, S., Haroutunian, V., Seeley, W. W., Huang, E. J., Shen, Y., Masliah, E., Mukherjee, C., Meyers, D., Cole, P. A., Ott, M. & Gan, L. (2010) Acetylation of tau inhibits its degradation and contributes to tauopathy. *Neuron,* 67(6)**,** 953-66.

Min, S. W., Sohn, P. D., Li, Y., Devidze, N., Johnson, J. R., Krogan, N. J., Masliah, E., Mok, S. A., Gestwicki, J. E. & Gan, L. (2018) SIRT1 Deacetylates Tau and Reduces Pathogenic Tau Spread in a Mouse Model of Tauopathy. *J Neurosci,* 38(15)**,** 3680-3688.

Mirbaha, H., Holmes, B. B., Sanders, D. W., Bieschke, J. & Diamond, M. I. (2015) Tau Trimers Are the Minimal Propagation Unit Spontaneously Internalized to Seed Intracellular Aggregation. *J Biol Chem,* 290(24)**,** 14893-903.

Mitchell, D. J., Kim, D. T., Steinman, L., Fathman, C. G. & Rothbard, J. B. (2000) Polyarginine enters cells more efficiently than other polycationic homopolymers. *J Pept Res,* 56(5)**,** 318-25.

Miyamoto, T., Stein, L., Thomas, R., Djukic, B., Taneja, P., Knox, J., Vossel, K. & Mucke, L. (2017) Phosphorylation of tau at Y18, but not tau-fyn binding, is required for tau to modulate NMDA receptor-dependent excitotoxicity in primary neuronal culture. *Mol Neurodegener,* 12(1)**,** 41.

Mizushima, N. & Yoshimori, T. (2007) How to interpret LC3 immunoblotting. *Autophagy,* 3(6)**,** 542-5.

Mokhtar, S. H., Bakhuraysah, M. M., Cram, D. S. & Petratos, S. (2013) The Beta-amyloid protein of Alzheimer's disease: communication breakdown by modifying the neuronal cytoskeleton. *Int J Alzheimers Dis,* 2013**,** 910502.

Molecular Probes, I. (2006) *HCS LipidTOX Neutral Lipid Stains* [Online]. Available at: https://www.fishersci.co.uk/shop/products/molecular-probes-lipidtox-hcs-lipidtox-deep-red-neutral-lipid-stain-cellular-imaging/10242283#:~:text=HCS%20LipidTOX%20Deep%20Red%20neutral%20lipid%20stain%20was,detected%20by%20fluorescence%20microscopy%20or%20an%20HCS%20reader.. Accessed 02.10.22.

Moloney, A. M., Griffin, R. J., Timmons, S., O'connor, R., Ravid, R. & O'neill, C. (2010) Defects in IGF-1 receptor, insulin receptor and IRS-1/2 in Alzheimer's disease indicate possible resistance to IGF-1 and insulin signalling. *Neurobiol Aging,* 31(2)**,** 224-43.

Moloney, C. M., Lowe, V. J. & Murray, M. E. (2021) Visualization of neurofibrillary tangle maturity in Alzheimer's disease: A clinicopathologic perspective for biomarker research. *Alzheimers Dement,* 17(9)**,** 1554-1574.

Monier, S., Parton, R. G., Vogel, F., Behlke, J., Henske, A. & Kurzchalia, T. V. (1995) VIP21-caveolin, a membrane protein constituent of the caveolar coat, oligomerizes in vivo and in vitro. *Mol Biol Cell,* 6(7)**,** 911-27.

Montaner, L. J., Da Silva, R. P., Sun, J., Sutterwala, S., Hollinshead, M., Vaux, D. & Gordon, S. (1999) Type 1 and type 2 cytokine regulation of macrophage endocytosis: differential activation by IL-4/IL-13 as opposed to IFN-gamma or IL-10. *J Immunol,* 162(8)**,** 4606-13.

Montesano, R., Roth, J., Robert, A. & Orci, L. (1982) Non-coated membrane invaginations are involved in binding and internalization of cholera and tetanus toxins. *Nature,* 296(5858)**,** 651-3.

Morales, I., Guzman-Martinez, L., Cerda-Troncoso, C., Farias, G. A. & Maccioni, R. B. (2014) Neuroinflammation in the pathogenesis of Alzheimer's disease. A rational framework for the search of novel therapeutic approaches. *Front Cell Neurosci,* 8**,** 112.

Morales, I., Jimenez, J. M., Mancilla, M. & Maccioni, R. B. (2013) Tau oligomers and fibrils induce activation of microglial cells. *J Alzheimers Dis,* 37(4)**,** 849-56.

Morris, M., Knudsen, G. M., Maeda, S., Trinidad, J. C., Ioanoviciu, A., Burlingame, A. L. & Mucke, L. (2015) Tau post-translational modifications in wild-type and human amyloid precursor protein transgenic mice. *Nat Neurosci,* 18(8)**,** 1183-9.

Mosconi, L., Pupi, A. & De Leon, M. J. (2008) Brain glucose hypometabolism and oxidative stress in preclinical Alzheimer's disease. *Ann N Y Acad Sci,* 1147**,** 180-95.

Mozersky, J., Roberts, J. S., Rumbaugh, M., Chhatwal, J., Wijsman, E., Galasko, D., Blacker, D. & Agreed (2022) Spillover: The Approval of New Medications for Alzheimer's Disease Dementia Will Impact Biomarker Disclosure Among Asymptomatic Research Participants. *J Alzheimers Dis,* 90(3)**,** 1035-1043.

Mufson, E. J., Mahady, L., Waters, D., Counts, S. E., Perez, S. E., Dekosky, S. T., Ginsberg, S. D., Ikonomovic, M. D., Scheff, S. W. & Binder, L. I. (2015) Hippocampal plasticity during the progression of Alzheimer's disease. *Neuroscience,* 309**,** 51-67.

Nabi, I. R. & Le, P. U. (2003) Caveolae/raft-dependent endocytosis. *J Cell Biol,* 161(4)**,** 673-7.

Nadimidla, K., Ismail, T. & Kanapathipillai, M. (2017) Tau peptides and tau mutant protein aggregation inhibition by cationic polyethyleneimine and polyarginine. *Biopolymers,* 107(9).

Nakaso, K., Yoshimoto, Y., Nakano, T., Takeshima, T., Fukuhara, Y., Yasui, K., Araga, S., Yanagawa, T., Ishii, T. & Nakashima, K. (2004) Transcriptional activation of p62/A170/ZIP during the formation of the aggregates: possible mechanisms and the role in Lewy body formation in Parkinson's disease. *Brain Res,* 1012(1-2)**,** 42-51.

Nara, A., Aki, T., Funakoshi, T. & Uemura, K. (2010) Methamphetamine induces macropinocytosis in differentiated SH-SY5Y human neuroblastoma cells. *Brain Res,* 1352**,** 1-10.

Narasimhan, S., Changolkar, L., Riddle, D. M., Kats, A., Stieber, A., Weitzman, S. A., Zhang, B., Li, Z., Roberson, E. D., Trojanowski, J. Q. & Lee, V. M. Y. (2020) Human tau pathology transmits glial tau aggregates in the absence of neuronal tau. *J Exp Med,* 217(2).

Neth, B. J. & Craft, S. (2017) Insulin Resistance and Alzheimer's Disease: Bioenergetic Linkages. *Front Aging Neurosci,* 9**,** 345.

Niblock, M. & Gallo, J. M. (2012) Tau alternative splicing in familial and sporadic tauopathies. *Biochem Soc Trans,* 40(4)**,** 677-80.

Nie, C. L., Wei, Y., Chen, X., Liu, Y. Y., Dui, W., Liu, Y., Davies, M. C., Tendler, S. J. & He, R. G. (2007) Formaldehyde at low concentration induces protein tau into globular amyloid-like aggregates in vitro and in vivo. *PLoS One,* 2(7)**,** e629.

Nih. (2017) *Symptoms and Diagnosis of Alzheimer's Disease - How Is Alzheimer's Disease Diagnosed?* [Online]. Available at: https://www.nia.nih.gov/health/how-alzheimers-disease-diagnosed. Accessed 02.08.2022.

Nikonenko, I., Boda, B., Steen, S., Knott, G., Welker, E. & Muller, D. (2008) PSD-95 promotes synaptogenesis and multiinnervated spine formation through nitric oxide signaling. *J Cell Biol,* 183(6)**,** 1115-27.

Nonaka, T., Watanabe, S. T., Iwatsubo, T. & Hasegawa, M. (2010) Seeded aggregation and toxicity of {alpha}-synuclein and tau: cellular models of neurodegenerative diseases. *J Biol Chem,* 285(45)**,** 34885-98.

O'leary, J. C., 3rd, Li, Q., Marinec, P., Blair, L. J., Congdon, E. E., Johnson, A. G., Jinwal, U. K., Koren, J., 3rd, Jones, J. R., Kraft, C., Peters, M., Abisambra, J. F., Duff, K. E., Weeber, E. J., Gestwicki, J. E. & Dickey, C. A. (2010) Phenothiazine-mediated rescue of cognition in tau transgenic mice requires neuroprotection and reduced soluble tau burden. *Mol Neurodegener,* 5**,** 45.

Oh, P., Mcintosh, D. P. & Schnitzer, J. E. (1998) Dynamin at the neck of caveolae mediates their budding to form transport vesicles by GTP-driven fission from the plasma membrane of endothelium. *J Cell Biol,* 141(1)**,** 101-14.

Ohtake, N., Saito, M., Eto, M. & Seki, K. (2014) Exendin-4 promotes the membrane trafficking of the AMPA receptor GluR1 subunit and ADAM10 in the mouse neocortex. *Regul Pept,* 190-191**,** 1-11.

Okamoto, Y., Ninomiya, H., Miwa, S. & Masaki, T. (2000) Cholesterol oxidation switches the internalization pathway of endothelin receptor type A from caveolae to clathrin-coated pits in Chinese hamster ovary cells. *J Biol Chem,* 275(9)**,** 6439-46.

Omega_Bio-Tek. (2022) *Product Manual; E.Z.N.A. Total RNA Kit I* [Online]. Available at: https://www.omegabiotek.com/product/total-cellular-rna-e-z-n-a-total-rna-kit-i/?cn-reloaded=1. Accessed 29.09.2022.

Opanasopit, P., Tragulpakseerojn, J., Apirakaramwong, A., Ngawhirunpat, T., Rojanarata, T. & Ruktanonchai, U. (2011) The development of poly-L-arginine-coated liposomes for gene delivery. *Int J Nanomedicine,* 6**,** 2245-52.

Oswald, M., Geissler, S. & Goepferich, A. (2016) Determination of the activity of maleimide-functionalized phospholipids during preparation of liposomes. *Int J Pharm,* 514(1)**,** 93-102.

Ott, S., Henkel, A. W., Henkel, M. K., Redzic, Z. B., Kornhuber, J. & Wiltfang, J. (2011) Pre-aggregated Abeta1-42 peptide increases tau aggregation and hyperphosphorylation after short-term application. *Mol Cell Biochem,* 349(1-2)**,** 169-77.

Ozcelik, S., Sprenger, F., Skachokova, Z., Fraser, G., Abramowski, D., Clavaguera, F., Probst, A., Frank, S., Muller, M., Staufenbiel, M., Goedert, M., Tolnay, M. & Winkler, D. T. (2016) Co-expression of truncated and full-length tau induces severe neurotoxicity. *Mol Psychiatry,* 21(12)**,** 1790-1798.

Paladugu, L., Gharaibeh, A., Kolli, N., Learman, C., Hall, T. C., Li, L., Rossignol, J., Maiti, P. & Dunbar, G. L. (2021) Liraglutide Has Anti-Inflammatory and Anti-Amyloid Properties in Streptozotocin-Induced and 5xFAD Mouse Models of Alzheimer's Disease. *Int J Mol Sci,* 22(2).

Palm-Apergi, C., Lonn, P. & Dowdy, S. F. (2012) Do cell-penetrating peptides actually "penetrate" cellular membranes? *Mol Ther,* 20(4)**,** 695-7.

Panda, D., Goode, B. L., Feinstein, S. C. & Wilson, L. (1995) Kinetic stabilization of microtubule dynamics at steady state by tau and microtubule-binding domains of tau. *Biochemistry,* 34(35)**,** 11117-27.

Pankiv, S., Clausen, T. H., Lamark, T., Brech, A., Bruun, J. A., Outzen, H., Overvatn, A., Bjorkoy, G. & Johansen, T. (2007) p62/SQSTM1 binds directly to Atg8/LC3 to facilitate degradation of ubiquitinated protein aggregates by autophagy. *J Biol Chem,* 282(33)**,** 24131-45.

Park, J. S., Kam, T. I., Lee, S., Park, H., Oh, Y., Kwon, S. H., Song, J. J., Kim, D., Kim, H., Jhaldiyal, A., Na, D. H., Lee, K. C., Park, E. J., Pomper, M. G., Pletnikova, O., Troncoso, J. C., Ko, H. S., Dawson, V. L., Dawson, T. M. & Lee, S. (2021) Blocking microglial activation of reactive astrocytes is neuroprotective in models of Alzheimer's disease. *Acta Neuropathol Commun,* 9(1)**,** 78.

Parkin, E. T., Hussain, I., Turner, A. J. & Hooper, N. M. (1997) The amyloid precursor protein is not enriched in caveolae-like, detergent-insoluble membrane microdomains. *J Neurochem,* 69(5)**,** 2179-88.

Parthsarathy, V., Mcclean, P. L., Holscher, C., Taylor, M., Tinker, C., Jones, G., Kolosov, O., Salvati, E., Gregori, M., Masserini, M. & Allsop, D. (2013) A novel retro-inverso peptide inhibitor reduces amyloid deposition, oxidation and inflammation and stimulates neurogenesis in the APPswe/PS1DeltaE9 mouse model of Alzheimer's disease. *PLoS One,* 8(1)**,** e54769.

Patterson, C. (2018) World Alzheimer Report 2018. The State of the Art of Dementia Research: New Frontiers. An Analysis of Prevalence, Incidence, Cost and Trends. *Alzheimer's Disease International*.

Pei, D. & Buyanova, M. (2019) Overcoming Endosomal Entrapment in Drug Delivery. *Bioconjug Chem,* 30(2)**,** 273-283.

Pelkmans, L., Kartenbeck, J. & Helenius, A. (2001) Caveolar endocytosis of simian virus 40 reveals a new two-step vesicular-transport pathway to the ER. *Nat Cell Biol,* 3(5)**,** 473-83.

Perez, M. J., Vergara-Pulgar, K., Jara, C., Cabezas-Opazo, F. & Quintanilla, R. A. (2018) Caspase-Cleaved Tau Impairs Mitochondrial Dynamics in Alzheimer's Disease. *Mol Neurobiol,* 55(2)**,** 1004-1018.

Perry, T., Lahiri, D. K., Sambamurti, K., Chen, D., Mattson, M. P., Egan, J. M. & Greig, N. H. (2003) Glucagon-like peptide-1 decreases endogenous amyloid-beta peptide (Abeta) levels and protects hippocampal neurons from death induced by Abeta and iron. *J Neurosci Res,* 72(5)**,** 603-12.

Petrucelli, L., Dickson, D., Kehoe, K., Taylor, J., Snyder, H., Grover, A., De Lucia, M., Mcgowan, E., Lewis, J., Prihar, G., Kim, J., Dillmann, W. H., Browne, S. E., Hall, A., Voellmy, R., Tsuboi, Y., Dawson, T. M., Wolozin, B., Hardy, J. & Hutton, M. (2004) CHIP and Hsp70 regulate tau ubiquitination, degradation and aggregation. *Hum Mol Genet,* 13(7)**,** 703-14.

Pham, W., Zhao, B. Q., Lo, E. H., Medarova, Z., Rosen, B. & Moore, A. (2005) Crossing the blood-brain barrier: a potential application of myristoylated polyarginine for in vivo neuroimaging. *Neuroimage,* 28(1)**,** 287-92.

Pickford, F., Masliah, E., Britschgi, M., Lucin, K., Narasimhan, R., Jaeger, P. A., Small, S., Spencer, B., Rockenstein, E., Levine, B. & Wyss-Coray, T. (2008) The autophagy-related protein beclin 1 shows reduced expression in early Alzheimer disease and regulates amyloid beta accumulation in mice. *J Clin Invest,* 118(6)**,** 2190-9.

Pickhardt, M., Neumann, T., Schwizer, D., Callaway, K., Vendruscolo, M., Schenk, D., St George-Hyslop, P., Mandelkow, E. M., Dobson, C. M., Mcconlogue, L., Mandelkow, E. & Toth, G. (2015) Identification of Small Molecule Inhibitors of Tau Aggregation by Targeting Monomeric Tau As a Potential Therapeutic Approach for Tauopathies. *Curr Alzheimer Res,* 12(9)**,** 814-28.

Pooler, A. M., Usardi, A., Evans, C. J., Philpott, K. L., Noble, W. & Hanger, D. P. (2012) Dynamic association of tau with neuronal membranes is regulated by phosphorylation. *Neurobiol Aging,* 33(2)**,** 431 e27-38.

Popova, N. V., Deyev, I. E. & Petrenko, A. G. (2013) Clathrin-mediated endocytosis and adaptor proteins. *Acta Naturae,* 5(3)**,** 62-73.

Pozueta, J., Lefort, R. & Shelanski, M. L. (2013) Synaptic changes in Alzheimer's disease and its models. *Neuroscience,* 251**,** 51-65.

Puri, V., Watanabe, R., Singh, R. D., Dominguez, M., Brown, J. C., Wheatley, C. L., Marks, D. L. & Pagano, R. E. (2001) Clathrin-dependent and -independent internalization of plasma membrane sphingolipids initiates two Golgi targeting pathways. *J Cell Biol,* 154(3)**,** 535-47.

Qiagen. (2016) *Quick-Start Protocol; QIAGEN Plasmid Mini, Midi, and Maxi Kits* [Online]. Available at: https://www.qiagen.com/us/resources/resourcedetail?id=c164c4ce-3d6a-4d18-91c4-f5763b6d4283&lang=en. Accessed 28.09.2022.

Qian, Z. M., Li, H., Sun, H. & Ho, K. (2002) Targeted drug delivery via the transferrin receptor-mediated endocytosis pathway. *Pharmacol Rev,* 54(4)**,** 561-87.

Qiang, L., Sun, X., Austin, T. O., Muralidharan, H., Jean, D. C., Liu, M., Yu, W. & Baas, P. W. (2018) Tau Does Not Stabilize Axonal Microtubules but Rather Enables Them to Have Long Labile Domains. *Curr Biol,* 28(13)**,** 2181-2189 e4.

Qiu, C., Kivipelto, M. & Von Strauss, E. (2009) Epidemiology of Alzheimer's disease: occurrence, determinants, and strategies toward intervention. *Dialogues Clin Neurosci,* 11(2)**,** 111-28.

Quintanilla, R. A., Matthews-Roberson, T. A., Dolan, P. J. & Johnson, G. V. (2009) Caspase-cleaved tau expression induces mitochondrial dysfunction in immortalized cortical neurons: implications for the pathogenesis of Alzheimer disease. *J Biol Chem,* 284(28)**,** 18754-66.

Rachmawati, H., Larasati, A., Adi, A. C. & Shegokar, R. (2020) *Chapter 2 - Role of nanocarriers and their surface modification in targeting delivery of bioactive compounds*. [In: Shegokar, R. (Ed.) Nanoparticles - Volume 1: Expectations and Realities of Multifunctional Drug Delivery Systems]. 17-43. Elsevier Inc.

Racoosin, E. L. & Swanson, J. A. (1989) Macrophage colony-stimulating factor (rM-CSF) stimulates pinocytosis in bone marrow-derived macrophages. *J Exp Med,* 170(5)**,** 1635-48.

Racoosin, E. L. & Swanson, J. A. (1993) Macropinosome maturation and fusion with tubular lysosomes in macrophages. *J Cell Biol,* 121(5)**,** 1011-20.

Rapoport, M., Dawson, H. N., Binder, L. I., Vitek, M. P. & Ferreira, A. (2002) Tau is essential to beta -amyloid-induced neurotoxicity. *Proc Natl Acad Sci U S A,* 99(9)**,** 6364-9.

Rauch, J. N., Olson, S. H. & Gestwicki, J. E. (2017) Interactions between Microtubule-Associated Protein Tau (MAPT) and Small Molecules. *Cold Spring Harb Perspect Med,* 7(7).

Reich, N. & Holscher, C. (2020) Acylated Ghrelin as a Multi-Targeted Therapy for Alzheimer's and Parkinson's Disease. *Front Neurosci,* 14**,** 614828.

Reis, C. R., Chen, P. H., Bendris, N. & Schmid, S. L. (2017) TRAIL-death receptor endocytosis and apoptosis are selectively regulated by dynamin-1 activation. *Proc Natl Acad Sci U S A,* 114(3)**,** 504-509.

Reynolds, C. H., Betts, J. C., Blackstock, W. P., Nebreda, A. R. & Anderton, B. H. (2000) Phosphorylation sites on tau identified by nanoelectrospray mass spectrometry: differences in vitro between the mitogen-activated protein kinases ERK2, c-Jun N-terminal kinase and P38, and glycogen synthase kinase-3beta. *J Neurochem,* 74(4)**,** 1587-95.

Roberson, E. D., Scearce-Levie, K., Palop, J. J., Yan, F., Cheng, I. H., Wu, T., Gerstein, H., Yu, G. Q. & Mucke, L. (2007) Reducing endogenous tau ameliorates amyloid beta-induced deficits in an Alzheimer's disease mouse model. *Science,* 316(5825)**,** 750-4.

Robertson, L. A., Moya, K. L. & Breen, K. C. (2004) The potential role of tau protein O-glycosylation in Alzheimer's disease. *J Alzheimers Dis,* 6(5)**,** 489-95.

Roda, A. R., Serra-Mir, G., Montoliu-Gaya, L., Tiessler, L. & Villegas, S. (2022) Amyloid-beta peptide and tau protein crosstalk in Alzheimer's disease. *Neural Regen Res,* 17(8)**,** 1666-1674.

Rohn, T. T. & Head, E. (2008) Caspase activation in Alzheimer's disease: early to rise and late to bed. *Rev Neurosci,* 19(6)**,** 383-93.

Ross, C. (2020) *The development of antibody loaded liposomes for the treatment of Alzheimer's Disease* [Online]. MSci Thesis, Biomedical and Life Sciences, Lancaster University, Lancaster. Available at: https://www.research.lancs.ac.uk/portal/en/publications/the-development-of-

antibody-loaded-liposomes-for-the-treatment-of-alzheimers-disease(76cefeb2-ac50-4da8-acf0-5b9998f29ef2).html.

Ross, C., Taylor, M., Fullwood, N. & Allsop, D. (2018) Liposome delivery systems for the treatment of Alzheimer's disease. *Int J Nanomedicine,* 13**,** 8507-8522.

Ross, R. A., Spengler, B. A. & Biedler, J. L. (1983) Coordinate morphological and biochemical interconversion of human neuroblastoma cells. *J Natl Cancer Inst,* 71(4)**,** 741-7.

Rothberg, K. G., Heuser, J. E., Donzell, W. C., Ying, Y. S., Glenney, J. R. & Anderson, R. G. (1992) Caveolin, a protein component of caveolae membrane coats. *Cell,* 68(4)**,** 673-82.

Ruan, G., Agrawal, A., Marcus, A. I. & Nie, S. (2007) Imaging and tracking of tat peptide-conjugated quantum dots in living cells: new insights into nanoparticle uptake, intracellular transport, and vesicle shedding. *J Am Chem Soc,* 129(47)**,** 14759-66.

Rye, K. A., Hime, N. J. & Barter, P. J. (1996) The influence of sphingomyelin on the structure and function of reconstituted high density lipoproteins. *J Biol Chem,* 271(8)**,** 4243-50.

Saar, K., Lindgren, M., Hansen, M., Eiriksdottir, E., Jiang, Y., Rosenthal-Aizman, K., Sassian, M. & Langel, U. (2005) Cell-penetrating peptides: a comparative membrane toxicity study. *Anal Biochem,* 345(1)**,** 55-65.

Sadleir, K. R., Kandalepas, P. C., Buggia-Prevot, V., Nicholson, D. A., Thinakaran, G. & Vassar, R. (2016) Presynaptic dystrophic neurites surrounding amyloid plaques are sites of microtubule disruption, BACE1 elevation, and increased Abeta generation in Alzheimer's disease. *Acta Neuropathol,* 132(2)**,** 235-256.

Saito, T., Chiku, T., Oka, M., Wada-Kakuda, S., Nobuhara, M., Oba, T., Shinno, K., Abe, S., Asada, A., Sumioka, A., Takashima, A., Miyasaka, T. & Ando, K. (2021) Disulfide bond formation in

microtubule-associated tau protein promotes tau accumulation and toxicity in vivo. *Hum Mol Genet,* 30(21)**,** 1955-1967.

Saman, S., Kim, W., Raya, M., Visnick, Y., Miro, S., Saman, S., Jackson, B., Mckee, A. C., Alvarez, V. E., Lee, N. C. & Hall, G. F. (2012) Exosome-associated tau is secreted in tauopathy models and is selectively phosphorylated in cerebrospinal fluid in early Alzheimer disease. *J Biol Chem,* 287(6)**,** 3842-9.

Sanders, D. W., Kaufman, S. K., Devos, S. L., Sharma, A. M., Mirbaha, H., Li, A., Barker, S. J., Foley, A. C., Thorpe, J. R., Serpell, L. C., Miller, T. M., Grinberg, L. T., Seeley, W. W. & Diamond, M. I. (2014) Distinct tau prion strains propagate in cells and mice and define different tauopathies. *Neuron,* 82(6)**,** 1271-88.

Sandusky-Beltran, L. A. & Sigurdsson, E. M. (2020) Tau immunotherapies: Lessons learned, current status and future considerations. *Neuropharmacology,* 175**,** 108104.

Santa-Maria, I., Perez, M., Hernandez, F., Avila, J. & Moreno, F. J. (2006) Characteristics of the binding of thioflavin S to tau paired helical filaments. *J Alzheimers Dis,* 9(3)**,** 279-85.

Santa-Maria, I., Varghese, M., Ksiezak-Reding, H., Dzhun, A., Wang, J. & Pasinetti, G. M. (2012) Paired helical filaments from Alzheimer disease brain induce intracellular accumulation of Tau protein in aggresomes. *J Biol Chem,* 287(24)**,** 20522-33.

Saraswathy, M. & Gong, S. (2013) Different strategies to overcome multidrug resistance in cancer. *Biotechnol Adv,* 31(8)**,** 1397-407.

Sato, Y., Naito, Y., Grundke-Iqbal, I., Iqbal, K. & Endo, T. (2001) Analysis of N-glycans of pathological tau: possible occurrence of aberrant processing of tau in Alzheimer's disease. *FEBS Lett,* 496(2-3)**,** 152-60.

Savioz, A., Leuba, G. & Vallet, P. G. (2014) A framework to understand the variations of PSD-95 expression in brain aging and in Alzheimer's disease. *Ageing Res Rev,* 18**,** 86-94.

Sayas, C. L. (2020) *Chapter 10 - Tau-based therapies for Alzheimer's disease: Promising novel neuroprotective approaches*. [In Gozes, I. and Levine, J. (Eds) Neuroprotection in Autism, Schizophrenia and Alzheimer's Disease.] 245-272. Academic Press.

Schaeffer, V., Lavenir, I., Ozcelik, S., Tolnay, M., Winkler, D. T. & Goedert, M. (2012) Stimulation of autophagy reduces neurodegeneration in a mouse model of human tauopathy. *Brain,* 135(Pt 7)**,** 2169-77.

Schoch, K. M., Devos, S. L., Miller, R. L., Chun, S. J., Norrbom, M., Wozniak, D. F., Dawson, H. N., Bennett, C. F., Rigo, F. & Miller, T. M. (2016) Increased 4R-Tau Induces Pathological Changes in a Human-Tau Mouse Model. *Neuron,* 90(5)**,** 941-7.

Schubert, M., Gautam, D., Surjo, D., Ueki, K., Baudler, S., Schubert, D., Kondo, T., Alber, J., Galldiks, N., Kustermann, E., Arndt, S., Jacobs, A. H., Krone, W., Kahn, C. R. & Bruning, J. C. (2004) Role for neuronal insulin resistance in neurodegenerative diseases. *Proc Natl Acad Sci U S A,* 101(9)**,** 3100-5.

Schweers, O., Schonbrunn-Hanebeck, E., Marx, A. & Mandelkow, E. (1994) Structural studies of tau protein and Alzheimer paired helical filaments show no evidence for beta-structure. *J Biol Chem,* 269(39)**,** 24290-7.

Seidler, P. M., Boyer, D. R., Rodriguez, J. A., Sawaya, M. R., Cascio, D., Murray, K., Gonen, T. & Eisenberg, D. S. (2018) Structure-based inhibitors of tau aggregation. *Nat Chem,* 10(2)**,** 170-176.

Selkoe, D. J. & Hardy, J. (2016) The amyloid hypothesis of Alzheimer's disease at 25 years. *EMBO Mol Med,* 8(6)**,** 595-608.

Sharma, V. K. & Singh, T. G. (2020) CREB: A Multifaceted Target for Alzheimer's Disease. *Curr Alzheimer Res,* 17(14)**,** 1280-1293.

Shi, N. Q., Qi, X. R., Xiang, B. & Zhang, Y. (2014) A survey on "Trojan Horse" peptides: opportunities, issues and controlled entry to "Troy". *J Control Release,* 194**,** 53-70.

Shimura, H., Schwartz, D., Gygi, S. P. & Kosik, K. S. (2004) CHIP-Hsc70 complex ubiquitinates phosphorylated tau and enhances cell survival. *J Biol Chem,* 279(6)**,** 4869-76.

Shin, J. S., Gao, Z. & Abraham, S. N. (2000) Involvement of cellular caveolae in bacterial entry into mast cells. *Science,* 289(5480)**,** 785-8.

Shipton, O. A., Leitz, J. R., Dworzak, J., Acton, C. E., Tunbridge, E. M., Denk, F., Dawson, H. N., Vitek, M. P., Wade-Martins, R., Paulsen, O. & Vargas-Caballero, M. (2011) Tau protein is required for amyloid {beta}-induced impairment of hippocampal long-term potentiation. *J Neurosci,* 31(5)**,** 1688-92.

Shogomori, H. & Futerman, A. H. (2001) Cholera toxin is found in detergent-insoluble rafts/domains at the cell surface of hippocampal neurons but is internalized via a raft-independent mechanism. *J Biol Chem,* 276(12)**,** 9182-8.

Sievers, S. A., Karanicolas, J., Chang, H. W., Zhao, A., Jiang, L., Zirafi, O., Stevens, J. T., Munch, J., Baker, D. & Eisenberg, D. (2011) Structure-based design of non-natural amino-acid inhibitors of amyloid fibril formation. *Nature,* 475(7354)**,** 96-100.

Simic, G., Babic Leko, M., Wray, S., Harrington, C., Delalle, I., Jovanov-Milosevic, N., Bazadona, D., Buee, L., De Silva, R., Di Giovanni, G., Wischik, C. & Hof, P. R. (2016) Tau Protein

Hyperphosphorylation and Aggregation in Alzheimer's Disease and Other Tauopathies, and Possible Neuroprotective Strategies. *Biomolecules,* 6(1)**,** 6.

Simon, D., Garcia-Garcia, E., Gomez-Ramos, A., Falcon-Perez, J. M., Diaz-Hernandez, M., Hernandez, F. & Avila, J. (2012) Tau overexpression results in its secretion via membrane vesicles. *Neurodegener Dis,* 10(1-4)**,** 73-5.

Sims, J. R., Zimmer, J. A., Evans, C. D., Lu, M., Ardayfio, P., Sparks, J., Wessels, A. M., Shcherbinin, S., Wang, H., Monkul Nery, E. S., Collins, E. C., Solomon, P., Salloway, S., Apostolova, L. G., Hansson, O., Ritchie, C., Brooks, D. A., Mintun, M., Skovronsky, D. M. & Investigators, T.-A. (2023) Donanemab in Early Symptomatic Alzheimer Disease: The TRAILBLAZER-ALZ 2 Randomized Clinical Trial. *JAMA,* 330(6)**,** 512-527.

Slaughter, T. & Black, M. M. (2003) STOP (stable-tubule-only-polypeptide) is preferentially associated with the stable domain of axonal microtubules. *J Neurocytol,* 32(4)**,** 399-413.

Small, S. A. & Duff, K. (2008) Linking Abeta and tau in late-onset Alzheimer's disease: a dual pathway hypothesis. *Neuron,* 60(4)**,** 534-42.

Smet-Nocca, C., Broncel, M., Wieruszeski, J. M., Tokarski, C., Hanoulle, X., Leroy, A., Landrieu, I., Rolando, C., Lippens, G. & Hackenberger, C. P. (2011) Identification of O-GlcNAc sites within peptides of the Tau protein and their impact on phosphorylation. *Mol Biosyst,* 7(5)**,** 1420-9.

Smillie, K. J. & Cousin, M. A. (2005) Dynamin I phosphorylation and the control of synaptic vesicle endocytosis. *Biochem Soc Symp*(72)**,** 87-97.

Smith, C. J., Anderton, B. H., Davis, D. R. & Gallo, J. M. (1995) Tau isoform expression and phosphorylation state during differentiation of cultured neuronal cells. *FEBS Lett,* 375(3)**,** 243-8.

Smith, J. A., Das, A., Ray, S. K. & Banik, N. L. (2012) Role of pro-inflammatory cytokines released from microglia in neurodegenerative diseases. *Brain Res Bull,* 87(1)**,** 10-20.

Soeda, Y., Saito, M., Maeda, S., Ishida, K., Nakamura, A., Kojima, S. & Takashima, A. (2019) Methylene Blue Inhibits Formation of Tau Fibrils but not of Granular Tau Oligomers: A Plausible Key to Understanding Failure of a Clinical Trial for Alzheimer's Disease. *J Alzheimers Dis,* 68(4)**,** 1677-1686.

Sohn, P. D., Tracy, T. E., Son, H. I., Zhou, Y., Leite, R. E., Miller, B. L., Seeley, W. W., Grinberg, L. T. & Gan, L. (2016) Acetylated tau destabilizes the cytoskeleton in the axon initial segment and is mislocalized to the somatodendritic compartment. *Mol Neurodegener,* 11(1)**,** 47.

Sousa De Almeida, M., Susnik, E., Drasler, B., Taladriz-Blanco, P., Petri-Fink, A. & Rothen-Rutishauser, B. (2021) Understanding nanoparticle endocytosis to improve targeting strategies in nanomedicine. *Chem Soc Rev,* 50(9)**,** 5397-5434.

Spires-Jones, T. L., De Calignon, A., Matsui, T., Zehr, C., Pitstick, R., Wu, H. Y., Osetek, J. D., Jones, P. B., Bacskai, B. J., Feany, M. B., Carlson, G. A., Ashe, K. H., Lewis, J. & Hyman, B. T. (2008) In vivo imaging reveals dissociation between caspase activation and acute neuronal death in tangle-bearing neurons. *J Neurosci,* 28(4)**,** 862-7.

Stamer, K., Vogel, R., Thies, E., Mandelkow, E. & Mandelkow, E. M. (2002) Tau blocks traffic of organelles, neurofilaments, and APP vesicles in neurons and enhances oxidative stress. *J Cell Biol,* 156(6)**,** 1051-63.

Steen, E., Terry, B. M., Rivera, E. J., Cannon, J. L., Neely, T. R., Tavares, R., Xu, X. J., Wands, J. R. & De La Monte, S. M. (2005) Impaired insulin and insulin-like growth factor expression and signaling mechanisms in Alzheimer's disease--is this type 3 diabetes? *J Alzheimers Dis,* 7(1)**,** 63-80.

Stoothoff, W., Jones, P. B., Spires-Jones, T. L., Joyner, D., Chhabra, E., Bercury, K., Fan, Z., Xie, H., Bacskai, B., Edd, J., Irimia, D. & Hyman, B. T. (2009) Differential effect of three-repeat and four-repeat tau on mitochondrial axonal transport. *J Neurochem,* 111(2)**,** 417-27.

Strang, K. H., Golde, T. E. & Giasson, B. I. (2019) MAPT mutations, tauopathy, and mechanisms of neurodegeneration. *Lab Invest,* 99(7)**,** 912-928.

Styren, S. D., Hamilton, R. L., Styren, G. C. & Klunk, W. E. (2000) X-34, a fluorescent derivative of Congo red: a novel histochemical stain for Alzheimer's disease pathology. *J Histochem Cytochem,* 48(9)**,** 1223-32.

Su, J. H., Zhao, M., Anderson, A. J., Srinivasan, A. & Cotman, C. W. (2001) Activated caspase-3 expression in Alzheimer's and aged control brain: correlation with Alzheimer pathology. *Brain Res,* 898(2)**,** 350-7.

Subramanian, J., Savage, J. C. & Tremblay, M. E. (2020) Synaptic Loss in Alzheimer's Disease: Mechanistic Insights Provided by Two-Photon in vivo Imaging of Transgenic Mouse Models. *Front Cell Neurosci,* 14**,** 592607.

Suk, J. S., Suh, J., Choy, K., Lai, S. K., Fu, J. & Hanes, J. (2006) Gene delivery to differentiated neurotypic cells with RGD and HIV Tat peptide functionalized polymeric nanoparticles. *Biomaterials,* 27(29)**,** 5143-50.

Sukumaran, S. K., Quon, M. J. & Prasadarao, N. V. (2002) Escherichia coli K1 internalization via caveolae requires caveolin-1 and protein kinase Calpha interaction in human brain microvascular endothelial cells. *J Biol Chem,* 277(52)**,** 50716-24.

Sultan, A., Nesslany, F., Violet, M., Begard, S., Loyens, A., Talahari, S., Mansuroglu, Z., Marzin, D., Sergeant, N., Humez, S., Colin, M., Bonnefoy, E., Buee, L. & Galas, M. C. (2011) Nuclear tau, a key player in neuronal DNA protection. *J Biol Chem,* 286(6)**,** 4566-75.

Sun, Q., Fan, W. & Zhong, Q. (2009) Regulation of Beclin 1 in autophagy. *Autophagy,* 5(5)**,** 713-6.

Sun, Y., Guo, Y., Feng, X., Jia, M., Ai, N., Dong, Y., Zheng, Y., Fu, L., Yu, B., Zhang, H., Wu, J., Yu, X., Wu, H. & Kong, W. (2020) The behavioural and neuropathologic sexual dimorphism and absence of MIP-3alpha in tau P301S mouse model of Alzheimer's disease. *J Neuroinflammation,* 17(1)**,** 72.

Tak, H., Haque, M. M., Kim, M. J., Lee, J. H., Baik, J. H., Kim, Y., Kim, D. J., Grailhe, R. & Kim, Y. K. (2013) Bimolecular fluorescence complementation; lighting-up tau-tau interaction in living cells. *PLoS One,* 8(12)**,** e81682.

Takahashi, M., Chin, Y., Nonaka, T., Hasegawa, M., Watanabe, N. & Arai, T. (2012) Prolonged nitric oxide treatment induces tau aggregation in SH-SY5Y cells. *Neurosci Lett,* 510(1)**,** 48-52.

Takara. *Tet-One technology overview* [Online]. Available at: https://www.takarabio.com/learning-centers/gene-function/inducible-systems/tet-inducible-systems/tet-one-technology-overview. Accessed 18.07.22.

Takara_Bio_Europe. (2011) *Titanium One-Step RT-PCR Kit User Manual* [Online]. Available at: https://www.takarabio.com/products/mrna-and-cdna-synthesis/cdna-synthesis-kits/titanium-one-step-kit. Accessed 29.09.2022.

Takeda, S., Wegmann, S., Cho, H., Devos, S. L., Commins, C., Roe, A. D., Nicholls, S. B., Carlson, G. A., Pitstick, R., Nobuhara, C. K., Costantino, I., Frosch, M. P., Muller, D. J., Irimia, D. & Hyman, B.

T. (2015) Neuronal uptake and propagation of a rare phosphorylated high-molecular-weight tau derived from Alzheimer's disease brain. *Nat Commun,* 6**,** 8490.

Takeuchi, H., Iba, M., Inoue, H., Higuchi, M., Takao, K., Tsukita, K., Karatsu, Y., Iwamoto, Y., Miyakawa, T., Suhara, T., Trojanowski, J. Q., Lee, V. M. & Takahashi, R. (2011) P301S mutant human tau transgenic mice manifest early symptoms of human tauopathies with dementia and altered sensorimotor gating. *PLoS One,* 6(6)**,** e21050.

Talbot, K., Wang, H. Y., Kazi, H., Han, L. Y., Bakshi, K. P., Stucky, A., Fuino, R. L., Kawaguchi, K. R., Samoyedny, A. J., Wilson, R. S., Arvanitakis, Z., Schneider, J. A., Wolf, B. A., Bennett, D. A., Trojanowski, J. Q. & Arnold, S. E. (2012) Demonstrated brain insulin resistance in Alzheimer's disease patients is associated with IGF-1 resistance, IRS-1 dysregulation, and cognitive decline. *J Clin Invest,* 122(4)**,** 1316-38.

Tan, J. M., Wong, E. S., Kirkpatrick, D. S., Pletnikova, O., Ko, H. S., Tay, S. P., Ho, M. W., Troncoso, J., Gygi, S. P., Lee, M. K., Dawson, V. L., Dawson, T. M. & Lim, K. L. (2008) Lysine 63-linked ubiquitination promotes the formation and autophagic clearance of protein inclusions associated with neurodegenerative diseases. *Hum Mol Genet,* 17(3)**,** 431-9.

Tanaka, T., Iqbal, K., Trenkner, E., Liu, D. J. & Grundke-Iqbal, I. (1995) Abnormally phosphorylated tau in SY5Y human neuroblastoma cells. *FEBS Lett,* 360(1)**,** 5-9.

Tanaka, T., Zhong, J., Iqbal, K., Trenkner, E. & Grundke-Iqbal, I. (1998) The regulation of phosphorylation of tau in SY5Y neuroblastoma cells: the role of protein phosphatases. *FEBS Lett,* 426(2)**,** 248-54.

Tanida, I., Ueno, T. & Kominami, E. (2008) LC3 and Autophagy. *Methods Mol Biol,* 445**,** 77-88.

Taniguchi, S., Suzuki, N., Masuda, M., Hisanaga, S., Iwatsubo, T., Goedert, M. & Hasegawa, M. (2005) Inhibition of heparin-induced tau filament formation by phenothiazines, polyphenols, and porphyrins. *J Biol Chem,* 280(9)**,** 7614-23.

Tarutani, A., Miyata, H., Nonaka, T., Hasegawa, K., Yoshida, M., Saito, Y., Murayama, S., Robinson, A. C., Mann, D. M. A., Tomita, T. & Hasegawa, M. (2021) Human tauopathy-derived tau strains determine the substrates recruited for templated amplification. *Brain,* 144(8)**,** 2333-2348.

Taylor, M., Moore, S., Mayes, J., Parkin, E., Beeg, M., Canovi, M., Gobbi, M., Mann, D. M. & Allsop, D. (2010) Development of a proteolytically stable retro-inverso peptide inhibitor of beta-amyloid oligomerization as a potential novel treatment for Alzheimer's disease. *Biochemistry,* 49(15)**,** 3261-72.

Taylor, M., Moore, S., Mourtas, S., Niarakis, A., Re, F., Zona, C., La Ferla, B., Nicotra, F., Masserini, M., Antimisiaris, S. G., Gregori, M. & Allsop, D. (2011) Effect of curcumin-associated and lipid ligand-functionalized nanoliposomes on aggregation of the Alzheimer's Abeta peptide. *Nanomedicine,* 7(5)**,** 541-50.

Terry, R. D., Masliah, E., Salmon, D. P., Butters, N., Deteresa, R., Hill, R., Hansen, L. A. & Katzman, R. (1991) Physical basis of cognitive alterations in Alzheimer's disease: synapse loss is the major correlate of cognitive impairment. *Ann Neurol,* 30(4)**,** 572-80.

Terwel, D., Lasrado, R., Snauwaert, J., Vandeweert, E., Van Haesendonck, C., Borghgraef, P. & Van Leuven, F. (2005) Changed conformation of mutant Tau-P301L underlies the moribund tauopathy, absent in progressive, nonlethal axonopathy of Tau-4R/2N transgenic mice. *J Biol Chem,* 280(5)**,** 3963-73.

Texido, L., Martin-Satue, M., Alberdi, E., Solsona, C. & Matute, C. (2011) Amyloid beta peptide oligomers directly activate NMDA receptors. *Cell Calcium,* 49(3)**,** 184-90.

The_Jackson_Laboratory. (2022) *B6N.Cg-Tg(Prnp-MAPT*P301S)PS19Vle/J, Stock No: 024841, Protocol 25393: Standard PCR Assay - Tg(Prnp-MAPT*P301S)PS19Vle alternate2, Version 1.2* [Online]. Available at: https://legacystrain.jax.org/Protocol?stockNumber=024841&protocolID=25393. Accessed 02.10.22.

Thermo_Fisher_Scientific_Inc. (2012) *pHrodo Red and Green Dextran Quick Reference* [Online]. Available at: https://www.thermofisher.com/order/catalog/product/P10361. Accessed 02.10.22.

Thermo_Fisher_Scientific_Inc. (2013) *LysoTracker and LysoSensor Probes* [Online]. Available at: https://www.thermofisher.com/order/catalog/product/L12492. Accessed 02.10.22.

Thermo_Fisher_Scientific_Inc. (2014) *CellLight Reagents *BacMam 2.0** [Online]. Available at: https://www.thermofisher.com/order/catalog/product/de/en/C10593. Accessed 02.10.22.

Thermo_Fisher_Scientific_Inc. (2019) *Product Sheet: CyQUANT LDH Cytotoxicity Assay Kit* [Online]. Available at: https://www.thermofisher.com/order/catalog/product/C20301#:~:text=The%20CyQUANT%20LDH%20Cytotoxicity%20Assay%20is%20a%20colorimetric,culture%20medium%20upon%20damage%20to%20the%20plasma%20membrane. Accessed 02.10.22.

Thies, E. & Mandelkow, E. M. (2007) Missorting of tau in neurons causes degeneration of synapses that can be rescued by the kinase MARK2/Par-1. *J Neurosci,* 27(11)**,** 2896-907.

Thomas, S. N., Funk, K. E., Wan, Y., Liao, Z., Davies, P., Kuret, J. & Yang, A. J. (2012) Dual modification of Alzheimer's disease PHF-tau protein by lysine methylation and ubiquitylation: a mass spectrometry approach. *Acta Neuropathol,* 123(1)**,** 105-17.

Timm, T., Marx, A., Panneerselvam, S., Mandelkow, E. & Mandelkow, E. M. (2008) Structure and regulation of MARK, a kinase involved in abnormal phosphorylation of Tau protein. *BMC Neurosci,* 9 Suppl 2**,** S9.

Tunnemann, G., Ter-Avetisyan, G., Martin, R. M., Stockl, M., Herrmann, A. & Cardoso, M. C. (2008) Live-cell analysis of cell penetration ability and toxicity of oligo-arginines. *J Pept Sci,* 14(4)**,** 469-76.

Uberti, D., Rizzini, C., Spano, P. F. & Memo, M. (1997) Characterization of tau proteins in human neuroblastoma SH-SY5Y cell line. *Neurosci Lett,* 235(3)**,** 149-53.

Uddin, M. S., Stachowiak, A., Mamun, A. A., Tzvetkov, N. T., Takeda, S., Atanasov, A. G., Bergantin, L. B., Abdel-Daim, M. M. & Stankiewicz, A. M. (2018) Autophagy and Alzheimer's Disease: From Molecular Mechanisms to Therapeutic Implications. *Front Aging Neurosci,* 10**,** 04.

Usardi, A., Pooler, A. M., Seereeram, A., Reynolds, C. H., Derkinderen, P., Anderton, B., Hanger, D. P., Noble, W. & Williamson, R. (2011) Tyrosine phosphorylation of tau regulates its interactions with Fyn SH2 domains, but not SH3 domains, altering the cellular localization of tau. *FEBS J,* 278(16)**,** 2927-37.

Van Dyck, C. H., Swanson, C. J., Aisen, P., Bateman, R. J., Chen, C., Gee, M., Kanekiyo, M., Li, D., Reyderman, L., Cohen, S., Froelich, L., Katayama, S., Sabbagh, M., Vellas, B., Watson, D., Dhadda, S., Irizarry, M., Kramer, L. D. & Iwatsubo, T. (2023) Lecanemab in Early Alzheimer's Disease. *N Engl J Med,* 388(1)**,** 9-21.

Vanier, M. T., Neuville, P., Michalik, L. & Launay, J. F. (1998) Expression of specific tau exons in normal and tumoral pancreatic acinar cells. *J Cell Sci,* 111 (Pt 10)**,** 1419-32.

Vercauteren, D., Vandenbroucke, R. E., Jones, A. T., Rejman, J., Demeester, J., De Smedt, S. C., Sanders, N. N. & Braeckmans, K. (2010) The use of inhibitors to study endocytic pathways of gene carriers: optimization and pitfalls. *Mol Ther,* 18(3)**,** 561-9.

Veronese, F. M. & Mero, A. (2008) The impact of PEGylation on biological therapies. *BioDrugs,* 22(5)**,** 315-29.

Villamil-Ortiz, J. G. & Cardona-Gomez, G. P. (2015) Comparative analysis of autophagy and tauopathy related markers in cerebral ischemia and Alzheimer's disease animal models. *Front Aging Neurosci,* 7**,** 84.

Vogel, J. W., Iturria-Medina, Y., Strandberg, O. T., Smith, R., Levitis, E., Evans, A. C., Hansson, O., Alzheimer's Disease Neuroimaging, I. & Swedish Biofinder, S. (2021) Author Correction: Spread of pathological tau proteins through communicating neurons in human Alzheimer's disease. *Nat Commun,* 12(1)**,** 4862.

Vogelsberg-Ragaglia, V., Bruce, J., Richter-Landsberg, C., Zhang, B., Hong, M., Trojanowski, J. Q. & Lee, V. M. (2000) Distinct FTDP-17 missense mutations in tau produce tau aggregates and other pathological phenotypes in transfected CHO cells. *Mol Biol Cell,* 11(12)**,** 4093-104.

Von Bergen, M., Barghorn, S., Li, L., Marx, A., Biernat, J., Mandelkow, E. M. & Mandelkow, E. (2001) Mutations of tau protein in frontotemporal dementia promote aggregation of paired helical filaments by enhancing local beta-structure. *J Biol Chem,* 276(51)**,** 48165-74.

Von Bergen, M., Friedhoff, P., Biernat, J., Heberle, J., Mandelkow, E. M. & Mandelkow, E. (2000) Assembly of tau protein into Alzheimer paired helical filaments depends on a local sequence motif ((306)VQIVYK(311)) forming beta structure. *Proc Natl Acad Sci U S A,* 97(10)**,** 5129-34.

Wang, C., Fan, L., Khawaja, R. R., Liu, B., Zhan, L., Kodama, L., Chin, M., Li, Y., Le, D., Zhou, Y., Condello, C., Grinberg, L. T., Seeley, W. W., Miller, B. L., Mok, S. A., Gestwicki, J. E., Cuervo, A. M., Luo, W. & Gan, L. (2022) Microglial NF-kappaB drives tau spreading and toxicity in a mouse model of tauopathy. *Nat Commun,* 13(1)**,** 1969.

Wang, D., Huang, X., Yan, L., Zhou, L., Yan, C., Wu, J., Su, Z. & Huang, Y. (2021) The Structure Biology of Tau and Clue for Aggregation Inhibitor Design. *Protein J,* 40(5)**,** 656-668.

Wang, J. Z., Grundke-Iqbal, I. & Iqbal, K. (1996a) Glycosylation of microtubule-associated protein tau: an abnormal posttranslational modification in Alzheimer's disease. *Nat Med,* 2(8)**,** 871-5.

Wang, J. Z., Grundke-Iqbal, I. & Iqbal, K. (1996b) Restoration of biological activity of Alzheimer abnormally phosphorylated tau by dephosphorylation with protein phosphatase-2A, -2B and -1. *Brain Res Mol Brain Res,* 38(2)**,** 200-8.

Wang, J. Z., Grundke-Iqbal, I. & Iqbal, K. (2007a) Kinases and phosphatases and tau sites involved in Alzheimer neurofibrillary degeneration. *Eur J Neurosci,* 25(1)**,** 59-68.

Wang, J. Z. & Liu, F. (2008) Microtubule-associated protein tau in development, degeneration and protection of neurons. *Prog Neurobiol,* 85(2)**,** 148-75.

Wang, P., Joberty, G., Buist, A., Vanoosthuyse, A., Stancu, I. C., Vasconcelos, B., Pierrot, N., Faelth-Savitski, M., Kienlen-Campard, P., Octave, J. N., Bantscheff, M., Drewes, G., Moechars, D. & Dewachter, I. (2017a) Tau interactome mapping based identification of Otub1 as Tau deubiquitinase involved in accumulation of pathological Tau forms in vitro and in vivo. *Acta Neuropathol,* 133(5)**,** 731-749.

Wang, R. & Reddy, P. H. (2017) Role of Glutamate and NMDA Receptors in Alzheimer's Disease. *J Alzheimers Dis,* 57(4)**,** 1041-1048.

Wang, R., Xu, X., Hao, Z., Zhang, S., Wu, D., Sun, H., Mu, C., Ren, H. & Wang, G. (2019) Poly-PR in C9ORF72-Related Amyotrophic Lateral Sclerosis/Frontotemporal Dementia Causes Neurotoxicity by Clathrin-Dependent Endocytosis. *Neurosci Bull,* 35(5)**,** 889-900.

Wang, Y., Balaji, V., Kaniyappan, S., Kruger, L., Irsen, S., Tepper, K., Chandupatla, R., Maetzler, W., Schneider, A., Mandelkow, E. & Mandelkow, E. M. (2017b) The release and trans-synaptic transmission of Tau via exosomes. *Mol Neurodegener,* 12(1)**,** 5.

Wang, Y. & Mandelkow, E. (2016) Tau in physiology and pathology. *Nat Rev Neurosci,* 17(1)**,** 5-21.

Wang, Y. P., Biernat, J., Pickhardt, M., Mandelkow, E. & Mandelkow, E. M. (2007b) Stepwise proteolysis liberates tau fragments that nucleate the Alzheimer-like aggregation of full-length tau in a neuronal cell model. *Proc Natl Acad Sci U S A,* 104(24)**,** 10252-7.

Weingarten, M. D., Lockwood, A. H., Hwo, S. Y. & Kirschner, M. W. (1975) A protein factor essential for microtubule assembly. *Proc Natl Acad Sci U S A,* 72(5)**,** 1858-62.

Wilson, D. M. & Binder, L. I. (1997) Free fatty acids stimulate the polymerization of tau and amyloid beta peptides. In vitro evidence for a common effector of pathogenesis in Alzheimer's disease. *Am J Pathol,* 150(6)**,** 2181-95.

Wirths, O. & Zampar, S. (2020) Neuron Loss in Alzheimer's Disease: Translation in Transgenic Mouse Models. *Int J Mol Sci,* 21(21).

Wischik, C. M., Edwards, P. C., Lai, R. Y., Roth, M. & Harrington, C. R. (1996) Selective inhibition of Alzheimer disease-like tau aggregation by phenothiazines. *Proc Natl Acad Sci U S A,* 93(20)**,** 11213-8.

Wischik, C. M., Harrington, C. R. & Storey, J. M. (2014) Tau-aggregation inhibitor therapy for Alzheimer's disease. *Biochem Pharmacol,* 88(4)**,** 529-39.

Wischik, C. M., Novak, M., Thogersen, H. C., Edwards, P. C., Runswick, M. J., Jakes, R., Walker, J. E., Milstein, C., Roth, M. & Klug, A. (1988) Isolation of a fragment of tau derived from the core of the paired helical filament of Alzheimer disease. *Proc Natl Acad Sci U S A,* 85(12)**,** 4506-10.

Wischik, C. M., Schelter, B. O., Wischik, D. J., Storey, J. M. D. & Harrington, C. R. (2018) Modeling Prion-Like Processing of Tau Protein in Alzheimer's Disease for Pharmaceutical Development. *J Alzheimers Dis,* 62(3)**,** 1287-1303.

Wischik, C. M., Staff, R. T., Wischik, D. J., Bentham, P., Murray, A. D., Storey, J. M., Kook, K. A. & Harrington, C. R. (2015) Tau aggregation inhibitor therapy: an exploratory phase 2 study in mild or moderate Alzheimer's disease. *J Alzheimers Dis,* 44(2)**,** 705-20.

Wood, J. G., Jones, B. C., Jiang, N., Chang, C., Hosier, S., Wickremesinghe, P., Garcia, M., Hartnett, D. A., Burhenn, L., Neretti, N. & Helfand, S. L. (2016) Chromatin-modifying genetic interventions suppress age-associated transposable element activation and extend life span in Drosophila. *Proc Natl Acad Sci U S A,* 113(40)**,** 11277-11282.

Wood, J. G., Mirra, S. S., Pollock, N. J. & Binder, L. I. (1986) Neurofibrillary tangles of Alzheimer disease share antigenic determinants with the axonal microtubule-associated protein tau (tau). *Proc Natl Acad Sci U S A,* 83(11)**,** 4040-3.

Wu, J. W., Herman, M., Liu, L., Simoes, S., Acker, C. M., Figueroa, H., Steinberg, J. I., Margittai, M., Kayed, R., Zurzolo, C., Di Paolo, G. & Duff, K. E. (2013) Small misfolded Tau species are internalized via bulk endocytosis and anterogradely and retrogradely transported in neurons. *J Biol Chem,* 288(3)**,** 1856-70.

Xia, D., Li, C. & Gotz, J. (2015) Pseudophosphorylation of Tau at distinct epitopes or the presence of the P301L mutation targets the microtubule-associated protein Tau to dendritic spines. *Biochim Biophys Acta,* 1852(5)**,** 913-24.

Xu, Y., Jin, M. Z., Yang, Z. Y. & Jin, W. L. (2021) Microglia in neurodegenerative diseases. *Neural Regen Res,* 16(2)**,** 270-280.

Xu, Y., Martini-Stoica, H. & Zheng, H. (2016) A seeding based cellular assay of tauopathy. *Mol Neurodegener,* 11**,** 32.

Yanamandra, K., Kfoury, N., Jiang, H., Mahan, T. E., Ma, S., Maloney, S. E., Wozniak, D. F., Diamond, M. I. & Holtzman, D. M. (2013) Anti-tau antibodies that block tau aggregate seeding in vitro markedly decrease pathology and improve cognition in vivo. *Neuron,* 80(2)**,** 402-414.

Yang, X. & Qian, K. (2017) Protein O-GlcNAcylation: emerging mechanisms and functions. *Nat Rev Mol Cell Biol,* 18(7)**,** 452-465.

Ye, H., Han, Y., Li, P., Su, Z. & Huang, Y. (2022) The Role of Post-Translational Modifications on the Structure and Function of Tau Protein. *J Mol Neurosci,* 72(8)**,** 1557-1571.

Ye, J., Yin, Y., Yin, Y., Zhang, H., Wan, H., Wang, L., Zuo, Y., Gao, D., Li, M., Li, J., Liu, Y., Ke, D. & Wang, J. Z. (2020) Tau-induced upregulation of C/EBPbeta-TRPC1-SOCE signaling aggravates tauopathies: A vicious cycle in Alzheimer neurodegeneration. *Aging Cell,* 19(9)**,** e13209.

Yin, H. & Kuret, J. (2006) C-terminal truncation modulates both nucleation and extension phases of tau fibrillization. *FEBS Lett,* 580(1)**,** 211-5.

Yin, Y., Gao, D., Wang, Y., Wang, Z. H., Wang, X., Ye, J., Wu, D., Fang, L., Pi, G., Yang, Y., Wang, X. C., Lu, C., Ye, K. & Wang, J. Z. (2016) Tau accumulation induces synaptic impairment and memory deficit by calcineurin-mediated inactivation of nuclear CaMKIV/CREB signaling. *Proc Natl Acad Sci U S A,* 113(26)**,** E3773-81.

Yoshiyama, Y., Higuchi, M., Zhang, B., Huang, S. M., Iwata, N., Saido, T. C., Maeda, J., Suhara, T., Trojanowski, J. Q. & Lee, V. M. (2007) Synapse loss and microglial activation precede tangles in a P301S tauopathy mouse model. *Neuron,* 53(3)**,** 337-51.

Yu, C. J., Ma, D., Song, L. L., Zhai, Z. N., Tao, Y., Zhang, Y., Cai, L. Y., Hou, Y. H., Chen, H. Y. & Wang, L. (2020) The role of GLP-1/GIP receptor agonists in Alzheimer's disease. *Adv Clin Exp Med,* 29(6)**,** 661-668.

Yusuf, M., Leung, K., Morris, K. J. & Volpi, E. V. (2013) Comprehensive cytogenomic profile of the in vitro neuronal model SH-SY5Y. *Neurogenetics,* 14(1)**,** 63-70.

Yuzwa, S. A., Cheung, A. H., Okon, M., Mcintosh, L. P. & Vocadlo, D. J. (2014) O-GlcNAc modification of tau directly inhibits its aggregation without perturbing the conformational properties of tau monomers. *J Mol Biol,* 426(8)**,** 1736-52.

Yuzwa, S. A., Shan, X., Macauley, M. S., Clark, T., Skorobogatko, Y., Vosseller, K. & Vocadlo, D. J. (2012) Increasing O-GlcNAc slows neurodegeneration and stabilizes tau against aggregation. *Nat Chem Biol,* 8(4)**,** 393-9.

Yuzwa, S. A., Yadav, A. K., Skorobogatko, Y., Clark, T., Vosseller, K. & Vocadlo, D. J. (2011) Mapping O-GlcNAc modification sites on tau and generation of a site-specific O-GlcNAc tau antibody. *Amino Acids,* 40(3)**,** 857-68.

Zalipsky, S. (1995) Chemistry of polyethylene glycol conjugates with biologically active molecules. *Advanced Drug Delivery Reviews,* 16(2-3)**,** 157-182.

Zareba-Paslawska, J., Patra, K., Kluzer, L., Revesz, T. & Svenningsson, P. (2020) Tau Isoform-Driven CBD Pathology Transmission in Oligodendrocytes in Humanized Tau Mice. *Front Neurol,* 11**,** 589471.

Zempel, H., Thies, E., Mandelkow, E. & Mandelkow, E. M. (2010) Abeta oligomers cause localized Ca(2+) elevation, missorting of endogenous Tau into dendrites, Tau phosphorylation, and destruction of microtubules and spines. *J Neurosci,* 30(36)**,** 11938-50.

Zerovnik, E. (2010) Protein conformational pathology in Alzheimer's and other neurodegenerative diseases; new targets for therapy. *Curr Alzheimer Res,* 7(1)**,** 74-83.

Zhang, B., Carroll, J., Trojanowski, J. Q., Yao, Y., Iba, M., Potuzak, J. S., Hogan, A. M., Xie, S. X., Ballatore, C., Smith, A. B., 3rd, Lee, V. M. & Brunden, K. R. (2012) The microtubule-stabilizing agent, epothilone D, reduces axonal dysfunction, neurotoxicity, cognitive deficits, and Alzheimer-like pathology in an interventional study with aged tau transgenic mice. *J Neurosci,* 32(11)**,** 3601-11.

Zhang, C., Tang, N., Liu, X., Liang, W., Xu, W. & Torchilin, V. P. (2006a) siRNA-containing liposomes modified with polyarginine effectively silence the targeted gene. *J Control Release,* 112(2)**,** 229-39.

Zhang, H., Cao, Y., Ma, L., Wei, Y. & Li, H. (2021a) Possible Mechanisms of Tau Spread and Toxicity in Alzheimer's Disease. *Front Cell Dev Biol,* 9**,** 707268.

Zhang, W., Falcon, B., Murzin, A. G., Fan, J., Crowther, R. A., Goedert, M. & Scheres, S. H. (2019) Heparin-induced tau filaments are polymorphic and differ from those in Alzheimer's and Pick's diseases. *Elife,* 8.

Zhang, X. & Song, W. (2013) The role of APP and BACE1 trafficking in APP processing and amyloid-beta generation. *Alzheimers Res Ther,* 5(5)**,** 46.

Zhang, X., Zhang, X., Zhong, M., Zhao, P., Guo, C., Li, Y., Wang, T. & Gao, H. (2020) Selection of a d-Enantiomeric Peptide Specifically Binding to PHF6 for Inhibiting Tau Aggregation in Transgenic Mice. *ACS Chem Neurosci,* 11(24)**,** 4240-4253.

Zhang, X. X., Tian, Y., Wang, Z. T., Ma, Y. H., Tan, L. & Yu, J. T. (2021b) The Epidemiology of Alzheimer's Disease Modifiable Risk Factors and Prevention. *J Prev Alzheimers Dis,* 8(3)**,** 313-321.

Zhang, Y., Li, H. L., Wang, D. L., Liu, S. J. & Wang, J. Z. (2006b) A transitory activation of protein kinase-A induces a sustained tau hyperphosphorylation at multiple sites in N2a cells-imply a new mechanism in Alzheimer pathology. *J Neural Transm (Vienna),* 113(10)**,** 1487-97.

Zhang, Y. J., Xu, Y. F., Liu, X. H., Li, D., Yin, J., Liu, Y. H., Chen, X. Q. & Wang, J. Z. (2008) Carboxyl terminus of heat-shock cognate 70-interacting protein degrades tau regardless its phosphorylation status without affecting the spatial memory of the rats. *J Neural Transm (Vienna),* 115(3)**,** 483-91.

Zheng, X., Shao, X., Zhang, C., Tan, Y., Liu, Q., Wan, X., Zhang, Q., Xu, S. & Jiang, X. (2015) Intranasal H102 Peptide-Loaded Liposomes for Brain Delivery to Treat Alzheimer's Disease. *Pharm Res,* 32(12)**,** 3837-49.

Zhou, X., Vink, M., Klaver, B., Berkhout, B. & Das, A. T. (2006) Optimization of the Tet-On system for regulated gene expression through viral evolution. *Gene Ther,* 13(19)**,** 1382-90.

9. Appendix

9.1. Vectors for stable transfection of Clone 4 SH-SY5Y cells

9.1.1. 2N4R Tau$_{441}$ gene (homo sapiens), EcoRV, BamHI, Kozak, P301L mutation

GGTGGTGATATCGCCACCATGGCTGAGCCCCGCCAGGAGTTCGAAGTGATGGAAGATCACGCTGGGACGT
ACGGGTTGGGGGACAGGAAAGATCAGGGGGGCTACACCATGCACCAAGACCAAGAGGGTGACACGGACGC
TGGCCTGAAAGAATCTCCCCTGCAGACCCCCACTGAGGACGGATCTGAGGAACCGGGCTCTGAAACCTCT
GATGCTAAGAGCACTCCAACAGCGGAAGATGTGACAGCACCCTTAGTGGATGAGGGAGCTCCCGGCAAGC
AGGCTGCCGCGCAGCCCCACACGGAGATCCCAGAAGGAACCACAGCTGAAGAAGCAGGCATTGGAGACAC
CCCCAGCCTGGAAGACGAAGCTGCTGGTCACGTGACCCAAGCTCGCATGGTCAGTAAAAGCAAAGACGGG
ACTGGAAGCGATGACAAAAAAGCCAAGGGGGCTGATGGTAAAACGAAGATCGCCACACCGCGGGGAGCAG
CCCCTCCAGGCCAGAAGGGCCAGGCCAACGCCACCAGGATTCCAGCAAAAACCCCGCCCGCTCCAAAGAC
ACCACCCAGCTCTGGTGAACCTCCAAAATCAGGGGATCGCAGCGGCTACAGCAGCCCCGGCTCCCCAGGC
ACTCCCGGCAGCCGCTCCCGCACCCCGTCCCTTCCAACCCCACCCACCCGGGAGCCCAAGAAGGTGGCAG
TGGTCCGTACTCCACCCAAGTCGCCGTCTTCCGCCAAGAGCCGCCTGCAGACAGCCCCCGTGCCCATGCC
AGACCTGAAGAATGTCAAGTCCAAGATCGGCTCCACTGAGAACCTGAAGCACCAGCCGGGAGGCGGGAAG
GTGCAGATAATTAATAAGAAGCTGGATCTTAGCAACGTCCAGTCCAAGTGTGGCTCAAAGGATAATATCA
AACACGTCCTGGGAGGCGGCAGTGTGCAAATAGTCTACAAACCAGTTGACCTGAGCAAGGTGACCTCCAA
GTGTGGCTCATTAGGCAACATCCATCATAAACCAGGAGGTGGCCAGGTGGAAGTAAAATCTGAGAAGCTT
GACTTCAAGGACAGAGTCCAGTCGAAGATTGGGTCCCTGGACAATATCACCCACGTCCCTGGCGGAGGAA
ATAAAAAGATTGAAACCCACAAGCTGACCTTCCGCGAGAACGCCAAAGCCAAGACAGACCACGGGGCGGA
GATCGTGTACAAGTCGCCAGTGGTGTCTGGGGACACGTCTCCACGGCATCTCAGCAATGTCTCCTCCACC
GGCAGCATCGACATGGTAGACTCGCCCCAGCTCGCCACGCTAGCTGACGAGGTGTCTGCCTCCCTGGCCA
AGCAGGGTTTGTGAGGATCCGCG

9.1.2. pIRESneo3_Tet-On3G vector

gacggatcgggagatctcccgatcccctatggtgcactctcagtacaatctgctctgatgccgcatagttaagcc
agtatctgctccctgcttgtgtgttggaggtcgctgagtagtgcgcgagcaaaatttaagctacaacaaggcaag
gcttgaccgacaattgcatgaagaatctgcttagggttaggcgttttgcgctgcttcgcgatgtacgggccagat
atacgcgttgacattgattattgactagttattaatagtaatcaattacggggtcattagttcatagcccatata
tggagttccgcgttacataacttacggtaaatggcccgcctggctgaccgcccaacgacccccgcccattgacgt
caataatgacgtatgttcccatagtaacgccaatagggactttccattgacgtcaatgggtggagtatttacggt
aaactgcccacttggcagtacatcaagtgtatcatatgccaagtacgccccctattgacgtcaatgacggtaaat
ggcccgcctggcattatgcccagtacatgaccttatgggactttcctacttggcagtacatctacgtattagtca
tcgctattaccatggtgatgcggttttggcagtacatcaatgggcgtggatagcggtttgactcacggggatttc
caagtctccaccccattgacgtcaatgggagtttgttttggcaccaaaatcaacgggactttccaaaatgtcgta
acaactccgccccattgacgcaaatgggcggtaggcgtgtacggtgggaggtctatataagcagagctctctggc
taactagagaacccactgcttactggcttatcgaaattaatacgactcactatagggagacccaagcttggtacc
gagctcggatcgatatctgcggcctagctagccaccatgtctagactggacaagagcaaagtcataaactctgct
ctggaattactcaatggagtcggtatcgaaggcctgacgacaaggaaactcgctcaaaagctgggagttgagcag
cctaccctgtactggcacgtgaagaacaagcgggccctgctcgatgccctgccaatcgagatgctggacaggcat
catacccactcctgccccctggaaggcgagtcatggcaagactttctgcggaacaacgccaagtcataccgctgt
gctctcctctcacatcgcgacggggctaaagtgcatctcggcacccgcccaacagagaaacagtacgaaaccctg
gaaaatcagctcgcgttcctgtgtcagcaaggcttctccctggagaacgcactgtacgctctgtccgccgtgggc
cactttacactgggctgcgtattggaggaacaggagcatcaagtagcaaaagaggaaagagagacacctaccacc
gattctatgcccccacttctgaaacaagcaattgagctgttcgaccggcagggagccgaacctgccttccttttc
ggcctggaactaatcatatgtggcctggagaaacagctaaagtgcgaaagcggcgggccgaccgacgcccttgac
gattttgacttagacatgctcccagccgatgcccttgacgactttgaccttgatatgctgcctgctgacgctctt
gacgattttgaccttgacatgctccccgggtaagcggccgcatagataactgatccagtgtgctggaattaattc
gctgtctgcgagggccagctgttggggtgagtactccctctcaaaagcgggcatgacttctgcgctaagattgtc
agtttccaaaaacgaggaggatttgatattcacctggcccgcggtgatgcctttgagggtggccgcgtccatctg
gtcagaaaagacaatctttttgttgtcaagcttgaggtgtggcaggcttgagatctggccatacacttgagtgac
aatgacatccactttgcctttctctccacaggtgtccactcccaggtccaactgcaggtcgagcatgcatctagg

gcggccaattccgcccctctcccccccccccctctccctcccccccccctaacgttactggccgaagccgcttgg
aataaggccggtgtgcgtttgtctatatgttattttccaccatattgccgtcttttggcaatgtgagggcccgga
aacctggccctgtcttcttgacgagcattcctaggggtctttcccctctcgccaaaggaatgcaaggtctgttga
atgtcgtgaaggaagcagttcctctggaagcttcttgaagacaaacaacgtctgtagcgacccctttgcaggcagc
ggaaccccccacctggcgacaggtgcctctgcggccaaaagccacgtgtataagatacacctgcaaaggcggcac
aaccccagtgccacgttgtgagttggatagttgtggaaagagtcaaatggctctcctcaagcgtattcaacaagg
ggctgaaggatgcccagaaggtaccccattgtatgggatctgatctggggcctcggtgcacatgctttacatgtg
tttagtcgaggttaaaaaaacgtctaggccccccgaaccacggggacgtggttttcctttgaaaaacacgatgat
aagcttgccacaacccgggataattcctgcagccaatatgggatcggccattgaacaagatggattgcacgcagg
ttctccggccgcttgggtggagaggctattcggctatgactgggcacaacagacaatcggctgctctgatgccgc
cgtgttccggctgtcagcgcaggggcgcccggttctttttgtcaagaccgacctgtccggtgccctgaatgaact
gcaggacgaggcagcgcggctatcgtggctggccacgacgggcgttccttgcgcagctgtgctcgacgttgtcac
tgaagcgggaagggactggctgctattgggcgaagtgccggggcaggatctcctgtcatctcaccttgctcctgc
cgagaaagtatccatcatggctgatgcaatgcggcggctgcatacgcttgatccggctacctgcccattcgacca
ccaagcgaaacatcgcatcgagcgagcacgtactcggatggaagccggtcttgtcgatcaggatgatctggacga
agagcatcaggggctcgcgccagccgaactgttcgccaggctcaaggcgcgcatgcccgacggcgatgatctcgt
cgtgacccatggcgatgcctgcttgccgaatatcatggtggaaaatggccgcttttctggattcatcgactgtgg
ccggctgggtgtggcggaccgctatcaggacatagcgttggctacccgtgatattgctgaagagcttggcggcga
atgggctgaccgcttcctcgtgctttacggtatcgccgctcccgattcgcagcgcatcgccttctatcgccttct
tgacgagttcttctgaggggatcaattctctagataactgatcataatcagccataccacatttgtagaggtttt
acttgctttaaaaaacctcccacacctcccccctgaacctgaaacataaaatgaatgcaattgttgttgttaactt
gtttattgcagcttataatggttacaaataaagcaatagcatcacaaatttcacaaataaagcatttttttcact
gcattctagttgtggtttgtccaaactcatcaatgtatcttaacgcgtcgagtgcattctagttgtggtttgtcc
aaactcatcaatgtatcttatcatgtctgtataccgtcgacctctagctagagcttggcgtaatcatggtcatag
ctgtttcctgtgtgaaattgttatccgctcacaattccacacaacatacgagccggaagcataaagtgtaaagcc
tggggtgcctaatgagtgagctaactcacattaattgcgttgcgctcactgcccgctttccagtcgggaaacctg
tcgtgccagctgcattaatgaatcggccaacgcgcggggagaggcggtttgcgtattgggcgctcttccgcttcc
tcgctcactgactcgctgcgctcggtcgttcggctgcggcgagcggtatcagctcactcaaaggcggtaatacgg
ttatccacagaatcaggggataacgcaggaaagaacatgtgagcaaaaggccagcaaaaggccaggaaccgtaaa
aaggccgcgttgctggcgtttttccataggctccgccccctgacgagcatcacaaaaatcgacgctcaagtcag
aggtggcgaaacccgacaggactataaagataccaggcgtttccccctggaagctccctcgtgcgctctcctgtt
ccgaccctgccgcttaccggatacctgtccgcctttctcccttcgggaagcgtggcgctttctcatagctcacgc
tgtaggtatctcagttcggtgtaggtcgttcgctccaagctgggctgtgtgcacgaacccccgttcagcccgac
cgctgcgccttatccggtaactatcgtcttgagtccaacccggtaagacacgacttatcgccactggcagcagcc
actggtaacaggattagcagagcgaggtatgtaggcggtgctacagagttcttgaagtggtggcctaactacggc
tacactagaagaacagtatttggtatctgcgctctgctgaagccagttaccttcggaaaaagagttggtagctct
tgatccggcaaacaaaccaccgctggtagcggtggttttttgtttgcaagcagcagattacgcgcagaaaaaaa
ggatctcaagaagatcctttgatcttttctacggggtctgacgctcagtggaacgaaaactcacgttaagggatt
ttggtcatgagattatcaaaaaggatcttcacctagatccttttaaattaaaaatgaagttttaaatcaatctaa
agtatatatgagtaaacttggtctgacagttaccaatgcttaatcagtgaggcacctatctcagcgatctgtcta
tttcgttcatccatagttgcctgactccccgtcgtgtagataactacgatacgggagggcttaccatctggcccc
agtgctgcaatgataccgcgagacccacgctcaccggctccagatttatcagcaataaaccagccagccggaagg
gccgagcgcagaagtggtcctgcaactttatccgcctccatccagtctattaattgttgccgggaagctagagta
agtagttcgccagttaatagtttgcgcaacgttgttgccattgctacaggcatcgtggtgtcacgctcgtcgttt
ggtatggcttcattcagctccggttcccaacgatcaaggcgagttacatgatcccccatgttgtgcaaaaaagcg
gttagctccttcggtcctccgatcgttgtcagaagtaagttggccgcagtgttatcactcatggttatggcagca
ctgcataattctcttactgtcatgccatccgtaagatgcttttctgtgactggtgagtactcaaccaagtcattc
tgagaatagtgtatgcggcgaccgagttgctcttgcccggcgtcaatacgggataataccgcgccacatagcaga
actttaaaagtgctcatcattggaaaacgttcttcggggcgaaaactctcaaggatcttaccgctgttgagatcc
agttcgatgtaacccactcgtgcacccaactgatcttcagcatcttttactttcaccagcgtttctgggtgagca
aaaacaggaaggcaaaatgccgcaaaaaagggaataagggcgacacggaaatgttgaatactcatactcttcctt
tttcaatattattgaagcatttatcagggttattgtctcatgagcggatacatatttgaatgtatttagaaaaat
aaacaaatagggttccgcgcacatttccccgaaaagtgccacctgacgtc

9.1.3. pTRE3G-mCherry_Tau$_{441}$ P301L vector

ctcgagtttactccctatcagtgatagagaacgtatgaagagtttactccctatcagtgatagagaacgtatgca
gactttactccctatcagtgatagagaacgtataaggagtttactccctatcagtgatagagaacgtatgaccag
tttactccctatcagtgatagagaacgtatctacagtttactccctatcagtgatagagaacgtatatccagttt
actccctatcagtgatagagaacgtataagctttaggcgtgtacggtgggcgcctataaaagcagagctcgttta
gtgaaccgtcagatcgcctggagcaattccacaacacttttgtcttataccaactttccgtaccacttcctaccc
tcgtaaagtcgacatggtgagcaagggcgaggaggataacatggccatcatcaaggagttcatgcgcttcaaggt
gcacatggagggctccgtgaacggccacgagttcgagatcgagggcgagggcgagggccgcccctacgagggcac
ccagaccgccaagctgaaggtgaccaagggtggccccctgcccttcgcctgggacatcctgtcccctcagttcat
gtacggctccaaggcctacgtgaagcaccccgccgacatccccgactacttgaagctgtccttccccgagggctt
caagtgggagcgcgtgatgaacttcgaggacggcggcgtggtgaccgtgacccaggactcctccctgcaggacgg
cgagttcatctacaaggtgaagctgcgcggcaccaacttcccctccgacggccccgtaatgcagaagaagaccat
gggctgggaggcctcctccgagcggatgtaccccgaggacggcgccctgaagggcgagatcaagcagaggctgaa
gctgaaggacggcggccactacgacgctgaggtcaagaccacctacaaggccaagaagcccgtgcagctgcccgg
cgcctacaacgtcaacatcaagttggacatcacctcccacaacgaggactacaccatcgtggaacagtacgaacg
cgccgagggccgccactccaccggcggcatggacgagctgtacaagtagcggccggcccctctccctcccccccc
ccctaacgttactggccgaagccgcttggaataaggccggtgtgcgtttgtctatatgttattttccaccatatt
gccgtcttttggcaatgtgagggcccggaaacctggccctgtcttcttgacgagcattcctaggggtctttcccc
tctcgccaaaggaatgcaaggtctgttgaatgtcgtgaaggaagcagttcctctggaagcttcttgaagacaaac
aacgtctgtagcgacccttgcaggcagcggaacccccacctggcgacaggtgcctctgcggccaaaagccacg
tgtataagatacacctgcaaaggcggcacaaccccagtgccacgttgtgagttggatagttgtggaaagagtcaa
atggctctcctcaagcgtattcaacaaggggctgaaggatgcccagaaggtaccccattgtatgggatctgatct
ggggcctcggtacacatgctttacatgtgtttagtcgaggttaaaaaaacgtctaggccccccgaaccacgggga
cgtggttttcctttgaaaaacacgatgataatatggccacaaccgggccggatatcgccaccatggctgagcccc
gccaggagttcgaagtgatggaagatcacgctgggacgtacgggttgggggacaggaaagatcaggggggctaca
ccatgcaccaagaccaagagggtgacacggacgctggcctgaaagaatctcccctgcagacccccactgaggacg
gatctgaggaaccgggctctgaaacctctgatgctaagagcactccaacagcggaagatgtgacagcacccttag
tggatgagggagctcccggcaagcaggctgccgcgcagccccacacggagatcccagaaggaaccacagctgaag
aagcaggcattggagacacccccagcctggaagacgaagctgctggtcacgtgacccaagctcgcatggtcagta
aaagcaaagacgggactggaagcgatgacaaaaaagccaaggggctgatggtaaaacgaagatcgccacaccgc
ggggagcagcccctccaggccagaagggccaggccaacgccaccaggattccagcaaaaaccccgcccgctccaa
agacaccacccagctctggtgaacctccaaaatcaggggatcgcagcggctacagcagccccggctccccaggca
ctcccggcagccgctcccgcaccccgtcccttccaaccccacccacccgggagcccaagaaggtggcagtggtcc
gtactccacccaagtcgccgtcttccgccaagagccgcctgcagacagcccccgtgcccatgccagacctgaaga
atgtcaagtccaagatcggctccactgagaacctgaagcaccagccgggaggcgggaaggtgcagataattaata
agaagctggatcttagcaacgtccagtccaagtgtggctcaaaggataatatcaaacacgtcctgggaggcggca
gtgtgcaaatagtctacaaaccagttgacctgagcaaggtgacctccaagtgtggctcattaggcaacatccatc
ataaaccaggaggtggccaggtggaagtaaaatctgagaagcttgacttcaaggacagagtccagtcgaagattg
ggtccctggacaatatcacccacgtccctggcggaggaaataaaaagattgaaacccacaagctgaccttccgcg
agaacgccaaagccaagacagaccacggggcggagatcgtgtacaagtcgccagtggtgtctggggacacgtctc
cacggcatctcagcaatgtctcctccaccggcagcatcgacatggtagactcgccccagctcgccacgctagctg
acgaggtgtctgcctccctggccaagcagggtttgtgaggatccaatgtaactgtattcagcgatgacgaaattc
ttagctattgtaatactctagaggatctttgtgaaggaaccttacttctgtggtgtgacataattggacaaacta
cctacagagatttaaagctctaaggtaaatataaaatttttaagtgtataatgtgttaaactactgattctaatt
gtttgtgtattttagattccaacctatggaactgatgaatgggagcagtggtggaatgcctttaatgaggaaaac
ctgttttgctcagaagaaatgccatctagtgatgatgaggctactgctgactctcaacattctactcctccaaaa
aagaagagaaaggtagaagaccccaaggactttccttcagaattgctaagtttttttgagtcatgctgtgtttagt
aatagaactcttgcttgctttgctatttacaccacaaaggaaaaagctgcactgctatacaagaaaattatggaa
aaatattctgtaacctttataagtaggcataacagttataatcataacatactgtttttttcttactccacacagg
catagagtgtctgctattaataactatgctcaaaaattgtgtacctttagctttttaatttgtaaaggggttaat
aaggaatatttgatgtatagtgccttgactagagatcataatcagccataccacatttgtagaggttttacttgc
tttaaaaaacctcccacacctcccccctgaacctgaaacataaaatgaatgcaattgttgttgttaacttgtttat
tgcagcttataatggttacaaataaagcaatagcatcacaaatttcacaaataaagcatttttttcactgcattc
tagttgtggtttgtccaaactcatcaatgtatcttatcatgtctgcggctctagagctgcattaatgaatcggcc
aacgcgcggggagaggcggtttgcgtattgggcgctcttccgcttcctcgctcactgactcgctgcgctcggtcg

ttcggctgcggcgagcggtatcagctcactcaaaggcggtaatacggttatccacagaatcaggggataacgcag
gaaagaacatgtgagcaaaaggccagcaaaaggccaggaaccgtaaaaaggccgcgttgctggcgtttttccata
ggctccgccccccctgacgagcatcacaaaaatcgacgctcaagtcagaggtggcgaaacccgacaggactataaa
gataccaggcgtttcccccctggaagctccctcgtgcgctctcctgttccgaccctgccgcttaccggatacctgt
ccgcctttctcccttcgggaagcgtggcgctttctcatagctcacgctgtaggtatctcagttcggtgtaggtcg
ttcgctccaagctgggctgtgtgcacgaaccccccgttcagcccgaccgctgcgccttatccggtaactatcgtc
ttgagtccaacccggtaagacacgacttatcgccactggcagcagccactggtaacaggattagcagagcgaggt
atgtaggcggtgctacagagttcttgaagtggtggcctaactacggctacactagaagaacagtatttggtatct
gcgctctgctgaagccagttaccttcggaaaaagagttggtagctcttgatccggcaaacaaaccaccgctggta
gcggtggtttttttgtttgcaagcagcagattacgcgcagaaaaaaaggatctcaagaagatcctttgatctttt
ctacggggtctgacgctcagtggaacgaaaactcacgttaagggattttggtcatgagattatcaaaaaggatct
tcacctagatccttttaaattaaaaatgaagttttaaatcaatctaaagtatatatgagtaaacttggtctgaca
gttaccaatgcttaatcagtgaggcacctatctcagcgatctgtctatttcgttcatccatagttgcctgactcc
ccgtcgtgtagataactacgatacgggagggcttaccatctggccccagtgctgcaatgataccgcgagacccac
gctcaccggctccagatttatcagcaataaaccagccagccggaagggccgagcgcagaagtggtcctgcaactt
tatccgcctccatccagtctattaattgttgccgggaagctagagtaagtagttcgccagttaatagtttgcgca
acgttgttgccattgctacaggcatcgtggtgtcacgctcgtcgtttggtatggcttcattcagctccggttccc
aacgatcaaggcgagttacatgatcccccatgttgtgcaaaaaagcggttagctccttcggtcctccgatcgttg
tcagaagtaagttggccgcagtgttatcactcatggttatggcagcactgcataattctcttactgtcatgccat
ccgtaagatgcttttctgtgactggtgagtactcaaccaagtcattctgagaatagtgtatgcggcgaccgagtt
gctcttgcccggcgtcaatacgggataataccgcgccacatagcagaactttaaaagtgctcatcattggaaaac
gttcttcggggcgaaaactctcaaggatcttaccgctgttgagatccagttcgatgtaacccactcgtgcaccca
actgatcttcagcatcttttactttcaccagcgtttctgggtgagcaaaaacaggaaggcaaaatgccgcaaaaa
agggaataagggcgacacggaaatgttgaatactcatactcttccttttcaatattattgaagcatttatcagg
gttattgtctcatgagcggatacatatttgaatgtatttagaaaaataaacaaatagggttccgcgcacatttc
cccgaaaagtgccacctgacgtctaagaaaccattattatcatgacattaacctataaaaataggcgtatcacga
ggccctttcgtcttcaagaattc

9.2. Selection of Clone 4 SH-SY5Y cells

9.2.1. Verification of Tet-On 3G expression

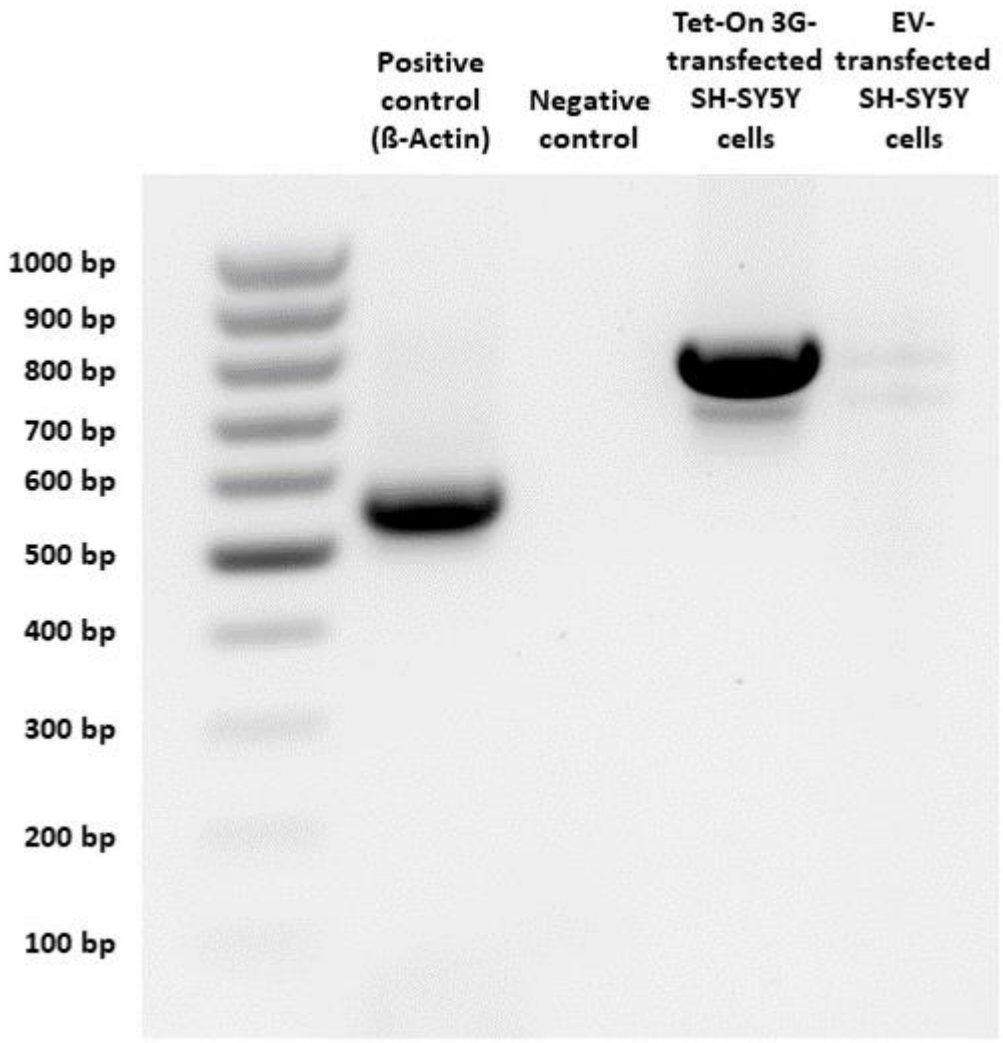

Figure 9.1: Tet-On 3G expression by SH-SY5Y_Tet-On3G cells following stable transfection. SH-SY5Y cells were transfected with pIRESneo3_Tet-On3G or empty vector (EV; pIRESneo3) and selected in the presence of 500 µg/mL G418 in the culture medium. RNA of the resulting polyclonal cell lines was purified, then reverse-transcribed to cDNA using forward and reverse primers for Tet-On 3G (746 bp). Shown is an agarose gel loaded with mouse liver RNA amplified with mouse β-Actin primers (540 bp; lane 1), RNA eluent (RNAse-free water) amplified with Tet-On 3G primers (lane 2) and either RNA derived from pIRESneo3_Tet-On3G- or empty vector-transfected SH-SY5Y cells amplified with Tet-On 3G primers (lane 3 and 4, respectively).

9.2.2. Confirmation of Dox-induced mCherry expression

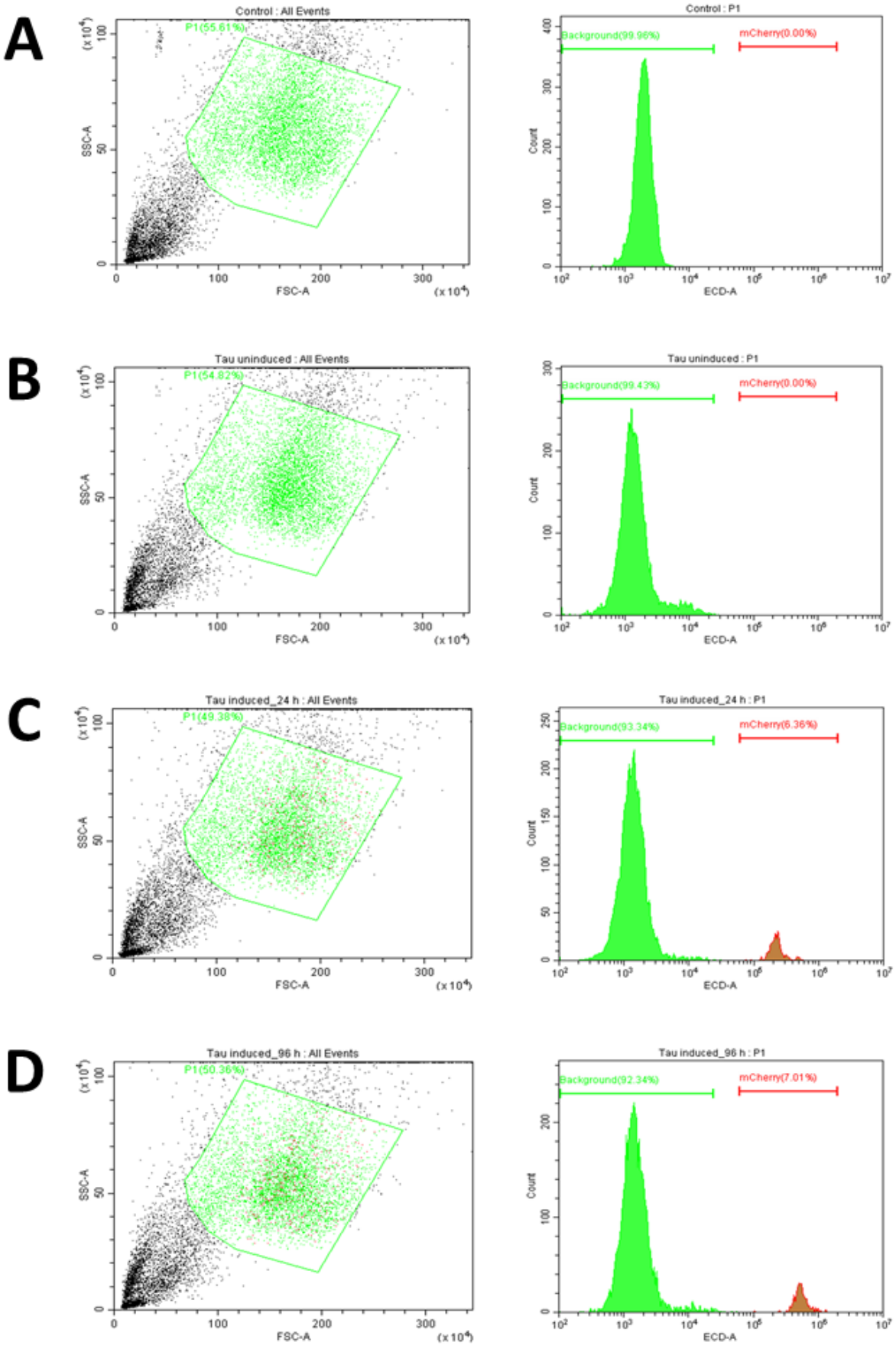

Figure 9.2: Dox-induced mCherry expression of polyclonal SH-SY5Y_Tet-On3G_Tau$_{441}$ P301L cells. SH-SY5Y cells were stably transfected with pIRESneo3_Tet-On3G vector DNA and selected by supplementation of the growth medium with 500 µg/mL G418, followed by stable transfection and selection using pTRE3G-mCherry_Tau$_{441}$ P301L plasmid DNA and 150 µg/mL Hygromycin B. The resulting SH-SY5Y_Tet-On3G_Tau$_{441}$ P301L cell line was cultivated in Dox-free medium and induced using 500 ng/µL Dox, followed by flow cytometry analysis. Shown are cell gating to exclude cell debris and clumps (forward scatter FSC-A versus side scatter SSC-A; left panels) and proportions of non-fluorescing (background) and mCherry-expressing cells (cell count versus fluorescence intensity ECD-A; right panels) of (A) untransfected SH-SY5Y cells, (B) SH-SY5Y_Tet-On3G_Tau$_{441}$ P301L cells in Dox-free medium and SH-SY5Y_Tet-On3G_Tau$_{441}$ P301L cells induced with Dox for 24 h (mCherry expression in 6.36 % of cells; C) and 96 h (mCherry expression in 7.01 % of cells; D). Notably, the ECD-A filter set ($\lambda_{Ex/Em}$ = 610/620 nm) poorly excites mCherry ($\lambda_{Ex/Em}$ = 587/610 nm), suggesting that the proportion of mCherry-expressing SH-SY5Y_Tet-On3G_Tau$_{441}$ P301L cells was underestimated.

9.3. Cell viability of SH-SY5Y cells following Dox as well as RI-AG03-polyR or scrambled RI-AG03-polyR exposure

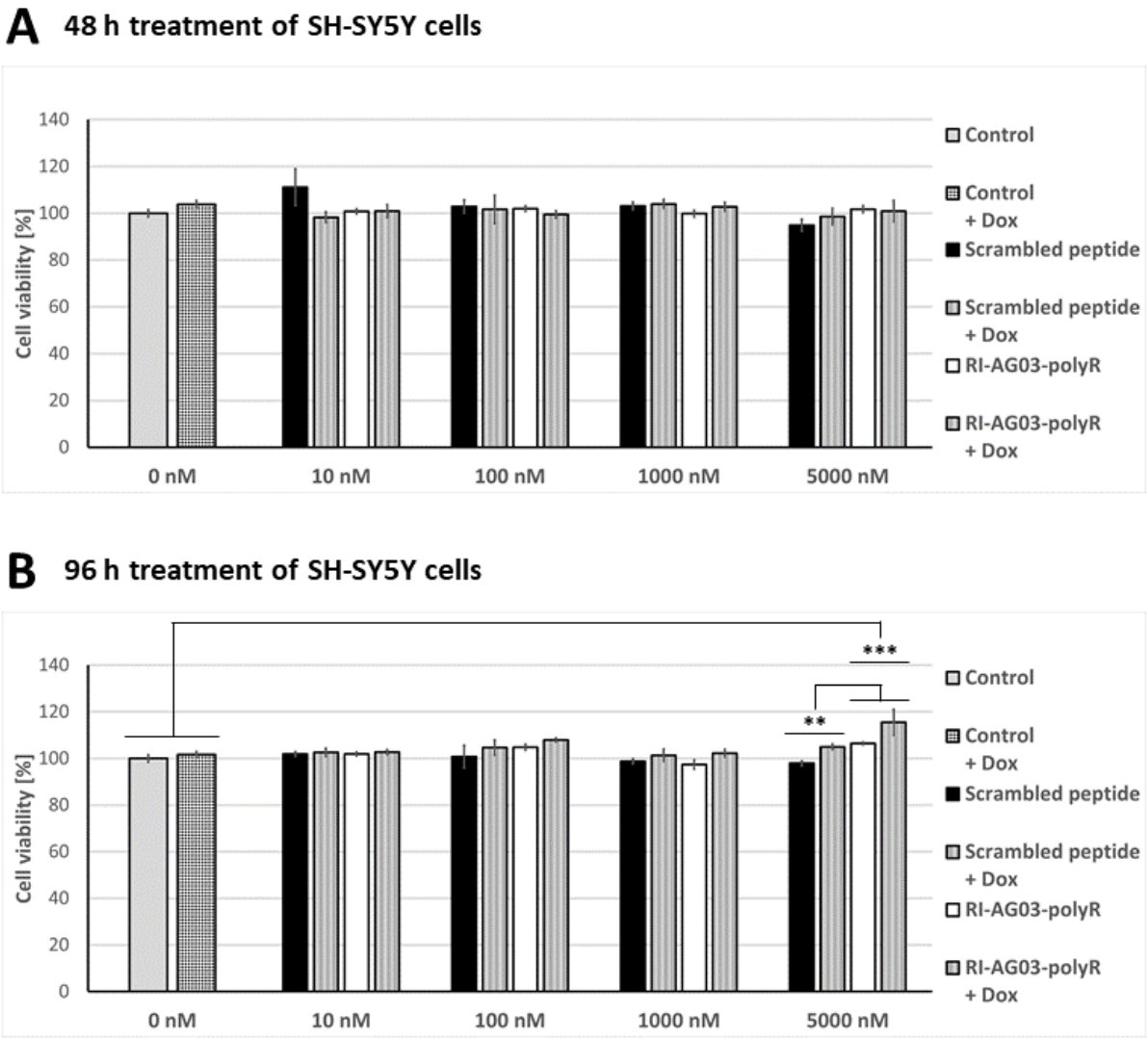

Figure 9.3: Impact of Dox and peptide treatments on the viability of SH-SY5Y cells. Cell viability of SH-SY5Y cells, as measured by the colorimetric conversion of WST-8, was assessed in the absence and presence of 500 ng/mL Dox and 10 - 5000 nM scrambled RI-AG03-polyR or RI-AG03-polyR peptide treatments for 48 h (A) and 96 h (B). Depicted is the mean ± SEM % of cell viability compared to fully untreated SH-SY5Y cells (n = 6 technical replicates; separate cell wells/flasks treated at the same time). Statistical testing involving three-way ANOVA followed by Tukey's post hoc showed that 5000 nM RI-AG03-polyR, but not a scrambled control peptide, significantly increased cell viability independent of Dox treatment (96 h). ** = $p < 0.01$ and *** = $p < 0.001$.

9.4. Cellular toxicity of unconjugated liposomes, peptide-conjugated liposomes and endocytosis inhibitors

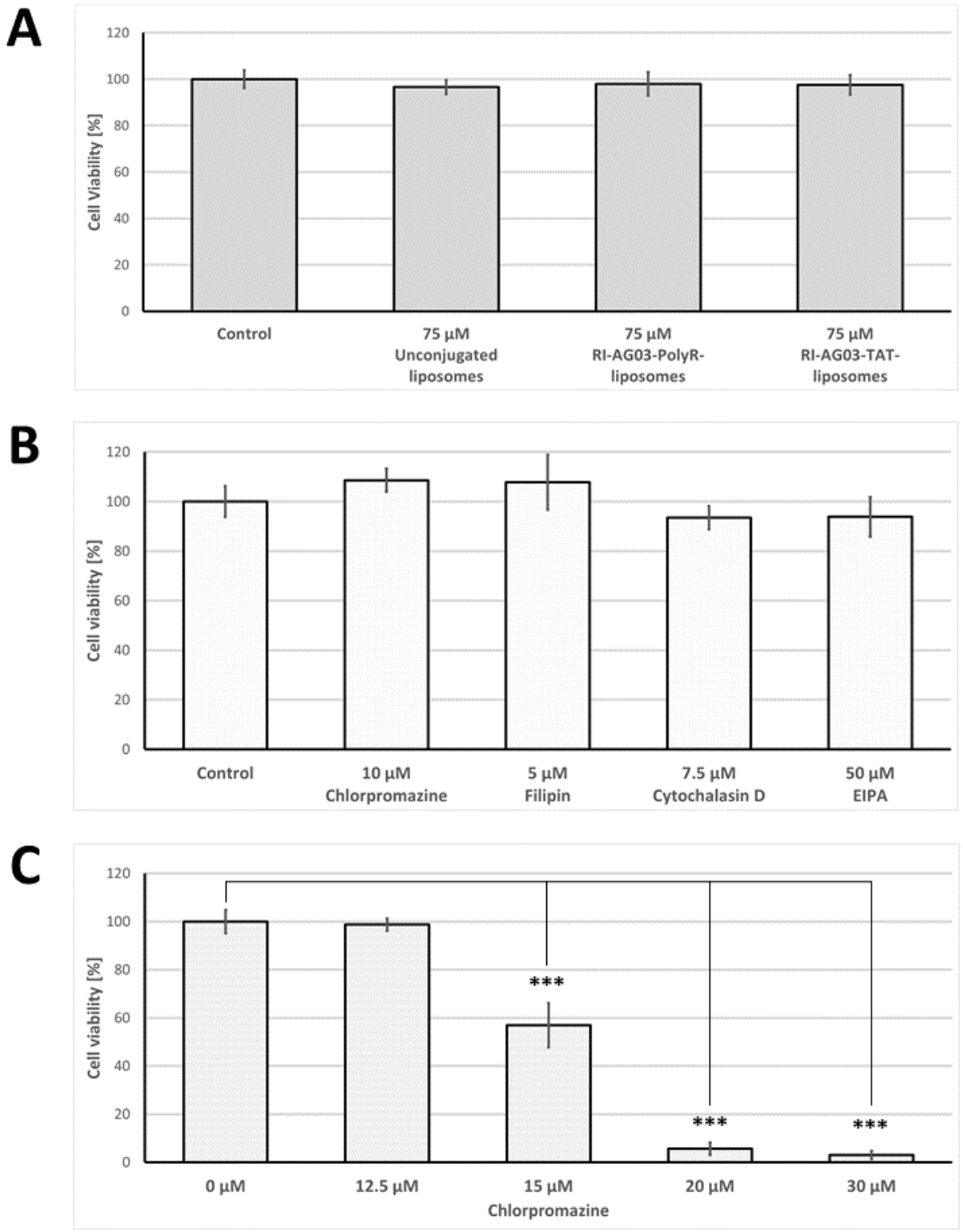

Figure 9.4: Toxicity of unconjugated liposomes, peptide-liposomes and endocytosis inhibitors used to study cellular uptake pathways. SH-SY5Y cells were treated with the indicated final

concentrations of unconjugated liposomes, RI-AG03-polyR-liposomes or RI-AG03-TAT-liposomes (A), various endocytosis inhibitors (B) or increasing Chlorpromazine concentrations (C) for 4.5 h. Shown is the average ± SEM % of cell viability relative to vehicle-treated control cells (n = 6 technical replicates; separate cell wells/flasks treated at the same time), as assessed by the colorimetric conversion of WST-8. One-way ANOVA and Tukey's Post-Hoc tests were applied to calculate significant differences. *** = $p < 0.001$.

9.5. Individual channels of the immunocytochemistry images in chapter 5

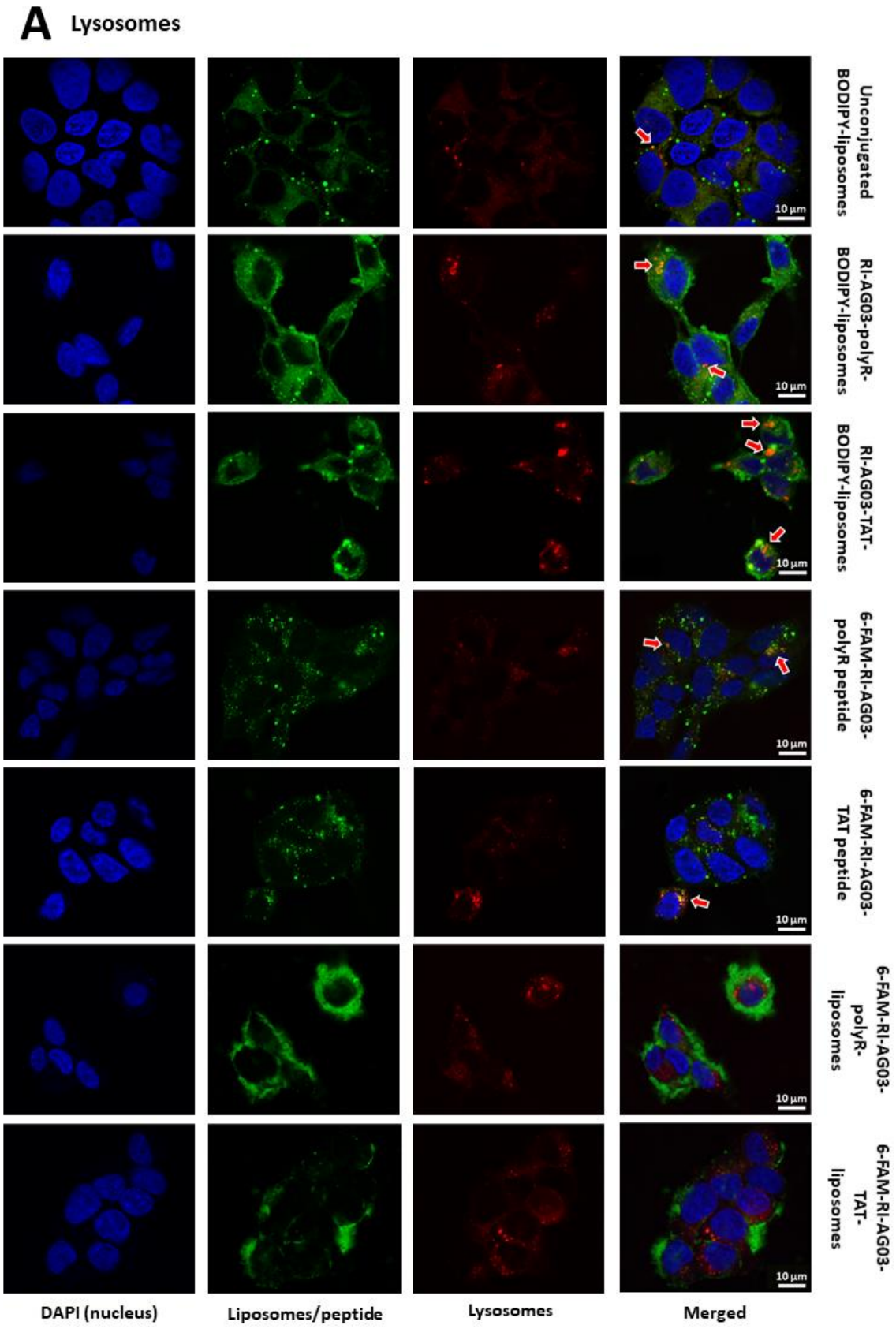

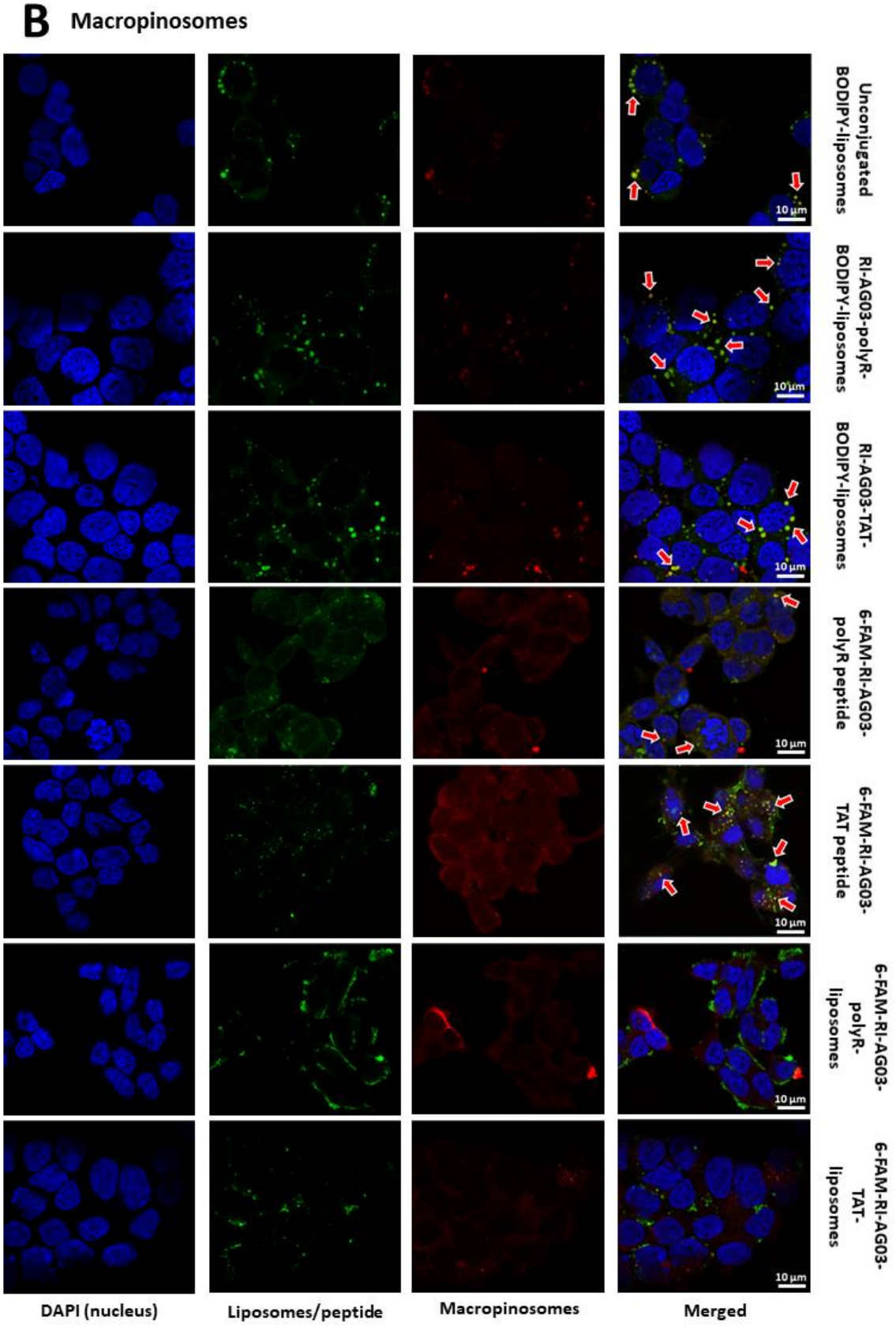
B Macropinosomes
Unconjugated BODIPY-liposomes
RI-AG03-polyR-BODIPY-liposomes
RI-AG03-TAT-BODIPY-liposomes
6-FAM-RI-AG03-polyR peptide
6-FAM-RI-AG03-TAT peptide
6-FAM-RI-AG03-polyR-liposomes
6-FAM-RI-AG03-TAT-liposomes
10 µm
DAPI (nucleus)
Liposomes/peptide
Macropinosomes
Merged

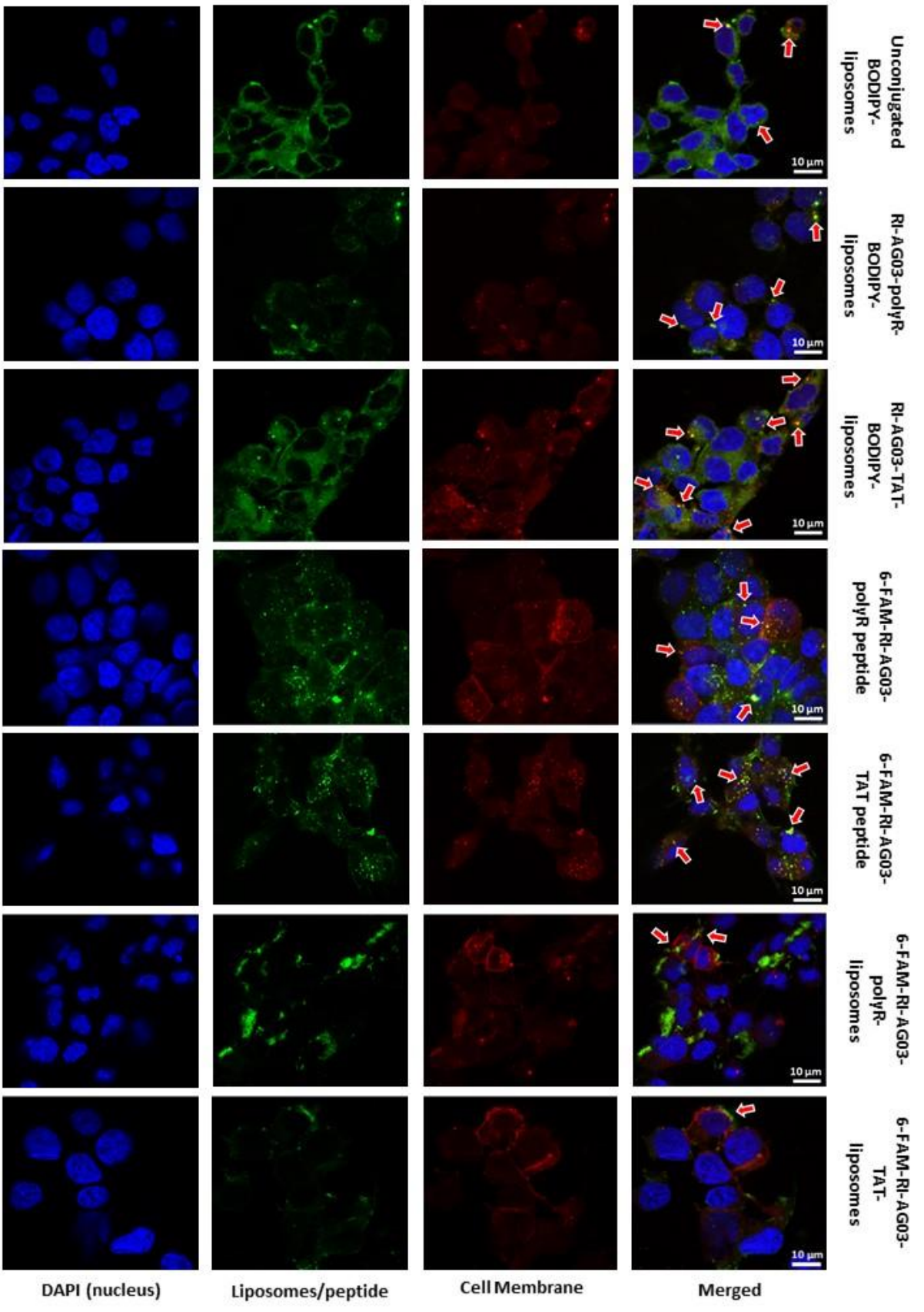
C Cell Membrane
Unconjugated BODIPY-liposomes
RI-AG03-polyR-BODIPY-liposomes
RI-AG03-TAT-BODIPY-liposomes
6-FAM-RI-AG03-polyR peptide
6-FAM-RI-AG03-TAT peptide
6-FAM-RI-AG03-polyR-liposomes
6-FAM-RI-AG03-TAT-liposomes
10 µm
DAPI (nucleus)
Liposomes/peptide
Cell Membrane
Merged

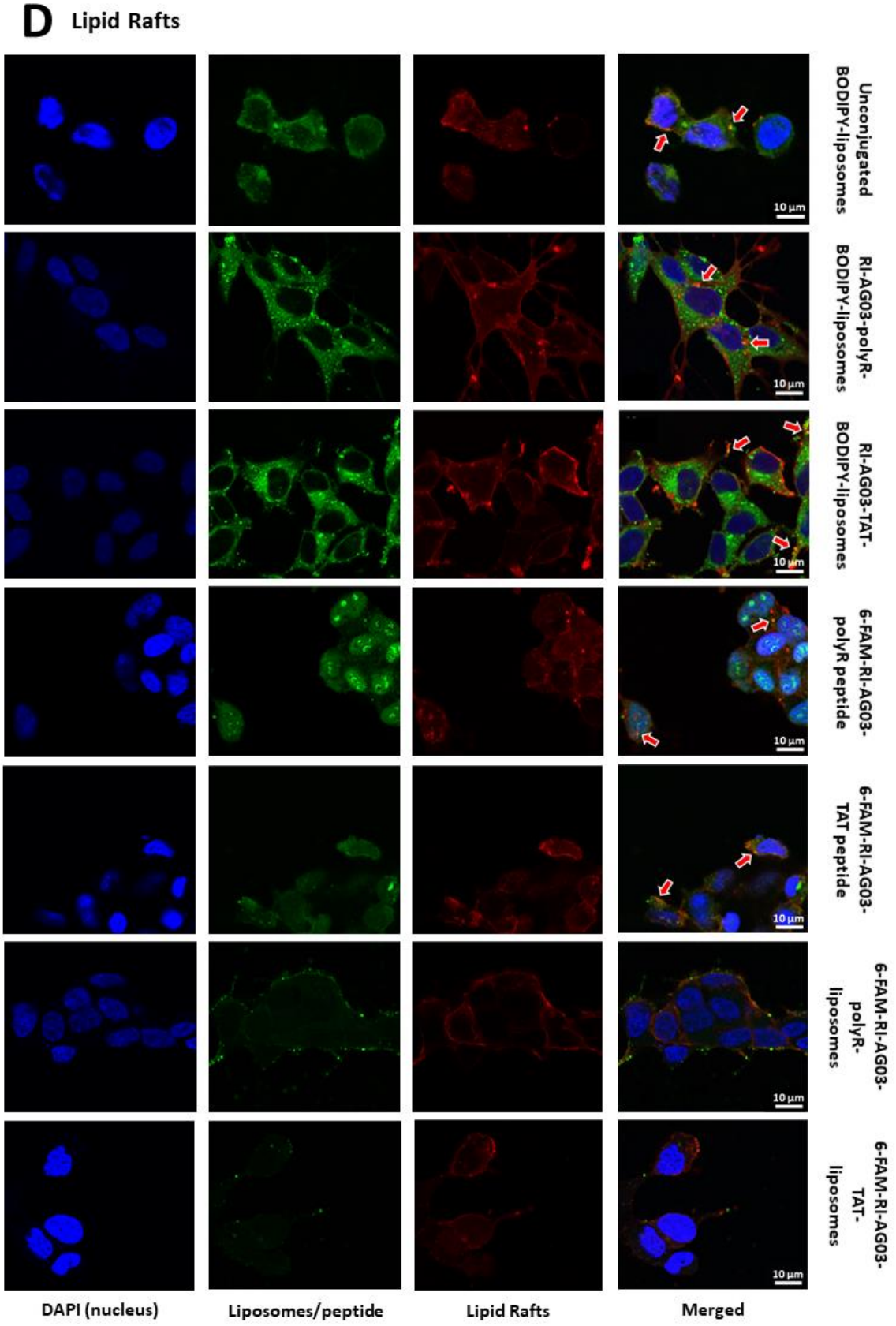
D Lipid Rafts
Unconjugated BODIPY-liposomes
RI-AG03-polyR-BODIPY-liposomes
RI-AG03-TAT-BODIPY-liposomes
6-FAM-RI-AG03-polyR peptide
6-FAM-RI-AG03-TAT peptide
6-FAM-RI-AG03-polyR-liposomes
6-FAM-RI-AG03-TAT-liposomes
10 µm
DAPI (nucleus)
Liposomes/peptide
Lipid Rafts
Merged

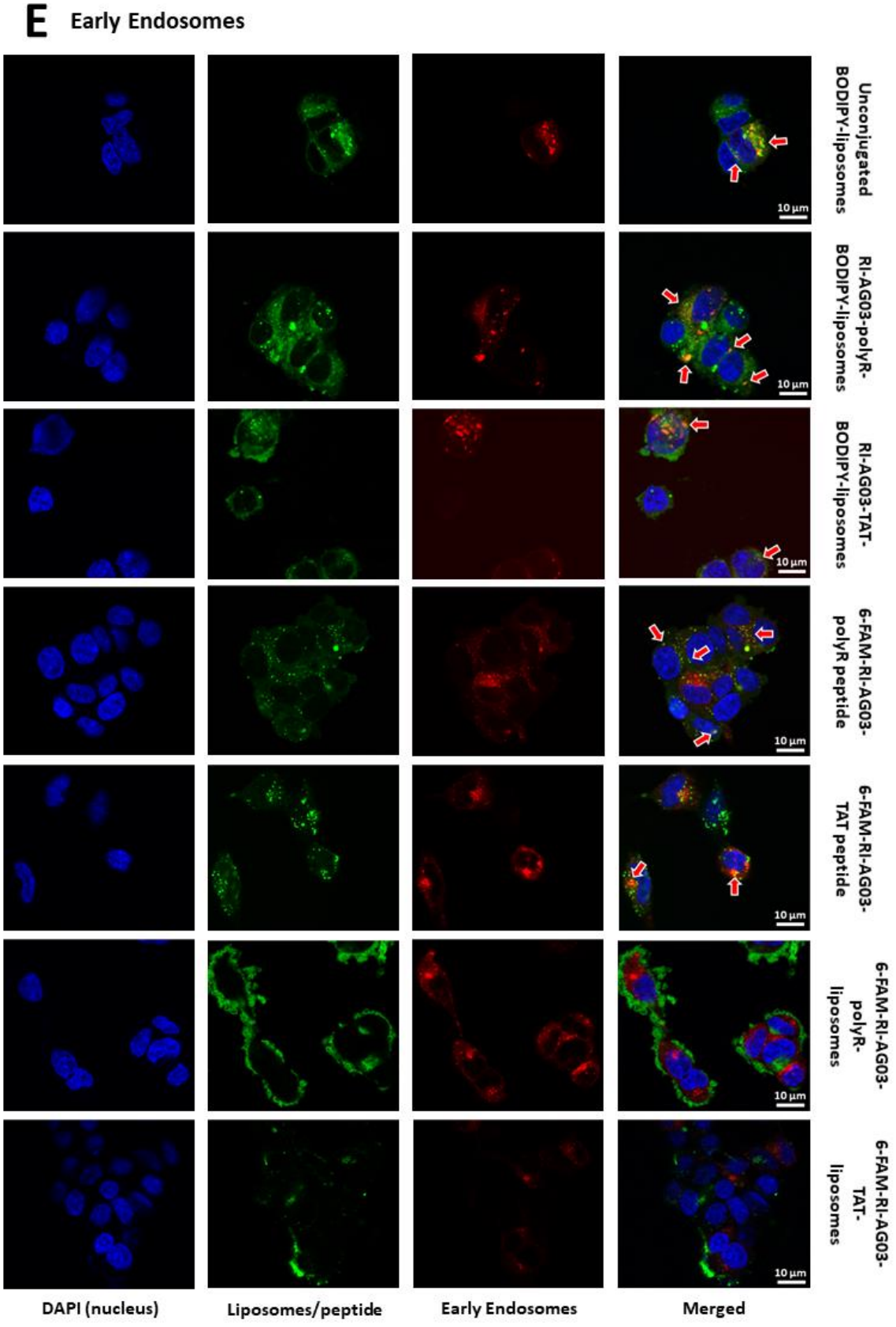
E
Early Endosomes
Unconjugated BODIPY-liposomes
RI-AG03-polyR-BODIPY-liposomes
RI-AG03-TAT-BODIPY-liposomes
6-FAM-RI-AG03-polyR peptide
6-FAM-RI-AG03-TAT peptide
6-FAM-RI-AG03-polyR-liposomes
6-FAM-RI-AG03-TAT-liposomes
10 µm
DAPI (nucleus)
Liposomes/peptide
Early Endosomes
Merged

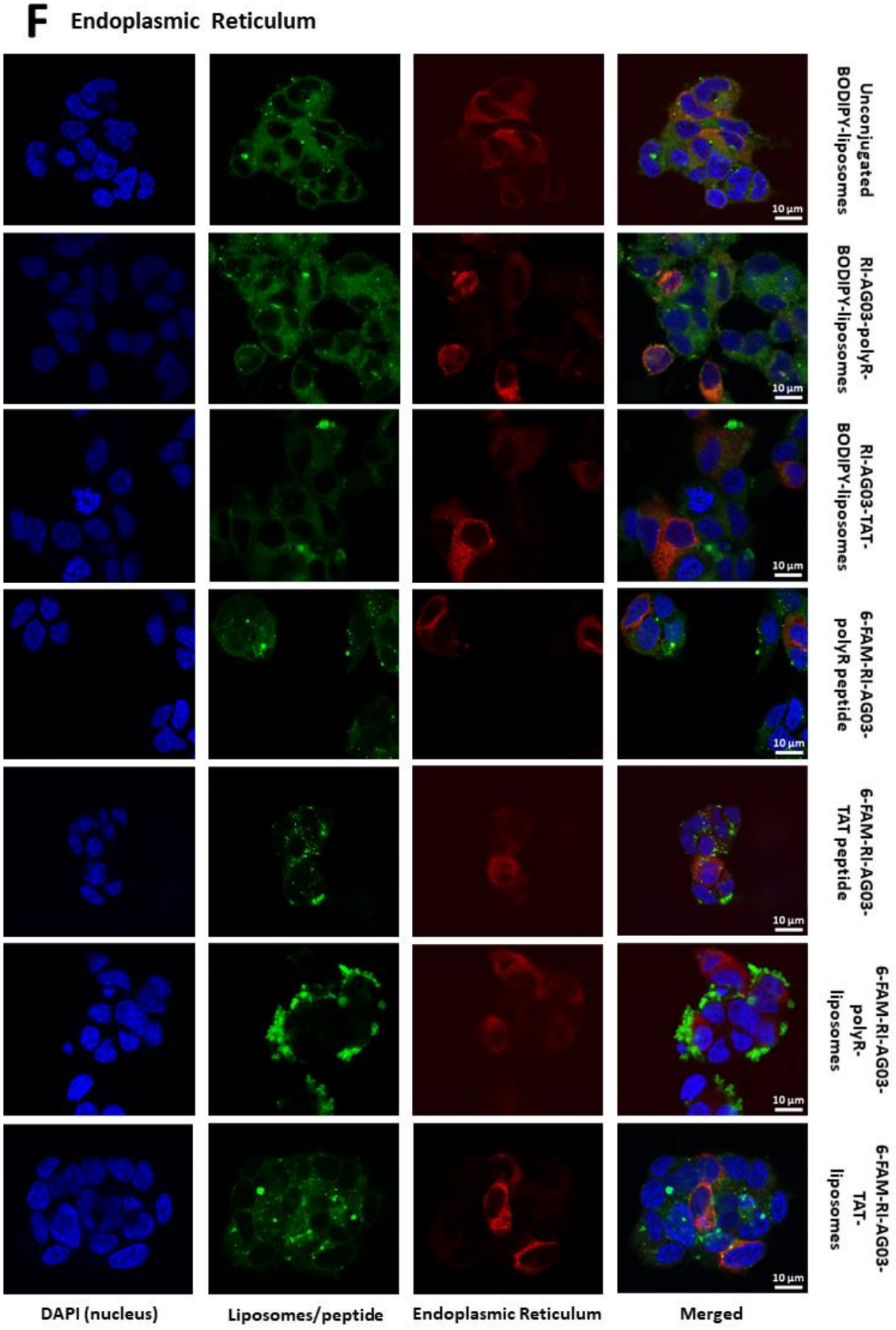
F Endoplasmic Reticulum
Unconjugated BODIPY-liposomes
RI-AG03-polyR-BODIPY-liposomes
RI-AG03-TAT-BODIPY-liposomes
6-FAM-RI-AG03-polyR peptide
6-FAM-RI-AG03-TAT peptide
6-FAM-RI-AG03-polyR-liposomes
6-FAM-RI-AG03-TAT-liposomes
10 µm
DAPI (nucleus)
Liposomes/peptide
Endoplasmic Reticulum
Merged

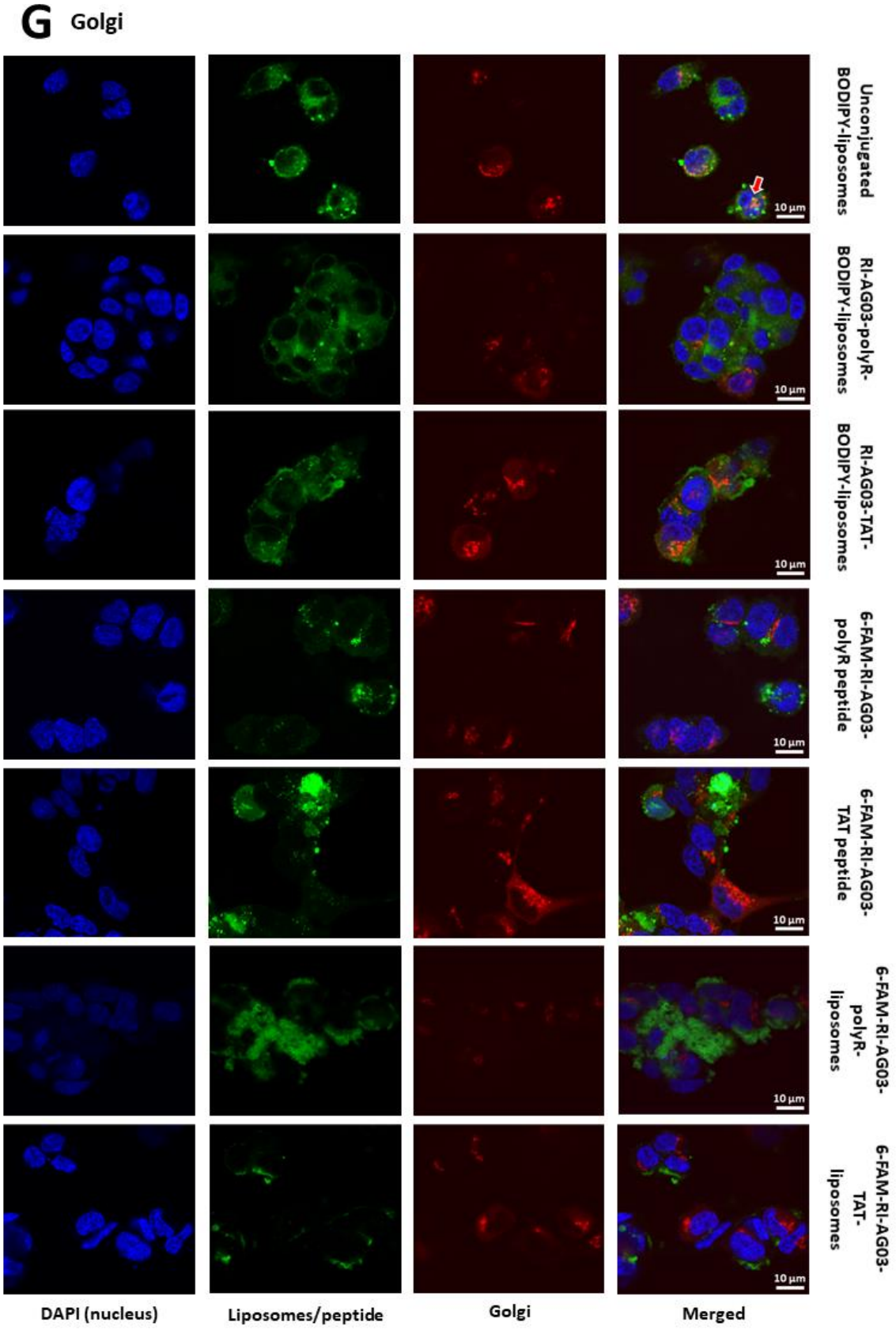

Figure 9.5: Intraorganellar trafficking of unconjugated liposomes, RI-AG03-polyR or RI-AG03-TAT and peptide-conjugated liposomes. SH-SY5Y cells were treated with fluorescent BODIPY-liposomes, fluorescent 6-FAM-peptides or peptide-conjugated liposomes (either with a fluorophore-coupled

liposome vehicle or peptide; all in green) and co-incubated with one of various live cell organelle markers (all in red) for 16 h. Cell organelle markers were LysoTracker Deep Red (lysosomes; A), pHrodo™ Red Dextran (macropinosomes; B), CellLight™ Plasma Membrane-RFP (cell membrane; C), Rab5a-RFP / CellLight™ Early Endosomes-RFP (early endosomes; E), CellLight™ ER-RFP (ER; F) or N-acetylgalactosaminyltransferase-RFP / CellLight™ Golgi-RFP (Golgi; G). In the case of lipid rafts (D), liposome and peptide constructs were co-incubated Cholera Toxin Subunit B (Recombinant), Alexa Fluor™ 594 Conjugates on ice for 30 min. Blue shows the nucleus (DAPI) and arrows emphasise co-localisation.

9.6. Failure to assess the trafficking of BODIPY-liposome constructs into caveosomes

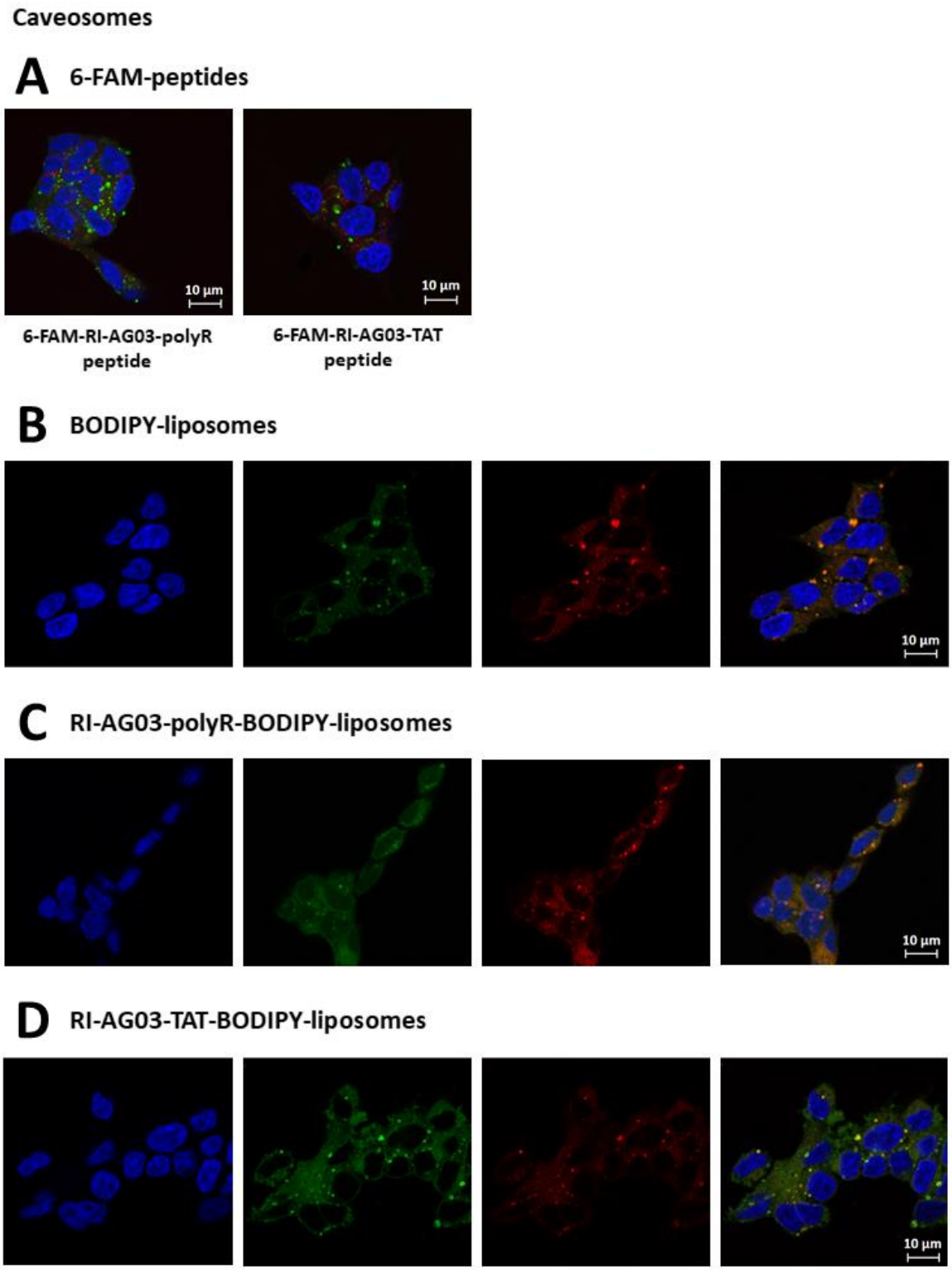

Figure 9.6: Unsuitability of HCS LipidTOX™ Deep Red Neutral Lipid Stain for caveosomes in SH-SY5Y cells. Cells were treated with 6-FAM-RI-AG03-polyR or 6-FAM-RI-AG03-TAT (A), BODIPY-liposomes (B), 6-FAM-RI-AG03-polyR-liposomes (C) or 6-FAM-RI-AG03-TAT-liposomes (D) (in green) for 16 h,

fixed in PFA and counterstained for the nucleus (DAPI; in blue). Subsequently, HCS LipidTOX™ Deep Red Neutral Lipid Stain (red) was applied and cells were subjected to confocal microscopy. Whilst the stain produced clear images for 6-FAM-peptides (A), perfect co-localisation of BODIPY-liposome species (green) with the dye (red) in (B - D) suggests that LipidTOX™ reagent stains internalised liposomes.